DISCRETE ELEMENT MODELLING OF THE DEFORMATION OF BULK AGRICULTURAL PARTICULATES

ABDULGANIY OLAYINKA RAJI

B.Sc (Hons.), M.Sc (Ibadan)

A thesis submitted for the degree of

Doctor of Philosophy on Agricultural Engineering

in the

Department of Agricultural and Environmental Sciences

at the

University of Newcastle upon Tyne

February, 1999

DEDICATION

This work is dedicated to the departed souls of my parents

Alhaji Raji Alagbe Ajao

and

Alhaja Sabitiyu Aderin Raji (Mrs)

(Nee: Adetayo)

Who departed this world during the course of this study.

May your soulsrest in perfect peace.

ABSTRACT

The Discrete Element Method (DEM) has been applied to numerical modelling of the bulk compression of low modulus particulates. An existing DE code for modelling the contact mechanics of high modulus particles using a linear elastic contact law was modified to incorporate non-linear viscoelastic contact, real containing walls and particle deformation. The new model was validated against experimental data from the literature and physical experiments using synthetic spherical particles, apple and rapeseed. It was then used to predict particle deformation, optimum padding thickness in a handling line and bulk compression parameters during oilseed expression.

The application of DEM has previously been limited to systems of hard particles of high compressive and shear modulii with relatively low failure strain. Material interactions have therefore commonly been modelled using linear contact law. For high modulus particles, particle shape change resulting from deformation is a not a significant factor. Most agricultural particulates however deform substantially before failure and their interaction is better represented with non-linear hysteretic viscoelastic contact relationship.

Deformation of geometrically shaped particles in DEM is usually treated as "virtual" deformation, which means that particles are allowed to overlap rather than deform due to contact force. Change to particle shape has not previously been possible other than in the case of particles modelled as 2-D polygons or where each particle is also modelled concurrently with an FE mesh. In this work a new approach has been developed which incorporates a non-linear deformation dependent contact damping relationship and a shape change while maintaining sufficient geometrical symmetry to allow the problem to be handled by the same DE algorithms as used for true spheres.

The method was validated with available experimental results on impact behaviour of rubber and the variations with different damping coefficients were simulated for a selected fruit. A fruit handling process dependent on the impact process was then simulated to obtain data required in the design of a fruit processing line.

Changes in shape of spherical synthetic rubber particles and rapeseeds under compression were predicted and validated with physical experiments. Images were taken and analysed using image processing techniques with 1:1 scaling. The method on shape change entails a number of simplifying assumptions such as uniform stress distribution and homogeneous material properties and uniform material distribution when deformed, which

are not observed in real agricultural materials and will tend to overestimate the true contact area between particles. In reality for fruits and vegetables, material redistribution is a complex process involving a combination of compaction and movement. However with the new method a better approximation of bed voidage (which standard DEM approaches underestimate) and stress were obtained in the compression of a synthetic material. This is a significant improvement on existing methods particularly with respect to stress distribution within a bulk particulate system comprising deforming elements where the size and orientation of contact surface between particles has a strong influence on the bulk modulus.

The new model was used for prediction of mechanical oil expression in four oilseed beds. Similar patterns in the variation of the characteristic parameters were obtained as observed in existing experimental data. The data could not be matched exactly as the quantity and arrangement of seeds in the initial seedbeds were not the same as those used in the experimental work. However the DE model gave approximate oil point data for seedbeds with the same physical properties and initial conditions as in the experiment. This suggests that the new model may be a useful tool in the study of mechanical seed-oil expression and other agricultural particulate compression processes.

TABLE OF CONTENTS

TABLE OF FIGURES

LIST OF TABLES

ACKNOWLEDGEMENTS

"*He who is not grateful to man can never be grateful to Allah*" (Ahmad and Trimidhi)

All praise is due to Allah who preserved my life, guard and guides me throughout this study.

I would like to thank my supervisor Dr. John F. Favier, for the overall supervision. Despite other commitments he painstakingly went through all the manuscripts. The encouragement I received at the initial stage and throughout the study has resulted in an un-quantifiable addition to my knowledge. I show my sincere gratitude with THANK YOU.

To my parents, even though we all thought we would meet again in this world, but that is no more possible. To Allah we belong and unto him we shall all return. However the role you played in my life which has brought me to this stage can never be forgotten. I enjoyed the nice upbringing, love, affection and those beautiful and useful advises. May God almighty in his infinite mercy forgive you and admit you to the Jannah (Paradise). I will always remember you. Though you are no more, but all the members of the family are living up to the tasks.

The support given and love shown by my other half, my loving wife, Muhibah Omodele and my children AbdulHameed Olayanju, AbdulBasit Olatunji (Jnr.) and Abdullah Olaitan (who both joined us during this study) must not be left unacknowledged. They all participated actively in the research in their own little ways. You are always with me while at work and the 'accidental' touch of some keys by the Junior Abduls (in the real sense a show of interest in what occupied dad's time) resulting in loss of data also helped in many ways (Dad must take a break!). Thanks for the company.

I am also indebted to all the other members of my family especially my uncles, brothers, sisters (The Harbahus, Tajudeen and Nasimot) and in-laws for their moral support both before and after the demise of my parents. Keep it up. May Allah reward you all abundantly (*Jazakumullah Khair*).

To all the brothers and sisters of the Islamic Society, Muslim Welfare House, the Nigerian Muslim Forum in Newcastle, other friends in the UK and across the globe who made me feel at home, the best to say is *Jazakumullah Khair*. A lot more deserves my thanks but could not be mentioned, I did not forget you.

I appreciate the assistance and co-operation by colleagues and members of staff of

the Agricultural and Environmental Sciences (AES) department and the faculty of Agricultural and Biological Sciences (ABS) in general.

This work was made possible with the Commonwealth Scholarship and Fellowship Plan (CSFP) awarded to me by the Association of Commonwealth Universities (ACU) and administered by the British Council. I therefore wish to thank all those involved both in Nigeria and the United Kingdom.

Finally I again turn with deep gratitude to Allah, saying *Alhamdulillah* for his mercy on me and pray for his continuous guidance and protection.

AbdulGaniy Olayinka RAJI

28th February, 1999

12th Dhu Al-Qa'adah, 1419.

1 INTRODUCTION

An understanding of the dynamic behaviour of particulate agricultural materials is necessary for optimal design and control of many primary agricultural production and post harvest operations. The increasing mechanisation of operations in agricultural produce harvesting, handling, transport, packaging and storage increase the likelihood of product damage. Minimal quality loss is desired during handling while efficient processing requires proper understanding of the behaviour of individual produce and the bulk. Although the stress-strain response and extent of damage of the produce in bulk have been studied, the phenomena underlying the bulk behaviour have yet to be fully explored.

The mechanisation of harvesting and processing of agricultural materials, especially fruits, seeds and vegetables, over the past fifty years has brought about a significant increase in research on their physical properties and behaviour during handling. Primary studies of the physical phenomena responsible for damage have usually entailed experimental measurements of the force-deformation relationship and other mechanical properties for single products. These type of empirical and semi-empirical study (Morrow and Mohsenin, 1968; Fridley *et al*, 1968; Holt *et al*, 1981; Lichtensteiger *et al*, 1988; Siyami *et al*, 1988) provide some useful information for some handling operations and are therefore still common (Matthew and Hyde, 1997; McGlone *et al*, 1997a; Chen and Tjan, 1998). This is because knowing the properties of an individual product is important for many processing operations in which the quality of the individual object requires protection. However most agricultural materials are handled in bulk during storage and handling.

The bulk system consists of a complex matrix of particles in which loading behaviour of the packed system is usually dramatically different from the loading behaviour of the individual product (Foultz *et al*, 1993). Recognising this, experimental studies have been extended to bulk systems (Manbeck and Nelson, 1972; Paulsen, 1978; Herum, 1979; Thompson and Ross, 1983; Horabik, *et al*, 1988; Foultz *et al*, 1993; Molenda *et al*, 1993). Such studies have involved full commercial scale using on-site measurements and laboratory scale models.

Experimental studies generally require time-consuming interpretation, hampered by lack of appropriate instrumentation and are restricted by the limited information provided on the behaviour within a bulk system i.e. what actually happens to individual particles in a bulk system. In order to gain more insight into the loading behaviour of a wide range of

products at both individual and bulk scales, various theoretical analyses and models involving development of constitutive equations have been explored (Chen and Fridley, 1972; Sherif *et al*, 1976; Hamman and Diehl, 1978; Mohsenin *et al*, 1978; Chen and Yasdani, 1991; Faborode and Dirinfo, 1994; Dielwiche *et al*, 1996). The theoretical method is useful for determining the material properties without the need to prepare samples but the derivation and solution of the equations are often not simple and sometimes difficult to handle due to lack of appropriate instrumentation for solution. However there is still a lack of appropriate constitutive equations that can represent the real behaviour for most agricultural particulates under load. Therefore most work has involved deduction from the existing equations for similar elastic and other engineering materials. Prominent among these is the classical solutions from the linear elastic theory for contact between spheres by Hertz (1882). This approach has been shown to be approximately applicable and has yielded good results especially for fruits whose strength is based on a mostly rigid structure surrounded by thin skin (Ruiz-Altisent, 1991). An additional feature of agricultural particulates is their time dependent behaviour, which differs for each product. This complication and other problems associated with the derivation and methods of solution, can result in formulation of equations whose solutions require many assumptions.

The central problem in the processing of agricultural particulate materials is the need for an improved understanding of the nature and the magnitude of the forces, deformation as well as changes in shape involved in particle to particle interactions. However up to date, what is not well understood is the extent to which the structure formed by the deforming and moving assembly of particles in a bulk system controls the overall material behaviour, quality and the final product in processing and usage. Also the way in which the inter-particle behaviour is affected by the spatial and size distributions of the constituent particles needs to be studied.

Experimental and analytical investigations are generally restricted by the limited quantitative information about what actually happens within particulate assemblies. Computational methods are promising alternatives that can essentially provide solutions to complicated equations, make accurate prediction of the stress-strain response during loading of the individual or bulk system and provide both microscopic and macroscopic information at any time on any subspace within a system.

The general objective of this study is therefore to study the behaviour of bulk systems of agricultural particulates under load using a numerical approach developed for particulate systems. Emphasis will be on the shape change of the individual particle resulting from

deformation, which is an important factor in bulk systems behaviour of agricultural particulates. In this chapter the general characteristics of particulate systems are discussed with the main numerical methods used for modelling their behaviour and the specific features of agricultural particulates are reviewed. The specific objectives of this study and a summary of chapter contents are then stated.

1.1 Properties and Analysis of Particulate Systems

Particulate or granular systems are comprised of distinct particles not physically connected to each other. Bulk mechanical behaviour of particulates depends on the movement and contact forces at the particle scale. The particles interact as discrete objects, displacing independently from one another and interacting only at contact points with each other and/or the container. The interaction between objects is transient with contacts forming and breaking resulting in flow and displacement. Bulk system of particulates usually consists of a combination of particles with different shapes and may be an ensemble of very small particles such as powders with sizes being about 10^{-6} of a metre in length or radius or an ensemble of large particles, the size of which is determined by the type of system. For agricultural systems, bulk systems of particulates with sphericity radius of between 1mm (grains) to 10mm (fruits) may be categorised as large particles while the range might be different in other fields such as geotechnical engineering where rock particles with larger sizes are handled. Inertial forces dominate the forces holding the particles together in a free (unloaded) system of particulates.

A number of methods have been used in studying the behaviour of granular assemblies. Some common procedures for solution to granular material behaviour as reviewed by Desai and Christian (1977) are as shown in Figure 1.1 (DEM has been added following this study). The problems associated with the experimental and analytical methods briefly discussed above on agricultural particulates apply generally to particulate systems. Laboratory models are sometimes used, though they provide useful information in some cases but extrapolation of the results to full industrial scale is most uncertain especially for cases where some measurements are very difficult (Ooi *et al,* 1998). The search for alternative methods that can provide both microscopic and macroscopic information within a particulate system and the emergence of high-speed computers has resulted in the increasing use of computational methods.

1.2 Computational Modelling

Two main computational methods have been used during the last two decades to model the behaviour of particulate solids. These are the continuum method (Finite and Boundary element methods; FEM and BEM) and the discrete element method (DEM) (Cundall and Strack, 1979; Munjiza *et al*, 1995; Becker, 1996; Holst e*t al*, 1999a and 1999b).

1.2.1 Finite and Boundary Element Methods

The basic steps of the FEM and BEM are discretisation, i.e. division of a continuum into an equivalent system of smaller continua called elements, derivation of element equations and assembling the element properties to form global differential equations describing the discrete systems. These equations are solved by converging to a minimal error or equilibrium state through approximation methods to obtain parameters describing the behaviour of each discrete section and provide information on macroscopic behaviour of the system.

The FEM has been used for a number of processes which include heat and mass transfer and stress-strain analysis for continuum and structural behaviour of bulk granular medium (Segerlind, 1984). Particulate materials with continuous bonding between particles, such as geo-material and some bulk systems of agricultural materials, have been considered as continua and successfully analysed using the FEM. These systems of closely packed particles treated as continua include bulk particulate systems in silos and other grain storage systems (Watson and Rotter, 1996; Xu *et al,* 1996; Meng *et al*, 1997a, 1997 b; Ooi and She, 1997). BEM on the other hand is advantageous due to non-negligible reduction of time and cost (Carini and Gioda, 1986) since only the boundaries of the system are discretised instead of its entire volume as required by the FEM. This gives accurate results (Olukoko *et al,* 1993; Becker, 1996) especially when dealing with problems with small strain such as those involving cavities. The BEM has therefore been used in the last decade for contact problems where partial or whole interior discretisation into elements gives approximately the same solution.

Finite Element, Boundary Element and Langrangian Finite Difference models employ interface elements or "slide lines" for modelling contacts between bodies. However their formulation is usually restricted in one or more of the following ways; (i) the logic

may break down when many intersecting interfaces are used, (ii) there may not be an automatic scheme for recognising new contacts and (iii) the formulations may be limited to small displacements and or rotation (Cundall and Hart, 1992). A model for discontinuous material such as granular media, with the first restriction might leave out some important factors such as recognition of non-contacting bodies and with the second, it is limited to a small number of bodies for which the interactions are known. Heinstein *et al* (1993) developed a contact detection algorithm in an attempt to address some of these difficulties associated with the simulation of contact in FEM. This was accomplished by monitoring the displacement of the slave nodes (a nodal point on the surface of the mesh) throughout the calculation for possible penetration of a master surface (the side of a finite element on the surface). There are no published figures on the results of their studies but illustrated examples of some operations were used to demonstrate the capabilities of this algorithm.

Despite the advantages of FEM and BEM the assumption of continuity is not always true for particulate systems, hence an alternative approach may be required for modelling or combined with the continuum method when discontinuity sets in during flow. A poor estimate may be obtained for systems comprising a small number of particles because the methods operate only at the bulk scale. Also homogeneity of physical properties is usually assumed within the spatial domain but the length scale of the microstructure of the materials (individual particle size) may be much smaller than the elements of the discretised region.

1.2.2 Discrete Element Method

Perhaps the most striking characteristic of a granular medium is its dual nature being both a disjoint, discrete material and a continuum. Although the individual particles of the medium are solids, they are not physically connected. The most basic mechanism is particle-to-particle interaction at contact points. Modelling such systems as discontinua is often more rewarding as new knowledge can be gained about the macroscopic behaviour when the microscopic mechanisms are understood (Isa and Nelson, 1989; Cundall and Hart, 1992; Williams and Rege, 1997). The major constraint in modelling such a system at the particle scale is the enormous number of contact points within a bulk system where the interaction has to be determined. This is a constraint related to memory size and computation time rather than physics. In recent years the possibility for numerical modelling of the dynamic behaviour of particle assemblies offered by the rapid increase in computer power has motivated further interest in contact problems in many fields of engineering and this has led

to the development of the relevant computer codes.

A numerical method later known as the Discrete Element Method (DEM) originally developed by Cundall (Cundall, 1971) was proposed by Greenspan (1974) as a method to describe the motion of an assembly and thereafter introduced for the computational analysis of granular soil and rock particles under load.

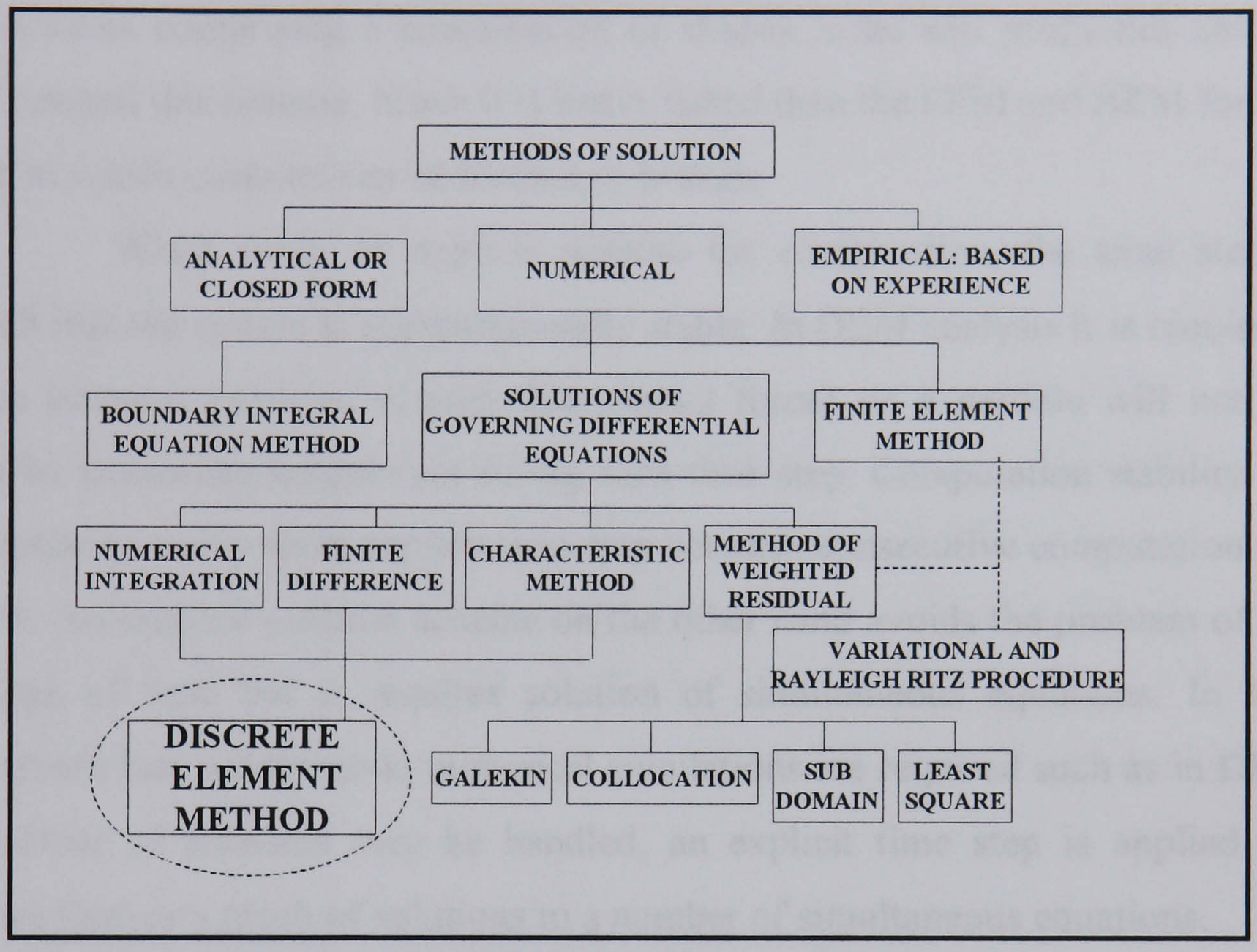

Figure 1.1 Common procedures of solution of granular materials analysis (Desai and Christian, 1977)

The origin of DEM can be traced to the late 1960's when simulation of the mechanical behaviour of jointed rocks was accomplished by introducing discontinuities into the existing continuum models (Munjiza *et al,* 1995). It was developed originally by Cundall in the early seventies for rock mechanics problems (Cundall, 1971; Dobry and Ng, 1992) and later extended to granular materials (Cundall and Strack, 1979). Cundall and Hart (1992) proposed the name Discrete Element Method (also referred to as Distinct Element Modelling or Distinct Particle Modelling) for any computer programme that; (i) allows finite displacement, rotation and detachment of discrete bodies and (ii) recognises new contacts automatically as the calculation progress.

The DEM is an explicit numerical scheme in which the interaction of particles in a bulk system is monitored contact by contact and the motion modelled particle by particle. The interaction between the particles is viewed as a transient problem with states of

equilibrium developing whenever the internal forces balance. The process involves solutions of the equation of motion of each particle using an explicit time finite difference algorithm. Deformation, contact forces and stress-strain response between contacting particles are directly determined using an appropriate force-displacement law during each time step.

The DEM is a collection of four methods; the distinct element programme, modal method, discontinuous deformation and the momentum exchange method. It is capable of handling systems comprising a combination of shapes, sizes and properties and considers both continua and discontinua, hence it is better suited than the FEM and BEM for modelling of systems in which contacts can be formed or broken.

When using an explicit scheme for computation, the time step must be chosen such that the system is computationally stable. In DEM analysis it is required that the disturbance between particles is such that contact forces on a particle will not propagate more than its immediate neighbours during each time step. Computation stability (in DEM) therefore requires a very short explicit time step between consecutive computation of particle interactions. An implicit solution scheme on the other hand avoids the problem of instability at any range of time but it requires solution of simultaneous equations. In large-scale problems where fast and dynamic numerical simulations are required such as in DEM where a large number of particles may be handled, an explicit time step is applied to reduce computation time as a result of solutions to a number of simultaneous equations.

1.2.2.1 Applications and Advantages of DEM

The DEM evolved from a wide range of disciplines but has largely been applied to problems in goemechanics involving a large number of separate distinct bodies. Researchers in the field of geomechanics have successfully predicted the behaviour of soil and rock particulate systems with this method. Such phenomena include complex mechanical interactions within multiple body systems and gross progressive discrete fracture in geotechnical, mining and many other fields.

Researchers on DEM have either used codes made available by Cundall such as BALL (Cundall, 1971) and TRUBAL (Cundall and Strack, 1979, Strack and Cundall, 1984) or have modified these two programmes to suit their needs; CONBAL (Ng, 1989; Ng and Dobry, 1990); DISC (Ting *et al*, 1989); Ning (1995); Sakaguchi *et al* (1994) and Rong *et al* (1995a). New codes based on the principle have also been developed; MASOM (Isa and Nelson, 1989), GLUE (Bathurst and Rotenburg, 1989), Walton *et al* (1988) and Williams

and O'Connor (1995).

1.2.2.1.1 Wider Scope and Usage

The nature of DEM (evolution from a wide range of disciplines) has made it more readily applicable to many other areas of science and industrial interest. One of the areas where the DEM has been successfully applied is in chemical and process engineering. It has been used in simulation of processes in the pharmaceutical industries involving powder and pellet handling such as impact breakage of chemical agglomerates (Thornton and Yin, 1991; Thornton *et al,* 1996; Ning *et al*, 1997a, 1997b), attrition of particulate solids (Hutchings, 1993; Ghadiri and Ning, 1997), fluidisation (Tsuji *et al*, 1993; Xu and Yu, 1997), mixing, pneumatic conveying and compaction. Other applications include research on flow studies such as simulation of plug flow of cohesionless spherical particles conveyed in horizontal pipe (Tsuji *et al*, 1992), with obstructions (Williams *et al*, 1996) and the study of formation of shear bands in flow problems (Williams and Rege, 1997). It has also recently been applied in agricultural process engineering (Rong *et al*, 1992; Sakaguchi *et al,* 1994 and 1998; Schembri and Harris, 1996).

1.2.2.1.2 Particle Shape, Size and Spatial Distribution

Systems made up of various particle shapes which include circular, elliptical and polygonal shapes for 2-D studies and spherical, ellipsoidal and polyhedral solids for 3-D studies have been handled with the DEM. Primitive shapes such as spheres and circles have the advantage of computational simplicity and most of the available contact theories can be applied to them. The difficulty that arises when using these common simple geometric shapes for modelling real granular particles whose shape is irregular is that the behaviour predicted may differ significantly from that of the real particles. Earlier work in the field of geomechanics used disc (Cundall and Strack, 1979) and spheres (Ng and Dobry, 1994).

More recently non-circular elements have been used to approximate more closely to the real material behaviour. These include ellipse (Ting *et al,* 1993; Sakaguchi *et al*, 1994) and polygons (Ghaboussi and Barbosa, 1990; Krishnasamy and Jakiela, 1995). Others are shapes formed by continuous function representation (CFR) of the surface of a body described implicitly by a function f(x, y) or f(x, y, z) in 2 and 3-D respectively such as ellipse and superquadrics (Barr, 1981; Williams and Pentland, 1989; Hogue, 1998) and

discrete function representation (DFR) using a parametric function to describe the surface. Williams and O'Connor (1995) define DFR as discretised representation of the body as a parametric function of one parameter. Hogue and Newland (1994) applied this method to generate 2-D particles using a polar descriptor to define the nodes on the surface of a particle defined by its function (radius and angle from a datum). Munjiza *et al* (1995) on the other hand used a set of boundary nodes and connectivity information to defined the shape. Polyhedron whose geometry is defined in terms of corners and edges given by a series of vectors from the centre have also been used. The main problem associated with all these methods is the computational cost in contact detection.

Computational efficiency associated with the use of spherical shapes led to the investigation of the generation of irregularly shaped particles by Abbaspour *et al* (1998) using a combination of spheres. Excessive computational time is reduced as the need for numerous points and nodes representing boundaries is eliminated. Shapes close to that of many fruits have been generated successfully and numerical trials on the flow and discharge from a silo showed a discharge rate dependent on the degree of irregularity.

The DEM has been successfully used to model bound or unbound systems with uniform size or a combination of different size distribution. Systems comprising small and large numbers of particles have been modelled with the DEM to predict the behaviour of a sub-domain of a larger system. Examples include modelling of soil loading with 684 and 1000 discs in two-dimensions (Ting *et al*, 1993; Barthurst and Rotenburg, 1989) and flow and discharge problem in a silo using 1980 spherical grains (Rong *et al,* 1995b) while Sakaguchi *et al* (1994) used 4700 spherical glass beads and 2600 white rice (modelled as elliptical particles). Schembri and Harris (1996) modelled the impact breakage of sugar cane using 2765 hexagonal elements to represents the cross sectional cellular structure. Kafui and Thornton (1993) simulated the impact of monodisperse primary spherical agglomerates against a wall in 2D and 3D with 1000 and 7912 respectively. Soil ploughing was modelled with 66544 soil particles of sizes ranging between 0.03-0.75mm by Hryciw *et al* (1997). In the impact studies the effect of impact velocity, strength and particle size among others were examined. Generally the particles or elements used are generated using a random number generator algorithm or specifying a matrix of uniformly arranged particles in 2 or 3-D.

The sizes of materials modelled with DEM ranged from small (0.1mm - 0.4mm) soil particles (Anandarajah, 1995), chemical agglomerates (4mm - 10mm) (Ning, 1995) to relatively large particles such as 4 - 10 mm spherical particles by Tsuji *et al* (1992 and 1993) in plug flow of cohesionless materials in a horizontal pipe and soil compression.

Earlier work on DEM was based on the assumption that each element was rigid, but later developments included local deformation, although the deformation is treated as virtual. This has permitted a more rigorous treatment of both the contact conditions and energy preservation requirement allowing the modelling of soft, weak, brittle or deformable materials such as rubber (Karakerezis and Khodabandehloo, 1996) and apple (Rong *et al*, 1993). In the works DEM has been found to modelled the mechanical behaviour of the assemblies qualitatively closer to real materials. However, quantitatively the predictions of flow rate and void have matched real systems but the predictions of some other parameters such as stress and friction need further research.

1.2.2.1.3 Combined DEM and FEM

The incorporation of deformation kinematics with the discrete element formulation has also led naturally to a combined discrete and finite element approach. This solution is particularly suited to problems in which progressive fracturing take place. Munjiza *et al* (1995) applied a combined finite and discrete element method to deformable solids starting from a continuum representation of the solid using finite elements. Progressive fracturing led to the formation of discrete elements composing of one or more deformable finite elements. The process continued until either the system came to rest or up to a time of interest. Lu *et al* (1997) developed a hybrid numerical model based on the FEM and DEM to predict the stress and velocity fields for particulate materials during discharge from silos. FEM was used to model the particulates as a continuum. The DEM was employed when the bulk solids no longer behaved as a continuum such as in the lower part of the hopper near the outlet and the intersections between the vertical bin walls and inclined hopper walls where there are large shear deformations. Negi *et al* (1997) reported that simulation results of wall pressure with the model successfully matched results from laboratory experiments involving gravity flow of soybean from a parallel wall bin with different outlets while Jofriet *et al* (1997) used the validated model to determine some parameters associated with hopper flow. Pan and Reed (1989) also used a combined model for large deformation analysis of rock masses.

1.2.2.2 Limitations

There are some limitations on the application of DEM to real systems. One problem is the use of appropriate particle shape but there has been increased interest in research on

this area as discussed earlier. The DEM is not suited for simulation of problems on a very large length or volume scale where the spatial domain may contain several millions of particles. This limitation is not associated with the method itself but with the available computing power, as modelling this number of particles will require a very high-speed computer with large memory. Moreover, the detailed output of such a calculation would be too excessive because of the size of the microscopic material and macroscopic space domain for which information is required. Such problems are usually best solved with continuum codes.

Another problem with the DEM is associated with the mode of application, which is related to the effect of scaling. As discussed in 1.2.2.1.2, most studies have used a few hundred or thousand particles. In systems composed of large number of small sized particles this number of particles will represent only a very small, possibly even negligible, part of the total spatial domain. For example Hryciw *et al* (1997) used approximately 66000 particles in their study of soil ploughing but the volume of the model system was negligible compared to the actual system. The experiment used for validation of the model consisted of a 300 x 150 x 8.5 mm^3 box filled with sand to a desired depth. The bulk volume of the model sand particles used in the simulation was approximately 1x 10^4 mm^3 while that of the experiment was about 12.5 x 10^4 mm^3 (1/3 full). This problem was recognised by Langston *et al* (1997) who selected large particles with visible grain boundaries to keep the critical time step within feasible limits and make image analysis easier. The same applies in the modelling of gravity flow in silos by Rong *et al* (1995b) and Sakaguchi *et al* (1994) where a few hundreds of particles were used to represent a large silo. Material physical properties were adjusted in some simulation work while completely different properties compared to the real system were used in some others. Hryciw *et al* (1997) and Langston *et al* (1997) reported that the strength properties of particles used in their simulation are between 4 - 8 orders of magnitude less than the real values.

The studies cited above actually went a little further by introducing image analysis and graphical presentation for validation in addition to the existing graphical parametric comparison of both experiment and simulation. Sakaguchi *et al* (1994 and 1998), Hryciw *et al* (1997) and Langston *et al* (1997) took images of the particulate assembly using a high-speed video camera. The pattern of particle movement in both experiment and simulation were compared and found to correlate well. However the image analysis still failed the scale effect test as only visual observation and comparisons between experimental and simulation results were reported while the question of quantitative determination of particle

arrangement and movement was neglected. A scaled image comparison by superimposing the two images is yet to be explored. Such an approach is not possible without addressing the problem of scaling.

1.3 Application of DEM to Agricultural Particulates

A close study of the physical structure of the systems to which DEM has been applied e.g. rock and soil particulate systems, shows a similarity with the structure of agricultural particulate systems. The mechanical and rheological properties may differ as agricultural particulates have relatively rough surfaces and generally low modulus compared to most engineering materials. Investigations incorporating the deformation kinematics and the introduction of viscous damping (which is a modification of the commonly used global damping) such as those of Tsuji *et al* (1992 and 1993) showed that the DEM can be successfully applied in the study, prediction and analysis of agricultural particulates. Since most agricultural materials exhibit a non-linear response to applied loads, the incorporation of viscoelastic behaviour into the DEM has increased potential for its application to agricultural particulates.

Rong *et al* (1993) used the DEM to model the dynamic behaviour of a single column of fruits (apples) packed in a container on a truck bed. The numerical experiment consisted of two series of tests each involving three treatments of two packing types and road irregularity input. Either a soft or hard response suspension unit was assigned to each series. The variations of vertical velocity and interaction forces of individual apples in a vertical column of five, in three different packaging arrangements were studied. Due to symmetry, as is the case in most simulation or theoretical work, the mechanical quantities of three marked elements in three layers, top, middle and bottom layers were presented. They observed larger variation of vertical velocity and interaction forces in the top and bottom layers than in the intermediate layer in all three set-ups. The results of the middle layer, which are in accord with experimental evidence by Holt *et al* (1985), were used to recommend optimum packaging arrangements.

Sakaguchi *et al* (1994) used the DEM to simulate gravity flow of white rice and validated the results with experiments. In the experiments, gravity flow and discharge phenomena of spherical beads and white rice flowing out of a hopper were recorded using a high-speed camera at a time interval of 0.01 s. The images were then analysed using a computer-based image processing application. The positions of the free surface obtained for

simulation in 2-D were found to agree reasonably well with the experimental results. However the rotation of the elements was not observable in the simulation for circular beads but only with the ellipse shaped rice particles. Using a similar set-up and analysis Sakaguchi *et al* (1998) modelled the separation of paddy and white rice using spherical particles.

Rong *et al* (1995a) simulated the mechanical behaviour of bulk solids using a model based on the DEM to obtain information on their flow and contact condition. They validated the model with experiments on the discharge of hollow cylindrical particles flowing from a hopper using particles physical properties within the range for agricultural materials. The results showed a general agreement between the numerical and measured values of the positions of ten particles in a given layer of the bin at different times.

Having validated the model Rong *et al* (1995b) used this DEM model to study the flow patterns through shear bands and material deformations of bulk solids with 780 - 1980 solid particles of 0.025 m diameter in different hopper shapes and inserts of different shapes near the hopper discharge. The movement of the particles was simulated and the results showed progressive changes in the shear lines along points of broken contacts representing the pattern of flow. Dramatic velocity changes and particle rotation were also observed near the transition from parallel to convergent flow with particles rotating along the walls in both the vertical and horizontal parts. The patterns also showed the vertical layers near the opposite walls rotating in opposite directions. They therefore concluded that the DEM could be used in study of shear bands and prediction of other flow problems such as in silos and other storage bins. However this work used a regular lattice of 2-D spheres and ignored the scale effect discussed earlier which severely limits the usefulness of the results

Schembri and Harris (1996) applied the DEM to the study of 2-D fracture of a cellular material (sugar cane) under impact load. A transverse section of the cane with storage cells represented by hexagonal elements was created in a 2-D section. An elastic bond between adjacent cells was applied to provide inter-cell cohesion that maintained the equilibrium positions of the elements in the presence of any external loading until the shear stress exceeded the bond strength. The failure of the simulated material under load was obtained by observing lines along broken contact points and obtaining information for contacts retained, formed or broken after bond failures. The simulated damage when compared to the experimentally observed result for 18 m/s radial impact of a 440 g projectile against a segment of cane showed that both produced a Y-shaped failure pattern very similar in dimension.

It is pertinent to note that in all the work reported emphasis was laid on the

calculation of some mechanical properties in flow studies. In agricultural materials, the damage in handling and energy or forces required for breakage or fracturing during processing is often of greater importance than the displacement of the material. Regardless of sample dimension, when a sample is deformed in compression or under load, the strain generated will decrease the height or length of the sample. This results in an increase in sample diameter (in the lateral direction) or width to a value dependent on the bulk modulus and Poisson ratio of the material. Therefore an insight into the shape changes as the particle deform can give the stress concentration point and eventually the potential failure point or reduction in quality and market value (extent of damage by bruising and shape changes). This phenomenon can also be used to study the energy requirement before failure of particles under any particular assembly of particles. This is typical of soft materials such as most agricultural and food materials. This information is of great importance in the design and planning of agricultural materials handling and processing operations and may not be of importance in other fields of engineering.

Karakeresiz and Khodabandehloo (1996) used some of these parameters and constants to predict deformation of agricultural products in 2-D with DEM. A system consisting of point mass elements connected to each other by discrete spring and dashpot links was used to represent the specimen in their model and a similar system was set up experimentally. The deformed shape of rubber and sponge specimens squeezed between two plates were obtained with the model using small elements connected together to represent the bulk system. Similarly deformation rate was computed for these materials and apple tissue although the deformed shape for apple tissue was not presented. A good correlation was obtained between the DEM and the experimental results.

The mechanical behaviour of an assembly of agricultural particulates such as fruits, vegetables and seeds is a complex integrated effect defined by the geometry of the containing structure and number and strength of the points of interaction (contacts). These are themselves a consequence of the shape, size, roughness and strength of the particles as well as any other external forces. Handling and processing operations result in non-linear behaviour (inelastic deformation) brought about by movement of stressed particles and possible fracture. Studies of this behaviour through experimentation have not produced comprehensive and reliable results on the behaviour of individual particles in the bulk system. Since the DEM has been shown to be a numerical method suitable for modelling the behaviour of discontinuous media of varying physical properties, it is therefore a promising approach to modelling bulk systems of soft, deformable particles. However its application to

this system will require modification of existing methods since there is a lack of appropriate existing DE code for bulk systems or single particle in 3-D with fixed boundaries incorporating particle deformation for viscoelastic materials which are typical of most agricultural handling and processing systems.

1.4 Objectives

The specific objectives of this study are to:

(i) Review existing theories on the behaviour of both geo- and bio-materials with respect to their physical and engineering properties,

(ii) Investigate the discrete element method (DEM) as applied in the field of geo and rock mechanics through an appraisal of one of the existing programmes developed for granular materials i.e. CONBAL with a view to modifying it for agricultural particulates.

(iii) Develop a generic programme (modified CONBAL or based on the principle of DEM) for the simulation of the handling and processing of particulate biomaterials with a view to:

  (a) Predict the behaviour of some bulk systems of agricultural particulates and the individual particles within it, under load, in specific operations such as compression and packing of fruits and seeds.

  (b) Obtain the resulting change in shape of the deformed particles within the system, which may lead to estimation of the damage done to the material under load.

1.5 Summary

An extensive review of contact mechanics theory in its general sense and as it applies to some specific problems especially viscoelastic materials which extend its use to agricultural materials is presented in Chapter Two. This includes the theory used in developing algorithms for the change in shape of particles under load. A review of the basic principles and theoretical background of DEM follow these.

In Chapter Three, an appraisal of the programme chosen for this study with the necessary modification as well as the mode of operation of the original and the new programme are presented.

In Chapter Four, the modified DE code with new extensions to incorporate particle

deformation are validated using data from the literature and new experiments on the bulk synthetic and biological particulates.

In Chapter Five key aspects of two agricultural particulates handling and processing operations are simulated using the new DE code. These are determination of the optimum thickness of contacting surfaces in a fruit processing line and simulation of the early stages of oil expression in seeds.

2 THEORETICAL BACKGROUND

2.1 Introduction

Hertz (1882) pioneered study of the response of a single contact between two particles. The theoretical understanding of the results of experimental investigations of particle-particle and/or particle-wall interaction for frictionless elastic bodies has been extended to include no-slip solution for spheres with different sizes (Mindlin, 1949; Goodman, 1962), tangential loading, twisting couples and sliding as well as influence of friction at the contact interface (McEwen, 1949; Mindlin, 1949; Smith and Liu, 1953; Mindlin and Deresiewicz, 1953), elastic-plastic deformation with surface roughness (Fuller and Tabor, 1975; Rogers and Reeds, 1984) and the effects of dynamic yield stress (Wall *et al,* 1989). Ning (1995) extensively reviewed the conditions for adhesive and non-adhesive contacts, loading, and types of impact. Further detail and review of recent developments in impact and contact mechanics theory, can be found in Lubkin (1962), Timoshenko and Goodier (1970) and Johnson (1992).

The DE method briefly reviewed in the previous chapter is partially based on the application of contact theory to particulate mechanics. A review of the contact mechanics theory and principles is necessary before further discussion of DEM. This chapter will therefore outline the theory of contact mechanics in general and as it applies to viscoelastic materials. The basic principles and theoretical background of DEM will then be presented.

2.2 Frictionless Elastic Contact in Smooth Bodies

Hertz (1882) developed a theory for the behaviour of convex elastic bodies with frictionless contact. The theory assumes that each body is homogeneous and isotropic, the load is static, the surfaces are smooth and the radii of curvature of the contacting bodies greatly exceeds the radius of the contact surface. When two non-conforming bodies are brought into contact, they touch initially at a point or along a line depending on their shape. Under the action of a static load they deform in the vicinity of the first point of contact so that they touch over a finite area, which is small, compared with the dimension of the bodies.

Hertz bodies are perfectly smooth which results in frictionless contact during interaction with only normal stress and negligible shear or tangential stress. In the Hertzian model the force deformation relation at contact is non-linear elastic (i.e. reversible with no energy dissipation during loading and unloading). The solution predicts a plane circular

contact area between two spherical elastic bodies in contact under a normal load having a radius of

$$a = (KF_n R^{-1})^{\frac{1}{3}} \qquad 2.1$$

where K is related to the material property, F_n is the normal contact force and R is a function of the geometry of the bodies in contact.

The approach of the centre of the spheres (α), which is the addition of the deformation of the two spheres (1 and 2), is related to the contact radius and the geometry of the material R,

$$\alpha = \alpha_1 + \alpha_2 = a^2 R \qquad 2.2$$

The relationship between the normal force and approach of the centres can be obtained from 2.1 and 2.2

$$F_n = K^{-1} R^{-\frac{1}{2}} \alpha^{\frac{3}{2}} \qquad 2.3$$

Therefore Hertz theory shows that for spherical elastic bodies in contact under a normal compressive load F_n, the load is proportional to the approach of the two sphere centres (i.e. deformation of both spheres at the contact area).

The normal contact stiffness C_n can be obtained from this non-linear equation by using the linear relation

$$dF_n = C_n d\alpha \qquad 2.4$$

substituting from (2.1) and (2.3) gives

$$C_n = \frac{dF_n}{d\alpha} = \frac{3}{2} K_n^{-1} R^{-\frac{1}{2}} \alpha^{\frac{1}{2}}$$

$$= \frac{3}{2} K_n^{-1} a \qquad 2.5$$

The material property constant K, is defined as

$$K = K_1 + K_2 = \frac{3}{4}\left(\frac{1-\nu_1^{\,2}}{E_1} + \frac{1-\nu_2^{\,2}}{E_2}\right) \qquad 2.6$$

where ν is the Poisson ratio and E is the modulus of elasticity.

For contact between a soft and a rigid surface, $E_1 <<< E_2$ hence $K_2 <<< K_1$ and K_2 (for rigid) can be neglected. If we substitute E with the shear modulus or coefficient of rigidity in (2.6) for

$$G = \frac{E}{2(1+\nu)}$$

then $$K = \frac{3}{8}\left(\frac{1-\nu_1}{G_1} + \frac{1-\nu_2}{G_2}\right) \qquad 2.7$$

The constant R is related to the radius of the contacting bodies by

$$R = \frac{1}{R_1} + \frac{1}{R_2} = \frac{R_1 + R_2}{R_1 R_2} \qquad 2.8$$

for two spheres having different radii. $R = {}^{1}\!/_{R_1}$ for a sphere of radius R_1 in contact with a rigid plane where ${}^{1}\!/_{R_2} \cong 0$ while in the case of a sphere and a concave surface of radius of curvature R_1, $R = \frac{R_1 - R_2}{R_1 R_2}$.

Substituting (2.7) and (2.8) in (2.1) and (2.3) gives

$$F_n = \frac{8}{3}\alpha^{3/2}\left(\frac{R_1 R_2}{R_1 + R_2}\right)^{1/2}\left[\frac{1-\nu_1}{G_1} + \frac{1-\nu_2}{G_2}\right]^{-1} \qquad 2.9$$

$$\alpha = \left\{\frac{3}{8}F_n\left[\frac{1-\nu_1}{G_1} + \frac{1-\nu_2}{G_2}\right]\left(\frac{R_1 + R_2}{R_1 R_2}\right)^{\frac{1}{2}}\right\}^{\frac{2}{3}} \qquad 2.10$$

and

$$a = \left\{\frac{3}{8}\pi F_n\left[\frac{1-\nu_1^{\,2}}{E_1} + \frac{1-\nu_2^{\,2}}{E_2}\right]\left(\frac{R_1 R_2}{R_1 + R_2}\right)\right\}^{\frac{1}{3}} \qquad 2.11$$

The mean pressure acting on the contact area of diameter $d = 2a$ is

$$P = \frac{Force}{Area} = \frac{4F_n}{\pi d^2} \qquad 2.12$$

The pressure distribution over the contact area is found to be represented by a hemisphere with a maximum at the centre, which is the point of action of the normal compressive force and minimum (≅0) at the edges. The maximum pressure was reported by Timoshenko and Goodier (1970) and Johnson (1992) to be 3/2 of the average pressure

$$P_{\max} = \frac{3}{2}P = \frac{6F_n}{\pi d^2} \qquad 2.13$$

Johnson (1992) derived the general equation for normal stresses and also for the radial and tangential stresses (not calculated by Hertz) on a circular region of radius 'a'.

These are

$$\sigma_n = -P_{\max}\left(1-\frac{r^2}{a^2}\right)^{3/2} \qquad 2.14$$

$$\sigma_r = P_{\max}\left[\frac{1-2\nu}{3}\left(a^2/r^2\right)\left\{1-\left(1-\frac{r^2}{a^2}\right)^{3/2}\right\}-\left(1-\frac{r^2}{a^2}\right)^{1/2}\right] \qquad 2.15$$

$$\sigma_\theta = -P_{\max}\left[\frac{1-2\nu}{3}\left(a^2/r^2\right)\left\{1-\left(1-\frac{r^2}{a^2}\right)^{3/2}\right\}+2\nu\left(1-\frac{r^2}{a^2}\right)^{1/2}\right] \qquad 2.16$$

where $r = 0$ at the centre and $r = a$ at the edge of the contact circle. This shows that the tangential and radial stresses are minimum (negligible fraction of P_{max}) at the centre while their maximum values occur at the boundary surface of the circle with

$$\sigma_r = \sigma_\theta = \pm P_{\max}\left(\frac{1-2\nu}{3}\right) \qquad 2.17$$

and the normal stress at the centre of the circle is

$$\sigma_n = -P_{\max} = -\frac{6F_n}{\pi d^2} \qquad 2.18$$

2.3 Mindlin's Solution for Rough Bodies: Tangential Forces

The Hertz contact theory is for smooth bodies (spheres) in contact subjected only to a normal force with neither friction nor tangential forces. Mindlin (1949) and Mindlin and Deresiewicz (1953) investigated the tangential load-displacement relation by a consideration of both the Hertz theory and the work of Cattaneo (1938). They considered the case of the contact between two elastic rough spheres, where friction is greater than zero, subjected to several loading sequences involving variations of a combination of normal and tangential forces. A number of closed form solutions were presented for each of the loading cases from which general procedural rules were identified. Walton (1978) and Dobry *et al* (1991) extended this work by considering the case of oblique contact in which simultaneous and arbitrarily varying tangential and normal loads are applied respectively. They noted that the solutions of Mindlin and Deresiewicz (1953) correspond to important simple loading histories and do not constitute general solutions that could be used to predict the displacement at contact for arbitrary normal and tangential force.

In their solution to the tangential problem Mindlin and Deresiewicz (1953) confirmed that consideration of symmetry showed that normal stress, force and displacement are not altered during the application of the tangential force. Hence the Hertz theory is still valid for

the normal force-displacement relation. However they also found that the changes in tangential stress and force-displacement relations are dependent not only on the initial state or current loading, but also upon the entire past history of loading as well as simultaneous rate of change of the normal and tangential forces. They derived the basic general procedural equation of the contact tangential force-displacement response and presented closed form solutions for the following particular cases, which were later verified experimentally by a number of researchers. The last on the list is an additional case investigated later by Dobry *et al* (1991). The cases are illustrated in Figures 2.1-2.6 and are:

- Varying normal force (F_n), and tangential force with components in two directions perpendicular to the direction of F_n, $F_{t_x} = F_{t_z} = 0$ (Hertz theory, Fig. 2.1)
- Constant F_n, increasing F_{t_x}, $F_{t_z} = 0$ (Fig. 2.2)
- Oscillating oblique forces $\frac{|dF_{t_X}|}{|dF_n|} > \mu$, (μ is the friction coefficient) $F_{t_z} = 0$ (Fig. 2.3)
- Oscillating oblique forces $\frac{|dF_{t_X}|}{|dF_n|} \leq \mu$, $F_{t_z} = 0$ (Fig. 2.4)
- Both F_n and F_{t_x} increasing or decreasing, $F_{t_z} = 0$ (Fig. 2.5)
- Constant F_n, $F_t = F_{t_x} + F_{t_z}$ (Fig. 2.6)

In all the cases only one component of the tangential force is considered and the normal f-d is still valid whatever the loading history and current value of F_t. The curves show that the tangential force is dependent on the magnitude of the normal force, hence the infinite set of geometrically similar F-D curves, each corresponding to a different value of the normal force (Thornton and Randall, 1988). However the past history dependence means that when tangential force is applied or generated by friction, no matter how small, the corresponding tangential displacement is not fully reversible, resulting in energy dissipation.

This shows that the material does not exhibit pure elastic behaviour but a non-linear elasticity with some elements of plastic behaviour (residual deformation) accounting for the energy dissipation. In viscoelastic materials this is recoverable with time provided the plastic limit has not been reached

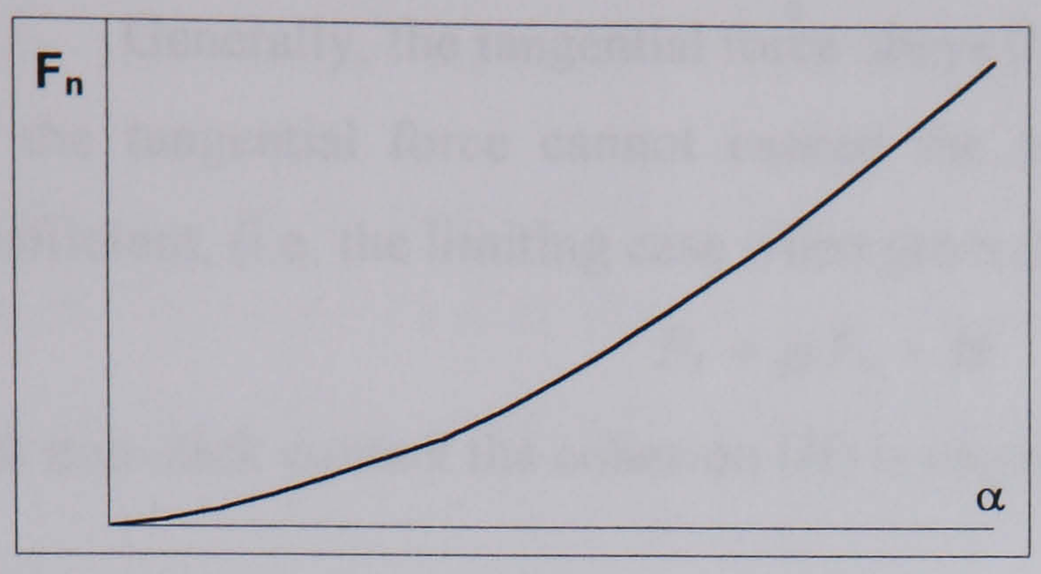

Figure 2.1 Non-linear normal F-D

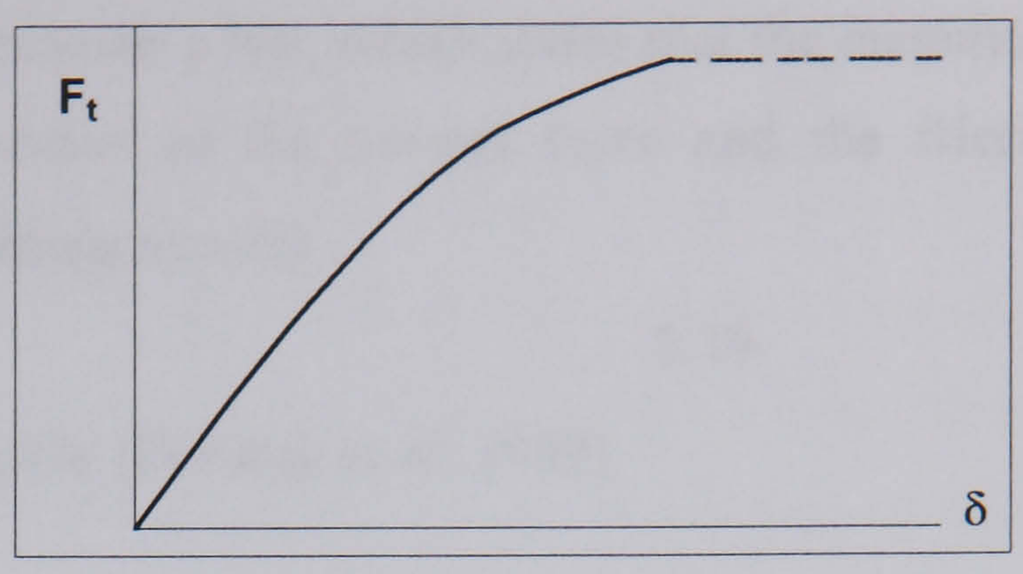

Fig. 2.2 Increasing tangential force (Const. F_N)

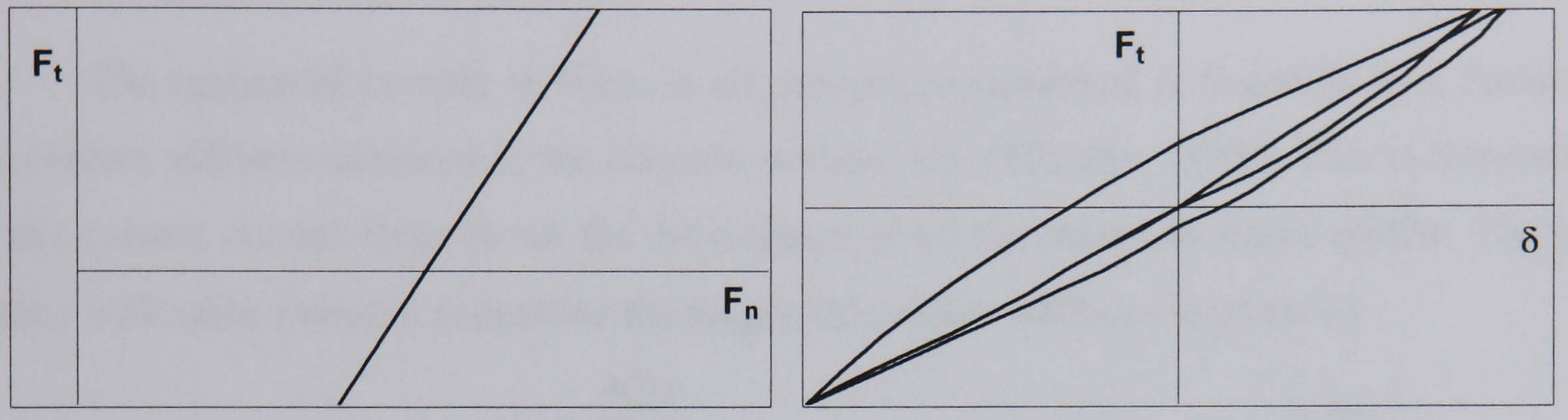

Figure 2.3 Oscillating tangential force ($\mu<dF_T/dF_N<\infty$) (a) Force path (b) F-D loop

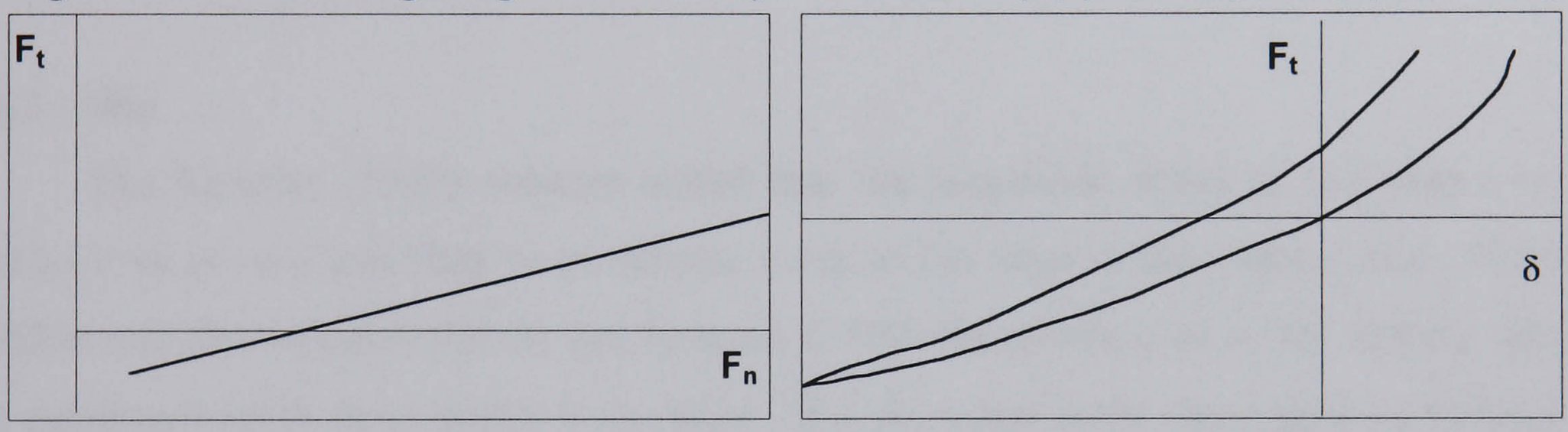

Figure 2.4 Oscillating tangential force ($0<dF_T/dF_N<\mu$) (a) Force path (b) F-D loop

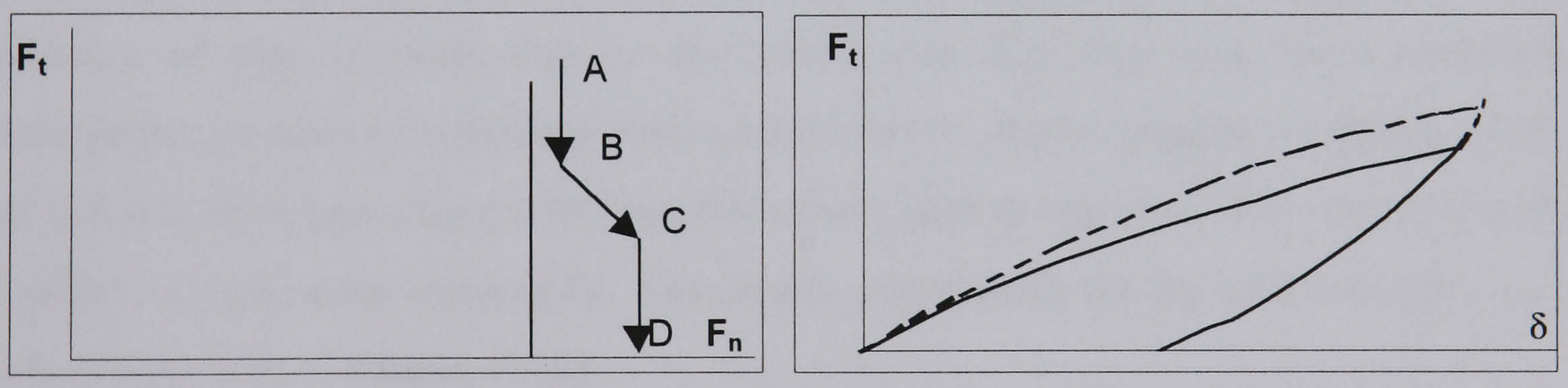

Figure 2.5 Changing normal and tangential forces (a) Force path (b) F-D loop

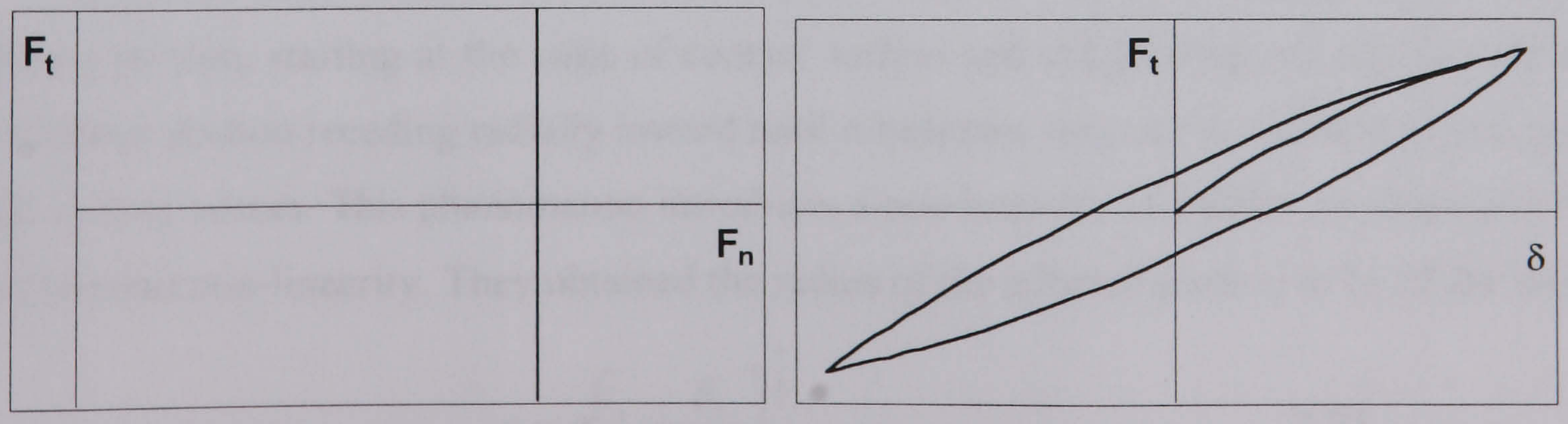

Figure 2.6 Oscillating tangential force ($dF_T/dF_N = \infty$) (a) Force path (b) F-D loop

Generally, the tangential force obeys Coulomb's law, which states that the magnitude of the tangential force cannot exceed the product of the normal force and the friction coefficient, (i.e. the limiting case when gross sliding occurs)

$$F_t = \mu F_n + H \qquad 2.19$$

For non-stick contact the cohesion (H) is negligible (Horabik *et al*, 1989).

2.3.1 Tangential Contact Stiffness

The tangential contact stiffness in all the cases considered is found to be a factor of the contact stiffness obtained in the solution without slip (Mindlin, 1949). This is dependent on the current normal force hence the dependence of all the others as stated earlier. For two bodies with same material properties the tangential contact stiffness is given by

$$C_t = \frac{4Ga}{2-\nu} \qquad 2.20$$

2.3.2 Slip

The Mindlin (1949) solution stated that the tangential stress at the centre of the contact area is zero and rises to an infinite value at the edge of the contact area. However Mindlin and Deresiewicz (1953) and Johnson (1992) found that this is not realistic though the maximum stress does occur at the edge. This deviation from the original prediction of infinite stress according to Mindlin and Deresiewicz (1953) is accounted for by the occurrence of slips or micro slips on the contact area. The slips occur as a result of the simultaneous variations in tangential and normal forces. As the tangential force exceeds the limit (μF_n) at the edges where it has the maximum value at any time, slip occurs to cushion this effect i.e. reduce the value of F_t. The process continues inwardly until it spread over the whole contact area (Johnson, 1982)

Two portions are created on the contact surface; an outer annulus of slip i.e. un-adhered portion, starting at the edge of contact surface and progressing radially inward and an adhered portion receding radially inward until it becomes zero at the centre at which point rigid sliding occurs. This phenomenon introduces a non-linearity of a different character than the Hertzian non-linearity. They obtained the radius of the adhered portion to be of the form

$$c = a\left(1 - \frac{F_t}{\mu F_n}\right)^{\frac{1}{3}} \qquad 2.21$$

This radius is also dependent on the loading history and therefore the term $F_t/\mu F_n$ changes with the type of loading. For each case two equations are obtained for the adhered and slipped regions. The tangential stress increases from the centre to the maximum just at the edge of the adhered portion or area with radius '*c*' and falls across the annulus of slip portion to zero at the edge of the normal contact radius '*a*'. The curve for the slip and no-slip is as shown in Figure 2.7.

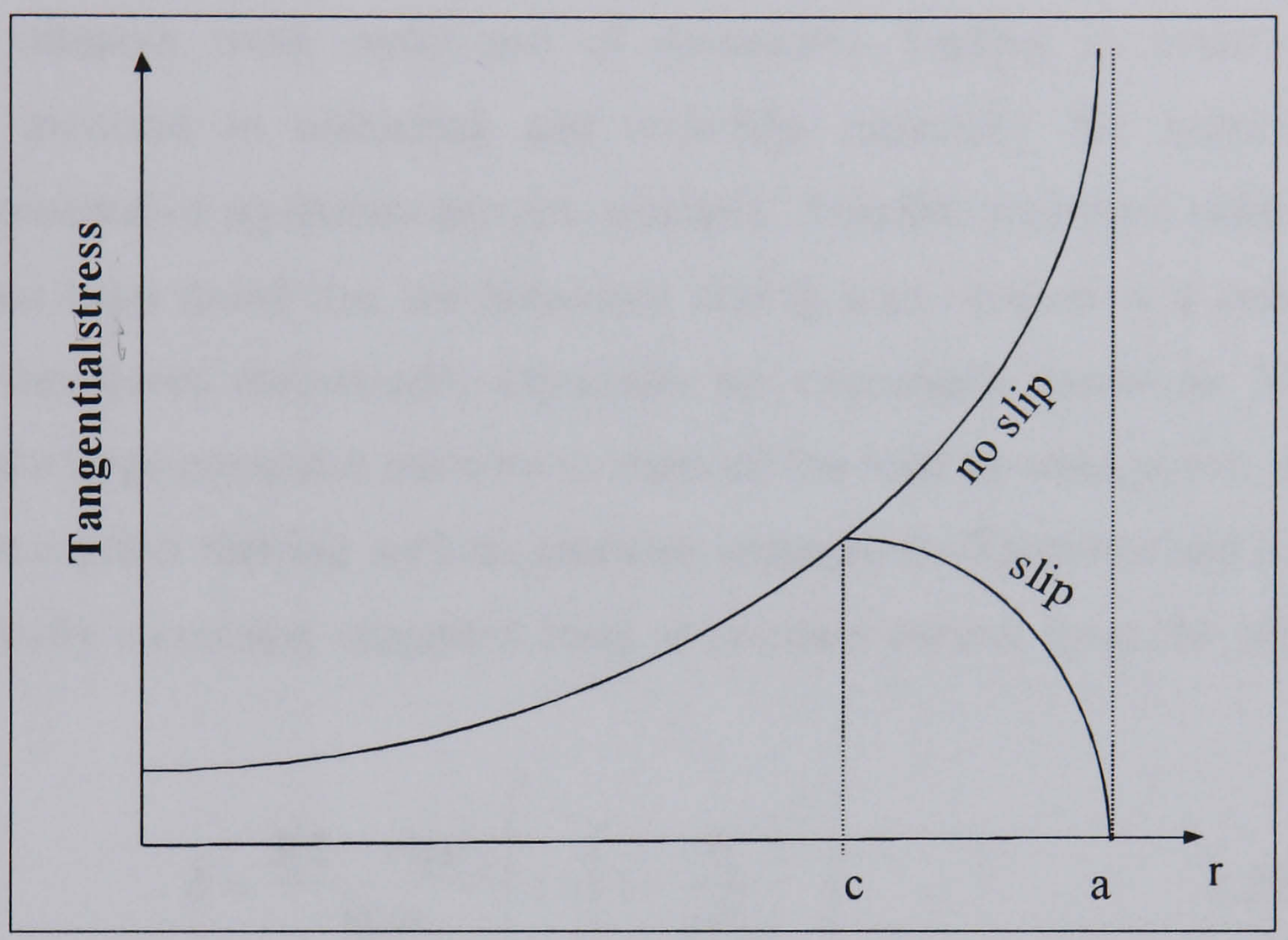

Figure 2.7 Distribution of stress across the contact surface (Mindlin, 1949)

The adhered portion shrinks until (2.19) is satisfied and at this point the displacement, with *c* becoming zero, reached its maximum resulting in gross rigid body sliding over the whole contact region. This is the difference between slip and sliding. For all the cases, the general solution obtained for the stress and displacement is of the form

$$\sigma_t = \frac{3\mu F_n}{2\pi a^3}\left(a^2 - r^2\right) \qquad c \le r \le a \qquad 2.22$$

$$\sigma_t = \frac{3\mu F_n}{2\pi a^3}\left[\left(a^2 - r^2\right)^{\frac{1}{2}} - \left(c^2 - r^2\right)^{\frac{1}{2}}\right] \qquad r \le c \qquad 2.23$$

while the Mindlin bulk relative tangential displacement is

$$\delta = \frac{3(2-\nu)\mu F_n}{8Ga}\left(1 \mp \frac{c^2}{a^2}\right) \qquad 2.24$$

or for two particles in contact, with different material properties

$$\delta = \frac{3\mu F_n}{16a}\left(\frac{(2-\nu_1)}{G_1}+\frac{(2-\nu_2)}{G_2}\right)\left(1 \mp \frac{c^2}{a^2}\right) \qquad 2.25$$

and

$$C_t = \frac{dF_t}{d\delta} = \frac{4G\,a}{2-\nu}\left(\frac{c}{a}\right) \qquad 2.26$$

This is not only dependent on the radius of the contact area but it also depends on the loading history.

Most research work make use of monotonic loading in order to avoid the complication involved in unloading and reloading especially for materials in which appropriate constitutive equations are not available. Mindlin presented solutions for these cases but it has been found that the behaviour during load reversal is a complex one that cannot easily be solved theoretically especially for viscoelastic materials. Modelling such problem require large computer memory to store all the load reversal points, most of which are not known a priori making such an exercise impractical (Thornton and Randall, 1988). For monotonically increasing tangential force at constant normal force the Mindlin solution predicts

$$\delta = \frac{3(2-\nu)\mu F_n}{8Ga}\left[1-\left(1-\frac{F_t}{\mu F_n}\right)^{\frac{2}{3}}\right] \qquad 2.27$$

$$F_t = \mu F_n\left\{1-\left[1-\frac{8Ga}{3(2-\nu)}\frac{\delta}{\mu F_n}\right]^{\frac{3}{2}}\right\} \qquad 2.28$$

and

$$C_t = \frac{dF_t}{d\delta} = \frac{4Ga}{2-\upsilon}\left(1-\frac{F_t}{\mu F_n}\right) \qquad 2.29$$

This solution illustrated in Figure 2.8 curve (B) shows that at the origin when $c = a$, (2.26) reduces to (2.20). As the tangential force approach the limiting value, c approaches zero with the displacement reaching the abscissa of point F (Figure 2.8, curve B) and after this point the displacement becomes indeterminate resulting in rigid body sliding, giving

$$\delta = \frac{3(2-\upsilon)\mu F_n}{8Ga} \qquad 2.30$$

where $F_t = \mu F_n$, $c = 0$, $C_t = 0$. In between these two points corresponds to a point on the curve represented by (2.27).

Further analysis of the loading cases by Thornton and Randall (1988) and Thornton

and Yin (1991) showed that the tangential incremental force for loading conditions of increasing tangential force, decreasing tangential force and then increasing tangential force after partly or fully decreasing (loading, unloading and reloading respectively) is

$$dF_t = \frac{8G^* a}{2-\nu}\Theta d\delta \pm \mu F_n(1-\Theta) \qquad 2.31$$

where $\frac{1}{G^*} = \frac{1}{G_1} + \frac{1}{G_2}$

and

$$\Theta^3 = 1 - (F_t + \mu F_n)\frac{1}{\mu F_n} \qquad \text{Loading} \qquad 2.32$$

$$\Theta^3 = 1 - (F_t^* - F_t + 2\mu F_n)\frac{1}{2\mu F_n} \qquad \text{Unloading} \qquad 2.33$$

$$\Theta^3 = 1 - (F_t - F_t^{**} + 2\mu F_n)\frac{1}{2\mu F_n} \qquad \text{Reloading} \qquad 2.34$$

except when $d\delta < dF_n \frac{2-\nu}{4G^* a}$ and *sign* $(d\delta)$ = *sign* (dF_n). The negative is only invoked during unloading. F^* is the peak force before unloading and F^{**} is the minimum force before reloading.

For both increasing F_n and F_t i.e. oblique loading which is the most common phenomenon in many situations, the solution predicts only one yield surface similar to the no-slip solution i.e. the surface yields when $F_t = \mu F_n$ with a constant C_t from the origin. This is the C_t obtained from the origin given by (2.20) resulting in a linear relation as shown in Figure 2.8 curve (A). The contact stiffness is therefore purely a function of the current normal force. The displacement is then

$$\Delta\delta = C_t \Delta F_t \qquad 2.35$$

This is a linear dependent law which does not predict the non-linear behaviour of the contact when $F_t < \mu F_n$.

2.3.3 Yield

Gross sliding or failure, i.e. yield occurs only when $F_t = \mu F_n$. In the Mindlin solution there are infinite number of yields in the form of slip or partial slip before this limiting condition. As stated earlier this is to correct the effect of the resulting infinite force/stress at the edge of the contact area. It results in a non-linear relation as opposed to the linear relation predicted by the no slip solution although with very little difference. The final yield occurs

when gross sliding occurs. Ng (1989) and Dobry *et al* (1991) presented a graphical representation of their investigation on this subject. They obtained series of cones representing the yield points with the inner cones representing a slip while the outer cone represents the gross sliding (final yield point). These cones were obtained in a plot of F_n, F_{tx} and F_{tz} as three perpendicular axes y, x and z respectively. The base of the cone is around the F_n axis while the apex faces the F_{tx}-F_{tz} plane starting from the origin. (Figure 2.9).

2.4 Energy Dissipation and Damping

Energy dissipation is important for particulate systems in flow, loading and impact. For small particles flowing through a fluid medium energy is lost through drag. On the other hand in impact processes energy dissipation resulting from internal friction and plastic deformation allows the assembly to reach a quasi-static equilibrium state otherwise oscillation continues indefinitely (purely elastic behaviour).

In non-elastic materials, the behaviour of the material leads to some energy dissipation in the form of plastic deformation for materials that exhibit plastic behaviour. On the other hand in the case of viscous and viscoelastic materials energy is absorbed leading to a delay in either deformation or recovery. In modelling and theoretical studies, these effects, i.e. plastic or viscous, are taken into consideration by introducing a viscous damper which is usually modelled or represented by one or more dashpots whose effect is like that of piston with a plunger.

2.4.1 Viscous Contact Damping

The interaction at the contact between two particles is commonly envisaged or modelled using the simplest rheological damping model, the Kelvin-Voigt model. This model assumes a linear spring and dashpot in parallel. The equations that governs the linear system for spring and dashpot respectively are

$$F_s = -kx$$
$$F_d = -D\frac{dx}{dT} = -D\dot{x} \qquad 2.36$$

where F_s is the spring (elastic) force, F_d is the viscous damping force, k is the spring stiffness, D the damping coefficient and x is the displacement of the particle from the initial position (the approach of the two centres for two spherical bodies in contact) while $\dot{x}$, is the first derivative of x with respect to time (the oscillation or relative velocity).

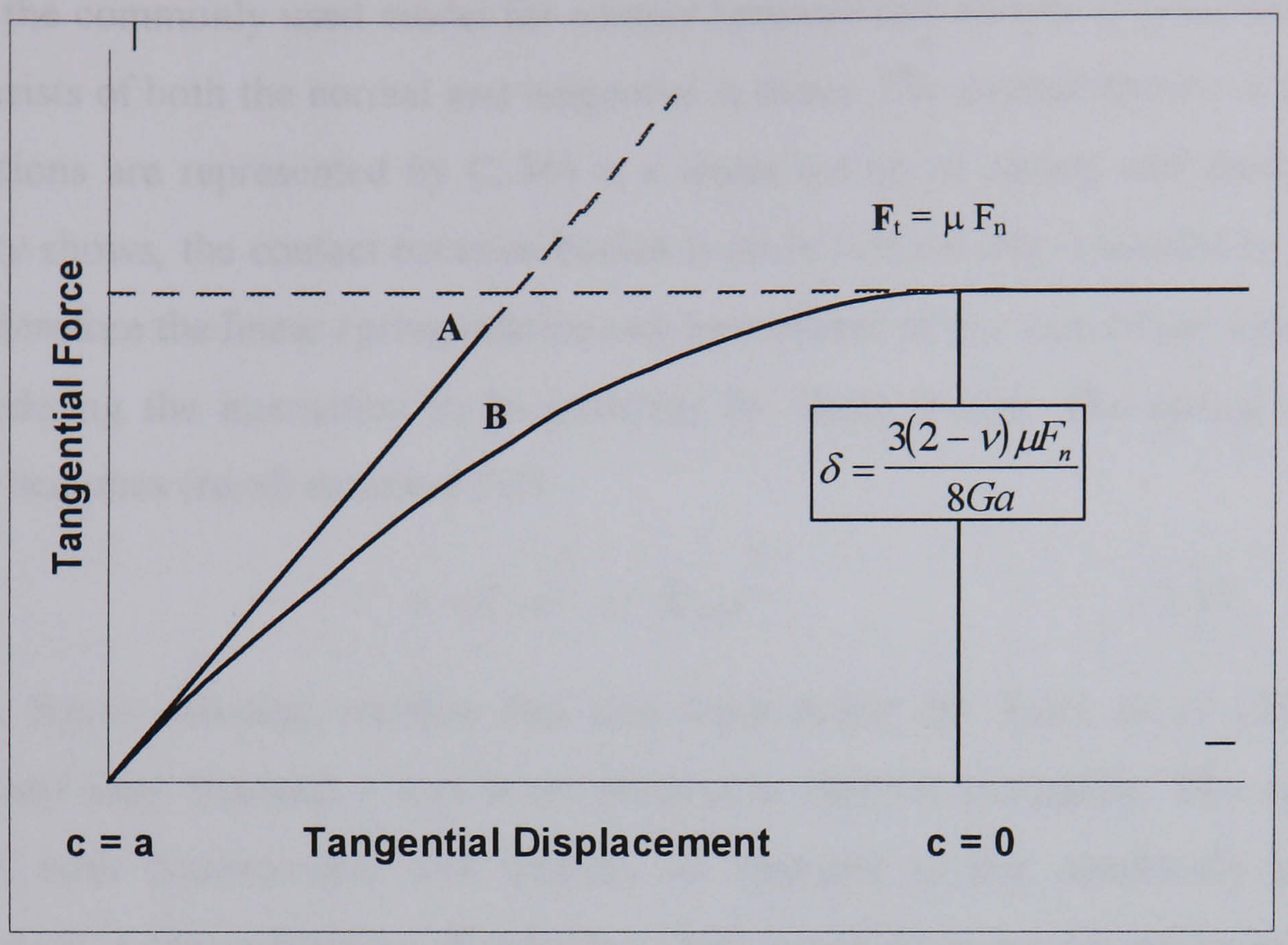

Figure 2.8 Tangential force-displacement

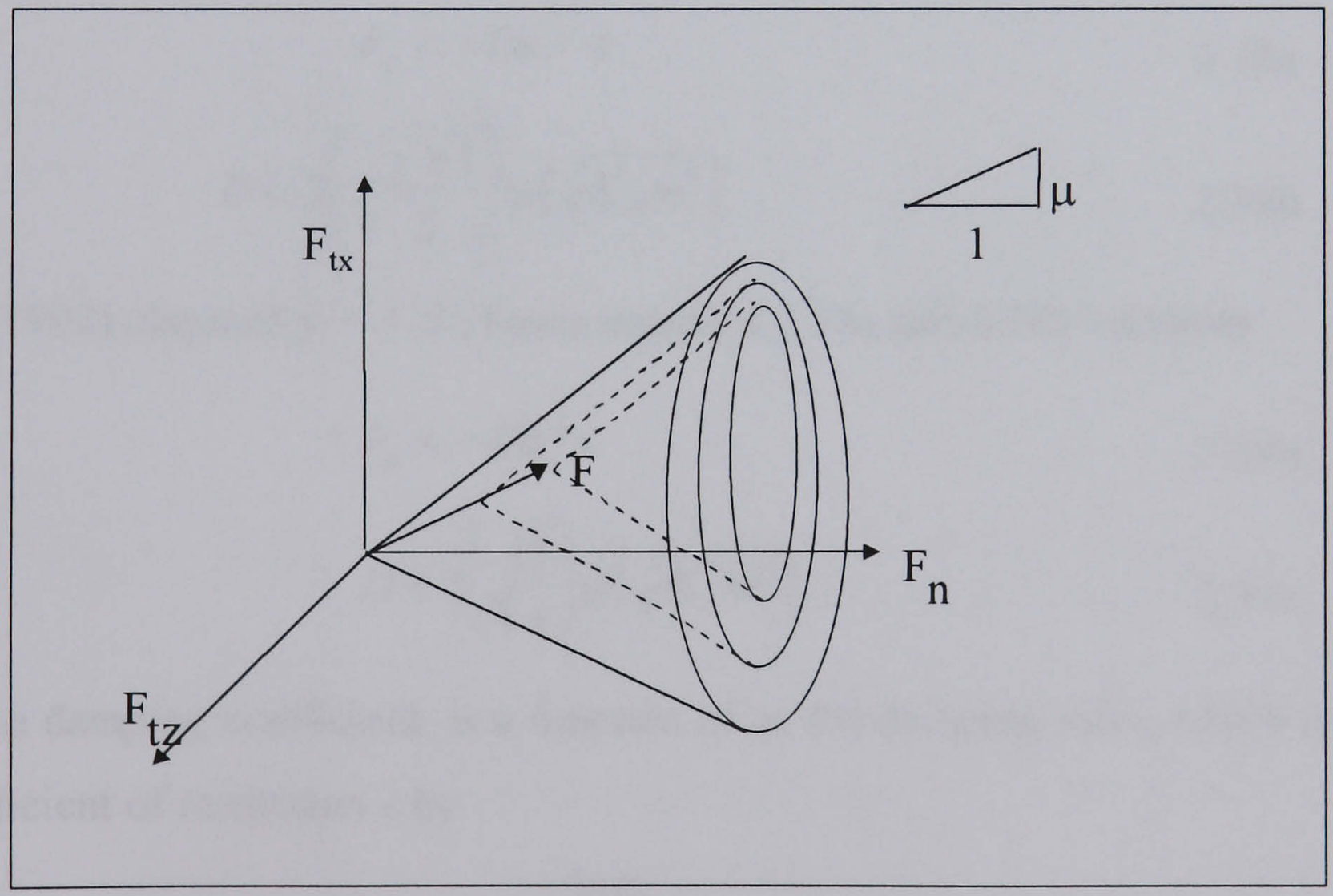

Figure 2.9 Contact force space and yield surface for elastic-plastic solution of increasing normal force and elastic force path $dF_t/dF_n < \mu$ (Dobry *et al*, 1991).

A typical spring and damper system between a body and a wall is shown in Figure 2.10 while the commonly used model for contact between two bodies is presented in Figure 2.11. It consists of both the normal and tangential systems. The system shown in Figure 2.11 whose relations are represented by (2.36) is a linear set-up of spring and dashpot, but as Hertz theory shows, the contact between bodies is more realistically modelled by non-linear systems. Therefore the linear spring relation can be replaced with a non-linear spring relation when considering the interaction to be governed by Hertz theory. The spring equation in (2.36) then becomes (recall equation 2.3)

$$F_s = -K_H x^{\frac{3}{2}} = -K_H \alpha^{\frac{3}{2}} \qquad 2.37$$

The linear damping relation has also been found by Tsuji *et al* (1992) to be unrealistic and they obtained a non-linear relation in their investigation. The relation is a function of both displacement and velocity as opposed to the commonly used linear equation, which is only a function of velocity. This type of damping according to Tsuji *et al* (1992) and from investigation by Zhang and Whitten (1996) gives a more realistic relation compared to the linear model. The general relationship is given by

$$F_d = -Dx^{\frac{y-1}{y}}\dot{x} \qquad 2.38a$$

where

$$D = 2\left(\sqrt{\frac{y+1}{2}}\right)\psi\left(\sqrt{K_H m^*}\right) \qquad 2.38b$$

Tsuji *et al* (1992) obtained $y = 3/2$, hence equation 2.38a and 2.38b becomes

$$F_d = -Dx^{\frac{1}{4}}\dot{x} \qquad 2.39a$$

$$D = 2\left(\sqrt{\frac{5}{4}}\right)\psi\left(\sqrt{K_H m^*}\right) \qquad 2.39b$$

where D, the damping coefficient, is a function of ψ, the damping ratio, which is dependent on the coefficient of restitution e by

$$\psi = -\frac{\ln e_n}{\sqrt{(\ln e_n)^2 + \pi^2}}. \qquad 2.40$$

and m^* a function of the mass of the bodies, is obtained in a similar way to R i.e.

$$\frac{1}{m^*} = \frac{1}{m_1} + \frac{1}{m_2} \qquad 2.41$$

From this general relation the normal damping coefficient can be expressed in terms of the

normal contact stiffness. Recalling equation (2.4)

$$C_s = C_n = \frac{dF_s}{d\delta} = \frac{3K_H}{2}\alpha^{\frac{1}{2}} \qquad 2.42$$

therefore

$$F_{d_n} = -2\sqrt{\frac{5}{6}}\psi\sqrt{C_n m^*}\,\dot{\alpha} \qquad 2.43$$

Similarly the tangential damping coefficient is·

$$F_{d_t} = -2\sqrt{\frac{5}{6}}\psi\sqrt{C_t m^*}\,\dot{\delta} \qquad 2.44$$

If C_n and C_t are constants then (2.43) and (2.44) represents a linear system while C_n and C_t are (2.5) and (2.20) for simple non-linear system. On the other hand if C_n and C_t are variables dependent on the deformation, (2.42), then (2.43) and (2.44) represent the damping forces in non-linear hysteretic system where residual deformation is predicted after unloading.

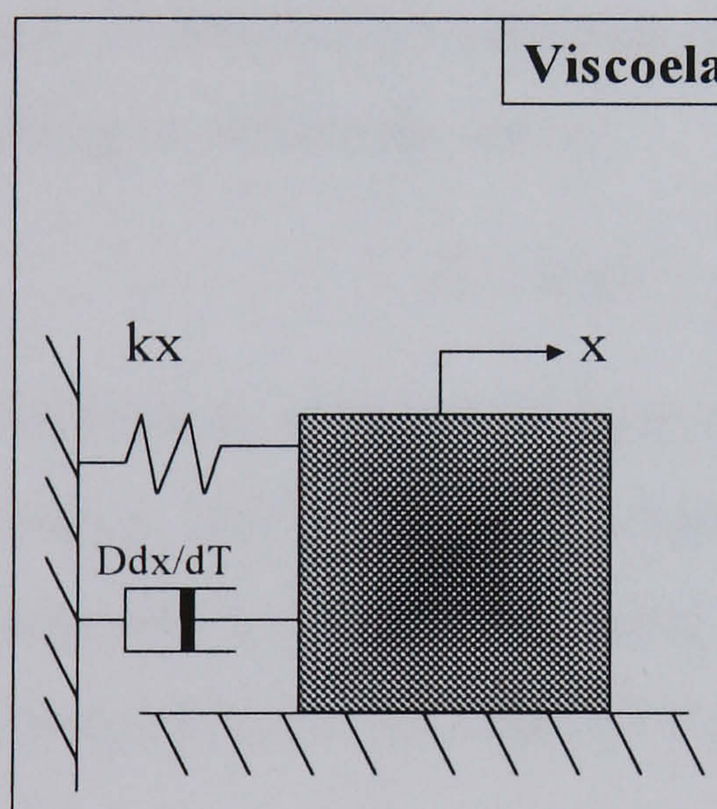

Figure 2.10 Single particle model

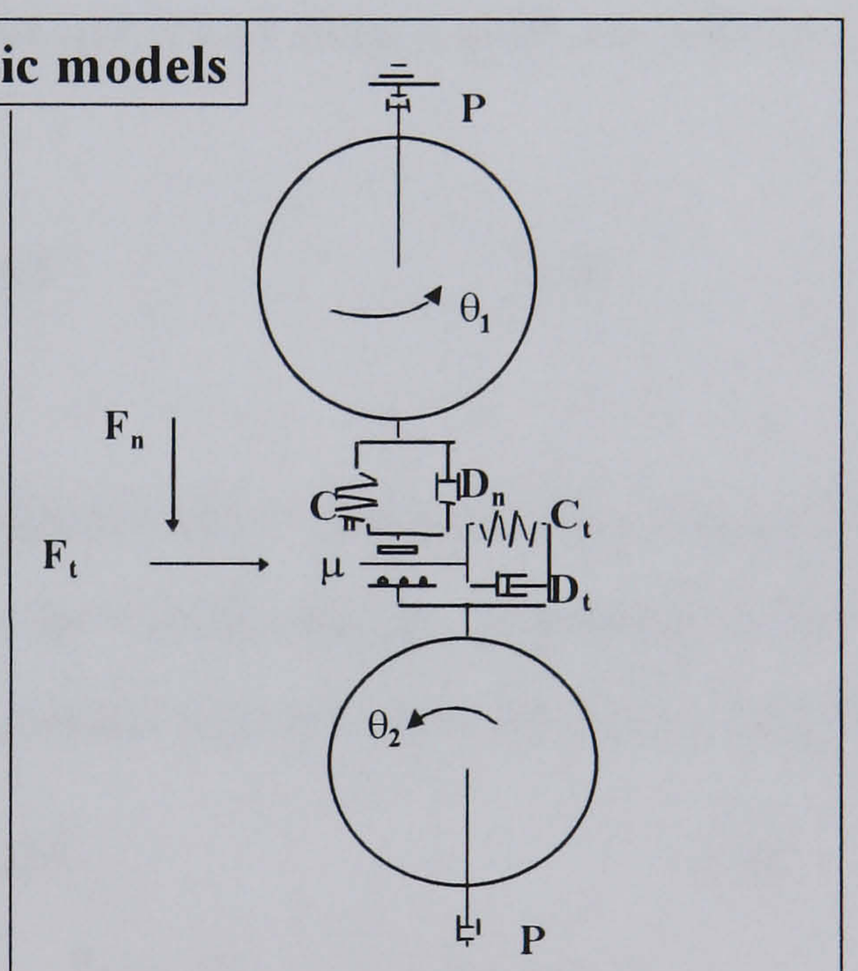

Figure 2.11 Contact model for two spherical objects

Negi *et al* (1992) reported that the normal and tangential contact stiffnesses are related to viscoelastic materials' flexural and stress moduli, the damping coefficient to the coefficient of restitution while both tangential spring stiffness and damping coefficient are proportional to the equivalent normal values. Tsuji *et al* (1992 and 1993) and Zhang and Whitten (1996) assumed equal spring stiffness for normal and tangential directions while Ning (1995) on the other hand computed the normal and tangential damping forces with each dependent on its spring stiffness.

For purely elastic materials where the system is not damped, $\psi = 0$ i.e. $e = 1$, then there is no energy dissipation while $0 < \psi < 1$ i.e. $0 > e > 1$ represents an oscillatory system that comes to rest after some time. The length of time depends on the value of ψ. On the other hand for $\psi > 1$ i.e. $e < 0$, the system of particles sticks to each other or to the target surface respectively.

The energy dissipated after contact of two bodies can be calculated using the following relationship representing the area within the resulting loop in the deformation curve for viscoelastic material.

$$E_r = \int_0^{u_m} F du - \int_{u_m}^{u_r} F du \qquad 2.45$$

where u_m is the maximum deformation and u_r is the residual deformation after break of contact.

For a body falling on a surface from a height h, the initial total energy is equal to the potential energy E_i which is proportional to the mass and drop height represented by the area under the loading or deforming curve.

$$E_i = mgh = \frac{1}{2} m V_0^2 \qquad 2.46$$

where V_o is the velocity at the start of impact.

The energy (E_f) on the object immediately after contact when the particle escapes from the surface with a velocity V_f is equal to the kinetic energy remaining in the object after contact. This is equal to the area behind the rebound contact recovery curve in a F-D plot.

$$E_f = \frac{1}{2} m V_f^2 \qquad 2.47$$

The difference between (2.46) and (2.47) gives the energy dissipated.

$$E_r = E_i + E_f \qquad 2.48$$

From (2.47) when sticking occurs, $V_i = V_c$, $V_f = 0$ and from (2.48) the critical velocity (V_c) below which sticking occurs is given by

$$V_c = \left(\frac{2}{m} E_r \right)^{\frac{1}{2}} \qquad 2.49$$

The coefficient of restitution when bouncing occurs ($V_i > V_c$) can be obtained in terms of the critical sticking velocity by combining (2.48) and 2.49)

$$e_c = [1 - \{V_c / V_o\}^2]^{1/2} \qquad 2.50$$

Incorporating the contact damping element, the resultant contact force becomes

$$F = F_s + F_d .$$

2.4.2 Global Damping

Global damping which is the damping applied equally to all particles is commonly used in DEM. It may be used to model a physical phenomenon such as drag during flow of small or lightweight material through a fluid medium or to reduce the time taken to reach equilibrium during particle generation stage in DEM. In some DEM simulations, a global damping factor is used for energy dissipation because the normal force is taken to be elastic while plasticity is considered to operate only in tangential direction as discussed earlier. Cundall and Strack (1979) used global damping to operate on the absolute velocity of the particles using a dashpot connecting each particle to the ground and this method is retained in most subsequent DE models. It is also used to bring the system to equilibrium during consolidation or deposition process

2.5 Deformation and Shape Change

The behaviour of granular materials has been taken to be purely elastic or elasto-plastic in nature and the deformation is either considered temporary (elastic) or permanent (plastic). In both cases there is a volumetric reduction of both the individual particle and the bulk system hence an assumption of material compressibility. The method involving the loss of deformed volume (overlapping particles) has been used for determination of porosity in most reported work. The phenomenon is therefore not realistic especially for incompressible material where the assumption or representation of behaviour by non-rigidity, and volume conservation are essential.

Loo (1958) considered these effects theoretically in two dimensions and obtained a relationship for both the lateral and transverse deformation/strain for circular objects. The relations obtained though partly based on Hertz theory are not applicable for most 3-D materials such as sphere but may be useful for 3D objects that can be modelled in 2D with a finite length in the third axis such as cylindrical objects. Anazodo and Chikwendu (1983) applied this principle to obtain the lateral and transverse deformation used in determining the Poisson ratio and elastic modulus of corn cob assuming the cob is a cylinder.

In a study on 3-D objects, Arzt (1982) considered a number of options for new shape formation during particle growth or expansion on the region outside the contact area of spherical powder particles during cold compaction and sintering. He stated that in

pressureless sintering process, rearrangement of the particles (growth) takes place by formation of necks around the contact region from the excess volume. On the other hand in compaction process the excess volume is distributed across the free surface of the sphere outside the contact region forming a new incomplete sphere (flat at the contact region) with a larger radius. In reality, the phenomenon of material distribution is a complex one with the geometry emanating from the contact edge expected to be higher midway between two contacts. In the powder densification study, Arzt applied the principle of conservation of volume, where the deformed part at the contact is uniformly distributed to the region outside the contact area. A Voronoi polyhedron was used to represent the volume in which each initially spherical particle is placed; the particle eventually deforming to this shape.

An equation was derived for the radius of the new sphere R'' formed when a sphere of unit radius in a Voronoi polyhedron expands to a sphere of radius R' touching and 'overlapping' the walls of the polyhedron based on this assumption. The equation for the radius of the incomplete sphere is

$$R'' = R' + \frac{4Z\left(R'+1\right)^2\left(2R'+1\right)+B\left(R'-1\right)^3\left(3R'+1\right)}{12R'\left[4R'-2Z\left(R'-1\right)-B\left(R'-1\right)^2\right]} \qquad 2.51$$

where Z is the number of contacts and B is a constant derived from the radial density function in powder densification

This equation may not be useful for many materials because of its attachment to a powder densification function. Using his theory and applying the mathematical relation for excess volume distribution for a system of spheres, a new equation for calculating the radius of the new sphere after excess volume distribution can be derived. The equation (Appendix A) giving

$$R_s^{\,3} - \frac{1}{4}\sum_{i=1}^{N}\left\{\left(R_s - d_i\right)^2\left(2R_s + d_i\right)\right\} = R^3 \qquad 2.52$$

can be solved numerically for R_s, the radius of the new sphere, where R is the initial radius before contact, d is the distance from the centre of the sphere to the point of contact and N is the number of contacts.

2.6 Application of the Contact Theory to Agricultural Materials

The numerical studies on soil and rock particles especially using the DEM has concentrated on elastic and plastic assumptions but recent findings indicated that under

repeated loading, sands and clays dissipate energy primarily by plastic process but secondary compression is clearly viscous. This shows that viscoelastic behaviour better represents their behaviour in compression than elasto-plastic as usually assumed. Recent studies such as Ning and Ghadiri (1997) on chemical agglomerates and powders incorporated contact damping for the materials considered to behave as viscoelastic and obtained good results.

Agricultural and food materials appear to behave as viscoelastic materials (possessing rheological properties associated with elastic solid and viscous fluid), when they are subjected to various conditions of stress or strain (Morrow and Mohsenin, 1968; Chen and Fridley, 1972; Mohsenin *et al*, 1978). The rheological representation is a body incorporating at least one spring (elastic character) and one dashpot (viscous character). The number of springs and dashpot in the body and the manner in which they are connected are manipulated to represent different types of material and their behaviour under stress and strain. The combination of the models vary from one material to the other and also within materials for different parts. The least combination has been widely used in most theoretical work due to its simplicity and minimal error predicted when compared to experimental results.

Generally this model either combines the elastic spring in parallel with a dashpot i.e. Kelvin-Voigt model or in series i.e. Maxwell model; a situation stated by Rao and Skinner (1986) as the minimum requirement. The various combinations emanating from different research reported by Rao and Skinner (1986) and Mohsenin (1986) include, generalised Kelvin model (a series of Kelvin bodies in series with a Maxwell model), Burgers model (Kelvin body in series with Maxwell), generalised Maxwell comprising of a finite number of Maxwell elements in parallel with each other and other combination of Maxwell or Kelvin models with one or more of a dashpot or spring (the number varies with the type of material). Various studies also confirmed that the behaviour of a material as a whole may be different for part of it e.g. the skin and the interior.

DEM has been used successfully for rigid or hard agricultural materials with emphasis laid on particle movement. There is a need to apply this method to soft materials with the availability of non-linear solution for the viscoelastic materials which suits most of these materials. However to date the best way to treat the behaviour of agricultural materials have not been found and this complex nature has always posed problems in both theoretical and numerical modelling of biomaterial behaviour.

In numerical methods the use of the simplest type of the model has been given prominence for ease of computation and the limited computer power as well as time. The

problem associated with the commonly used Kelvin-Voigt model is the computation of the time dependent deformation recovery, an area that is calling for attention in research. This probably explains why most research make use of monotonic loading to avoid load reversal. In this study this model will also be used as a starting point for the use of DEM for flexible soft biomaterials. The extension and trial of the other types of model are for future work where introduction of time dependent behaviour might be considered but there will still be limitations as to the number of particles that can be handled even with supercomputers.

2.7 Principles of the Discrete Element Method

The Discrete Element Method is a numerical method for modelling the mechanical behaviour of granular materials. In DEM bulk systems are treated as an assemblage of distinct particles with each particle interacting with its neighbours through particle to particle contact governed by physical laws. The new position, deformation and forces acting on each particle is identified at every short time interval. This is repeated over several time steps or calculation iterations referred to as calculation cycles until a stable system is obtained with balanced forces. Therefore, DEM basically makes direct determination of the contact behaviour possible, considering the external and internal forces on the particles and viewing their interaction as a transient problem until a state of equilibrium is developed when the internal forces balance.

The important components of any DEM are the representation of the workspace or system to be modelled, particle types, shape and the formulation for interaction between the particles resulting from the existence of contacts at the point of discontinuity.

2.7.1 Material Generation and Classification

In DEM, generation of an assembly of particles is usually the very first task to be accomplished. The particle generation method is dependent on the type of system to be modelled and the particles constituting the system. The shape, size distribution and the typical particle arrangement as well as the need for boundaries such as walls are necessary components that determine the generation algorithm. The process of generation involves specifying the centre co-ordinates and the radius. The generation process in modelling is either by random generation employing random-number-generators or a regular sequence of particles placed on top of each other in rows and columns or offset diagonally in both 2&3D.

2.7.1.1 Particle Properties

Generally most of the studies on the DEM used regular particle shapes with circles and spheres being the most widely used due to their computational efficiency. In reality most particles are irregular in shape and modelling by assuming the closest regular shapes has produced some reasonable predictions that have made understanding of the particulates behaviour clearer.

A number of investigators have therefore worked on generation of irregular particles but the problem associated with this has limited most of the reports to the generation method without any considerable results on the trials. Some of the generation methods proposed were reviewed by Hogue (1998) and are briefly presented in 1.2.2.1.2

DEM can generally be used to model all types of distinct or granular particles, which are discontinuous in nature. The differences in these particles may be in their properties such as strength, shape, and size. The materials, except when bonded together or in free flow operations, are usually in an enclosure surrounded by either rigid or flexible walls through which the external force can be transmitted. There are three important steps before developing algorithms for analysis and programming in DEM. These are representation of contact, solid materials and detection and revival of contact.

2.7.1.2 Representation of Contact

An important component of any DEM in discontinuous systems is the method for representing interaction between the particles resulting from the existence of contacts at the point of discontinuity. Contacts are classified as either SOFT or HARD with the type determined by the strength properties of the material in use.

In a system where particles make soft contact they deform at contact points as a result of friction and stress. In DEM modelling, the deformation is represented as inter-penetration of the two contacting particles at the contact point, although physically, surface deformation occurs rather than inter-penetration. The physical assumption in the case of hard contact is that no inter-penetration occurs between the two bodies, only shear movement (sliding), rolling and loss of contact can occur. The sliding and rubbing at the contact point which occur due to the small stress and no friction result in high-speed interaction by collision involving energy loss. Momentum balance is used in the calculation of the normal force at contact point. Hard contact is not applicable to most biomaterials except in handling of dry grains and seeds. The type of contact is based on physics rather than on numerical convenience. Therefore, in this study, soft contact will be assumed considering the physics

of biomaterials.

2.7.1.3 Representation of Solid Materials

The classification criteria in this case are similar to those on contact representation. Particles are classified as rigid or deformable with most of the rigid particles exhibiting hard contact while deformable exhibit soft contact. Generally, these particles are either generated using the computer random-number-generation method or a regular arrangement specified.

2.7.2 Main Features of Discrete Element Analysis

The distribution of external loads between interparticle contacts in a granular assembly is achieved in DEM by repeated application of Newton's law of motion to monitor the motion of the discrete particles and by using appropriate force-displacement laws to compute the interaction contact by contact using an explicit numerical scheme. Each cycle is carried out over a time step, the length of which is chosen so that during a single time step disturbance cannot propagate from any particle further than its immediate neighbours.

2.7.2.1 Calculation Cycles and Simulation Steps

The main features of Discrete Element Method and a typical calculation cycle shown in Figures 2.12 and 2.13 involve the following steps:

(1) Compute the relative velocities over the time step (dT) at interparticle contact from the known initial velocity (V) for two particles a and b

$$dV_r = V_a - V_b \qquad 2.53$$

(2) Integrate to obtain relative displacement (du_r)

$$du_r = (V_a - V_b)\, dT \qquad 2.54$$

(3) Employ a suitable force-displacement law, to determine the current interparticle contact force (F).

$$F = k\, du \qquad 2.55$$

where k is the stiffness coefficient.

(4) Apply Newton's second law of motion to each particle and compute their acceleration (ü)

$$\ddot{u} = \frac{F}{m} \qquad 2.56$$

where m is the mass.

(5) Integrate the acceleration to obtain the new velocity

$$\dot{u} = \int \left(\frac{F}{m}\right) dT \qquad 2.57$$

(6) Update the locations of the particles, locate new and delete broken contacts.

$$u = \int \left[\left(\frac{F}{m}\right) dT\right] dT \qquad 2.58$$

These series of calculations which alternate between the force-displacement and Newton's law of motion are repeated until equilibrium contact forces and displacement are obtained.

In the general case of an assembly of many particles, these steps are applied at each contact and the vectorial sum of the parameters including displacement, forces and stresses, for the system as well as those at contact are determined. The detailed calculation procedures are presented in the following passages for three-dimensional co-ordinates.

2.7.2.2 Particle Position and Movement

Particle position is specified as the co-ordinates of the centre of gravity with respect to the reference point. For a system with n particles, the positions are $u_1, u_2, \ldots, u_n$ i.e.

$$u_i = (x_i, y_i, z_i) \quad i = 1, n \qquad 2.59$$

Considering two particles with centres at distance L as shown in Figure 2.14. The angles of inclination of the centre line to the 3D-axes are α, β and ϕ for the x, y, and z axes respectively. The unit vector joining the two centres is $\mathbf{e_i}$

$$e_i = \cos\alpha\hat{i} + \cos\beta\hat{j} + \cos\phi\hat{k} \qquad 2.60$$

$$L = \sqrt{(x_1 - x_2)^2 + (y_1 - y_2)^2 + (z_1 - z_2)^2} \qquad 2.61$$

and a unit vector $\boldsymbol{t_i}$ obtained by a vertical clockwise rotation of $\boldsymbol{e_i}$ through 90° is

$$\mathbf{t_i} = \cos\alpha\hat{i} - \cos\beta\hat{j} + \cos\phi\hat{k} \qquad 2.62$$

The velocity is $V_i = (\dot{x}_i, \dot{y}_i, \dot{z}_i) = \dot{u}_i \quad \text{i} = 1,\text{n} \qquad 2.63$

The angular velocities $\theta_1, \theta_2, \ldots, \theta_n$ are considered positive in the clockwise direction.

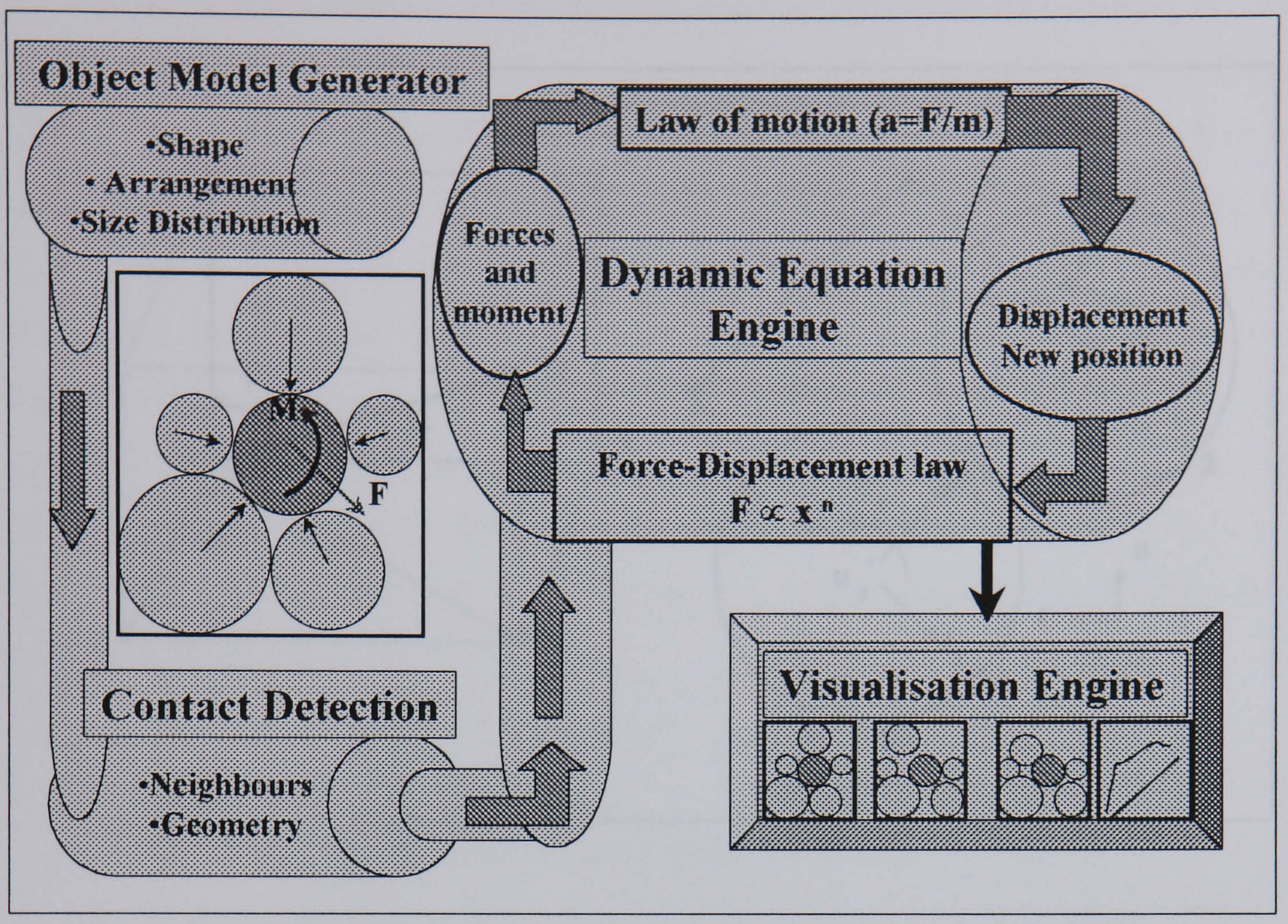

Figure 2.12 DEM analysis pipeline

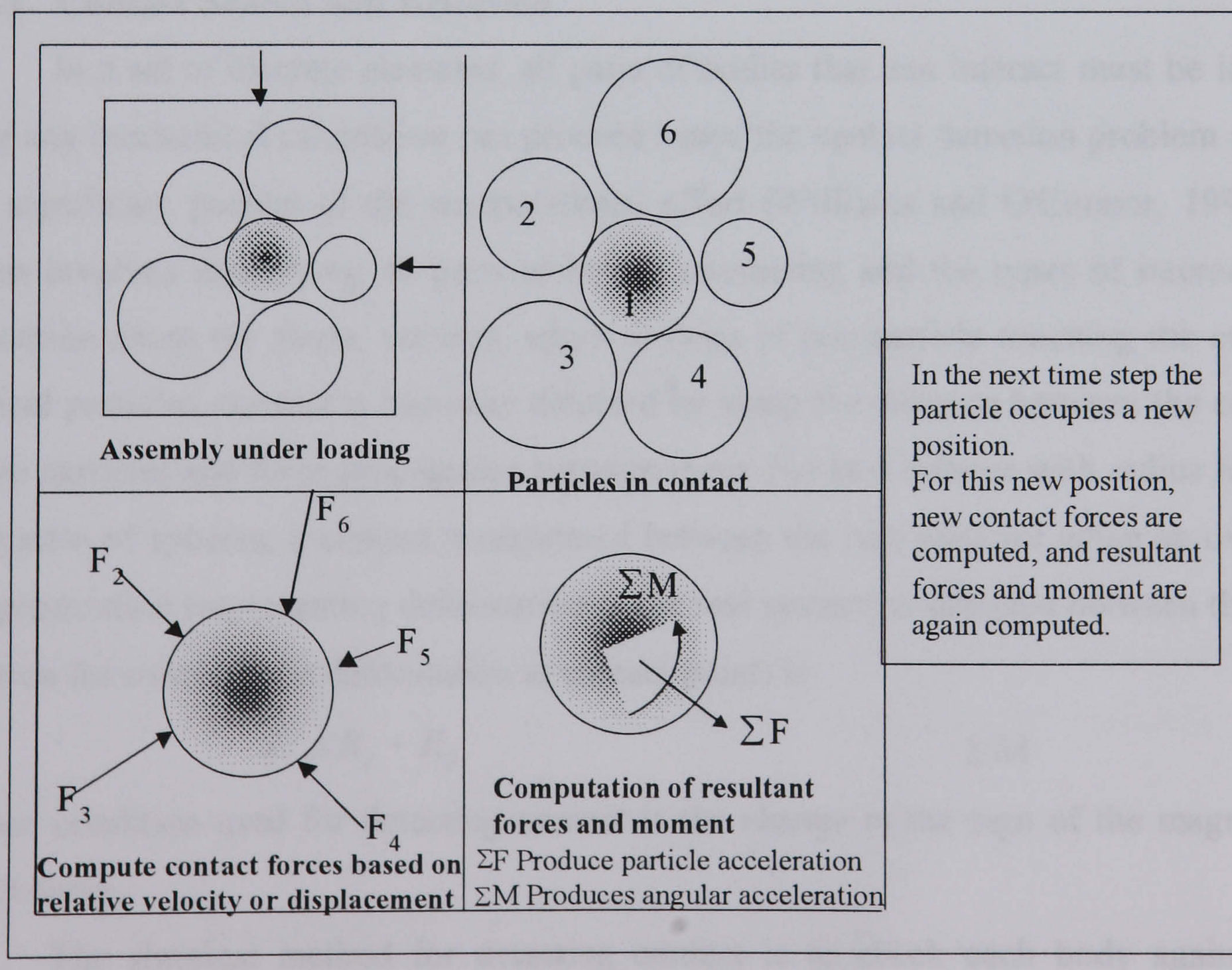

Figure. 2.13 Main features of DEM

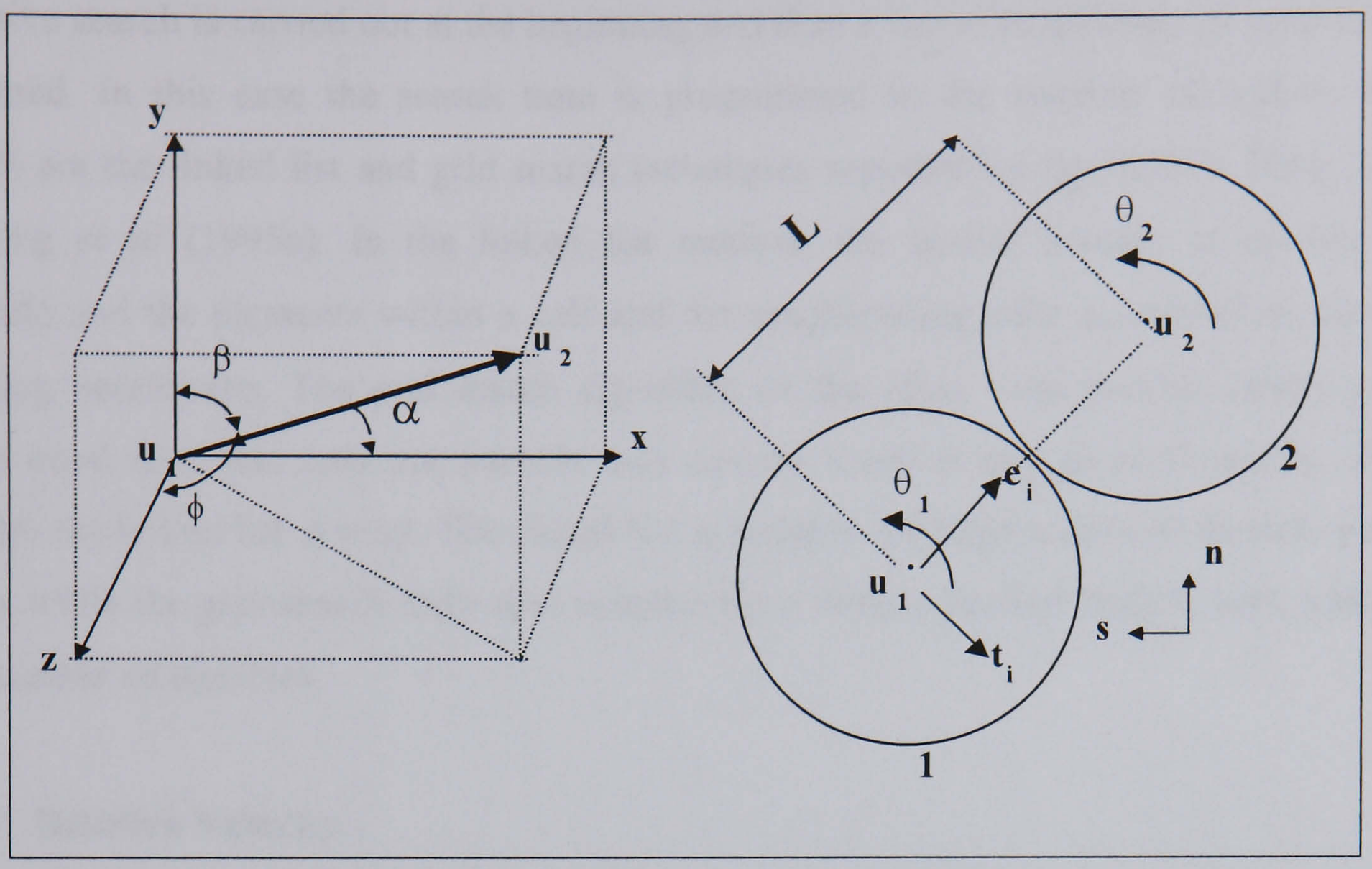

Figure. 2.14 Pair of spherical particles in contact

2.7.2.3 Contact Search and Detection

In a set of discrete elements, all pairs of bodies that can interact must be identified before any mechanical calculation can proceed hence the contact detection problem accounts for a significant portion of the computational effort (Williams and O'Connor, 1995). This process involves identifying all pairs of bodies interacting and the types of interaction i.e. information about the shape, vertices, edges or faces of one particle touching the other. For spherical particles, contact is basically detected by using the distance between the centres of the two particles and force propagation between them. For two spheres with radius R_1 and R_2 in a system of spheres, a contact is registered between the two particles when an overlap or inter-penetration (representing deformation in the real system) is detected between them. The condition for overlap (the deformation at contact point) is

$$L \leq R_1 + R_2 \qquad 2.64$$

Another condition used for detecting contact is the change in the sign of the magnitude of contact force.

The simplest method for detecting contact is to check each body against every other. This method requires a large computation time proportional to n^2 for n elements. The

second method is the automatic-neighbourhood-updating first used by Hocking (1989). An exhaustive search is carried out at the beginning and then a list of neighbours of each body is maintained. In this case the search time is proportional to the number of bodies. Other methods are the linked list and grid search techniques reported by Ng (1989), Ning (1995) and Rong *et al* (1995a). In the linked list method, the spatial domain is divided into grids/cells and the elements within a cell and the neighbouring cells are noted as potential contacting neighbours. The grid search algorithm on the other hand involve creating cells that are sized such that only one particle may occupy a cell at any given time (Ng, 1989), thereafter the linked list is used. The linked list is suitable for large scale and densely packed systems while the grid search technique is better for a loosely packed system with relatively small number of particles.

2.7.2.4 Relative Velocity

The relative velocity of the contacting bodies is given by

$$\Delta V_r = V_1 - V_2 = \dot{u}_1 - \dot{u}_2 \qquad 2.65$$

If a rotation factor is introduced, then

$$\Delta V_r = (V_1 - V_2) - \left(\theta_{(1)} R_{(1)} + \theta_{(2)} R_{(2)}\right) t_i \qquad 2.66$$

This relative velocity when resolved onto the global axis, yields the normal ($\dot{n}$) and tangential ($\dot{s}$) components, i.e. the projections of ΔV_r onto $\mathbf{e}_i$ and $\boldsymbol{t}_i$ respectively

$$\dot{n} = \Delta V_r \, \mathbf{e}_i = \Delta V_n = (V_1 - V_2)\mathbf{e}_i - \left(\theta_{(1)} R_{(1)} + \theta_{(2)} R_{(2)}\right) t_i \mathbf{e}_i$$

$$\Delta V_n = (V_1 - V_2)\mathbf{e}_i \qquad 2.67$$

$$\dot{s} = \Delta V_r t_i = \Delta V_s = \left(V_1 - V_2\right) t_i - \left(\theta_{(1)} R_{(1)} + \theta_{(2)} R_{(2)}\right) t_i t_i$$

$$= (V_1 - V_2) t_i - \left(\theta_{(1)} R_{(1)} + \theta_{(2)} R_{(2)}\right)$$

$$\Delta V_s = (V_1 - V_2) - (n e_i) - \left(\theta_{(1)} R_{(1)} + \theta_{(2)} R_{(2)}\right) \qquad 2.68$$

Note: The indices in parenthesis are not summed while Einstein summation convention is adopted for the parameters with indices (i.e. vectorial sum of the co-ordinates for each parameter).

2.7.2.5 Relative Displacement

The incremental relative displacements are obtained by integrating the velocities with respect to the time step.

$$\Delta \mathrm{n} = \dot{n}\ \Delta T = \{ (V_1 - V_2)\mathbf{e}_i \}\ \Delta T \qquad 2.69$$

$$\Delta \mathrm{s} = \dot{s}\ \Delta T = \left[(V_1 - V_2)t_i - \left(\theta_{(1)} R_{(1)} + \theta_{(2)} R_{(2)} \right) \right] \Delta T \qquad 2.70$$

2.7.2.6 Normal and Tangential Contact Forces

The incremental normal and tangential or shear contact forces are obtained by applying an appropriate force-displacement law such as those discussed above. Recalling from (2.4) that the F-D relation

$\Delta F = C_{st}(\Delta d)$ for linear elastic materials

$\Delta F = C_{st}(\Delta d) + D(\Delta v)$ for linear viscoelastic materials

hence $\Delta F_n = \mathrm{C_n}(\Delta\alpha)$ 2.71

$\Delta F_t = C_t(\Delta\delta)$ 2.72

where C_{st} is the contact stiffness, D, the dashpot factor or coefficient of damping, (Δd) the incremental displacement and α and δ represents normal and tangential displacement respectively. The normal incremental force for the linear case is therefore

$$\Delta F_n = C_n \{ (V_1 - V_2)\mathbf{e}_i \}\ \Delta T \qquad 2.73$$

and the tangential is

$$\Delta F_t = C_t \left[(V_1 - V_2)t_i - \left(\theta_{(1)} R_{(1)} - \theta_{(2)} R_{(2)} \right) \right] \Delta T \qquad 2.74$$

In most non-linear DEM modelling the Hertz and Mindlin F-D law for normal and tangential relations respectively are used. This involves the use of material properties such as elastic modulus, Poisson ratio and geometry of the materials to determine the "contact stiffnesses" dynamically i.e. equations (2.5 and 2.20) unlike in the linear case above where a predetermined contact stiffness is specified for each material as a constant. The normal and tangential forces determined (2.9 and 2.28) are added vectorially to obtain the resultant force and then resolved onto the global axis.

Having determined the incremental force over the time step (ΔT), the normal and tangential contact forces at each contact at any time (T) are then updated for two particles (1) and (2) in contact using the relation

$$F_T = F_{T-\Delta T} + \Delta F$$

$$i.e\ F_{(1)T} = F_{(1)T-\Delta T} + \Delta F, and, F_{(2)T} = F_{(2)T-\Delta T} + \Delta F \qquad 2.75$$

Ting *et al* (1993) noted that summing incremental normal contact forces at each time step could lead to significant accumulated error. Instead they recommend computing

the total normal overlap (displacement) at each instant, then using this to obtain the total contact force while the tangential forces are still obtained using incremental forces.

The resultant normal and tangential components for each particle can then be obtained from the vectorial sum of the components in the 3-D axes

$$F_n = \sqrt{\sum_{i=1}^{3} F_{n_i}{}^2} = \sqrt{F_{n_x}{}^2 + F_{n_y}{}^2 + F_{n_z}{}^2} \qquad 2.76$$

$$F_t = \sqrt{\sum_{i=1}^{3} F_{t_i}{}^2} = \sqrt{F_{t_x}{}^2 + F_{t_y}{}^2 + F_{t_z}{}^2} \qquad 2.77$$

The vectorial sum of (2.76) and (2.77) gives the resultant total force on the particle

$$F_{(1)res} = \sqrt{F_n{}^2 + F_t{}^2}$$

$$= \sum_{i=1}^{3} F_{(1)_i} = \sqrt{F_{(1)_x} + F_{(1)_y} + F_{(1)_z}} \qquad 2.78$$

where $F_{(1)_x}, F_{(1)_y}, F_{(1)_z}$ are the components of the total force resolved into the global axes. The resultant force on each particle is the sum of all the forces at each contact. For a particle (1) making contact with (k-1) particles, then

$$F_{(1)_x} = \sum_{i=2}^{k} F_{(1)i_x} \qquad 2.79$$

where $F_{(1)_x}$ is the resultant force on particle (1) wrt the x axis and $F_{(1)i_x}$ is the contact force between particle (1) and particle (i) with respect to the x axis. This force can then be used to obtain the new particle position.

2.7.2.7 Moment

The moment acting on each particle is calculated as the product of the tangential force and the perpendicular distance (R_c) from its line of action to the centroid of the particle

$$M_{(1)res} = F_t R_c$$

$$= \sum M_{(1)} = \sum_{i=2}^{k} R_{c(1)i} F_{t\,(1)i} \qquad 2.80$$

2.7.2.8 Friction and Sliding

Particle sliding occurs whenever the friction force is overcome and the Coulomb friction law is satisfied

$$F_t = F_n Tan\varphi_n \qquad 2.81$$

Friction damping occurs during sliding whenever the absolute value of the shear

force at any contact is equal to the maximum possible shear force ($F_{t_{max}}$) hence

$$\left|(F_t)_{\max}\right|_t = \left|(F_n)\right| Tan\varphi_n = \mu\left|(F_n)\right| \qquad 2.82$$

where φ_n is the smaller of the interparticle friction angles of the two particles in contact and μ is the friction coefficient.

2.7.3 Determination of Critical Time Step

In a granular system the majority of the energy transmission between individual particle is carried by Rayleigh waves which travel along the surface of the solid. For a single particle there is a time during which force is transmitted from one contact point to another along the particle surface. In DEM an explicit time step is applied as it permits direct step-by-step evaluation, hence the choice of the actual time step is crucial to ensure numerical stability. It should be as large as possible for simulation efficiency and yet small enough such that it is less than the time it takes for the wave energy to transverse the minimum sized particle in the assembly.

Two equations have been used for computing the critical time step in DEM. Both are based upon the frequency determined from a single degree of freedom in the system of particle(s) with the mass element connected to the ground. The first, uses the frequency of propagation of Rayleigh surface waves on one of the elastic bodies on application of force (Ning, 1995, Ning and Ghadiri, 1997)

$$V_R = \Phi\sqrt{\frac{G}{\rho}} \qquad 2.83$$

where ρ is the density and Φ is a parameter dependent on the Poisson ratio (ν) and can be approximately given as

$$\Phi = 0.1631\nu + 08766 \qquad 2.84$$

The critical time step is therefore

$$\Delta T_c = \frac{\pi R_{\min}}{V_R} = \frac{\pi R_{\min}}{\Phi}\sqrt{\frac{\rho}{G_{\max}}} \qquad 2.85$$

where $R_{\min}$ is the radius of the smallest particle and $G_{\max}$ is the maximum rigidity modulus in the assembly. The minimum and maximum values of the parameters are chosen such that the least value from those determined from different materials within a system is used. Taylor and Preece (1992) recommended that the critical time step should be determined by the highest eigenvalue of the system and that any value higher than this renders the calculation

unstable.

The other method is the Cundall and Strack (1979) criterion using the natural frequency ($\omega = \sqrt{m/C_x}$) in a linear spring system giving

$$\Delta T_c = \frac{2\pi}{\omega} = 2\pi\sqrt{\frac{m_{\min}}{C_{\max}}} \qquad 2.86$$

where $m_{\min}$ is the mass of the lightest particle and $C_{\max}$ is the largest contact stiffness. This is suitable for systems where contact stiffness is known or chosen for the study. Ning and Ghadiri (1997) showed that the difference in the values calculated using (2.85 and 2.86) are negligible. When damping was introduced for viscoelastic materials the constant in (2.86) was found to be proportional to the damping ratio (2.40) (Negi *et al*, 1992; Tsuji *et al*, 1992) giving

$$\Delta T = \frac{\pi}{\sqrt{\frac{C_{\max}}{m_{\min}}\left(1 - \frac{\ln^2 e}{\pi^2 + \ln^2 e}\right)}} \qquad 2.87$$

The time step calculated with (2.87) in most cases is not short enough to guarantee numerical stability. This is because relative particle movement is not considered in the derivation of the natural frequency and the Rayleigh wave frequency. Therefore a fraction of the theoretical critical time step { $\Delta T_{actual} = (frac)\Delta T_c$ } was used in almost all reported work. During simulation, if numerical instability occurs the time step is reduced further by *frac*. A specified time step can also be chosen arbitrarily (Sakaguchi *et al,* 1994, Hryciw *et al,* 1997)

2.7.4 Motion: Acceleration

In order to update the position of the particle, the acceleration of the particle has to be obtained. Having obtained the resultant forces, the translation and rotational accelerations of each particle are calculated by applying the Newton's Second Law of Motion.

$$m_{(1)}(\ddot{u}_{(1)})_i = \sum F_{(1)_i} \quad \text{i} = 1, 2, 3 \qquad 2.88$$

and

$$I_{(1)}\ddot{\theta}_{(1)} = \sum M_{(1)} \qquad 2.89$$

where I is the moment of inertia.

The new particle velocity after the time step ΔT can be obtained from

$$\Delta \dot{u} = \int \ddot{u} \Delta T \qquad 2.90$$

Wronski and Jean (1995) stated that a simple and effective solution to integrate

dynamic equations with contact is to employ a first order finite difference approximation, FDA, (see appendix B). This does not introduce any regularity constraints on the kinematics variables and avoid errors.

In DEM it is assumed that the acceleration and velocity are constant over each time step. By incorporating the leapfrog integration scheme proposed by Cundall and Strack (1979), the velocity of the particle can be obtained at the next HALF TIME step $T+\frac{1}{2}\Delta T$ with the assumption that the force and moment are acting on the particle at time T within the time step. This is called the time-centred system. Therefore

$$(\dot{u}_{(1)})_{i_{T+\frac{1}{2}\Delta T}} = (\dot{u}_{(1)})_{i_{T-\frac{1}{2}\Delta T}} + \left[\frac{\sum F_{(1)_i}}{m_{(1)}}\right]_T \Delta T \qquad 2.91$$

$$(\dot{\theta}_{(1)})_{i_{T+\frac{1}{2}\Delta T}} = (\dot{\theta}_{(1)})_{i_{T-\frac{1}{2}\Delta T}} + \left[\frac{\sum M_{(1)}}{I_{(1)}}\right]_T \Delta T \qquad 2.92$$

The gravitational force must be added to the resultant force to obtain the actual resultant force where necessary.

$$F_{(1)res} = \sum_{i=1}^{3} F_{(1)_i} = \sqrt{F_{(1)_x} + F_{(1)_y} + F_{(1)_z}} + m_{(1)} g_i \qquad 2.93$$

2.7.5 Updating Location

Integrating equation (2.91) and (2.92) using the FDA gives

$$(u_{(1)})_{i_{T+\Delta T}} = (u_{(1)})_{i_T} + \left[\dot{u}_{(1)}\right]_{T+\frac{1}{2}\Delta T} \Delta T \qquad 2.94$$

$$(\theta_{(1)})_{i_{T+\Delta T}} = (\theta_{(1)})_{i_T} + \left[\dot{\theta}\right]_{T+\frac{1}{2}\Delta T} \Delta T \qquad 2.95$$

Introducing the contact damping factor and taking the global damping force into account in the equations of motion (2.88) and (2.89), then

$$m_{(1)} (\ddot{u}_{(1)})_i = \sum\left(F_{(1)_i} + F_{d(1)_i}\right) - P\dot{u}_i \qquad 2.96$$

$$I_{(1)} \ddot{\theta}_{(1)} = \sum\left(M_{(1)}\right) - \bar{P}\dot{\theta}_{(1)} \qquad 2.97$$

where P and $\bar{P}$ are the coefficients of global damping and are proportional to the mass and moment of inertial of the particles,

$$P = fm_{(1)} \quad and \quad \bar{P} = fI_{(1)} \qquad 2.98$$

where f is the proportionality constant.

Using FDA the velocity equations (2.91 and 2.92) can be updated using (2.96), (2.97) and (2.98).

$$(\dot{u}_{(1)})_{i_{T+\frac{1}{2}\Delta T}} = \left\{(\dot{u}_{(1)})_{i_{T-\frac{1}{2}\Delta T}}\left[1 - f\frac{\Delta T}{2}\right] + \left[\frac{\sum F_{(1)_i} + D_{(1)_i}}{m_{(1)}}\right]_T \Delta T\right\} \Big/ \left[1 + f\frac{\Delta T}{2}\right] \qquad 2.99$$

$$(\dot{\theta}_{(1)})_{i_{T+\frac{1}{2}\Delta T}} = \left\{(\dot{\theta}_{(1)})_{i_{T-\frac{1}{2}\Delta T}}\left[1 - f\frac{\Delta T}{2}\right] + \left[\frac{\sum M_{(1)}}{I_{(1)}}\right]_T \Delta T\right\} \Big/ \left[1 + f\frac{\Delta T}{2}\right] \qquad 2.100$$

Equations (2.99) and (2.100) now replace (2.91) and (2.92) as the expression for the velocity having considered all the necessary conditions on the particles.

2.8 Constitutive Equation of Motion

The general dynamic equation of equilibrium governing particle motion can then be written as

$$m\frac{d^2u}{dT^2} + P\frac{du}{dT} + F_s + F_d + F_e = 0 \qquad 2.101$$

where the first term is the mass element (LHS in Equation 2.88), the second is the global damping element, the third and fourth are the internal resorting forces from the elastic and viscous elements respectively and the fifth is any other externally applied force. The second to fifth term added to give the RHS term in (2.88). Note that the appropriate sign convention for each force has to be considered.

Zhang and Whitten (1996) reviewed this general equation of motion following Tsuji *et al* (1992 and 1993). They obtained theoretical solutions for a single degree of freedom for two colliding particles and presented the results for deformation, velocity and force at contact using both linear and non-linear equations

The governing linear equation of motion of the impacting particles from which these parameters were obtained is expressed as

$$m\frac{d^2u}{dT^2} + D\frac{du}{dT} + Cu(T) = 0 \qquad 2.102$$

Normalising (2.102) to simplify the calculation gives

$$\frac{d^2\hat{u}}{d\hat{T}^2} + 2b\frac{d\hat{u}}{d\hat{T}} + \hat{u}(\hat{T}) = 0 \qquad 2.103$$

where $u = \hat{u}/C$, $T = \hat{T}(m/C)^{1/2}$ and b = $D/[2(mC)^{1/2}]$.

Zhang and Whitten (1996) defined these as $u = \hat{u}/D$, $T = \hat{T}\left(m/D\right)^{\frac{1}{2}}$ and $b = C\left\{2(mD)^{\frac{1}{2}}\right\}^{-1}$ which is likely to be typographical error.

The solution of (2.103) for $\hat{u}(\hat{T})$ gives the relative position of one of the particles at time T as given in Appendix C with the normalised velocity and forces and these are shown graphically in Figure 2.15 (a – c). From the figures the displacement variation with time shows an increase from zero to a maximum before returning to zero for different values of b. The velocity on the other hand decreases to zero and reverses direction while the force-time curve show results in an unusual trend. The magnitude of the forces (except $b = 0$) starts from non-zero and reduces to zero during collision process. They therefore concluded that this is due to the problem with the linear modelling. A similar process with the non-linear model whose general equation is expressed as

$$m\frac{d^2u(T)}{dT^2} + b(mC)^{\frac{1}{2}}u(T)^{\frac{1}{4}}\frac{du(T)}{dT} + Cu(T)^{\frac{3}{2}} = 0 \qquad 2.104$$

They made each term in the equation non-dimensional by replacing the displacement and time with $u = (mv_0 / C)^{2/5}\hat{u}$, $T = \{(mv_0 / C)^{2/5} / v_0\}$ giving (2.104) in normalised form as

$$\frac{d^2\hat{u}(\hat{T})}{d\hat{t}^2} + b\hat{u}(\hat{T})^{\frac{1}{4}}\frac{d\hat{u}(\hat{T})}{d\hat{t}} + \hat{u}(\hat{T})^{\frac{3}{2}} = 0 \qquad 2.105$$

from which the curves in Figure 2.15 (d-f) were obtained.

These plots as can be seen and as they concluded showed a reasonable prediction although subject to experimental confirmation. Similar to the linear case, the velocity started increasing and the force reversed before the displacement, which rose to the maximum, returned to zero. This non-linear model when used to predict the behaviour of basalt stones gave a closer result to that from experiment.

2.9 Summary

Theories for smooth contact (frictionless) and rough contact (with friction) for two elastic bodies commonly used in DEM and theories for handling interaction between spherical bodies and a flat plane as well as a concave surface have been reviewed. The theory for elastic contact with flat and curved walls (typical of most agricultural particulate handling systems)

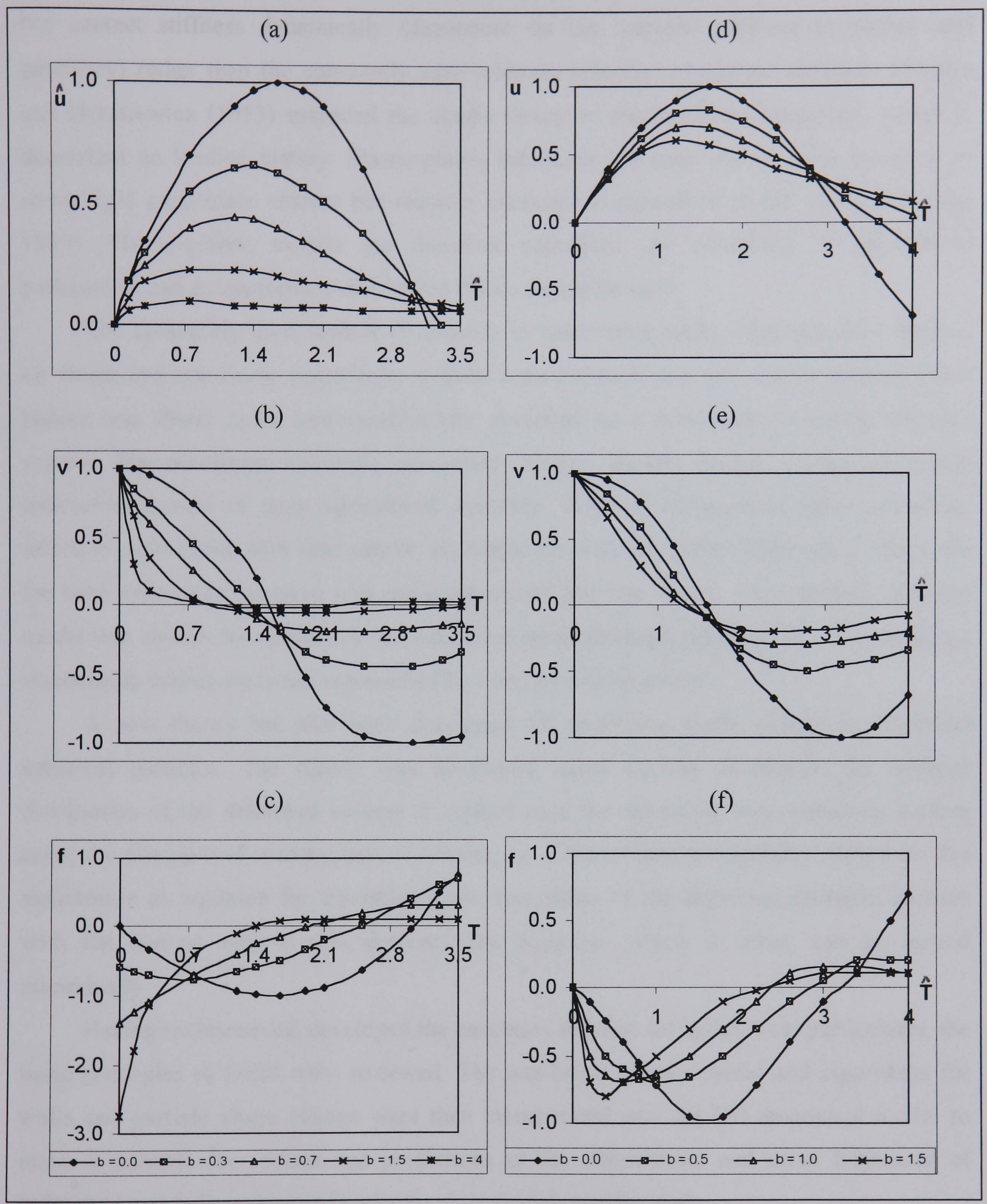

Figure 2.15(a, b, and c) Plot of normalised position, velocity and force during collision between two identical spherical particles using linear equation 2.36 and (d, e, and f) with non-linear equation 2.39 (Zhang and Whitten, 1996).

was developed. Hertz (1882) and Mindlin (1949) elastic theories were used for calculating the contact stiffness dynamically (dependent on the material stiffness properties and geometry) rather than the commonly used arbitrary selection of contact stiffness. Mindlin and Deresiewicz (1953) extended the elastic theory to elastic-plastic behaviour, which is dependent on loading history. Elastic-plastic behaviour has been shown to be common in some rigid particulate objects but requires excessive computation in DE modelling (Ng, 1989). Elastic-plastic models are therefore unrealistic for modelling of agricultural particulates and an appropriate alternative theory should be used.

The commonly used models of contacts in deformable (soft), incompressible bodies, i.e. linear and non-linear viscoelastic models, were reviewed and the contact between these bodies was found to be more realistically modelled by a non-linear hysteretic inelastic system. The non-linear hysteretic viscoelastic theory, models energy dissipation during interaction typical of most agricultural materials. Residual deformation after unloading, which is recoverable with time can be accounted for with this theory although in this work the time dependent recovery was not incorporated into the theory. The simplest damping model was chosen for reasons of computational speed although the behaviour of interacting viscoelastic bodies are better represented by a more complex model.

A new theory has also been developed for modelling shape change in deformed spherical particles. The theory was developed based on the assumption of uniform distribution of the deformed volume at contact over the remaining non-contacting surface using the principle of conservation of volume, i.e. material incompressibility. Based on this assumption an equation for determining the new shape of the deformed spherical particle with flat contact regions was derived. The equation, which is cubic, can be solved numerically.

Having reviewed and developed the necessary theories for agricultural particulates, the basic principles of DEM were reviewed. The non-linear contact model and algorithms for walls and particle shape change were then incorporated into the DE theoretical model to make it suitable for studies and predictions of the deformation and other behaviour of individual and bulk systems of agricultural particulates under load.

3 APPRAISAL AND MODIFICATION OF CONBAL

The discrete element method has been widely applied to the study of the behaviour of granular systems using a variety of codes as discussed in 1.4.2.1. This study takes as its starting point a code based on the original DEM code written by the pioneering researcher (Cundall, 1971). The code (called CONBAL) is first appraised and then the modifications and additions required to achieve the stated objectives are presented.

3.1 Introduction

CONBAL is a computer programme developed for modelling two and three-dimensional granular systems surrounded by a virtual boundary called the periodic space. In this study the CONBAL version of Ng (1989) and Ng and Dobry (1990) was modified by replacing the periodic space with walls. Particle-to-wall contact relationship was incorporated based on similar contact theory for particle-to-particle interaction as used in the original programme. An algorithm to monitor the particle shape change as a result of deformation (usually modelled as virtual deformation, i.e. interparticle penetration) was also introduced. These are necessary since the modified programme is intended for handling both high-modulus (hard) particles (for which the original programme was developed) and low-modulus (soft) agricultural particles. These particles also require the incorporation of conditions for viscoelasticity such as viscous contact damping relations and removal of the elastic-plastic based algorithm.

In the modified version the principle for calculation of contact forces is based on the Hertz (1882) and Mindlin and Deresiewicz (1953) theories for normal and tangential forces respectively as these were used in the original algorithm. However, the loading history dependent algorithm, which is of more use for elasto-plastic condition, was changed to a single yield surface contact stiffness relationship with the tangential component dependent on the normal component. Also in this work, the loading type did not involve oscillating (dynamic) load, hence the combined factors for the loading, unloading, reloading were simplified for monotonic loading. This may be necessary in flow simulation, which is not the main focus of this study. However the modification of the code is such that it can be easily adapted for simulation of unloading, reloading and simulation of any or a combination of the particulate handling processes listed below.

The current programme retains the use of spherically shaped particles otherwise

referred to as balls or particles. It can be used for simulation or modelling of one or more particles, free fall, settling, impact collision with a wall or another surface or particle. A number of other processes including compression or shearing of bulk systems of particulate material, damage in the form of deformation, flow and discharge of materials from a silo (flat and inclined bottomed) and conveying can also be modelled with the new programme. The new code was used for test simulations on all these processes but this report covers only those relevant to the stated objectives. Load application, which can be static, quasi-static or dynamic, is through one or more walls in orthogonal and or tangential directions for normal and shear loading respectively. These operations which can be categorised under material transport, handling and compression are typical operations in agricultural material processing.

3.2 CONBAL Development

3.2.1 Structure of CONBAL

CONBAL is a result of the combination of two codes written in FORTRAN-77 based on the DEM; **CON**TACT to compute the contact force using a non-linear force-deformation relation and TRU**BAL** for monitoring particle motion using a linear relation. Ng (1989) reported that the later version of TRUBAL by Zhang and Cundall (1986) was modified to incorporate a non-linear pressure dependent force-displacement (F-D) relation.

3.2.1.1 TRUBAL

TRUBAL was developed by Cundall and Strack (1979) as an improved version of an earlier programme BALL (Cundall, 1971). It is a 3-D programme for determining the dynamic response of random arrays of spheres in a periodic space as against the static response in 2-D BALL. The space is obtained by numerically connecting the opposite faces of an imaginary cube containing the spheres thus allowing a sphere to leave the box through one side and re-enter through the opposite side during simulation.

In TRUBAL and BALL, an arbitrary linear contact stiffness (spring) is specified by the user to calculate the normal and tangential forces having obtained the relative displacement from particle movement. The contact force increment is then added to the contact force at time T to obtain the new force at time $T + \Delta T$.

Using the basic principles of DEM discussed in Chapter Two i.e. 2.7, forces acting

on a particle are summed to obtain the resultant force passing through the centre of the particle and the resultant moment around the centre which induce respectively translation and angular accelerations on the particle. The accelerations are then integrated to obtain the velocity from which a new particle position at the end of the time step can be computed.

During loading, a prescribed uniform strain field is applied to the periodic space and all the particles at each time step, resulting in movement. The forces resulting from particle interaction and the stress field for the bulk volume are then computed. Space periodicity did not allow box distortion in TRUBAL unlike in BALL when normal and shear strains are applied. Therefore the box retained its shape and this limits the programme to simulations of consolidation and volumetric changes in directions perpendicular to the box surfaces. Since the particles are not deformable, the movement of one wall leads to the movement of perpendicular boundaries in the opposite direction.

3.2.1.2 CONTACT

The algorithm CONTACT (Dobry *et al*, 1991) for a given contact load increment as described briefly by Ng (1989), is a computer programme developed to:

i) Calculate normal displacement (relative displacement) between centres of contacting spheres from the normal components of the load increment and the Hertzian contact law,

ii) Determine the type of loading (elastic and inelastic-plastic) and use the corresponding tangential stiffness to calculate the tangential displacement (Mindlin theory),

iii) Find the position, size, and stiffness of the currently achieved surfaces and update the yield surfaces, and

iv) Handle spheres of different sizes having identical elastic and friction properties by using the concept of equivalent radius.

This flow rule was reversed by Ng (1989) who modified the programme to compute forces from specified displacement as against calculating displacement from loading.

3.2.1.3 CONBAL

CONBAL was developed by Ng (1989) who incorporated CONTACT as a subroutine to TRUBAL. In the resulting programme named CONBAL all the above processes are the same, but the displacement calculated from TRUBAL is used in CONTACT to calculate the tangential force for elastic-plastic materials based on Mindlin's

solution. CONBAL also uses most of the concepts found in the original TRUBAL which include grid masking to identify particle neighbours, linked list data structure to store neighbour information, secondary displacement accumulations to maintain greater accuracy and the calculation cycle. However there are several other significant differences such as improved particle generation, specification of material properties to obtain the contact stiffness as opposed to choosing an arbitrary linear contact stiffness (as in TRUBAL) as well as the use of a non-linear F-D law.

There are different types of CONBAL developed both in 2-D (initially used to reduce computational time and complications involved in 3-D) and 3-D as reported by Ng and Dobry (1990). The 3-D CONBAL programme was used in this study since most processes are 3-D and modelling in 2-D is only suitable for model development. Also the simulations in this study did not involve a large number of particles as the operations (loading, compression and packing of seeds and fruits) to be modelled (except in flow and discharge operations) did not involve large numbers of particles. However the model was developed to handle a large number of particles, the limit of which is determined by available computing facillities.

The two types of CONBAL in 3-D are CONBAL3-1 and CONBAL3-4

CONBAL3-1- computes one yield surface in contact, making use of the linear tangential force-dependent law. Particle rotation is allowed, hence the only yield is due to sliding. This may be applicable for particle flow operations.

CONBAL3-4 on the other hand keeps track of four yield surfaces. Particle rotation is not allowed but only forced to translate, by assuming an infinite polar mass moment of inertia for all particles making the angular acceleration zero. Both programmes will only be useful for this work if the elasto-plastic conditions are modified and replaced with viscoelastic conditions. In the new programme rotation may be allowed or not depending on the operation being modelled.

3.3 CONBAL3: Operational mode

CONBAL as described earlier makes possible the direct determination and monitoring of particle movement, forces, deformation and stress in a loaded system. The components and subroutines of CONBAL3 with their sequence of calls are shown in Figure 3.1. The operations performed by each of the routine in the original programme with modifications made for this study and other additional routines added are presented in

Appendix D and presented as comments on each routine in the full programme (supplied on a disk with this thesis). Figure 3.2 shows a flowchart of the mode of operation of the original code (subroutines involved in each operation are presented in italics).

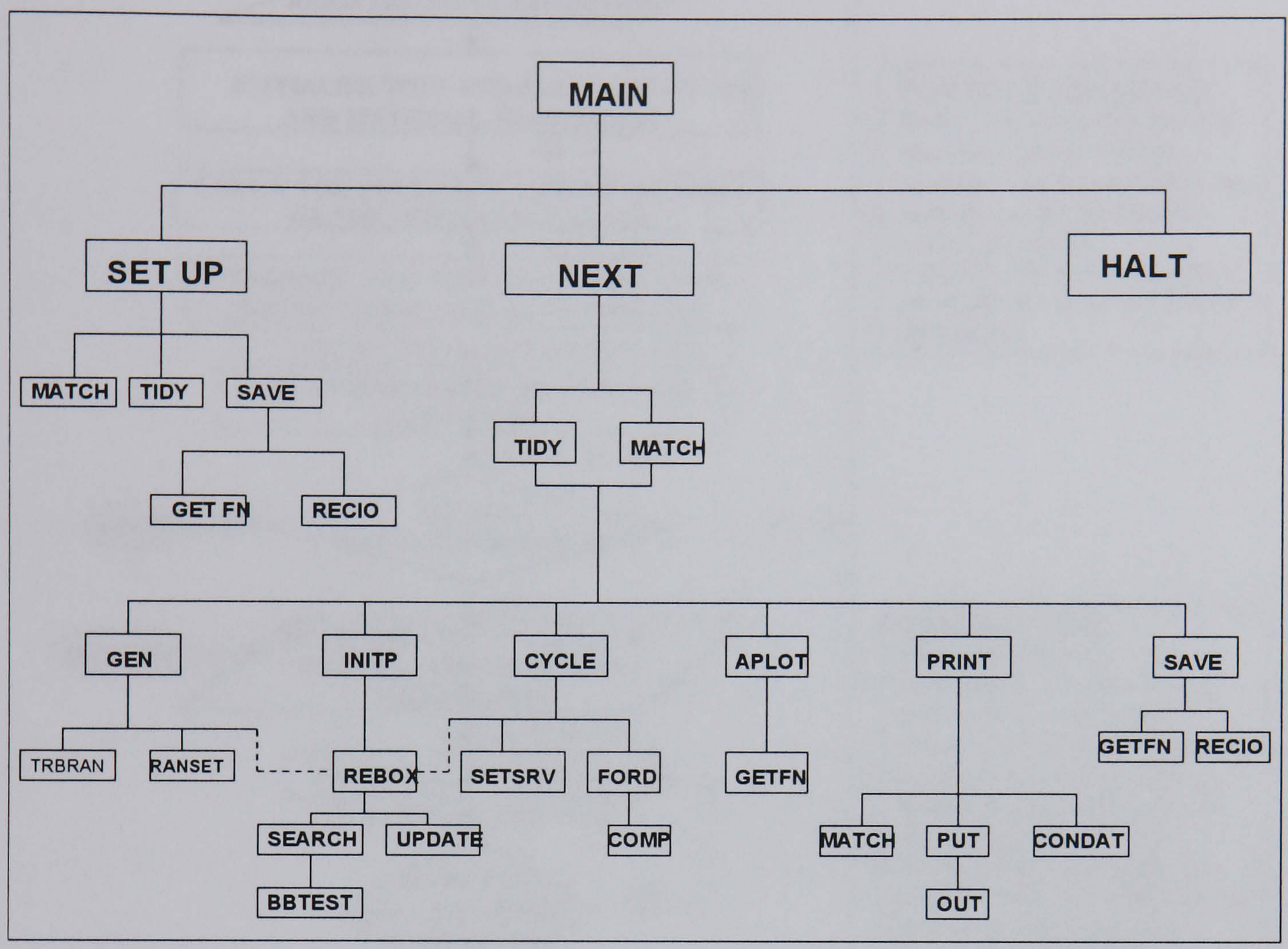

Figure 3.1 Structure of CONBAL3

3.3.1 Classification of CONBAL Programmes

The theory of DEM discussed in 2.7 represents what takes place in CONBAL with the exception of subroutine COMP whose principle is based on some of the theories discussed in 2.1. A brief summary of the theory of COMP as applied by Ng (1989) and discussed extensively by Dobry *et al* (1991) is given below. CONBAL classifications are based on the type of tangential contact stiffness used. Three types of contact laws for the tangential stiffness have been implemented in three different versions of CONBAL. However the normal load and displacement response, the Hertzian non-linear elastic response is the same in all.

The first tangential F-D response is the complete Mindlin solution applied by Ng (1989). This is a non-linear response depending on the load history of the normal and tangential forces for elasto-plastic materials as discussed in 2.3 and further details can be found in Mindlin and Deresiewicz (1953) and Dobry e*t al* (1991). It predicts a tangential stiffness given by (2.20) at the origin and zero at $F_t = \mu F_n$.

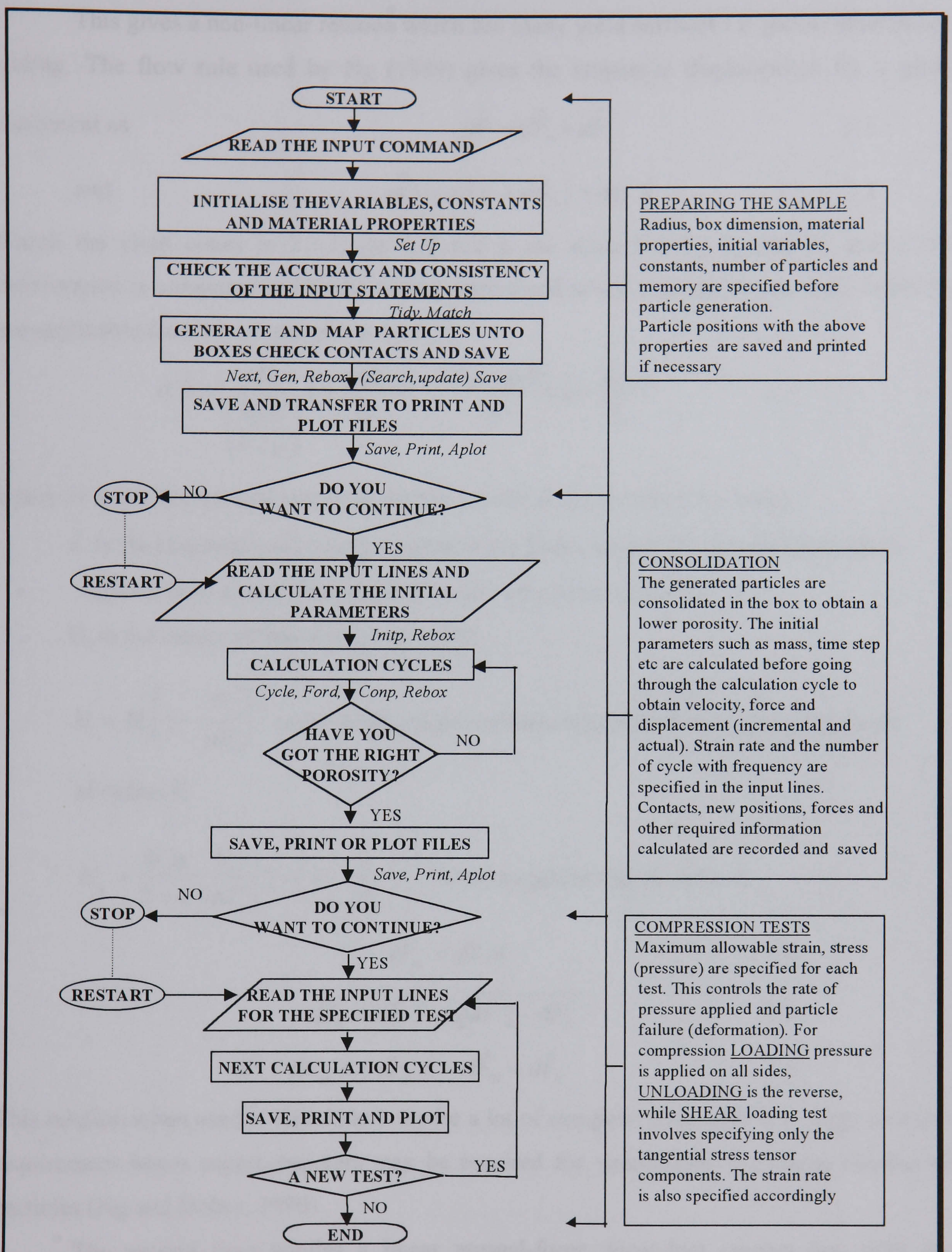

Figure 3.2 Flow Chart for CONBAL3

This gives a non-linear relation which has many yield surfaces i.e. partial slips before sliding. The flow rule used by Ng (1989) gives the tangential displacement for a given increment as

$$\vec{dF} = \vec{dF_n} + \vec{dF_t} \qquad 3.1$$

and

$$\vec{dD} = d\delta_x \hat{i} + d\delta_y \hat{j} + d\alpha\ \hat{k} \qquad 3.2$$

Recall the yield cones in 2.3.3; the **i, j** and **k** are along the F_x, F_z and F_n axes. This deformation is computed in COMP having determined which loading history and conditions are applicable from all or part of the term

$$d\vec{D} = \frac{dF_n}{\left(\frac{2Ga}{1-\upsilon}\right)}\hat{k} + \frac{\mu dF_n}{H_o}\hat{n} + \frac{dF_{tn} - \mu dF_n}{H}\hat{n} + \frac{dF_{tt}}{H_p}\hat{t} \qquad 3.3$$

where $\hat{n}$ is the normal unit vector to the yield circle at the current force point,

$\hat{t}$ is the tangential unit vector tangent to the yield circle at the current force point

(Note: both $\hat{n}$ and $\hat{t}$ are coplanar with in the plane of F_x-F_z)

H_o is the elastic stiffness given in (2.20)

$H = H_0\left(1 - \frac{F_t}{\mu F_n}\right)^{\frac{1}{3}}$ is the elasto-plastic stiffness corresponding to the yield circle of radius K

$H_p = \frac{8Ga}{2-\upsilon}\frac{F_t}{3\mu F_n}\left[1 - \left(1 - \frac{1}{\mu F_n}\right)\right]^{\frac{2}{3}}$ is the tangential elastic stiffness

$$dF_{tn} = d\vec{F}.\hat{n} \qquad 3.4$$

$$dF_{tt} = d\vec{F}.\hat{t} = \sqrt{dF^2 - dF_{tn}^2} \qquad 3.5$$

$$d\vec{F} = dF_{tn}.\hat{n} + dF_{tt}.\hat{t} = \vec{dF_{tn}} + \vec{dF_{tt}} \qquad 3.6$$

This relation when used in simulation require a lot of computer time with very large memory requirement hence supercomputers may be required for simulations with large number of particles (Ng and Dobry, 1990)

The second case applies a linear normal-force dependent contact law with the tangential contact stiffness being a function of the current normal force. It has the value of the Mindlin stiffness at the origin and this is used until sliding. This case therefore retains only one yield surface and does not predict the non-linear behaviour at contact for all $F_t < \mu F_n$.

The third case is also a Mindlin's solution but with four yield surfaces.

3.4 Input Commands

Input operative commands having various functions defining material properties, constants, dimensions and parameter controls for programme execution were used in CONBAL. Each line of the input file or commands has a list of the parameters following a keyword for a particular operation. The programme detects and recognises only the first three letters (listed as data in the programme) in the keyword. These series of three letters are indices or links to the part of the programme where the parameters are read. The keyword can also be written in full and the data or information (the keyword and each parameter) are separated from each other by a space or a comma (multiple separators are treated as one). The whole command input can be written in a file and compiled or input one by one as commands.

These types of operative commands are very efficient and flexible in use because different problems can be handled without re-writing the programme. The complete list of input commands used in CONBAL are given and explained in detail by Ng and Dobry (1990). A list of some of the new commands in the modified version developed in this study are given below with the necessary letters in the keywords written in upper case letters. A full list of the operative commands including the new and those used with the original code (modified or retained) to be used for different studies are presented in Appendix E.

The command for starting the programme specifying the box dimensions d_i, number of particles to be generated, ***nballm***, number of cubic sub-boxes to be created, ***nbox***, and the number of walls, ***nwall***, (added in this version) is: **STA**rt, d_1, d_2, d_3, *nballm, nbox, nwall*.

WALpar, *hiho, angl, gigu, vel1, vel2, vel3*: is the command for creating a discharge chute of dimension ***hiho***, for a silo whose bottom is inclined at an angle ***angl*** to the vertical. The discharge chute is at a vertical distance ***gigu***, from a conveyor moving with velocities of ***vel1, vel2, vel3*** in x, y and z. Discharge and conveying operations are indicated with **DIS**charge, idisch where idisch is 0 or 1(indicating the chute is closed or open respectively).

In the original programme the damping command specified the global damping coefficient while in the modified version a second parameter i.e. the coefficient of restitution was added to calculate the viscous contact damping ratio required for computation of the damping coefficient, hence the command is **DAM**ping, *global, cores*. In all the simulations in this work the global damping was set to zero.

For the calculation cycles and loading, **COM**press, *cx, cy, cz, mx, my, mz* is the command line specifying the indices for compression for loading walls in x, y or z axis. An index of 1 indicate the wall in that axis is a loading wall while ***mx, my*** and ***mz*** are real values

indicating the distance through which the loading wall is to be moved to touch the nearest ball before compression. The command used for quasi-static and dynamic loading is the same command used for specifying strain rate applied on both the particles and the periodic space at the same time in the original programme. The function was changed to specify the strain rate or the loading speed for only the loading wall used for compression in strain based loading. This is **GRI**d, *strx, stry, strz, strtx, strty, strtz,* specifying the normal (***str***) and shear (***strt***) strain rates for loading walls x, y and z with the appropriate sign indicating the direction of movement. In dynamic loading the signs are reversed intermittently at the appropriate times or after specified number of cycles. Both **GRI**d and **COM**press must precede **CYC**le command when needed. Static loading is indicated by **DED**load, *dedmas* with ***dedmas*** specifying the weight of the loading wall or any dead load placed on it. The calculation cycle command is similar to the original but a rotation index has been added. This is given by **CYC**le, *ncy, ntime, irot* which specify the number of cycles and number of times that ***ncy*** is to be repeated while ***irot*** is the index for rotation (0 = no rotation, 1= rotation allowed).

The command for activating the calculation and storage of information for the shape change of the deformed particle, is simply **SHA**pe.

3.5 Particle Generation

Particle generation is through a single command line **GEN**erate, *nbup, ntypes, ntyp1, ntyp2..ntypi* (Appendix E) specifying the number of bulk of particles per time (nbup) and the number of types of particles (ntypes) to be created as well as the distribution of the number per type (ntyp)within the bulk number that has to be generated. The first particle generated is placed at the centre of the periodic space/box and others are uniformly distributed outwardly, though randomly placed. Random numbers (using Fortran RAN generator) are generated and used to determine the angles of inclination (vertical and horizontal) of the new ball with reference to the first ball. The direction cosines of the line joining the centre of the new ball and the first ball in the 3-D axes are then calculated. This new sphere becomes a new ball provided it is within the box and there is no overlap between it and any other ball near it (in the same quadrant) before being mapped into the box(es) it occupies. The balls are generated in the order of types specified in the input line and the generation ceases if this condition is no longer satisfied after a number of trials have been made indicating that there is no more space to be filled.

In this study the generation algorithm was modified such that the first particle to be

generated is placed at the centre of the base of the box or workspace which is typical of most loading and container filling processes. The generation from the centre of the workspace suits the original programme with periodic space (imaginary boundary). This is because the system modelled is usually a small domain of a much larger system. Generation of a single column set of particles was also introduced to be able to obtain a system whose image can easily be analysed and compared with experimental results. This is achieved by setting the horizontal angular inclination with respect to the first particle to zero.

The particles can also be created directly by specifying the co-ordinates of their centre points using **CRE**ate command (Appendix E). This is useful for systems with known particles positions or for regularly placed particle. The particle type (ptype) indicated by size is also specified in the input command with the coordinates, hence the command is **CRE**ate x, y, z , ptype.

3.6 Wall Generation

The original programme did not have an algorithm for wall generation, therefore the conditions discussed in this section are those used to develop the algorithm for wall generation and recognition in the new programme. An inclined, vertical or horizontal wall can be generated by specifying its position (centre co-ordinates) and angle of inclination (for inclined-bottomed bins) through the command WALpar in 3.4. A total of eleven walls fixed or movable relative to each other can be generated. These are the four sides, the cover or top wall, the base which could be just flat plane or a combination of four flat or inclined walls with a fifth movable flat wall as the cover for the discharge chute. The eleventh is a wall created at a specified distance from the base of the box as the discharge base and can be converted to a conveyor by specifying velocity or acceleration in any direction. Conveyors or any other walls or partitions can also be created in any part within or outside the workspace. The weight of any of the loading walls could be specified when needed otherwise the positions are the only necessary specifications.

In this study, for monotonic unidirectional compression, the top wall was used as the loading wall. Loading as stated earlier can either be by applying a constant strain rate (or loading speed) on the wall or under its own weight or with a specified load or stress applied on such wall.

3.7 Contact Search, Detection and Data Storage

The original programme identifies a cubic workspace (specified by the user in the start command) which is divided up to form series of cubic sub-boxes or grid-cells. For cubic workspace the number of sub-boxes per side is the cube root of the total the total number of boxes specified. The dimension of each sub-box must be greater than or equal to the diameter of the largest ball i.e. it must be able to accommodate at least one ball, indicating that the maximum number of boxes that a ball can occupy (partially) is eight and one (fully). However this is not a fixed condition, it can be changed when necessary.

The original programme was modified such that the workspace may not necessarily be cubic but the three sides are multiples of each other in dimension. This allows the creation or generation of a workspace of different dimension in the three axes. However the minimum box dimension possible is equal to the diameter of the largest particle. The new code retained the cubic sub-boxes system during initial particle generation but their dimensions change during simulation to non-cubic. This is because at any time during simulation the dimension of the workspace along each axis is taken as the distance from the reference point to the outer surface of the farthest particle along the axis. This eliminates the empty spaces outside the area occupied by the particle from being searched for contacts, minimising the computational requirement. The number of sub-boxes per side remains the same throughout the simulation hence they become non-cubic with equal dimensions along any axis. When any particle moves outside the container e.g. during conveying and discharge operations, sub-boxes are created at these regions using the same principle as within, for locating and searching for contacts.

3.7.1 Ball and Wall Mapping

During the process of generation and the entire operation, each ball (and wall in the modified version for this study) is mapped into the sub-box(es) which it occupies (note that each box also has a linked list associated with it which is linked to the identification of all the balls that are mapped into it). Ball or wall is mapped by calculating the positions of the surface of each ball along its diameter on each axis. For a ball whose position along the x-axis is P_x with radius R, then

$$P_{xmax} = P_x + R \; and \; P_{xmin} = P_x - R \qquad 3.7$$

By dividing P_{xmax} and P_{xmin} by the grid size along the x-axis the numbers of the sub-box(es) which this particle occupies in x are obtained. This is done similarly for y and z-axes. If the same values are obtained after the division, it means the particle is located in only one box. If the edge of the particle is tangent to the side of a sub-box (just at the boundary of two sub-boxes), it is assigned to the previous box (with respect to P_{xmin}) or the next box (wrt P_{xmax}). This is because the other parts are located in the next or previous box. Checking for contact means three boxes will be checked i.e. box into which P_{xmin}, other parts (center) and P_{xmax} falls.

All the balls (and walls) mapped into the same sub-box are potential neighbours that can form contact, therefore when considering a ball in a sub-box only its immediate neighbours in that sub-box are searched for contact. Stability of the programme is tested before each contact search by determining the next ball position using its present velocity. If the new position is such that the ball will not obey the DEM law i.e. propagate more than its immediate neighbour or move a distance greater than a specified tolerance value, in the next time step, which will render the programme unstable, the programme will be terminated. This results from excessive resultant force on a particle or a large time step producing large "overlap".

3.7.2 Contact Detection

Only the particles and walls mapped into the same sub-box(es) with a ball are recognised as its immediate neighbours and are the only ones considered during a contact check. This is the linked list method, which make use of the grid cells to link list of balls in the grid. Note that walls are not checked for contacts as one or more balls must make a contact with one or more walls. Once detected each resulting contact is allocated a memory block specific to that contact and the two balls involved. Therefore when considering contact of ball A in a sub-box with another ball B among the immediate neighbours in that sub-box the list linking the two is allocated a space in the memory block with an identification number for that contact. Two balls might be detected in more than one sub-box and a contact can be allocated identification number and list twice. In the modified code another array *con(a,b) = contact identification number* is used to prevent repeated contacts allocation which was not taken care of in the original code. When searching for contacts with ball B, and A being one of the immediate neighbours to be considered, if *con(a,b)* is not empty i.e. = 0, then it has not been tested with B otherwise the search between B and A is skipped. The memory block is used to store all information about this contact. When a contact is broken,

its memory space is added to an empty list, which string together all unused memory and are the first to be tried when new memory is required for a new contact. Generally this method allows fast reallocation of memory and saves computer time and space. Any particle that has moved over a certain distance is remapped so as to update the boxes it occupies.

3.7.3 Data Storage and Memory Partition

Information storage in CONBAL is by means of a single array A(I). It contains information on particle position, forces, boxes and contact data. It is subdivided into three parts for storage of ball, box and contact data, the dimensions of which are determined by the number of balls and boxes. The memory array for particle information storage starts from $I = M_1$ to a value given by

$$M_2 = nballm \times nvarb + M_1 \qquad 3.8$$

Where $M_1 = 1$ and $nvarb$ = the number of dimensional axes used (e.g. 3 for 3-D modelling). Therefore the position of the balls are stored by the components along the axes i.e. 3 arrays per ball for 3-D leaving a free memory space. The array for box information storage starts from M_2 up to an upper limit given by

$$M_{3a} = 2 \times nbox + M_2 \qquad 3.9$$

These numbers between M_2 and M_{3a} are also used for box identification in the linked list. The first box is identified by a number denoted by $NB = M_3 = M_2$ and the identification for the other boxes are in a step of 2 i.e. $NB+2i$ (i is the number of box). The free number in between for each box is used as a dynamic storage space in the memory block for storing the address of the immediate previous contact detected in a box.

The array for the string of contact data and lists starts from M_{3a} up to the maximum limit usually specified during declaration of array $A(I)$. This is used to store data such as the contact force, position, direction cosine etc. When a contact is detected, its identification number or address is denoted by a number IAD (greater than or equal to M_{3a}). A memory block containing $nvarc$ spaces (where $nvarc$ = 50 in CONBAL) is allocated to each contact indicating that 50 data values can be stored for each contact with the first being $A(IAD)$ and the last as $A(IAD+49)$. The IAD for the next contact detected is $(IAD+50)$ and its memory block is from $(IAD+50)$ to $(IAD+50+49)$.

The following is the distribution of the data stored in this memory block for each contact. [Note that for simplicity the arrangement below i.e. $A(K)$ indicates that $K = IAD+K-1$, hence $A(2) = A(IAD+1)$.

A(1) - A(3) = Tangential contact force components in the three axes (x,y,z)

A(4) = Normal contact force

A(5) - A(6) = Address for the two balls in contact

A(7) = Identification number for the previous contact detected in the same box

A(8)- A(10) = Direction cosine for normal deformation

A(11)-A(13) = Direction cosine for the tangential deformation in x-direction

A(14)-A(16) = Direction cosine for the tangential deformation in z-direction

A(17)-A(19) = Sliding index

A(20)-A(50) = Data related to the contact stiffness and other information from the Mindlin solutions for the elastic-plastic case (load history).

This array allocation is retained in the modified programme because it is an easy way to recall or print information in just a call of one array but the memory space for each contact data has been reduced to 30 since the elasto-plastic data storage are not needed.

3.7.4 Updating Contact

The identification number *IAD* linking any two contacting balls and the sub-box in which they were found is one of the list of numbers for the links detected in the system hence the term linked list. This number *IAD* is stored in the space for the free number associated with the box i.e. *A(NB+1) = IAD*. When a new contact is detected in the box, the *IAD* for the immediate previous contact which was stored in the array *A(NB+1)* is transferred to one of the memory spaces of new contact, *A(IAD+7)*. The new *IAD* for the new contact detected is then stored in the free space i.e. *A(NB+1)*. During the calculation cycles or any other operations where contact data such as force, deformation and contact area are calculated for each contact, each box is called and the necessary calculations are made for each contact starting backwards form the last contact. Note that each subsequent contact as it is detected has information about the identification of the immediately previous contact as stated above. The first contact which is the last to be called during the computation cycle, has an empty memory space A(*IAD+7*), which is an indication that the next box should be called as there are no more contacts in this box. This reduces computation time by avoiding the checking of particles that are not in contact. It also makes recording and calling of contact data per box and particles easier during plotting and printing.

When a contact is lost, its address (*IAD*) is saved in a dead link. Whenever a new contact is detected and an address required, this dead link is checked and one of the stored

addresses (the last to be added) is used. The series of saving and calling of addresses in the dead link is similar to that of contact address. Any immediate past address added to the dead link is saved in a memory block using the previous address i.e *A(new) = previous*.

3.8 Simulation Procedures

Generally the procedures described in Ng and Dobry (1990) for the numerical simulations in the original CONBAL are similar to those needed to run an experiment in the laboratory. The main stages (shown schematically in Figure 3.2) are

(i) Preparation of a sample or assembly generation

(ii) Consolidation of the sample to predetermined porosity or state of stress

(iii) Application of predetermined strain to shear or compress the sample.

3.8.1 Sample Generation and Preparation

In preparing a sample for test the material properties are specified and the required number of particles that can fill a specified periodic space are generated using a random-number generator algorithm. Each particle is then mapped as described in 3.7.1. These information, which also include the particles positions, are saved. The procedure is the same in the modified version used for this study but the necessary modification in generation of particles and walls discussed earlier were taken into consideration.

3.8.2 Sample Consolidation

In CONBAL the consolidation process is carried out to reduce the porosity of the generated sample which in most cases is loosely packed with some particles possibly hanging in space. The particle movement algorithm is strain based because the particles handled in CONBAL are supposedly very small and lightweight. Using a very small time step the movement of the particles will require excessive computational time before any movement is noticeable. Therefore a constant strain rate is applied to both the periodic space and the particles during each time step to speed up the movement. Generally in CONBAL3-4 the tangential strain rate is set to zero since rotation is not allowed. Also the number of calculation iterations (cycles) are specified; i.e. the calculation cycles are performed a specified number of times before output of data. Some initial parameters such as mass, time

step etc are calculated before each calculation cycle. During cycling both the actual forces, velocity, and displacement and their incremental values are calculated and the particles are re-boxed when necessary i.e. positions are updated and particles remapped into box(es) if necessary.

The cycling process is repeated until the required porosity is obtained due to the movement of the particles. Since the point at which the required porosity is reached is not known the consolidation takes place slowly (small strain rate) and the porosity monitored by saving or printing out the information onto a file or screen at the end of a number of cycles. This method as used by Ng (1989) could have saved some computation time if the method employed in the new code was used. This involved introduction of an index to save information and terminate the programme or start the next process when the desired porosity is reached or the porosity stabilised during consolidation

3.8.3 Loading Test

The consolidated particles can be tested for behaviour under compressive loading, unloading or shear loading of the bulk system. This is achieved by specifying the mode of load application (compressive, tensile or shear) and direction of the maximum allowable strain rate and displacement based on the type of test. Loading is also strain based as the strain rate corresponding to a situation when a given load is applied in any direction is specified and applied to all the particles and the periodic space. Subsequent operations are similar to the consolidation process but with faster particle movement and re-arrangement.

Information on the number of contacts, the particles in contact, deformation, particle positions, contact forces, resultant normal and tangential forces with direction on each particle and contact as well as unbalance forces, porosity and stress tensor in the bulk system are obtained as the output. The particles only deform at contact points, therefore they maintain their shape by overlapping at the contact point.

3.9 New Simulation Procedures

In the modified version, the assembly generation procedures were almost the same except for the placement of the first particle at the centre of the lower box (base wall). This filling method reflects loading from bottom up to the top typical of most real systems. The particles are also more closely packed than in the original and generation of a single column

of particles was made possible. The latter is to enable setting up of a system for compression or loading of a stack of material that can be verified experimentally. The particles can be created in any position and arrangement required using the create command.

The method of consolidation has been changed to gravity flow of particles i.e. deposition under self-weight. This procedure which eliminates the use of strain rate on the particles can be used to determine height of stack since the deformation of the particles can be monitored layer by layer. However the cyclic calculation process is still the same.

The test procedure is also the same as in the original code but without strain rate assisted movement of particles. The strain assisted load application is similar to that in the original code but rather than an imaginary boundary one or more of the walls act as the loading wall(s) and moved at a loading speed specified or generated by specified strain rate. Other algorithms were introduced in the modified version for other forms of loading as described earlier while some parts of the original programme were deleted.

3.10 Summary

The original programme, CONBAL, developed for rigid spherical particulates has been modified to make it suitable for simulation of handling and processing operations of agricultural particulates. The following is a summary of the modifications, new algorithms and processes introduced to the original DE code.

- The particle generation algorithm has been modified to suit the type of systems to be modelled. In the modified version the first particle is placed at the bottom centre and the others generated randomly around it. This reflects more closely normal container filling. In order to verify the simulation, the facility to generate a single column particle system was added to allow direct comparison between single column experiments and simulations. Necessary modifications were also made to the input commands, particle boxing, contact detection and searching method as well as data storage.
- Wall option: Most agricultural materials are either packed or transported in containers unlike in many application of DEM where the system is a large spatial domain or long structures made up of a very large number of particles and only a sub-domain of this continuous system is modelled with an imaginary boundary. Therefore a wall option was used and a particle-wall interaction law was introduced. Provision was made in the code such that flat or inclined walls, movable or stationary walls, chutes for discharge, as well as conveyors (flat or inclined) can all be created.

- Viscous contact damping (since the particles under consideration are viscoelastic) as opposed to the global damping in the original programme was introduced. The damping model introduced is the velocity and deformation dependent damping that is capable of modelling residual deformation in unloading. The loading and unloading FD curve are non-linear as opposed to the more commonly used linear system.
- Algorithms were added for calculation of the stress and other necessary parameters such as deformation and contact radius of each contact area and other bulk volume parameters in addition to the stress calculated in the original programme.
- A method was introduced for obtaining the resulting shape of the deformed balls. This was required because most biomaterials deform and change shape under load due to their viscoelastic nature though part or all the deformation may be regained (regaining shape). Their shape changes are noticeable even under small strain in some cases unlike most other engineering materials considered in DE models.
- The simulation procedures were also modified as discussed in 3.9.

4 MODEL VALIDATION

4.1 Introduction

The theories governing the behaviour of agricultural particulates presented in Chapter Two were used in the development of a new code for this study as explained in Chapters Two and Three. This Chapter is divided into two parts: validation of contact models and the shape change under compression. In the first part results of simulations of impact of single particles on other surfaces using the new code are compared with experimental data from the literature. In the second part validation of the code against physical experiments using the results of compression of synthetic and natural spherical shaped particles is presented.

4.2 Validation of Contact Models

When dropped vertically down on to a flat surface a viscoelastic material will bounce a number of times, losing energy at each impact before coming to rest on the surface. The damage and stress distribution on impacting fruits under static and dynamic loads have been studied extensively using various experimental methods resulting in a number of published parametric results on the behaviour of fruits. Efforts have also been made to develop predictive models for these results using theoretical analysis. The problem usually associated with these models is inexact assumptions of material behaviour leading to the use of approximate theories in prediction models.

The programme developed for this study as discussed in the previous chapters has incorporated a non-linear deformation-dependent viscoelastic model for spherical materials which according to reports (Tsuji *et al*, 1992, 1993; Zhang and Whitten, 1996) is more realistic than the more commonly used linear elastic and viscoelastic models to approximate the behaviour of agricultural materials. In order to validate the contact theory in the model, one each out of the available experimental and theoretical results on impact experiment using a drop test was chosen.

These studies are the work of Lichtensteiger *et al* (1988) and Zhang and Whitten (1996). Lichtensteiger *et al* (1988) measured the impact force on tomatoes and some other spherical non-agricultural materials (rubber) dropped on a very rigid and heavy base. The force data at equal time intervals were recorded via a force transducer connected to an

oscilloscope and recorded or saved on a microcomputer. A sampling rate of 2–10 μs per point, which gave adequate precision, was used for defining the force-time curve and tests were repeated at a slower sampling rate of 100 - 500 μs per point to obtain the time between the first and second bounces. Using the force-time information during contacts simple equations based on Newton's law of motion and finite difference approximation were developed to determine the velocity, acceleration and displacement during contact on a plate placed on a very heavy and rigid surface. The coefficient of restitution and energy dissipated during impact were also determined. In the model development the assumptions made are that the products are spherical, the centre of mass and the centre of the sphere remained coincident during contact, all the mass was subjected to the same acceleration and vibrations were negligible. This study was chosen because of the precision in data recording.

Table 4.1 shows the physical properties of the rubber balls used in the experiment. The properties of tomatoes used were not reported. The force-time curves in Figures 4.1 (a and b) diagrammatically illustrate the effect of maturity and mass on the contact force for tomatoes and ADRUB rubber balls respectively, obtained in the study. The contact force plotted as a function of time and displacement for Indoor Lacrose Ball (ILB) and outdoor (OLB) are as shown in Figures 4.2 (a and b). The F-T curves for artificially made and natural 'composite' products with relatively thin shells or coverings having different properties than the internal elements are also illustrated in the report. They reported that a phenomenon known as the shell effect accounted for the sudden change in slope of the F-T curves shortly after contact. This effect was also observed in red and pink tomatoes and some other fruits, apple and blueberries (Fluck and Ahmed, 1973).

4.2.1 Simulation

Numerical simulations of the impact of rubber balls and apples were performed using the new computer programme with the rheological model for viscoelastic materials (the incorporated non-linear deformation-dependent viscoelastic model for spherical materials) as presented in 2.4 and explained in Chapter Three. The properties of the materials from the experiment of Lichtensteiger *et al* (1988) (Table 4.1) were used in the computer simulation for rubber balls while those of apple were obtained from the literature (Mohsenin, 1986). The rigidity modulus of the rubber material is 3.0 MPa.

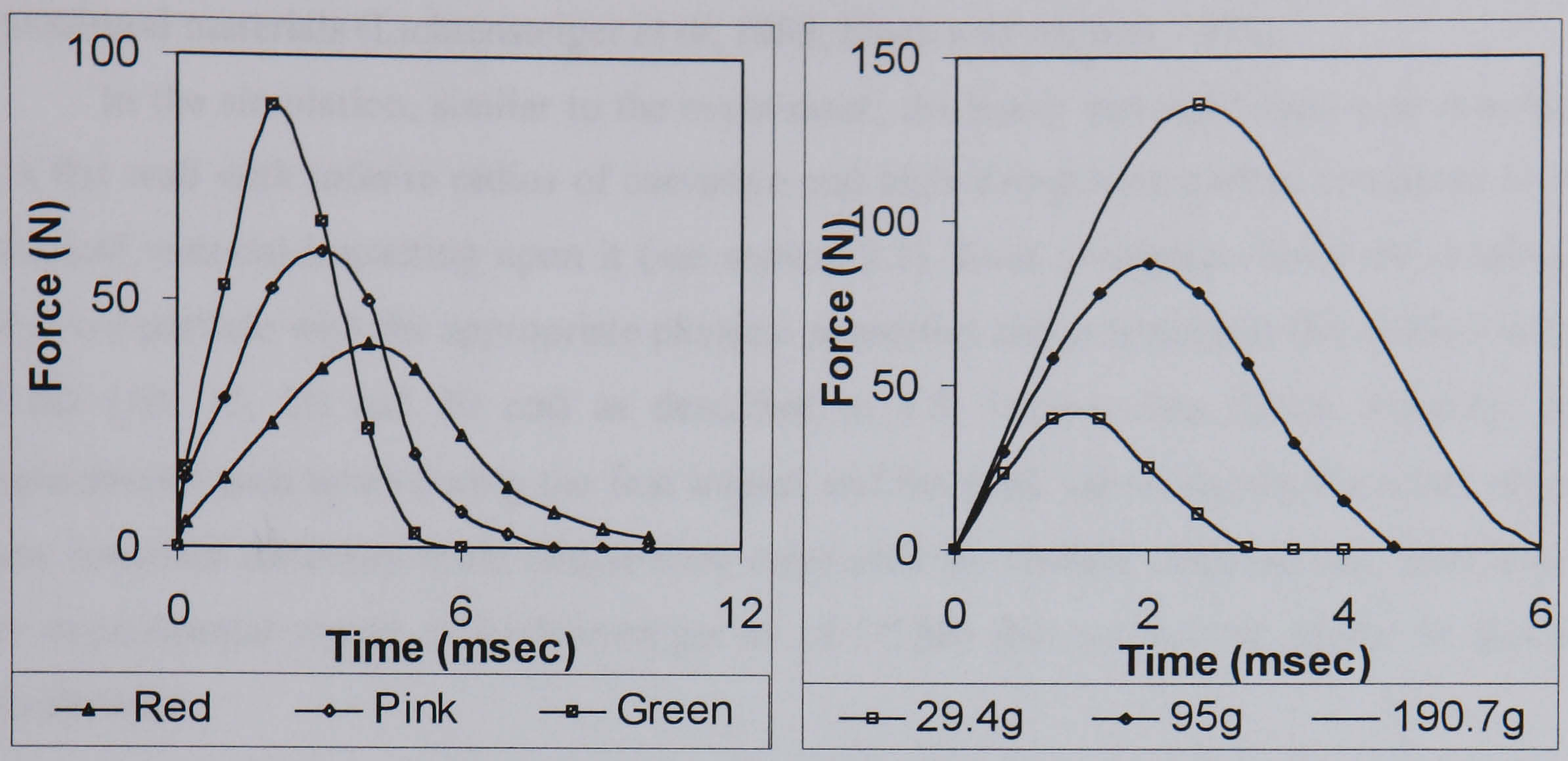

Figure 4.1 (a) Effect of tomato maturity on impact force (b) Effect of mass on the impact force for ADRUB balls (Lichtensteiger *et al*, 1988)

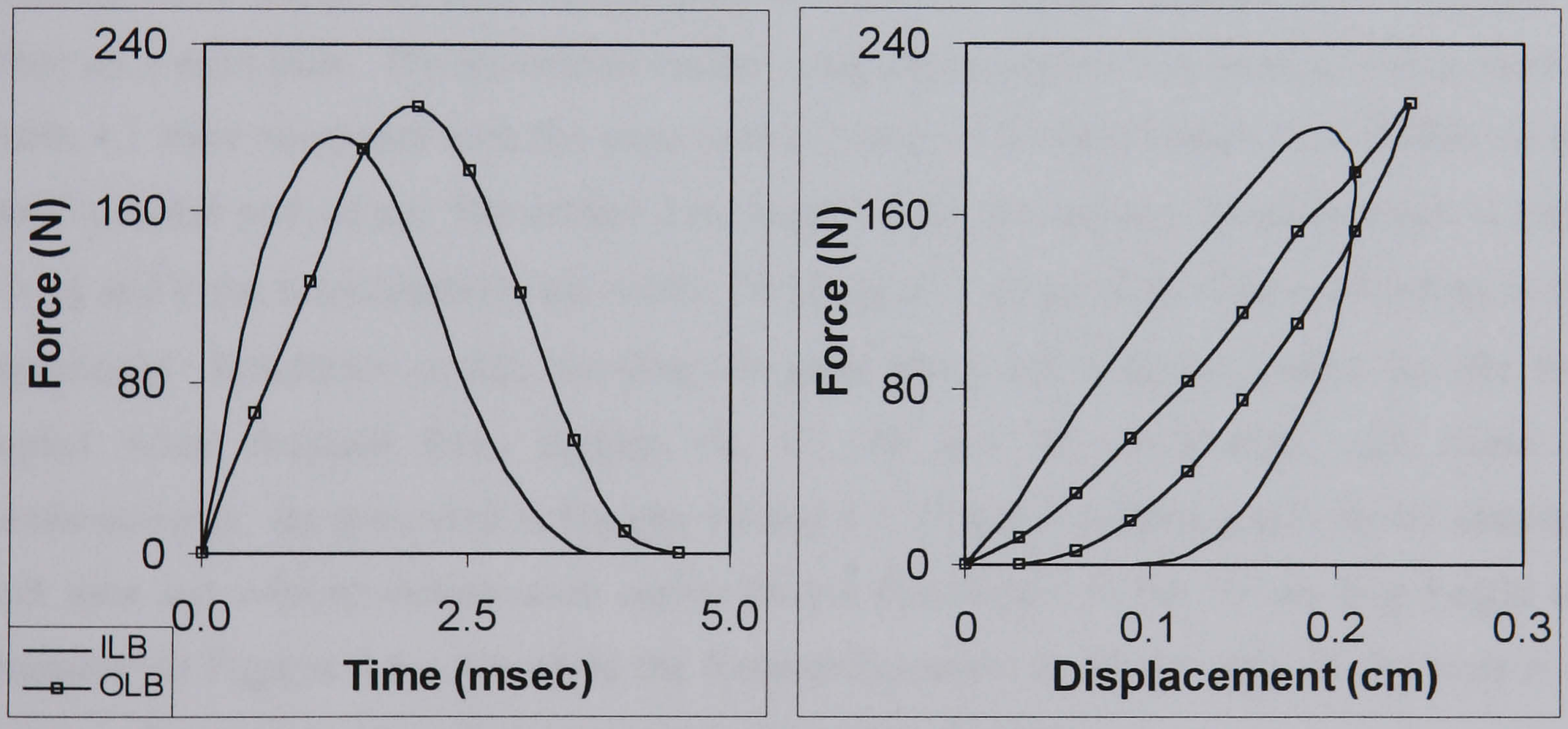

Figure 4.2 Force as a function of (a) time and (b) displacement for indoor and outdoor lacrose balls (Lichtensteiger *et al*, 1988).

The simulation results obtained for the rubber ball were compared with the experimental results reported by Lichtensteiger *et al* (1988) as a form of validation of the contact model and suitability of the DEM for the experiments discussed above. Since the details of the properties of apple are obtained from the literature validation was on the basis of agreement with the general solutions by Zhang and Whitten (1996) which are in turn in

agreement with the available results from experimental work on viscoelastic particulate agricultural materials (Lichtensteiger *et al*, 1988; Fluck and Ahmed, 1973).

In the simulation, similar to the experiment, the heavy and rigid base was simulated as a flat wall with infinite radius of curvature and high strength properties compared to the spherical material impacting upon it (see section 2.1). Each simulation involved creating a spherical particle with the appropriate physical properties and geometry at the desired height of fall (10, 15, 20 and 30 cm) as described in 3.5. Impact data (force, velocity, and displacement with time) during the first impact and the peak values during the other impact were recorded for every cycle (single time step) until the particle came to rest. The data in the experimental report in Lichtensteiger *et al* (1988) did not extend as far as particle equilibrium.

4.2.2 Results and Discussion

4.2.2.1 Impact

Figure 4.3 shows the force-time curves during the first impact and the effect of mass obtained from impact of three rubber balls of different weight dropped from a height of 10cm on a rigid plate. The simulation results using the properties and geometry presented in Table 4.1 were compared with the experimental result of Lichtensteiger *et al* (1988) on the same material and set up. The critical time steps for the simulations range between 4.1 and 4.6 μs and these coincidentally are within the range of 2-10 μs used in data recording in the experiment. Simulation results showing the peak force and time of contact for the first impact when dropped from heights 10, 15, 20 and 30 cm plotted with those of Lichtensteigers' are presented in Figures 4.4 and 4.5. The deformation and velocity obtained with time and velocity-deformation curves for the first impact in the 10 cm drop height are presented in Figures 4.6 - 4.8 while the force-deformation curve for each of the tests is as shown in Figure 4.9 although these are not reported by the group.

Good agreement was obtained between the simulation results and Lichtensteigers' data as can be seen in Figure 4.3. The peak forces predicted by the simulation were 42.5, 85.2 and 137.7 N as compared to 40, 87, and 136 N from the experiment for balls with weights of 29.4, 95 and 190.7 g respectively. The predicted time of contact is slightly lower in all cases. This trend is also similar in the simulation of drop impact for the heaviest ball, (191 g), from different heights.

Table 4.1 Data used in simulation as obtained from Lichtensteiger *et al* (1988) for ADRUB balls (Height of drop: 10, 15, 20 and 30 cm, Rigidity Modulus: 3.00 MPa, Friction coefficient: 0.5, Poisson ratio: 0.31).

Diameter (cm)	Mass (g)	Coefficient of restitution	Time step (μs)
3.76	29.4	0.636	4.1
5.47	95.0	0.639	4.4
7.04	190.7	0.629	4.6

(Walls have infinite radius and EM_w is assumed to be far greater than that of the rubber ball hence $1/R_w$ and $1/EM_w$ are negligible)

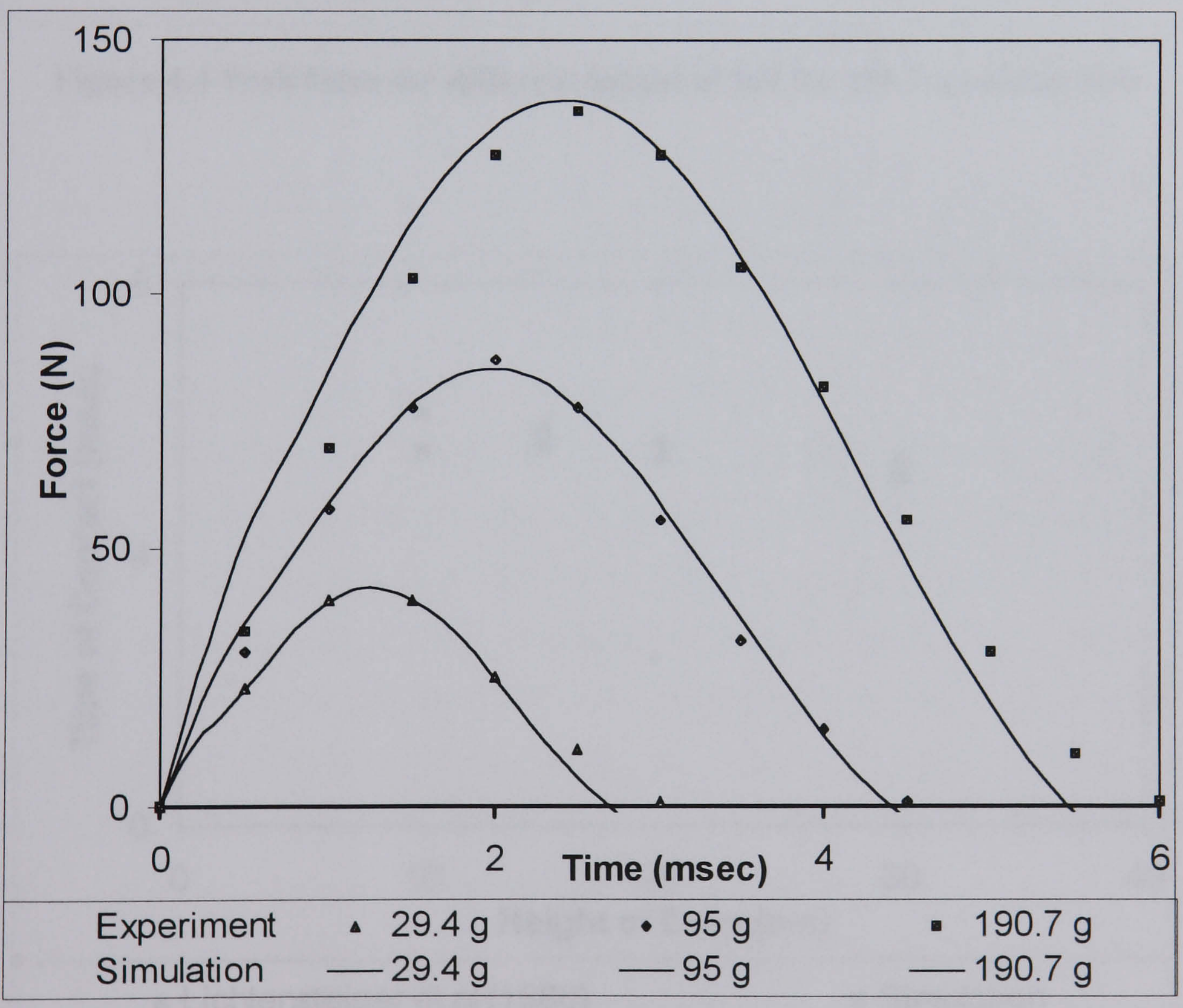

Figure 4.3 Force-time for rubber balls falling from a height of 10 cm (Data points show the results of Lichtensteiger *et al*, 1988)

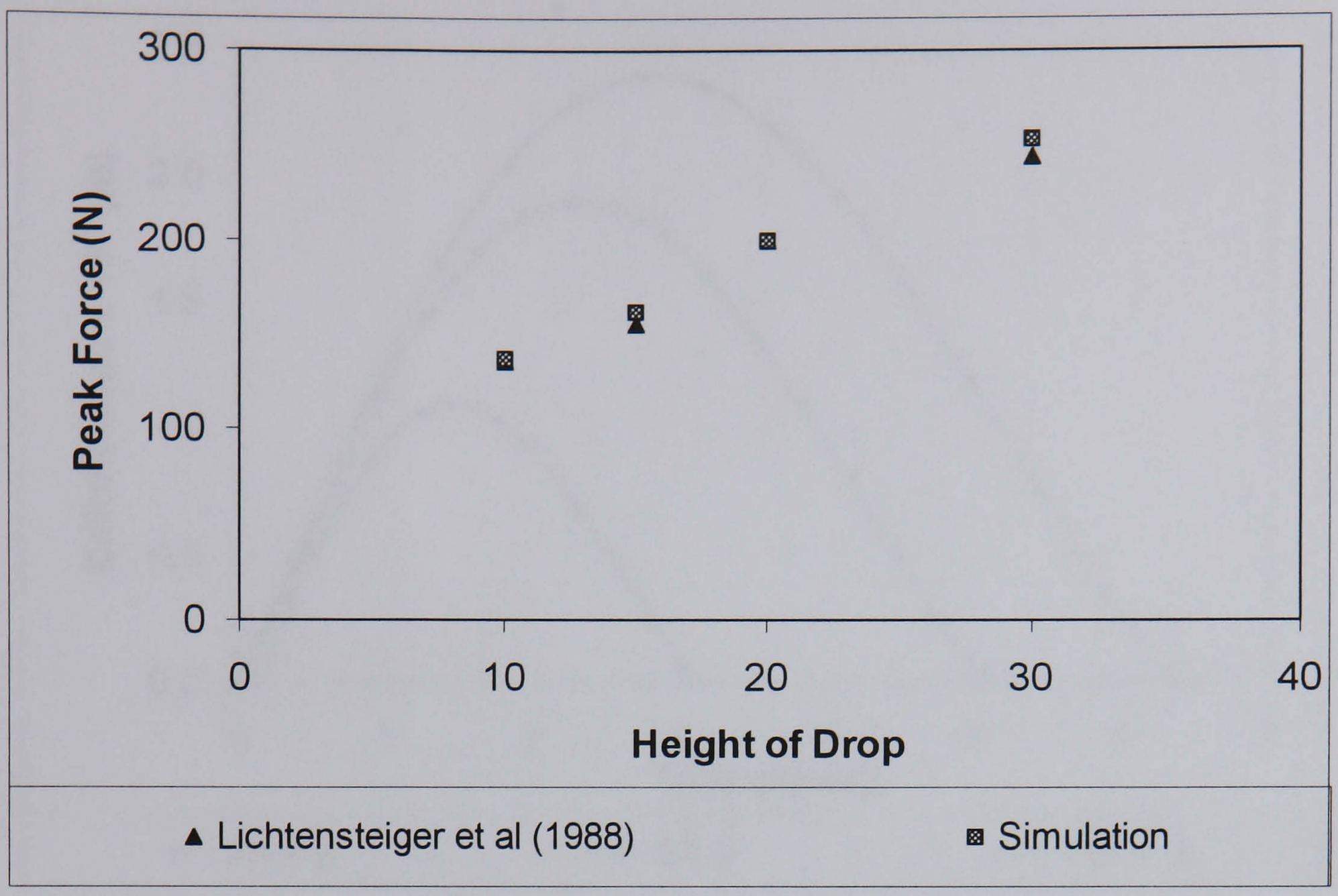

Figure 4.4 Peak force for different height of fall for 190.7 g rubber ball

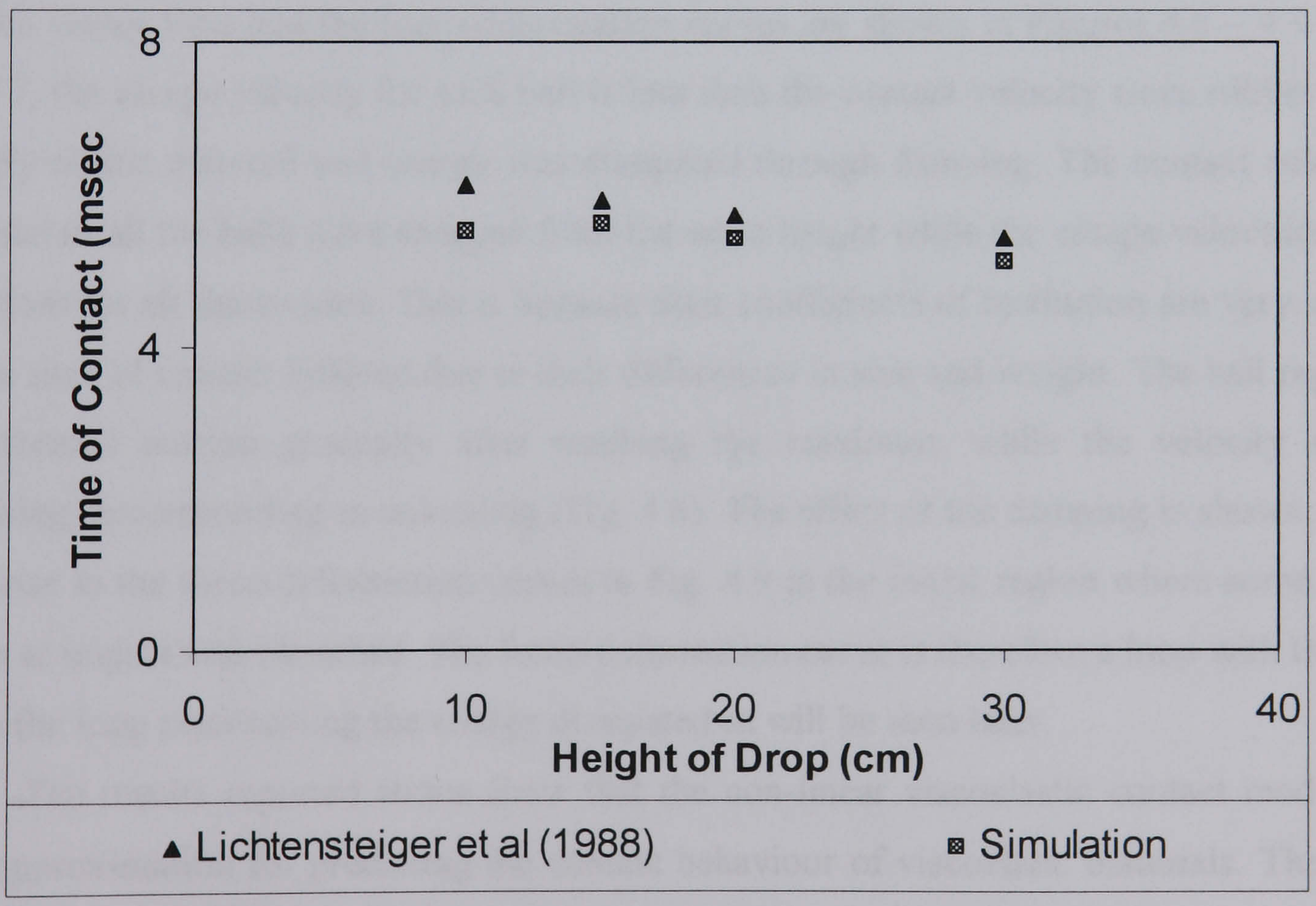

Figure 4.5 Time of contact for different height of fall for 190.7 g rubber ball

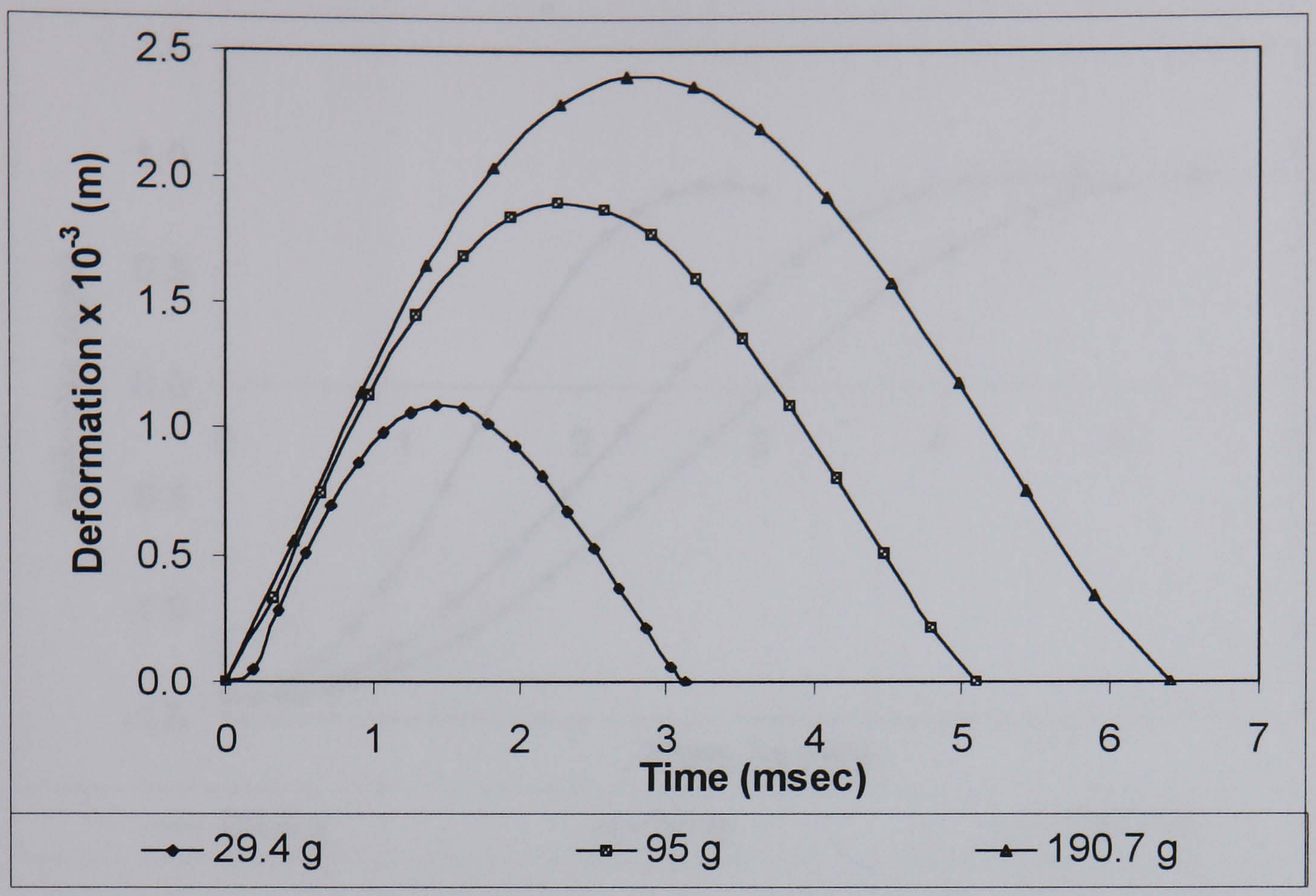

Figure 4.6 Deformation predicted during the first contact.

Additional parameters not reported by Lichtensteiger; deformation versus time, velocity versus time and the force-deformation curves are shown in Figures 4.6 – 4.9. From Fig. 4.7, the escape velocity for each ball is less than the contact velocity since rubber is not a purely elastic material and energy was dissipated through damping. The contact velocities are equal as all the balls were dropped from the same height while the escape velocities were very close for all three cases. This is because their coefficients of restitution are very similar but the time of contact differed due to their differences in size and weight. The ball regained its deformed portion gradually after reaching the maximum while the velocity started increasing, corresponding to unloading (Fig. 4.8). The effect of the damping is shown with a sharp rise in the force-deformation curves in Fig. 4.9 at the initial region where some of the energy at impact was absorbed. The force-deformation curve is therefore a loop with the area within the loop representing the energy dissipated as will be seen later.

The results reported above show that the non-linear viscoelastic contact model is a good approximation for predicting the contact behaviour of viscoelatic materials. Therefore this model was used for further studies on predicting the behaviour during impact for a viscoelastic material. The data presented in Table 4.2 are properties of apple fruit used for simulation of impact tests of the fruit when dropped from a height of 20 cm.

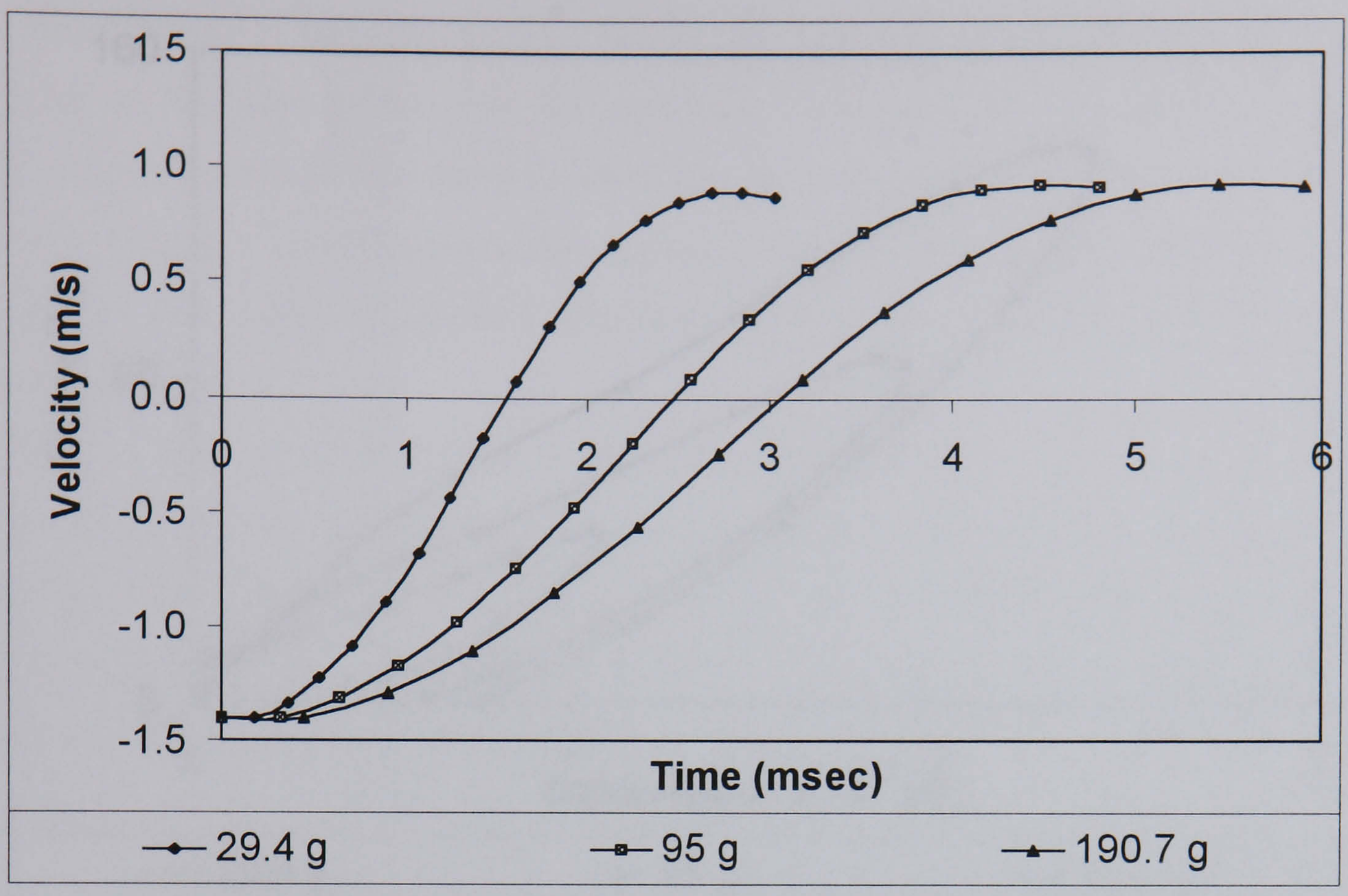

Figure 4.7. Velocity during the first contact (Negative indicates downward movement).

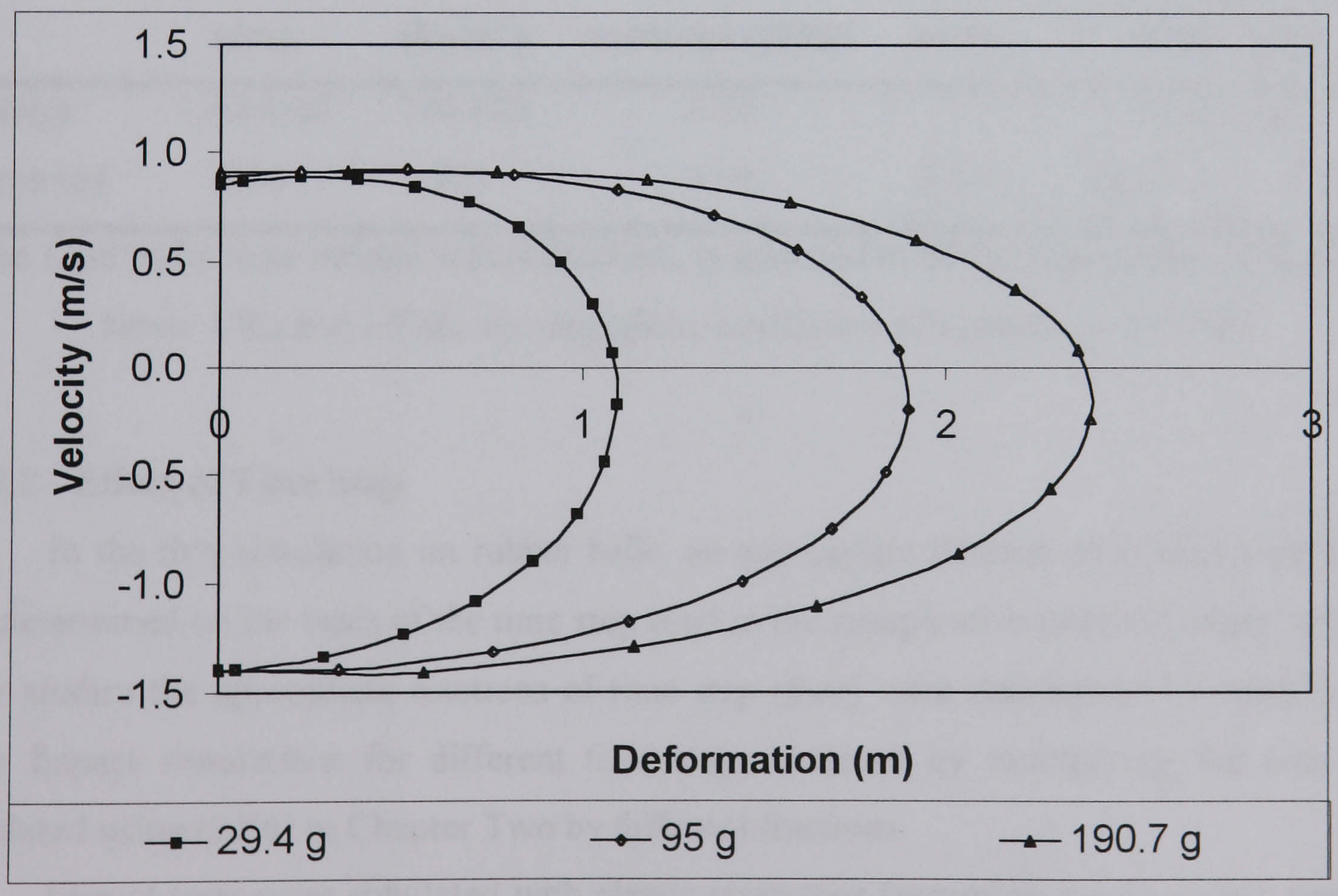

Figure 4.8 Velocity versus deformation during contact

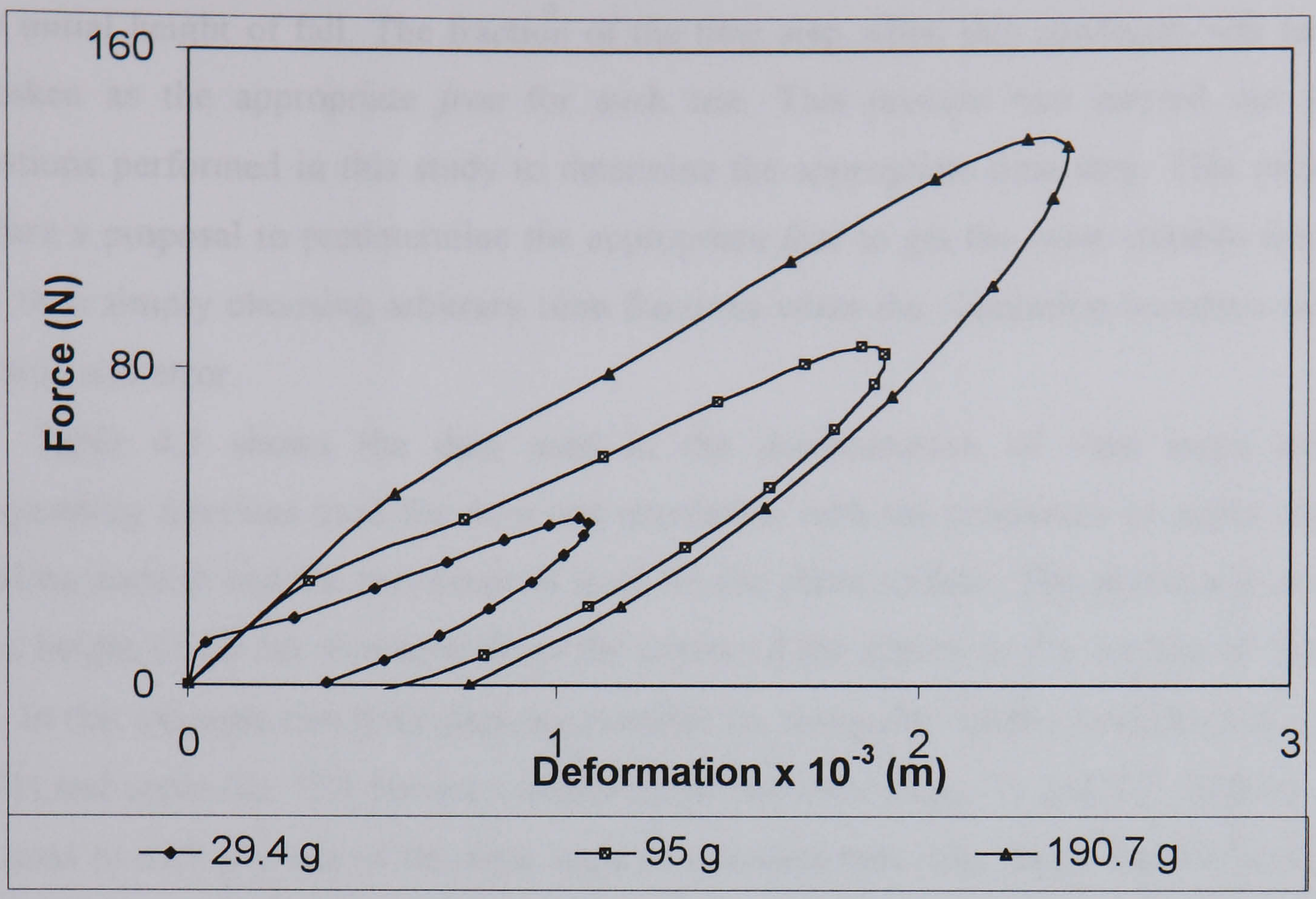

Figure 4.9 Force-Deformation curves

Table 4.2 Properties of apple used in simulation (Mohsenin, 1986)

	Diameter (cm)	Density (kg/m^3)	Elastic modulus (MPa)	Poisson ratio	Friction coefficient	
					Wall	Ball
Range	5.00-8.00	700-900	1-10	-	0.32-0.44	
Selected	7.00	801	4.66	0.31	0.35	0.35

(The rigid walls have infinite radius and EM_w is assumed to be far greater than of the fruit hence $1/R_w$ and $1/EM_w$ are negligible, coefficient of restitution: 0.4-0.8)

4.2.2.2 Effect of Time Step

In the first simulation on rubber balls, an appropriate fraction of critical time (*frac*) was determined on the basis of the time step used in the comparative physical experiment. In other studies the appropriate fractions of time step (*frac*) were determined by carrying out some impact simulations for different time steps obtained by multiplying the time step calculated using (2.86) in Chapter Two by different fractions.

Impact tests were simulated with elastic properties (assuming purely elastic particle) to obtain the variation in the behaviour due to the effect of the duration of the time step. The particle, when dropped from a height, is expected as an elastic material to bounce continuously with the same maximum force at each impact and the ball should be rising back

to the initial height of fall. The fraction of the time step when this condition was satisfied was taken as the appropriate *frac* for such test. This process was carried out for all simulations performed in this study to determine the appropriate time step. This method is therefore a proposal to predetermine the appropriate *frac* to get the most suitable time step rather than simply choosing arbitrary time fractions when the simulation becomes unstable or by trial and error.

Table 4.3 shows the data used in the determination of time steps and the corresponding fractions used for drop test simulation with the properties of apple used for the falling particle and the properties of steel for the plane surface. The object was dropped from a height of 20 cm measured from the centre of the sphere to the surface of the rigid plane. In this example two time steps are possible i.e. using the rigidity modulus (G) of steel (for T1) and apple (for T2). Having calculated the two time steps, T1 and T2, different *fracs* were used to multiply one of the time steps to calculate new time steps. Each of these was used in impact simulation and the results plotted. Figure 4.10 – 4.12 shows the results obtained for some of the *frac* tabulated in Table 4.3.

From Figures 4.10 - 4.12 show the force–time, displacement–time and the contact and escape velocity. Stable conditions with minimal errors were obtained with time steps less than or equal to 5.66×10^{-05} corresponding to *fracs* of 33.4 and 0.10 for time steps T1 and T2 respectively. With these time steps, uniform peak contact force of 203 N was obtained in all the contacts from which the first three are plotted (Figure 4.10). Also the particle rose back to the same height during the process (Figure 4.11) while the escape velocity was the same as the contact velocity during the first contact (Figure 4.12) when these fractions were used. In the other cases the escape velocity after the first contact was less than the contact velocity and this led to the loss of height (Figure 4.11) and eventually a lower peak force during the second contact. This process was repeated for the other contacts leading to gradual reduction of peak force in subsequent contacts, a phenomenon associated with energy dissipation not expected for elastic case as will be seen later. This process was as a result of the size of the time step, which determined the range of time at which data were recorded. With a wider time range the peak position may fall in between range hence it may not be recorded or calculated. Using a very high time step will result in excessive stepwise movement which may result in excessive contact force (a particle entering too deep into the other or the surface). It may also result in lack of contact as a result of the falling particle position being below the plane surface at a time when contact is expected. This will lead to the particle falling indefinitely i.e. outside the area of interest.

From the above it can be seen that for this particular case the smallest time step T1 is suitable as it is less than the determined time step and can be chosen as the time step. However this may not be applicable in all cases and also in this case this time step is far less than the minimum possible. Therefore using the *frac* will increase the time step and consequently reduce the number of iteration cycles during simulation saving computer time and memory.

Table 4.3 Material stiffness properties and fraction of critical time step

***Frac* for time step calculated with the following shear modulus, G (N/m^2)**			
s/no	**G (Steel plate) = 76.33×10^9 N/m^2, Time step = 1.69516×10^{-6} s = T1**	**G (Apple) = 17.95×10^5 N/m^2, Time step = 5.66346×10^{-4} s = T2**	**Time step obtained**
frac1	3.34	0.01	5.66×10^{-6}
frac2	16.70	0.05	2.83×10^{-5}
frac3	33.40	0.10	5.66×10^{-5}
frac4	167.00	0.50	2.83×10^{-4}
frac5	334.00	1.00	5.66×10^{-4}

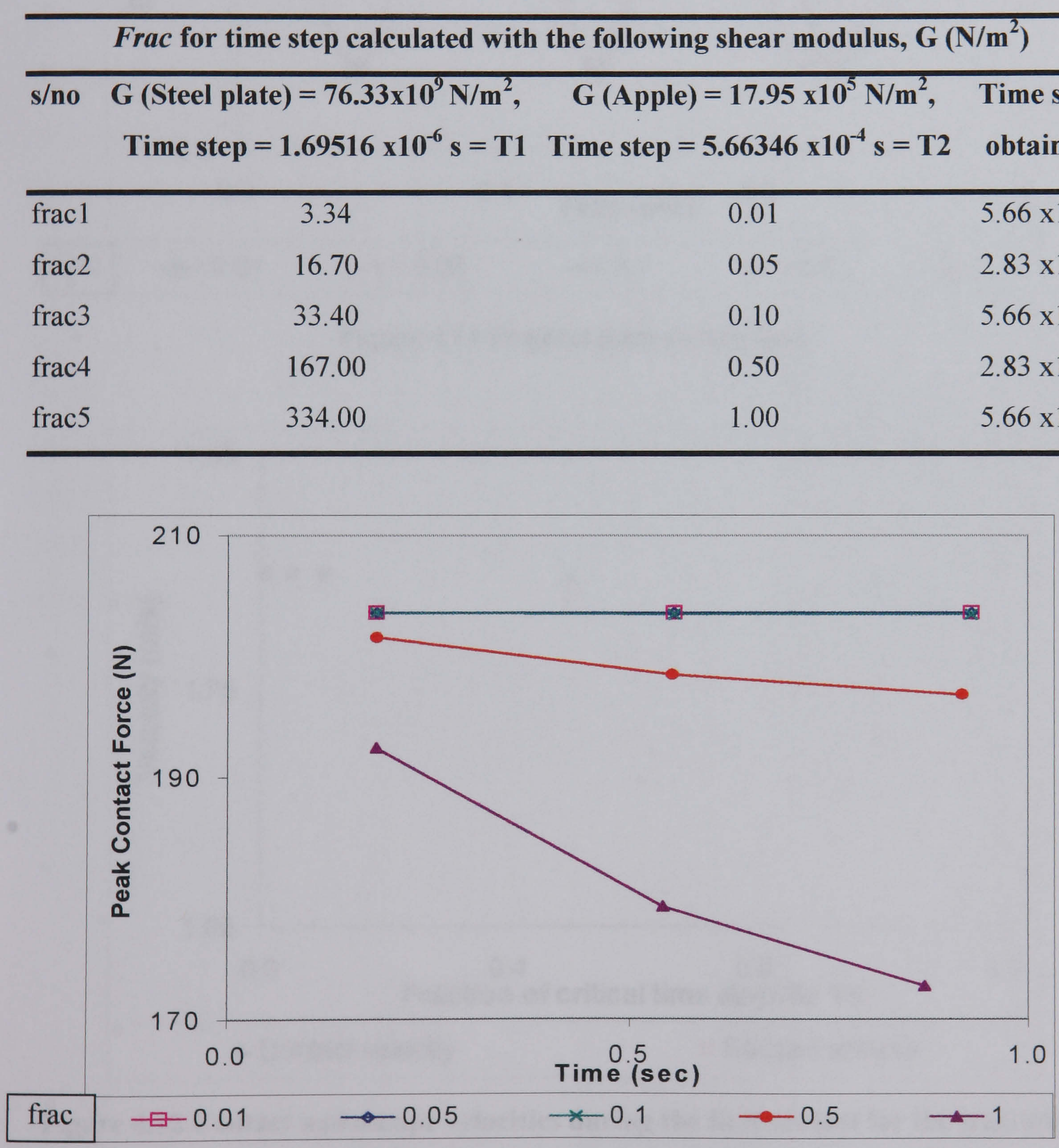

Figure 4.10 Peak force during the first three contacts of apple falling on heavy and rigid plane surface (The fractions of time step are shown in Table 4.3)

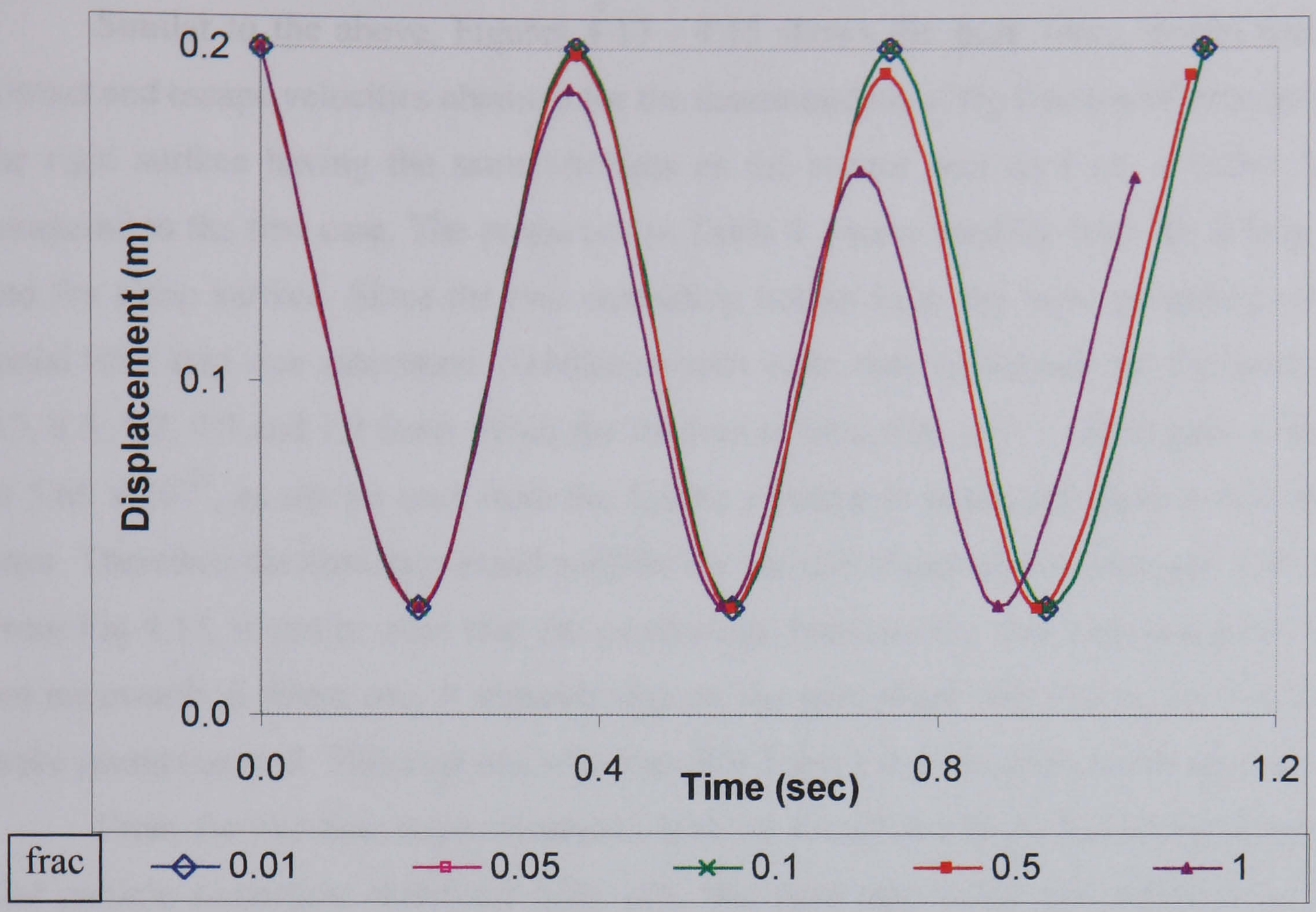

Figure 4.11 Displacement versus time

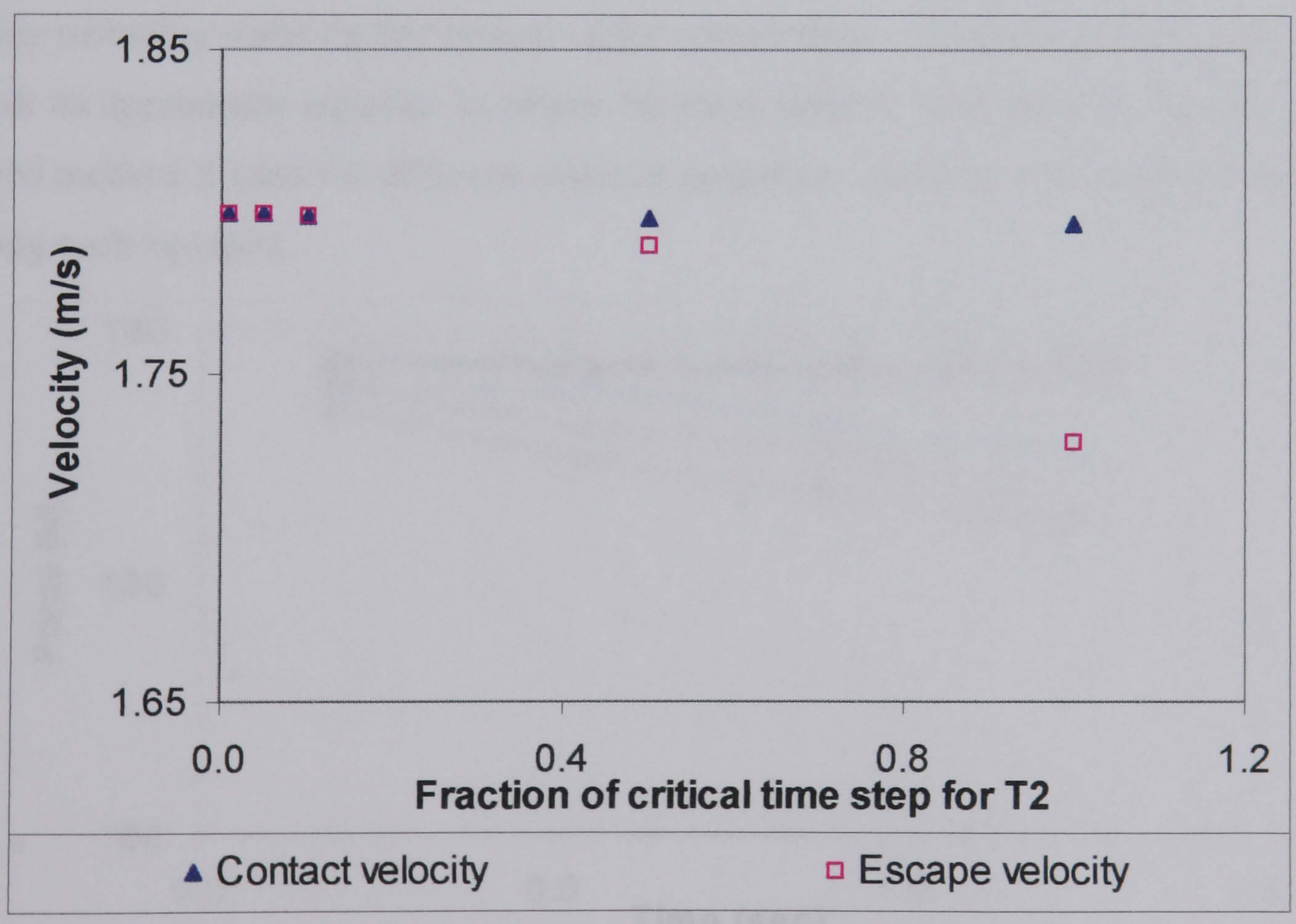

Figure 4.12 Contact and escape velocities during the first contact for the fractions of time step in Table 4.3

Similar to the above, Figures 4.13 - 4.15 shows the peak force, displacement and contact and escape velocities obtained for the determination of the fraction of time step when the rigid surface having the same stiffness as the sphere was used i.e. a softer material compared to the first case. The properties in Table 4.2 were used for both the falling sphere and the plane surface. Since the two contacting bodies have the same properties only one initial time step was calculated. Simulation tests were then performed for fractions of 0.1, 0.3, 0.5, 0.7, 0.9 and 1.0 from which the fraction of time step of 0.1 which gave a time step of 5.66×10^{-05}, as can be seen from the figures resulted in stable calculation with minimal error. Therefore the time step found suitable for particle to particle contact was 5.66×10^{-05}. From Fig 4.13, it can be seen that the relationship between the time step and peak force is not necessarily a direct one, it depends also on the immediate step before the two surfaces make contact as well. This explains why frac of 0.7 and 1.0 deviated from the normal trend.

From the two time steps calculated, both are found to stabilised at the same time step. The particle–to-particle stabilised fully with this time step while full stabilisation for the particle-to-wall time step (Figure 4.10) was at a lower time step. In order to ensure adequate precision, a time step less than the above value is recommended for simulation of any assembly including walls for the system under consideration. A separate study is required to establish an appropriate equation to obtain the most suitable time steps for simulation. The proposed method if used for different material properties could be a promising approach at obtaining such equation.

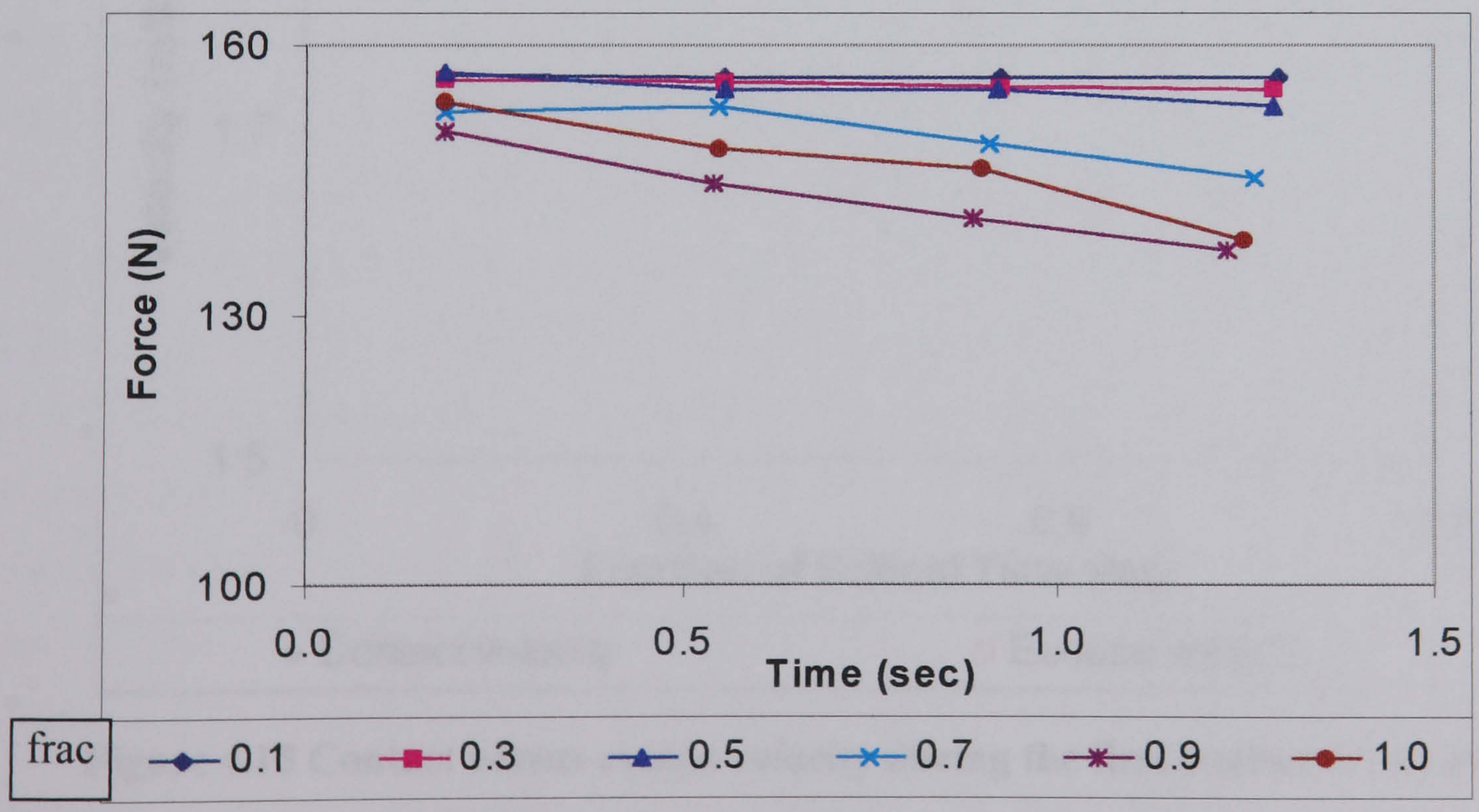

Figure 4.13 Peak force during the first four contacts of apple falling on a plane surface with same material properties at different fractions of time step

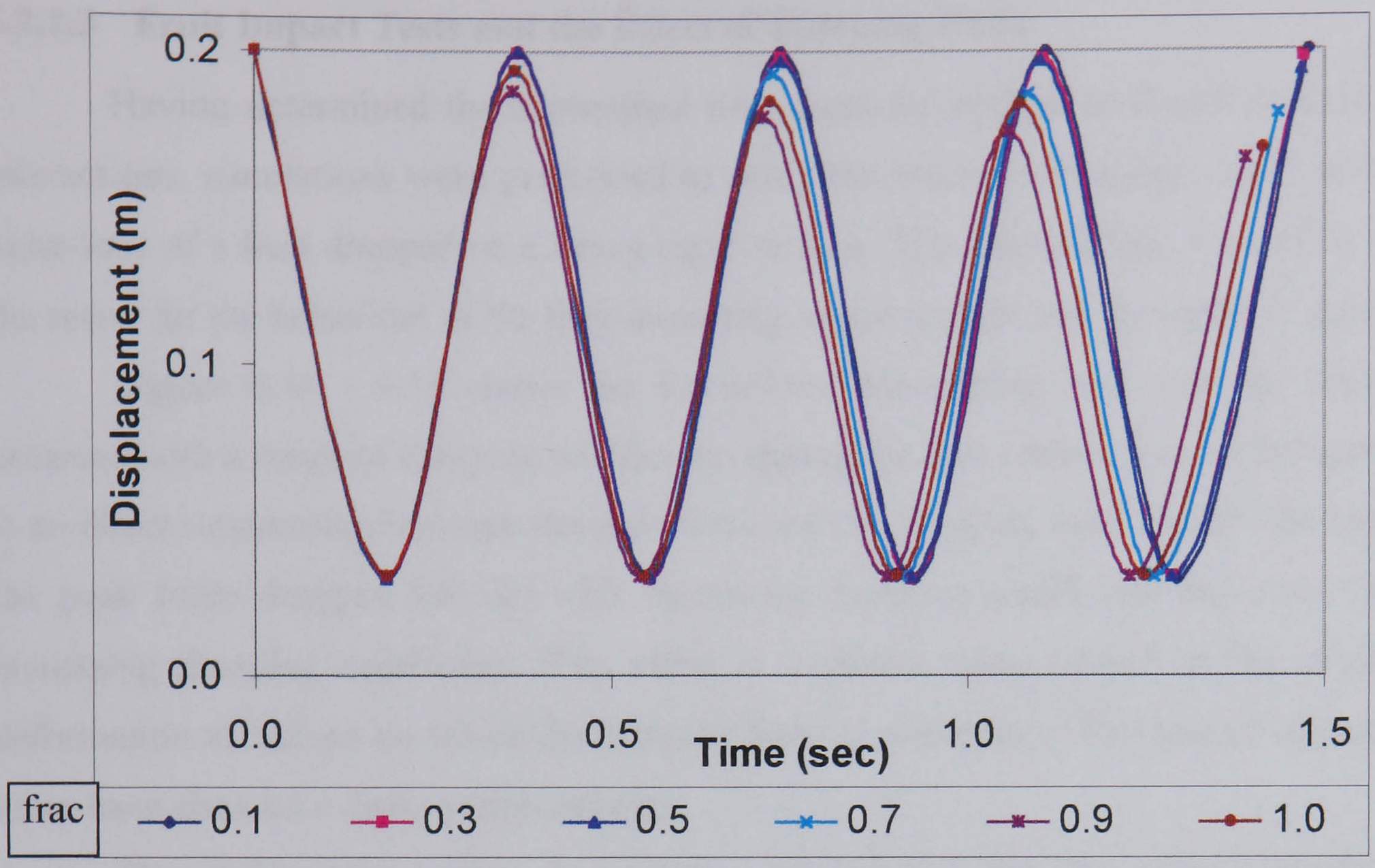

Figure 4.14 Corresponding displacement versus time curve during the first four contacts for apple falling on a plane surface with same stiffness different fractions of time step

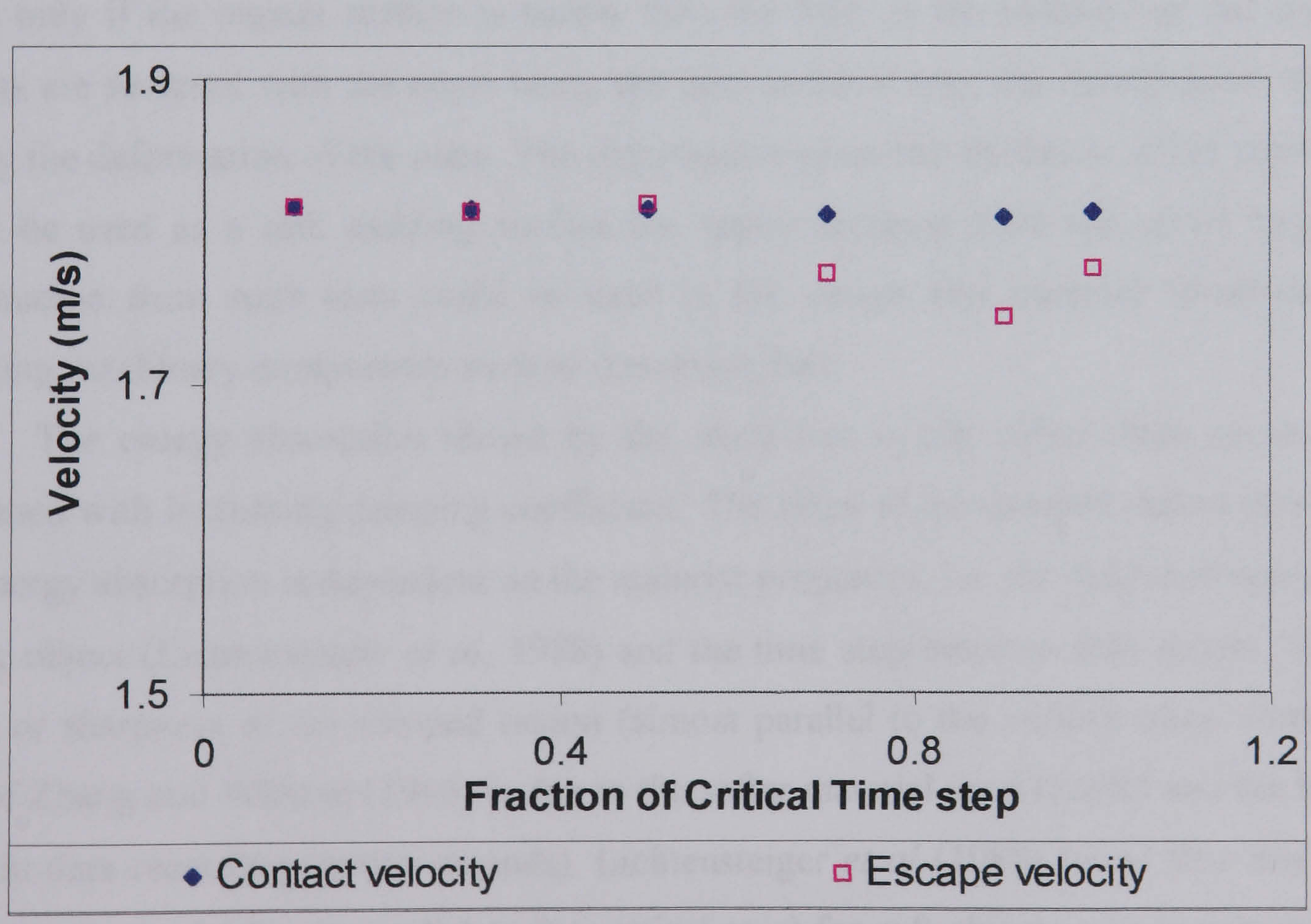

Figure 4.15 Contact versus escape velocity during the first contact for apple falling on a surface with same stiffness.

4.2.2.3 Fruit Impact Tests and the Effect of Damping Ratio

Having determined the appropriate time steps for particle-wall and particle-particle interactions, simulations were performed to study the effect of damping coefficient on the behaviour of a fruit dropped on a heavy rigid surface. The results (Figs. 4.16-4.21) serve as the result for the behaviour of the fruit impacting a hard surface and the effect of damping.

Figure 4.16 - 4.18 shows the force-time, deformation and velocity time curves obtained with a range of damping coefficients during the first contact. From the figures there is no direct relationship between the peak force and the damping ratio. Within the range used the peak force dropped initially with increasing damping coefficient but later rose with increasing damping coefficient. This effect is a phenomenon related to the velocity and deformation variations on which the damping force is dependent. The time of contact on the other hand showed a direct proportionality.

The deformation curve is perfectly symmetrical for the elastic condition (no damping) while the skewness increased with increasing damping resulting from longer time for recovery process. This is in agreement with the theoretical results of Zhang and Whitten (1996) shown in Figure 2.15. The deformation determined represents the deformation in apple only if the impact surface is harder than the fruit. If the stiffness of the contacting objects are reversed with the apple being the hard material then the deformation represents purely the deformation of the plate. The deformation gives the thickness of the material that could be used as a safe padding surface for apples dropped from the given height. The information from such tests could be used in the design and material specification for handling machinery components such as conveying belt.

The energy absorption shown by the sharp rise in the initial slope on the curves increased with increasing damping coefficient. The slope of the damped region representing the energy absorption is dependent on the material properties, i.e. the degree of homogeneity of the object (Lichtensteiger *et al*, 1988) and the time step between data points. The steep slope or sharpness of the damped region (almost parallel to the y-axis) when compared to that of Zhang and Whitten (1996) is due to the softer material used (apple) and the time step used in data recording (micro seconds). Lichtensteiger *et al* (1988) found that this slope is more pronounced (almost parallel to the vertical axis) for soft objects with tough skin which they referred to as the skin effect but this is not modelled in this study.

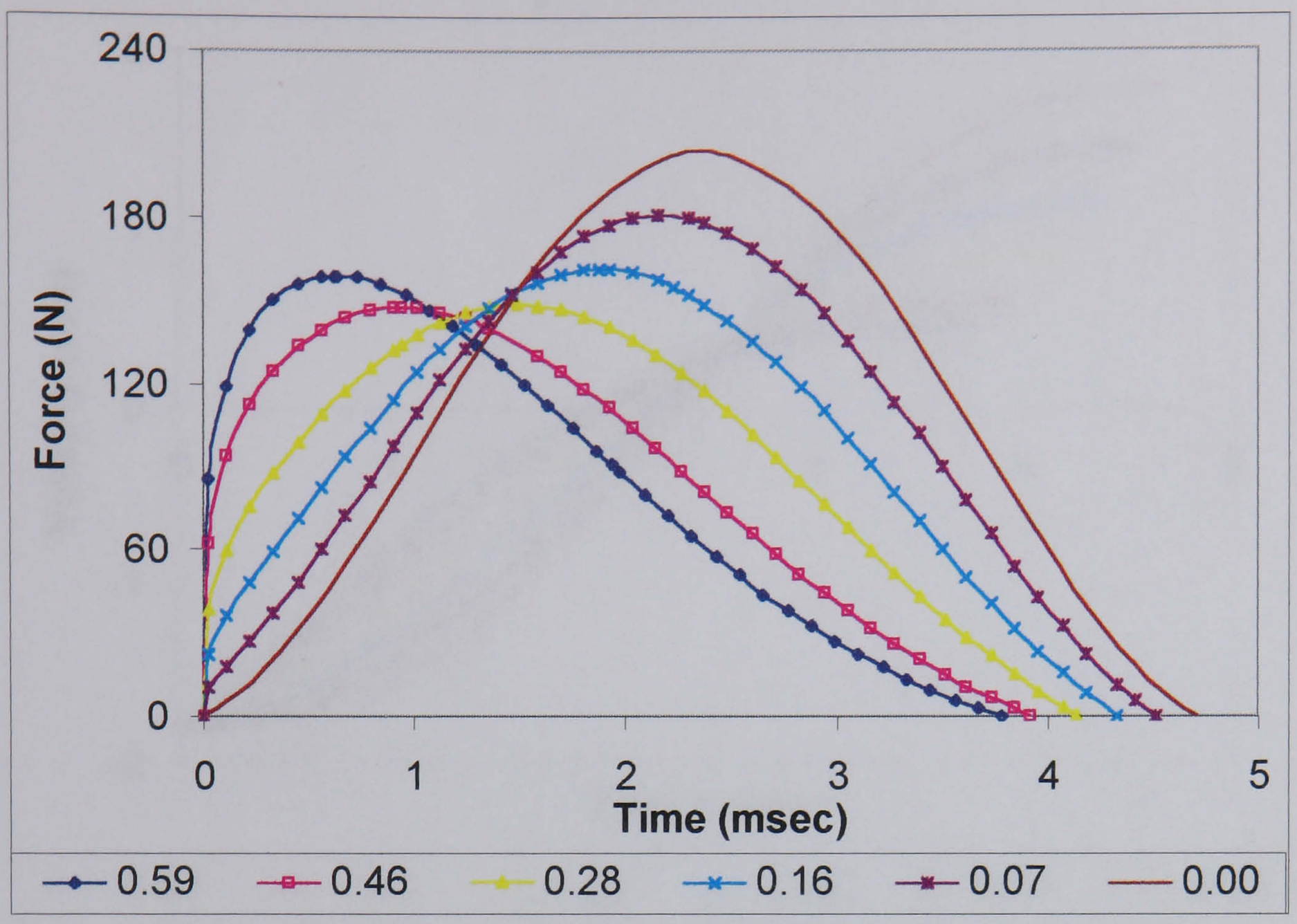

Figure 4.16 Force-time relationship for different damping coefficient for apple falling on a rigid flat surface

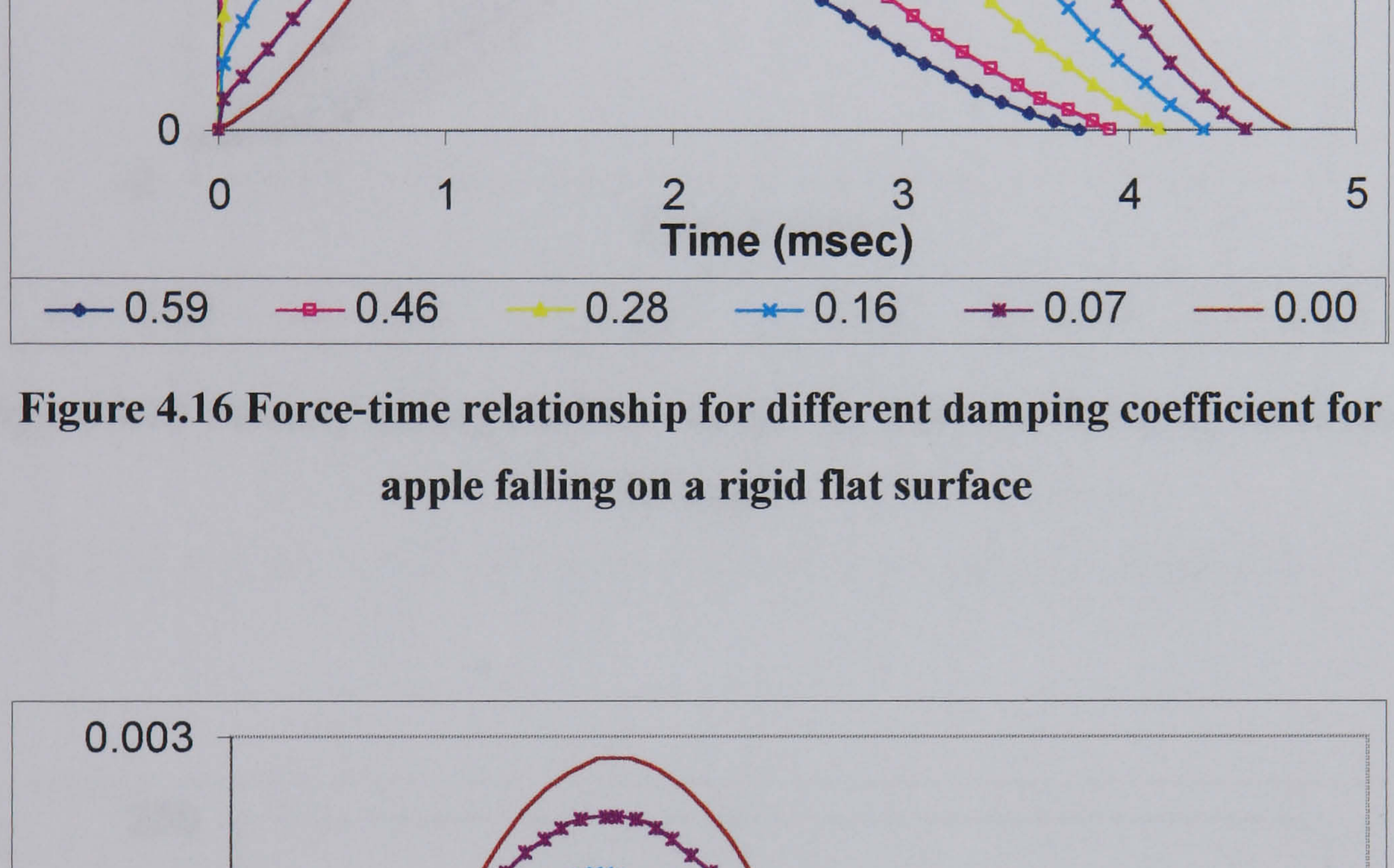

Figure 4.17 Deformation at contact for different damping coefficient for apple

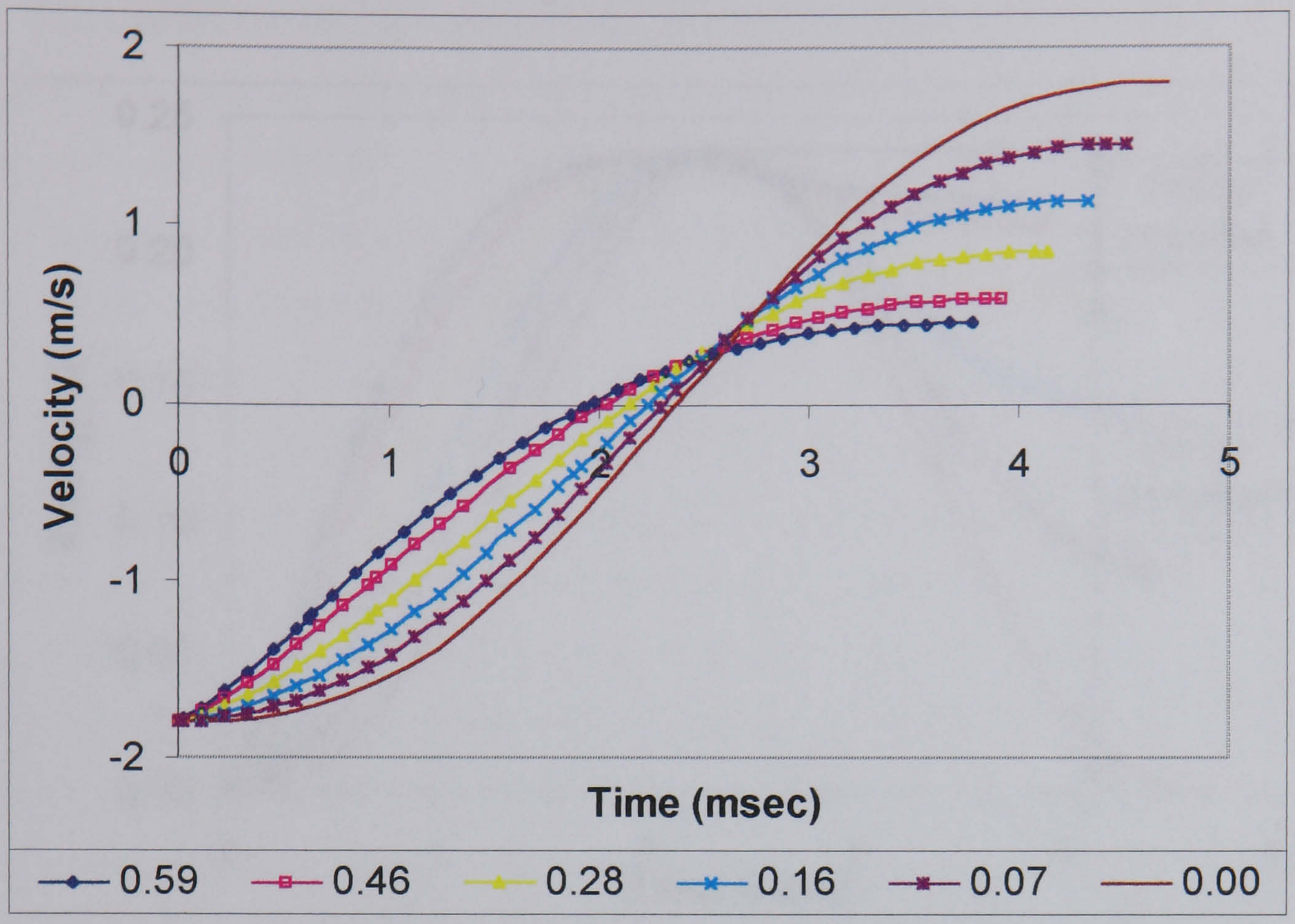

Figure 4.18 Velocity during the first contact for different damping coefficient for apple

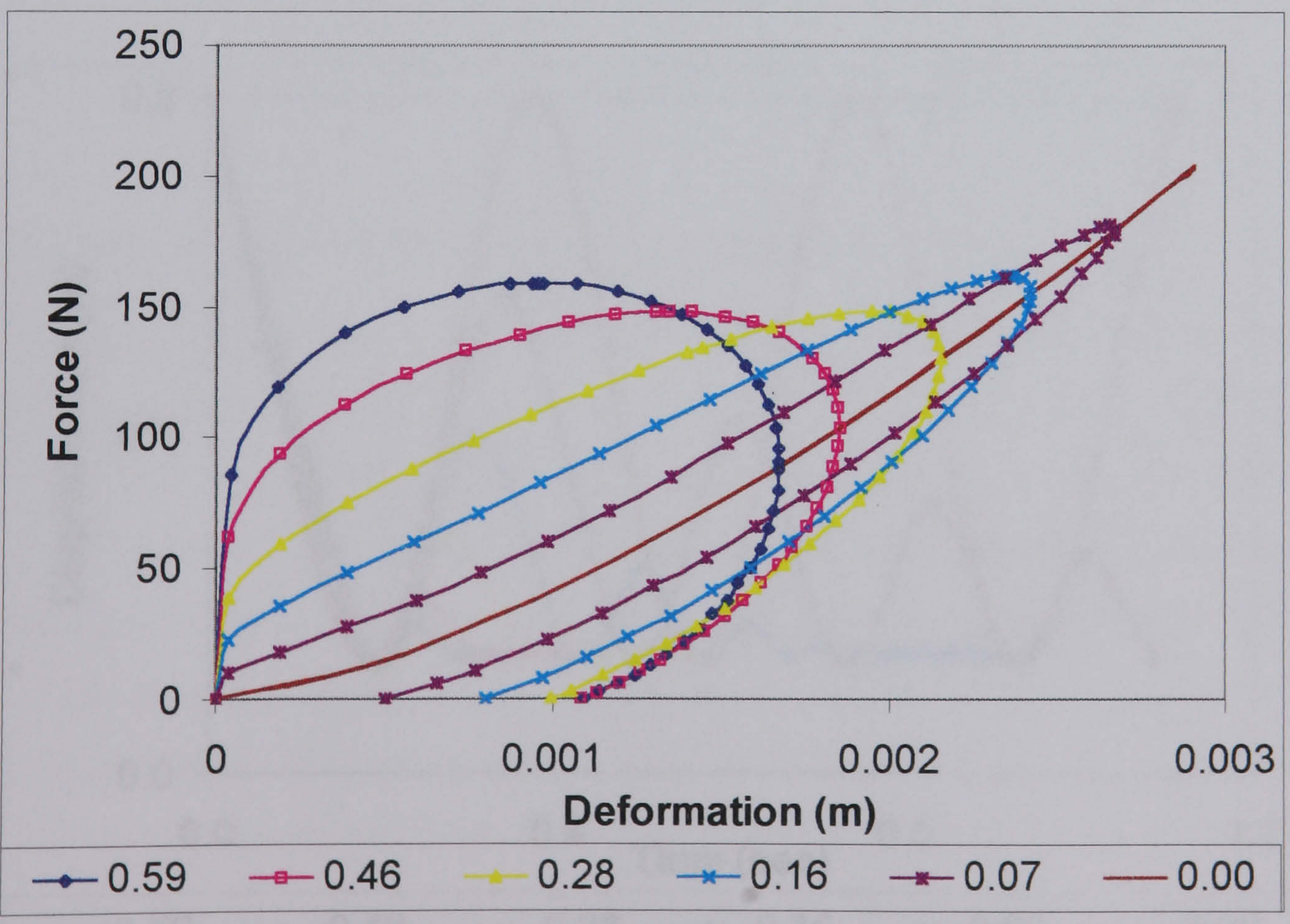

Figure 4.19 Force-Deformation relationship for different damping coefficient for apple

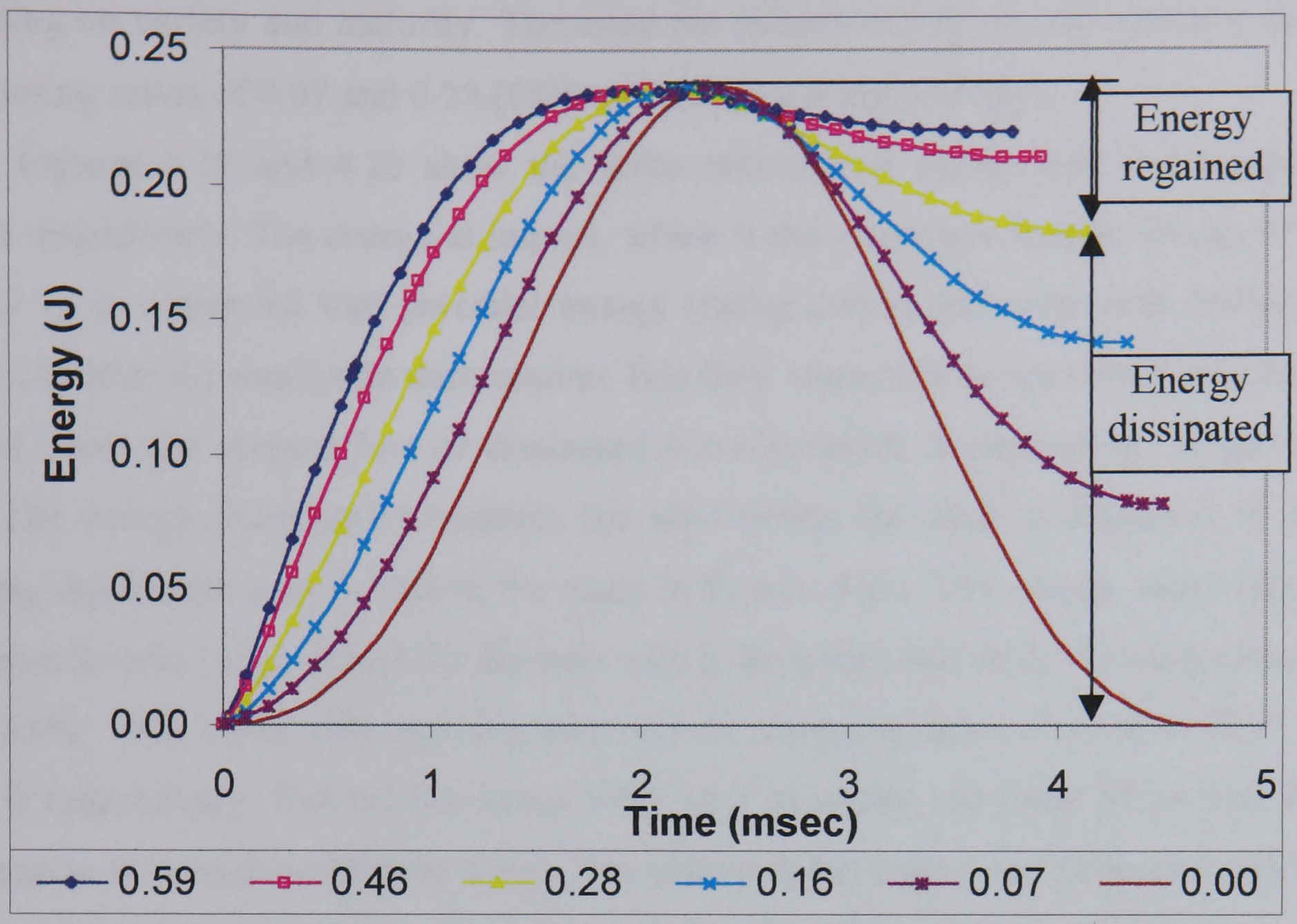

Figure 4.20 Energy used with time during contact

(The energy dissipated and regained are labelled for damping coefficient of 0.28)

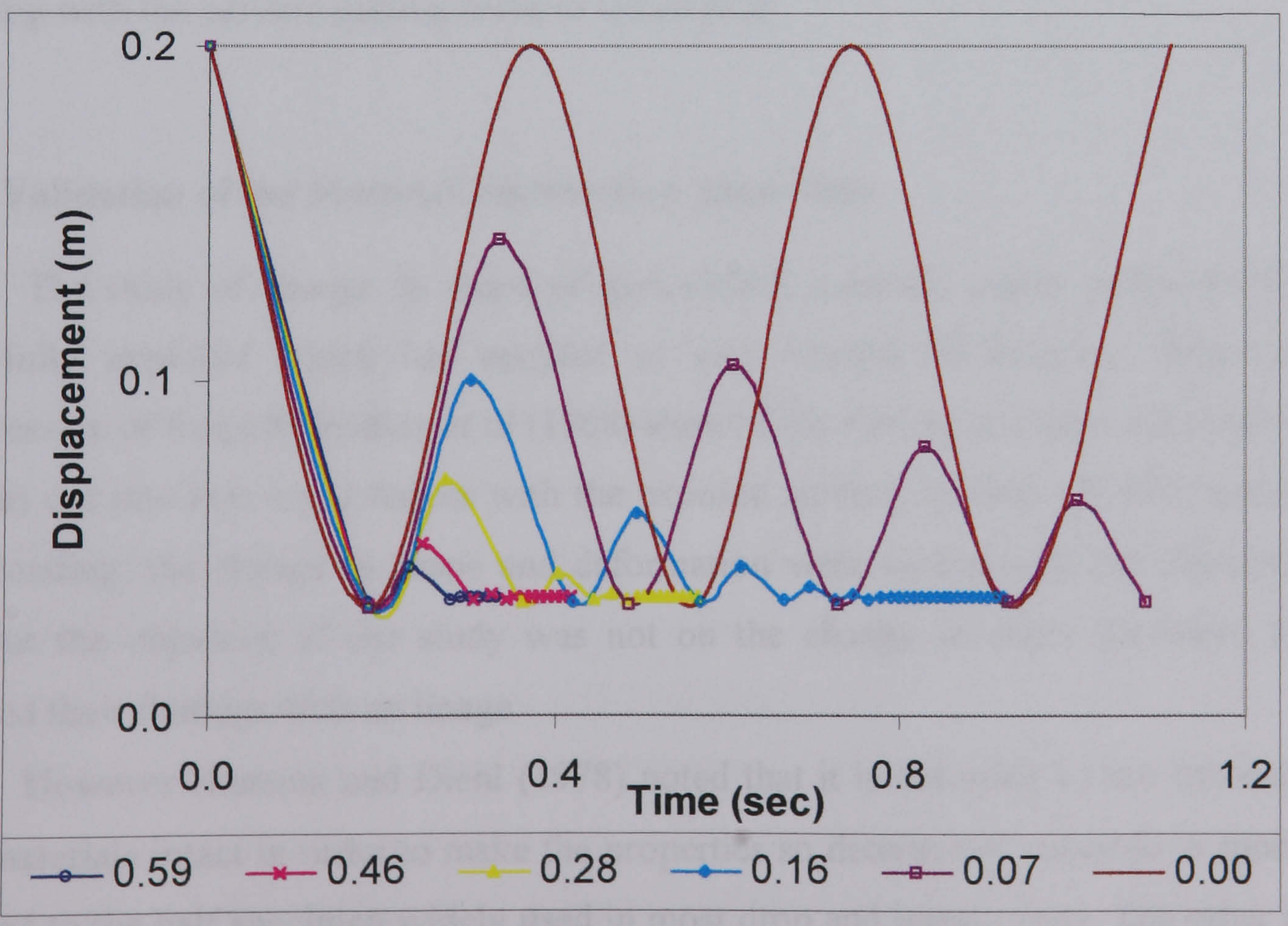

Figure 4.21 Particle movement

The coefficient of restitution (COR) of apple reportedly lies between 0.4 and 0.7 depending on variety and maturity. Therefore the behaviour lies on and between the curves for damping ratios of 0.07 and 0.28 (COR of 0.8 and 0.4 respectively).

Figures 4.19 and 4.20 show the force-deformation curves and the energy during contact respectively. The energy at impact, which is the maximum kinetic energy of the ball (0.2369 J), is converted into potential energy (rising curve) and recovered (falling curve) (Fig. 4.20) after the maximum deformation. It is fully recovered in the elastic case and in the damped cases the amount lost or dissipated (un-recovered) is dependent on the damping ratio. The energy dissipated represents the area within the loop in Figure 4.19 for each damping coefficient and is shown for each in Figure 4.20. The energy was almost fully converted to heat i.e. absorbed for the case with a damping ratio of 0.59 losing almost 90 % while 85%, 75%, 60%, 35% and 0% were lost for damping ratios of 0.46, 0.28, 0.16, 0.07 and 0.0 respectively. For all the cases with high damping the peak force and the peak deformation occurred at different times. The displacement-time curve (Figure 4.21) showing the movement during the entire process for each case until the particle came to rest, showed that at damping ratio of 0.59, the system was almost fully damped. This may not be applicable to apple, as it may not have a damping ratio of 0.59 except when rotten but served to illustrate the effect of damping. The range applicable to apple fruit as stated earlier is between 0.07 and 0.28. It is expected that damping ratio greater than 0.59 will result in full damping with the particle getting stuck to the surface.

4.3 Validation of the Material Distribution Algorithm

The study of change in shape of agricultural materials under compression has not been fully explored which has resulted in very limited information. Experiments on compression of fruits by Fridley *et al* (1968) showed the change in shape and deformation of peaches cut into two equal halves with the exposed surface marked off with grids. During plate loading, the change in shape and deformation were visible with the changing square grid but the objective of the study was not on the change in shape therefore they only reported their findings with an image.

However Hamann and Diehl (1978) noted that it is desirable to test inhomogeneous food materials intact in order to make the properties so determined valuable in modelling as opposed to the half specimen widely used in most drop and impact tests. The other report on this study is the work of Anazodo and Chikwendu (1983) on the compression of cylindrical

shaped objects. However this is a 2D scenario that is not applicable to most non-cylindrical agricultural materials.

An algorithm for modelling the change in shape of spherical materials (3D) derived from Arzt's approach (Arzt, 1982) was incorporated into the DE programme developed for this study. Models developed for materials exhibiting complex behaviour are generally validated by using simple objects that are close in shape and properties to the real objects or by simple comparison with available results from the literature. Normally a separate experimental study is needed in order to obtain information that could be used for comparison and correlation with the result from the simulation but this is hardly carried out. In this study, the model for the shape change was validated using spherical synthetic materials and the results validated against those from experiments set up using the same materials and a natural biomaterial.

In this section a brief description of the experimental work carried out to obtain the information required for the deformation and shape change of spherical materials under compression is presented. The theory and method of image processing used for analysis of the images taken during the experiment to obtain information for comparison with simulation results are also discussed.

4.3.1 Experimental Apparatus

Compression test of bulk systems requires that the particles be placed in a test box or an enclosure, which should be able to withstand the resulting wall pressure. A clear view of the system is also necessary to obtain images of the balls as they deform. A test box rig satisfying these requirements was designed and constructed for the experimental studies.

The test box, shown in perspective in Figure 4.22 consisted of the main frame made up of eight 3mm thick 30mm angle iron bars. The base and the upper support frames had slotted holes for adjusting the system width by moving of the vertical frames. The lateral movements of the vertical frames were prevented during loading by two bolts. The side-walls were formed from a combination of 6mm thick 30 mm wide steel bars. The number of these bars combined determined the width of the side-wall. The front and back of the assembly were covered with transparent Perspex to enable a clear view of the particle arrangement and deformation before and during operations. These Perspex covers were positioned through the gap between the frames and the side-walls which acted as supports on all the edges to prevent buckling. Two compression plates with appropriate studs or

connecting bars for attachment to a compressive machine were also designed for the system. All the parts of the rig were made separately and connected together by bolts and nuts making it easy to connect and dismantle. The slotted holes for frame movement and the combination of a number of bars making up the side-wall made the test box dimension adjustable in width and length to accommodate balls of different sizes.

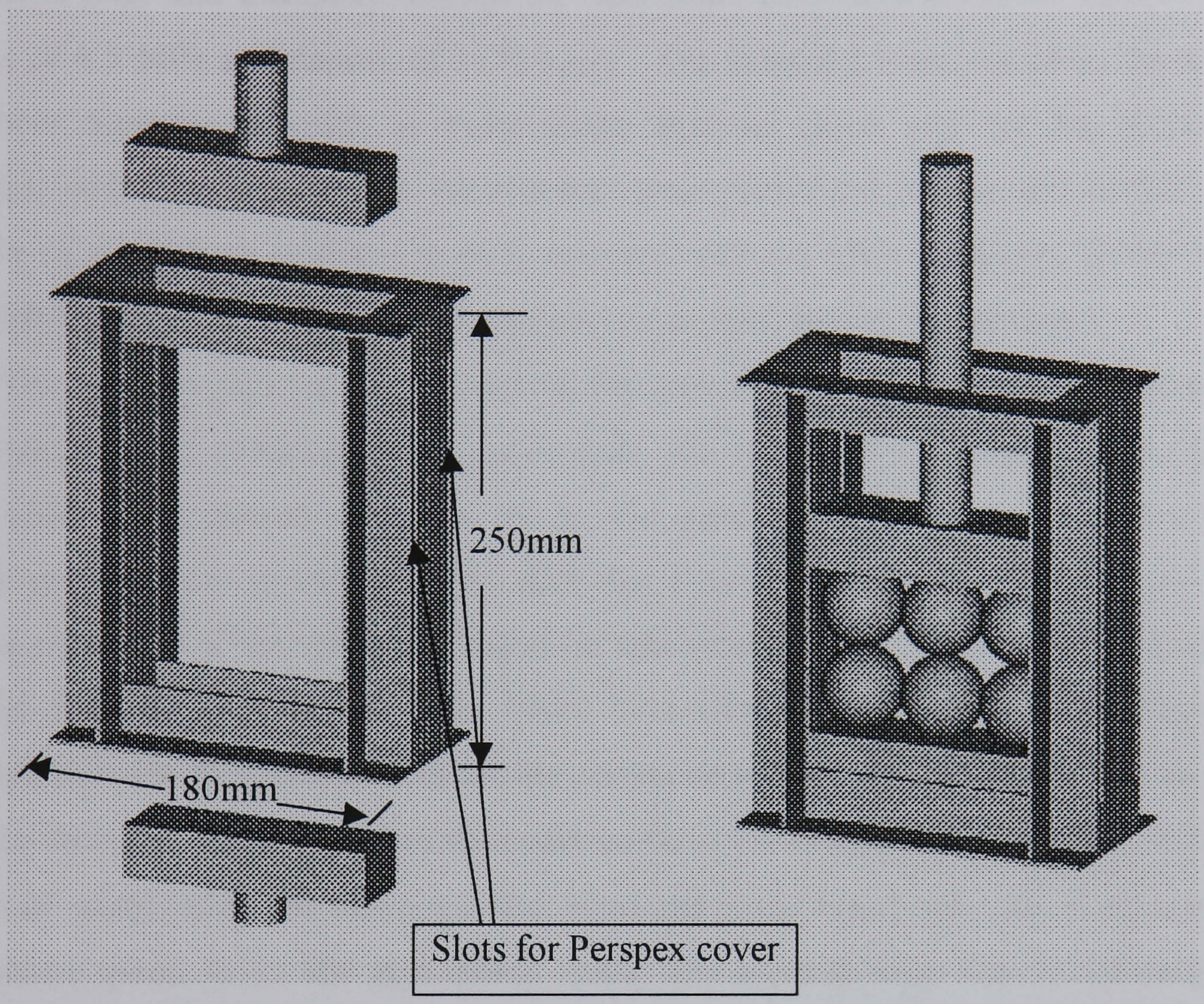

Figure 4.22 CAD perspective view of the test box (left) and the test box loaded with six spheres (right).

4.3.2 Imaging

Images of the system were taken using a CCD camera set up on the same plane as the compressive machine and positioned such that the view was orthogonal to the major vertical plane of the test box. The camera was connected to a PC and frames were grabbed using a Sprynt 40MHz 1870 frame grabber (Synoptics Limited, Cambridge UK) via a software interface (PC Image Foster Findlay, Newcastle, UK). Images were displayed on another screen monitor connected to the PC and grabbed at a predetermined time or strain interval during loading and then saved as digitised image. Background lighting was provided using two florescent tubes (35Watts) placed in a light box covered with 3mm thick translucent Perspex to diffuse the light resulting in clear white background. Front lighting consisted of two Tungsten bulbs (40W) attached to the upper part of the frame holding the camera.

4.3.3 Experimental Procedure

Experiments were conducted to validate the simulation process using spherical rubber materials with physical properties, which are close to some fruit and a bed of rapeseed in single column. (the set-up procedures are described in 4.4). The 33mm diameter rubber balls (Ley and Company, Liverpool) were made from natural rubber with an elastic modulus of 6.5 MPa and density of 1196 kg/m^3. The sphere(s) were placed in the test box one sphere diameter in width to make image analysis easier and for the purposes of correlation with simulation results. Experiments were carried out on one sphere (S1) and an assembly of six spheres arranged in three columns with the spheres directly on top of each other (S6R) or diagonally (S6D). This resulted in two rows for the six spheres.

The test box (rig) was set in place on the compressive machine for each experiment having adjusted the chamber to the appropriate size in length and breadth and the balls placed inside. The camera was then set on the same plane as the compressive testing machine and the focus of view adjusted such that a parallel or close to parallel view of the rig and a clear view of the spheres arrangement was obtained. The lighting was then adjusted to obtain clear background and front views. Live viewing and capturing of images was controlled from the PC. Having obtained the correct view, the compressive die was moved to a position such that it just contacted the upper surface of the upper layer of sphere(s) prior to the start of compression. At this point, the stress and strain scales were set to zero, and the compression speed set to the appropriate value. The spheres were then compressed uni-directionally by loading from the top via the flat loading plate connected to the load cell and driven by the compressive testing machine.

Force and displacement during compression were recorded via a data logger connected to the compressive machine. The deformation of the assembly observed through the camera positioned orthogonal to the major vertical plane of the box was captured at equal strain interval and stored in Tiff file format. Figure 4.23 shows the experimental set up with all the components connected.

4.3.4 Image Analysis

The captured images normally contained some parts of the frames and plunger, therefore, the first task was to segment the image, i.e. subdivide the image into its constituent parts or objects to extract the object of interest. This analysis was convenient using a

parts or objects to extract the object of interest. This analysis was convenient using a combination of image processing software on the PC (Paint Shop Pro) and the UNIX platform (XV).

The images were transferred to the Unix platform before or after the extraction depending on the method used for extraction and further image analysis and processing carried out using programmes written in Fortran. These analyses produced data and digital image files for shape and other features extracted, which are needed for comparison with the simulation results.

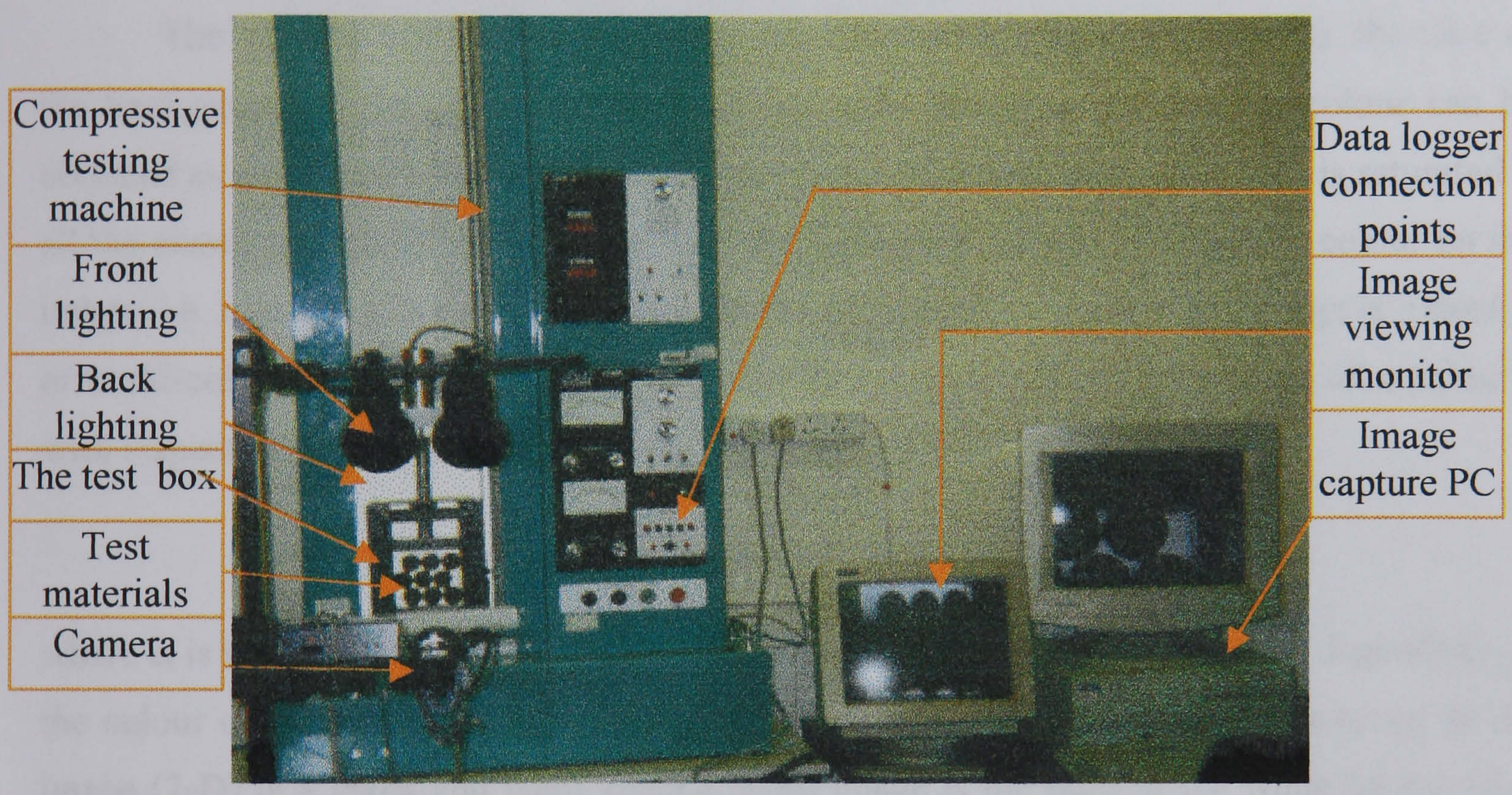

Figure 4.23 Full view of the experimental set-up

4.3.4.1 Image Extraction and Segmentation

A finite subset matrix [A] with elements a(f, g) can be extracted from a set of integral lattice points z(i, j) of a super-matrix [Z] having a set of Z x Z lattice points representing a particular digital image. In this super matrix [Z] a digital image with matrix [A] whose grey scales a(f, g) lie within z(m-k, n-r) is related to any element of [Z] matrix by $z_{p,q} = a_{p+1-k,q+1-r}$ where (from Figure 4.24) i and j are row and column number of element/pixel in [Z], f and g are elements position in [A] with $k \leq p \leq m$, $r \leq q \leq n$, $f = m - k$ and $g = n - r$. Using this matrix representation of images, parts or whole images can be pieced together, segmented, expanded or reduced by applying the normal arithmetic rules of matrix (Dougherty and Giardina, 1987). This principle was used in algorithm development for image analysis in this study.

(a) $\begin{bmatrix} z_{11} & - & - & - & z_{1j} \\ & - & - & - & \\ - & - & z_{kr} & z_{kn} & - & - \\ - & - & - & - & - \\ - & - & z_{mr} & z_{mn} & - & - \\ & - & - & - & \\ z_{i1} & - & - & - & z_{ij} \end{bmatrix}$ (b) $\begin{bmatrix} z_{kr} & - & z_{kn} \\ - & - & \\ z_{mr} & - & z_{mn} \end{bmatrix} = \begin{bmatrix} a_{11} & - & a_{1g} \\ - & - & \\ a_{f1} & - & a_{fg} \end{bmatrix}$

Figure 4.24 (a) Matrix representation of an image and (b) Extracted image

4.3.4.2 Information Density or Porosity

The porosity (voidage) of an image or separation to different colour i.e. the ratio of the background to the object or other colours with respect to a reference colour can be obtained as a measure of the pixel information density for each part. An image is saturated if all the elements (pixels) in the matrix have the same grey scale representing a colour on the image, i.e. it is a single coloured image. On the other hand an unsaturated image is a double or multi-coloured image and the density $u(e_i)$ is a measure of the percentage of a colour i with respect to all the colours making up the image.

$$u(e) = \frac{e_i}{E} \qquad 4.1$$

where $\mathbf{e_i}$ is the number of pixels with grey scale i or less than or greater than i, depending on the colour of interest and **E** is the total number of pixels in the image. The porosity of the image (2-D) in a black and white (background) image is the ratio of the white background pixels to the total pixels in the image. The porosity of an image taken for a single column stack of sphere can be obtained with this method.

4.3.4.3 Thresholding and Edge detection

In image processing the shape features of objects can be obtained by tracing or detecting the edges. This method was used in this study to extract the shape and deformation of objects during loading. In an image, an edge is the boundary between two regions with relatively distinct grey levels and a form of threshold can be used to detect edges. Threshold provides perhaps the most obvious way of locating objects in grey scale images (Davies, 1991). It is also a method used to extract a figure or a feature of a particular interest from within an image. This is different from the segmentation where a portion (rather than feature of an object) within the image is extracted. The threshold generator, THRESH, produces binary image or an image having only two grey scales or range of grey scales (Dougherty

and Giardina, 1987). All grey scales less than or greater than a particular grey scale or a range are threshed (discarded) or their values changed to the same scale (0 or 1 for binary image) and the reference scale retained or changed to another. THRESH is defined generally for an image z(i, j) within a grey scale of $0 \leq t \leq p$ having a total pixel of (i x j) and t as the reference scale as

$$\text{THRESH}(z;t)(i,j) = \begin{cases} t & \text{if } z(i,j) \geq t \\ * & \text{if } z(i,j) < t \end{cases} \qquad 4.2$$

A modified THRESH operator was used for edge detection of images in this study i.e. instead of thresholding the intensity of the image, an edge map which produced only the object boundaries was obtained. This involved returning the pixel numbers ($x \leq i$ and $y \leq j$) rather than the grey scale at the transition point between two range of scales defining the edge of an object while no value was returned for those outside those range.

$$\text{EDGE}(z;t)(i,j) = \begin{cases} x = k,\ y = n, & \text{if } z(k-1,n) \geq t \text{ and } z(k,n) < t \\ x = k-1,\ y = n, & \text{if } z(k-1,n) < t \text{ and } z(k,n) \geq t \\ \text{skip} & \text{if } z(k-1,n) \geq t \text{ and } z(k,n) \geq t \\ & \text{if } z(k-1,n) < t \text{ and } z(k,n) < t \end{cases} \qquad 4.3$$

where for the pixel number; $1 \leq k \leq i$ and $1 \leq n \leq j$ and the boundary grey scale was t. These data (x, y) were saved as a file or stored in memory (for online graphics) and read as data for plotting the edges of objects in an image on a 2-D curve rather than converting back to an image.

If it was desired to convert back to an image with just the object edges shown, then the 'skip' had to be recorded as another grey scale which represents the background or a distinct colour from that represented by t.

In this study since the images were in grey scale, the background grey scale for white was chosen as t, i.e. 255. This boundary scale has to be reduced when there are a lot of noise on the background. Any portion of the image file that is not a background pixel forms part of the image whose edge is to be detected. As Davies (1991) observed different edge detectors vary in effectiveness with which they produce edge maps resulting in thick boundaries, which are inaccurate in some cases. This problem was encountered in this study as attempts at using the XV edge detection on the UNIX workstation produced a thick edge therefore a programme was written for this process. This is as a result of the fact that the default setting on the software works for computer generated images with sharp edges usually devoid of noise. To overcome this, image thinning was needed which required writing a thinning algorithm thereby entailing writing a complete programme for the edge detection.

4.3.4.4 Determination of Sphere Centroids

The position of the centre of each sphere in the box was required for setting up a similar arrangement for simulation. The edges represented the intersection of the surface of the spheres with the vertical plane through the centre of the box (i.e. approximately through the centres of the spheres) thus each particle appeared as a circular object. To detect the centres of circular objects in digital images the Hough and Randon transform methods are the most widely used (Dougherty and Giardina, 1987; Davies, 1991; Princen *et al*, 1991; Leavers, 1991) although other methods also using image edge data were reported (Pei and Horng, 1996).

Generally the process involved the assumption that each edge point is a point on the boundary of a circle satisfying the function defining the surface from the centre of the circular object. Knowing the radius of the circle, a candidate centre point can be obtained by moving a distance equal to the radius from the edge point along the direction of the local edge normal. A peak location technique (Princen *et al*, 1991) can then be used to obtain an accurate centre from a set of accumulated centre points from all the points. An alternative approach is to use only three of the edge points to develop simultaneous equation with the x, y variables as the centre co-ordinates/pixels of the circle. This method was used in this study for spherical balls with circular cross-section. The first approach is computationally slower but more accurate for an irregular object whose shape is very close to a circle. It also needs another algorithm to erode the surfaces of the object where the edges are joined in an assembly containing many objects. The erosion method is the third method, which is more appropriate for irregular objects. In this method, the edges of the objects are eroded uniformly inward. This separates the objects and eventually reduces each object to a cluster of pixels around its centre from where the peak location technique can also be used. This method was also used in this study for irregularly shaped seeds as discussed in 4.4.

4.3.5 Simulation and Data Correlation

Computer simulations of the compression of a similar set-up to the experimental set-up described in 4.3.3 whose images are analysed as presented in 4.3.4 were carried out in order to validate the volume distribution algorithm. The compression of the assembly was simulated using the same physical properties and loading parameters as in the experiment. The centre points of the spheres prior to compression obtained from the image analysis (see 4.3.4.4) were used to generate a similar arrangement of spheres as used in the experiment

(see 3.5). A monotonic, uni-directional load was then applied by advancing a simulated loading plate by a constant increment over each time step, corresponding to a constant rate of strain equivalent to the loading speed in the experiment. Forces, deformation, stress, strain, porosity, volume change, shape and size changes were calculated and recorded at the uniform strain intervals.

Similar to the experimental image analysis, a vertical section through the centre of the system was plotted to reveal the position and shape of each object as modelled by the new algorithm and what it would have been if the algorithm were not applied (original DEM). The edges of the spheres extracted from the images of the experiment were superimposed on those from the edges calculated by the model for each corresponding strain increment. On-line graphics using the FORTRAN graphic library (NAG graphic library) was used to obtain the plots of the positions and shapes of the spheres within the system during the simulation and the edges of the image from the experiment were then superimposed on the simulated shapes. The simulations on rapeseed took a very long time hence on-line display and capture of the images were not possible. Therefore centre co-ordinates were recorded at uniform intervals and AVS graphics with fast rendering mode was used to obtain the images.

4.3.6 Results and Discussions

Results will be presented for the compression tests conducted on the three rubber ball specimens S1, S6R and S6D and a single column bed of rapeseed. The assemblies of rubber balls were compressed with a loading speed of 10 mm/s (compressive plate displacement) until the compressive load reached 500N. The load and strain were recorded at bulk deformation interval of 0.003m. In the simulation a strain rate of 0.3, 0.15 and 0.2 per second corresponding to the same loading speed in the experiment was applied on the top wall simulated as the loading plate for S1, S6R and S6D respectively.

4.3.6.1 Shape Change

Figures 4.25 (a – e) shows the extracted images obtained from the experiment (left) and the plots of their edges superimposed on the cross section of the sphere from the simulation as predicted with the new code and what it would have been if the uniform material distribution algorithm was not used (dashed lines). The images for compression of one sphere were taken at a bulk strain interval of 0.09 (3mm deformation) during compression. For graphical clarity only a subset of edge points detected for the edge

contours of the spheres from the experiment are shown. The actual edges of the spheres from the experiment are represented by blue circular dots or square box symbols, the continuous red line represents the shape estimated by the model using the new material distribution algorithm and the black dashed lines represent the estimated shape without redistribution of deformed material. It can be seen from the figures that the edge predicted by the new model (incorporating the material redistribution function) is much closer to the actual than that predicted by the standard model.

The images from the compression of six spheres are shown in Figure 4.26 (a – e) taken at bulk deformation stages of 3mm (strain of 0.18). The behaviour showed the same trend as that from the compression of a single sphere. The effect of light reflection resulting in lighter surface can be seen on the edges of some of the spheres with slight deviation from the normal curve. This can be corrected by thresholding, for systems where smooth edged images are required. An irregularity in shape of the sphere at the bottom left side used in the experiment resulted in the gap that could be noticed at the middle left side on the superimposed figures. The images and superimposed figures for the compression of S6D are shown in Figures 4.27 for bulk deformation of 0 and 12mm. Similar to the single sphere the edge predicted by the new model was much closer to the actual edge than that predicted by the standard model.

From the figures, a good visual correlation was obtained between the experimental and simulation results with material distribution algorithm. Prediction with the normal DE code without the use of the shape and size change algorithm on the other hand showed a divergent relationship with both experiment and new code. Visually the edges predicted with the three methods appeared very close in S6R and S6D hence other analytical comparisons are required.

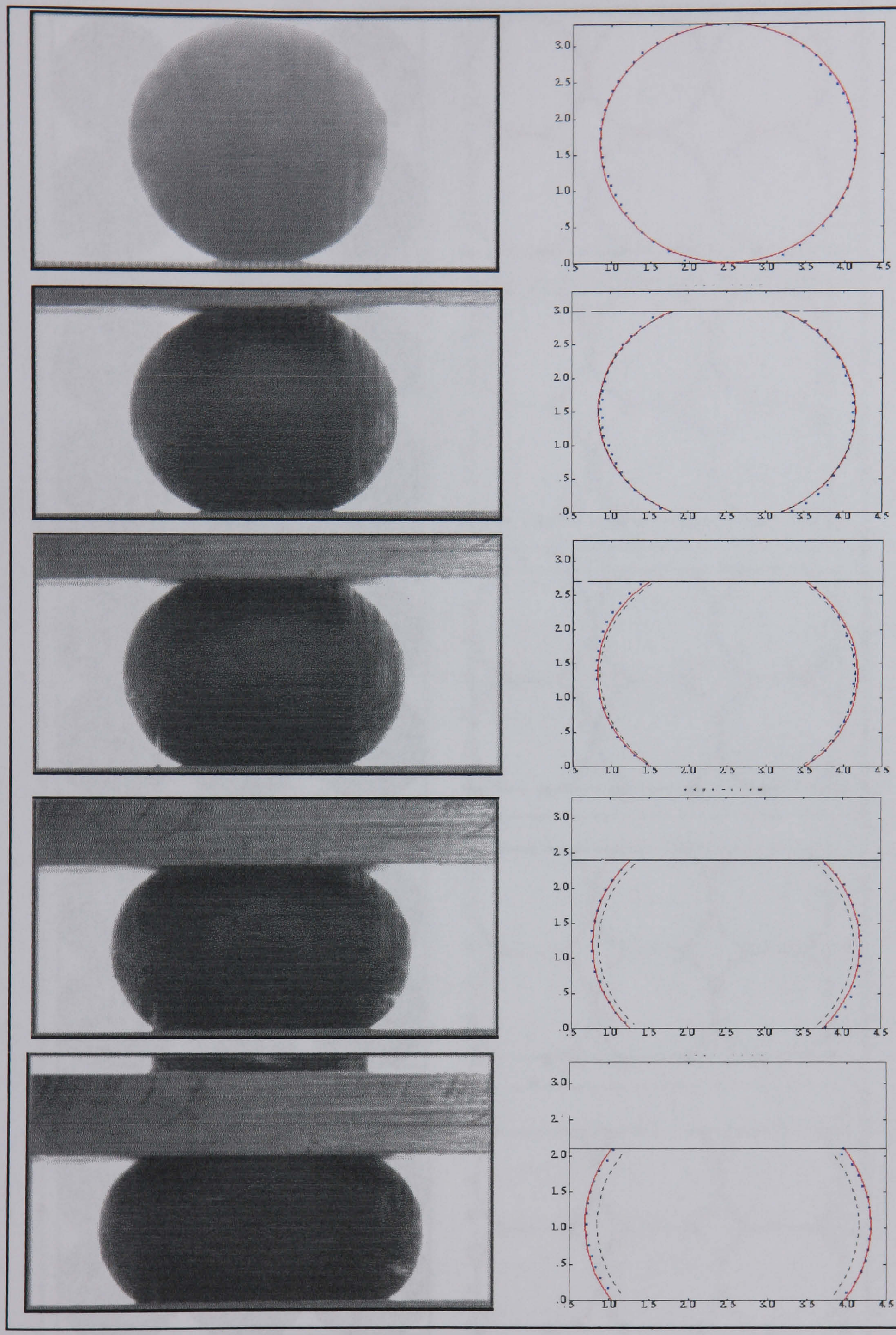

Figure 4.25 Captured images of a single sphere during compression (left.) and superimposed experiment and simulation images (right) at deformation of 0, 3, 6, 9, 12 mm (see text for details)

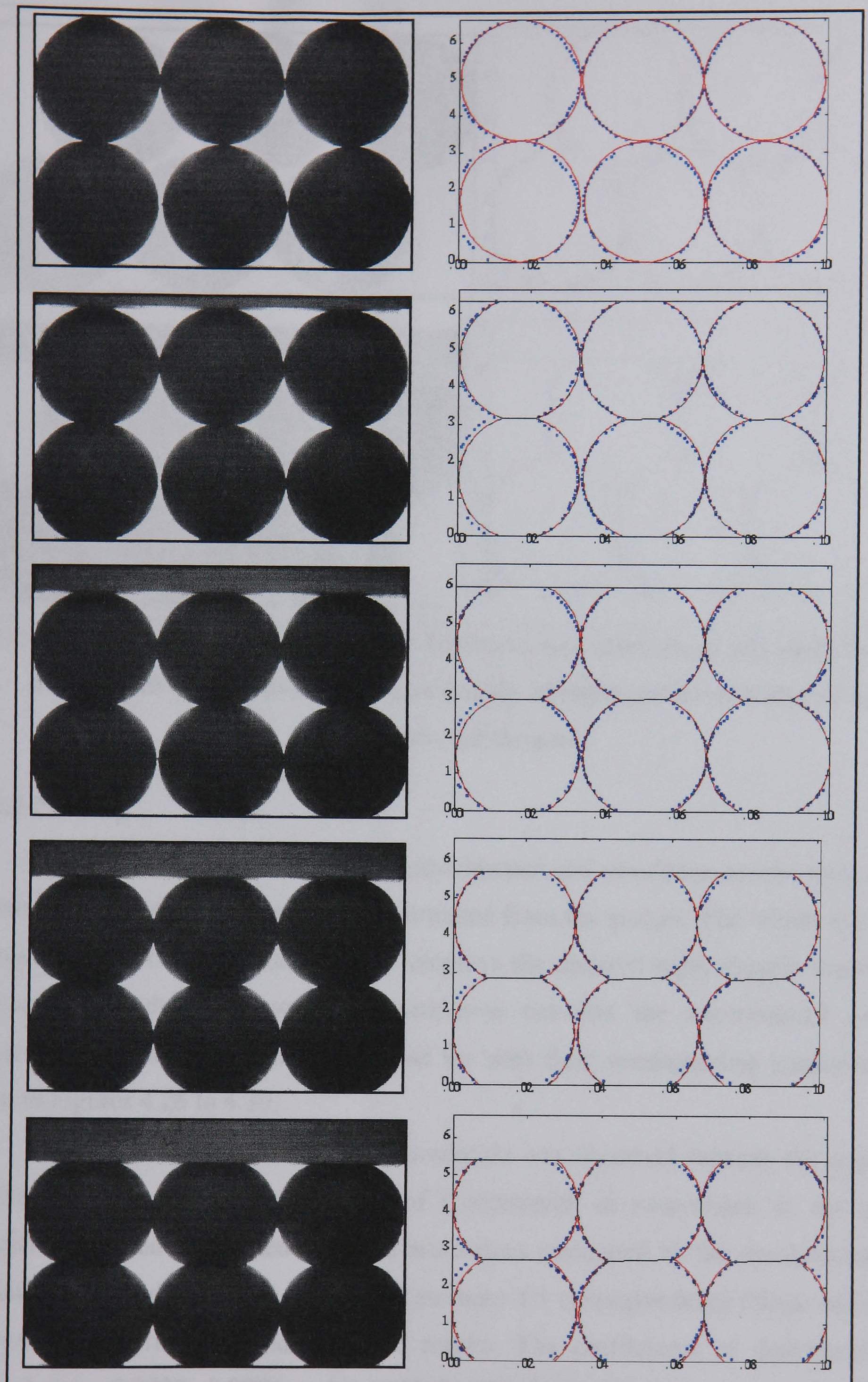

Figure 4.26 Captured images of S6R during compression (left.) and superimposed experiment and simulation images (right) at deformation of 0, 3, 6, 9, 12 mm (see text for details)

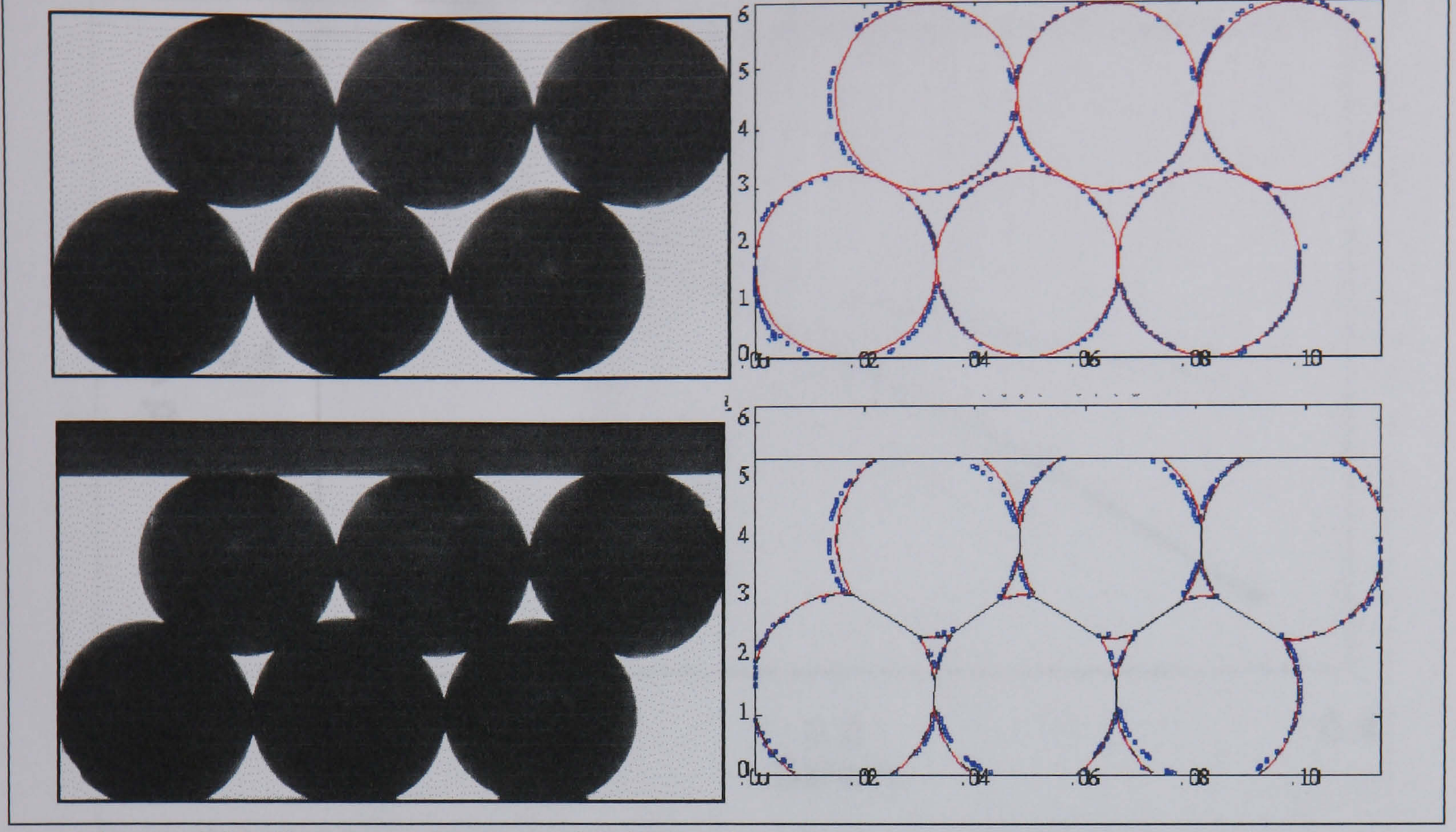

Figure 4.27 Captured images of S6D during compression (left) and superimposed experiment and simulation images (right) at deformation of 0 and 12 mm (see text for details)

4.3.6.2 Porosity

The correspondence between the experimental and simulation results were quantified by comparison of the 2-D bed voidage estimated from the images. The results are shown in Figures 4.28 - 4.30 where "new model" employs the material redistribution function while the standard model does not. The correlation between the experimental and model predictions was fitted statistically. The line fits with their corresponding equations are also shown in Figures 4.28 to 4.30.

From these figures a very good correlation was observed between the experimental and the predicted values at all stages of compression in comparison to the increasing divergence between experimental values and values calculated by the standard model. The correlations showed that there was almost an exact 1:1 correspondence (slope and intercept) between the experimental and predicted results. The coefficients of determination (R2) obtained were 0.9938, 0.9984 and 0.9952 for S1, S6R and S6D respectively, which are closer to the perfect fit (1.0) for the new model. The standard model predictions on the other hand when fitted against the experiment have good line fits (R2 of 0.9783 0.9835 and 0.9860 for S1, S6R and S6D respectively) but showed divergent relationship (slope and intercept).

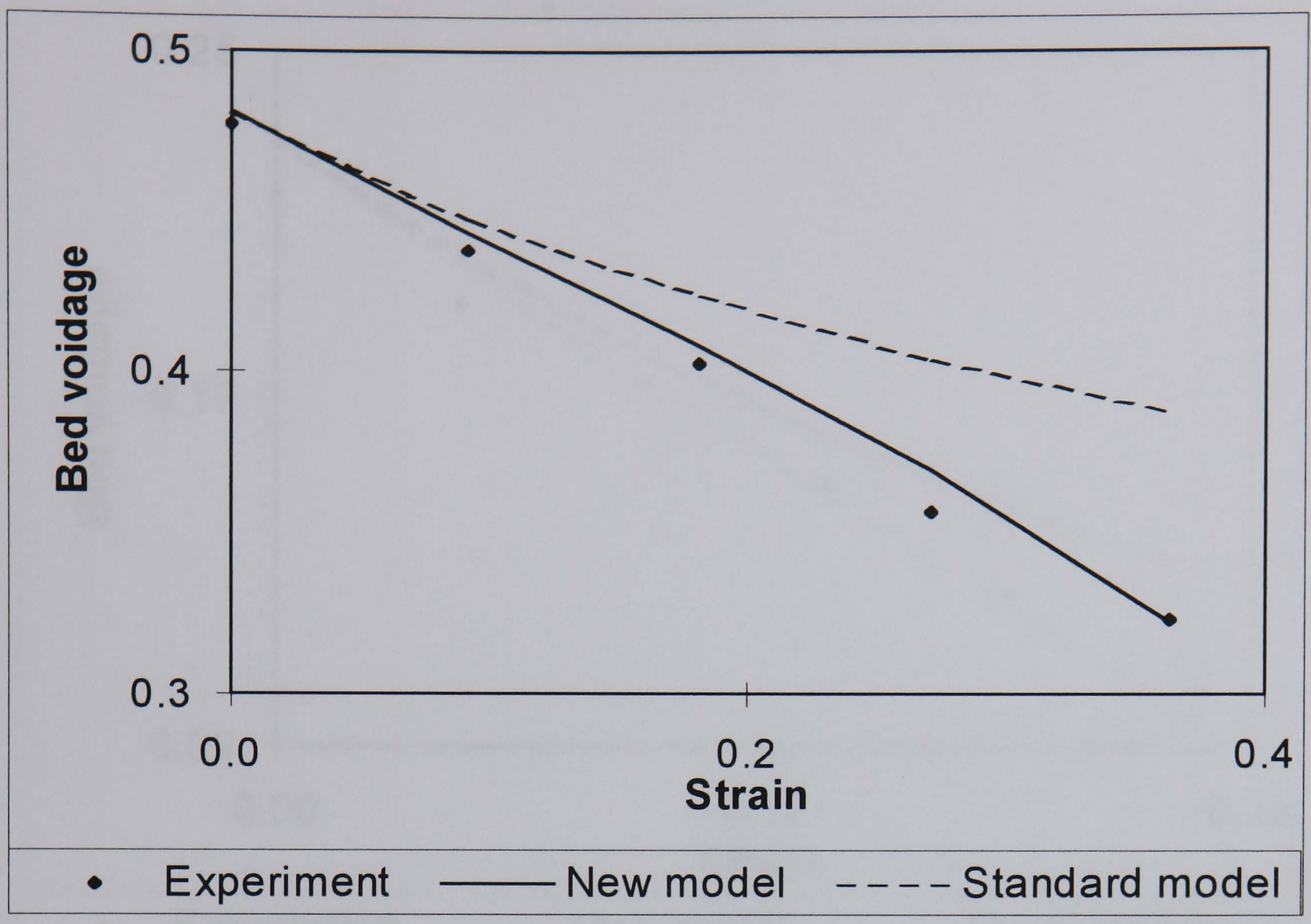

(a)

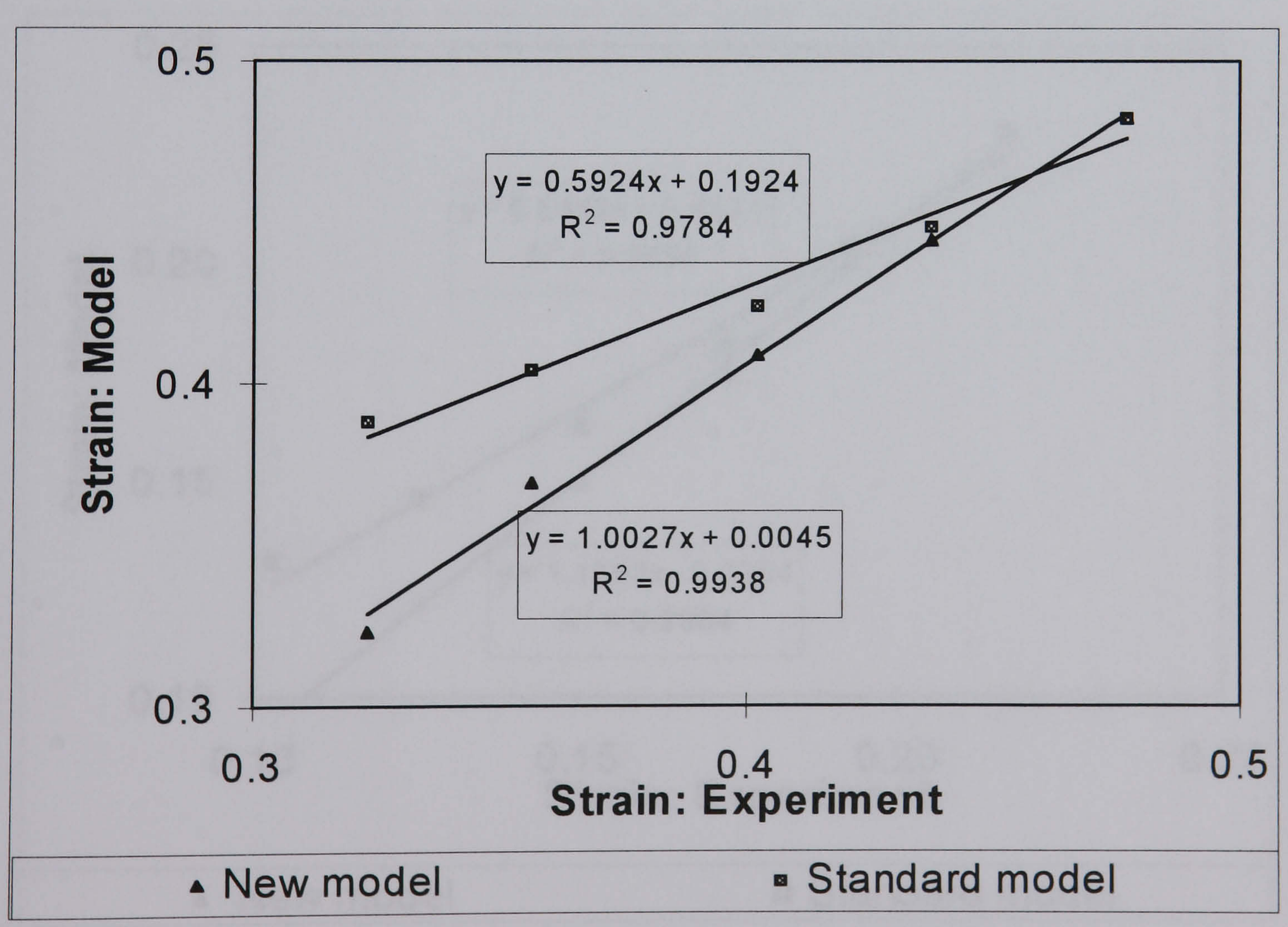

(b)

Figure 4.28 (a) Bed voidage and (b) Line fit plot for single sphere

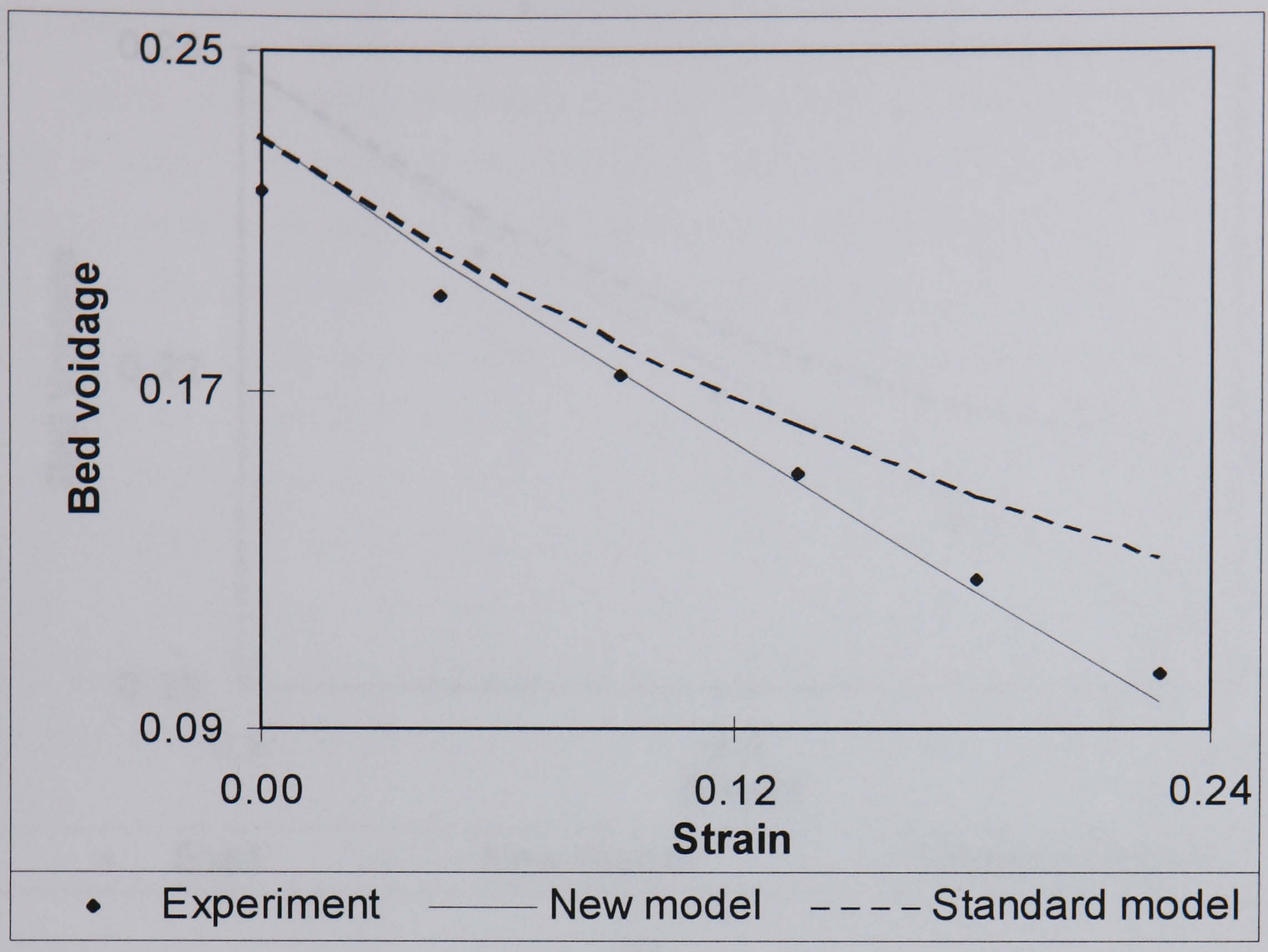

(a)

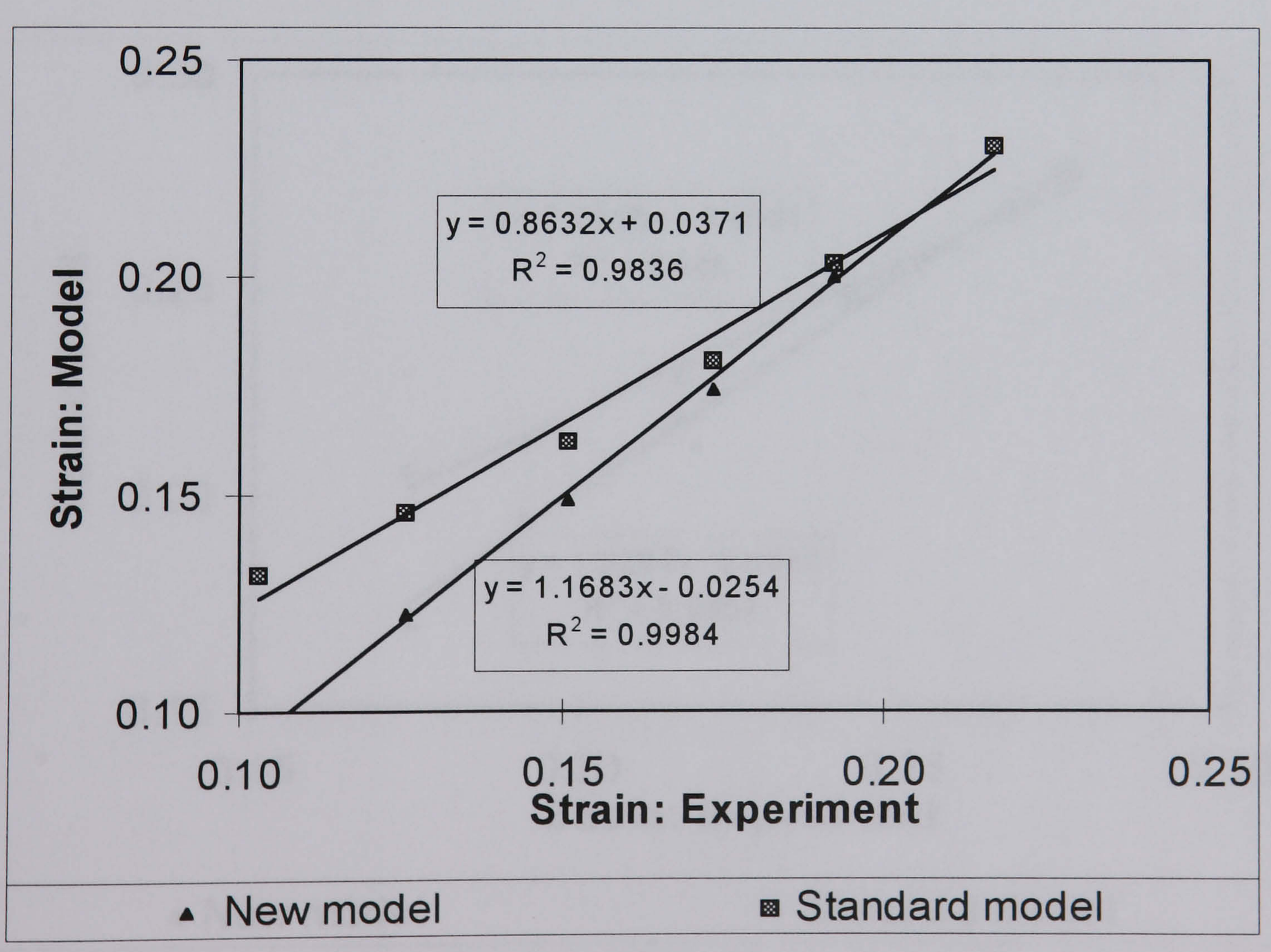

(b)

Figure 4.29 (a) Bed Voidage and (b) Line fit plot for S6R

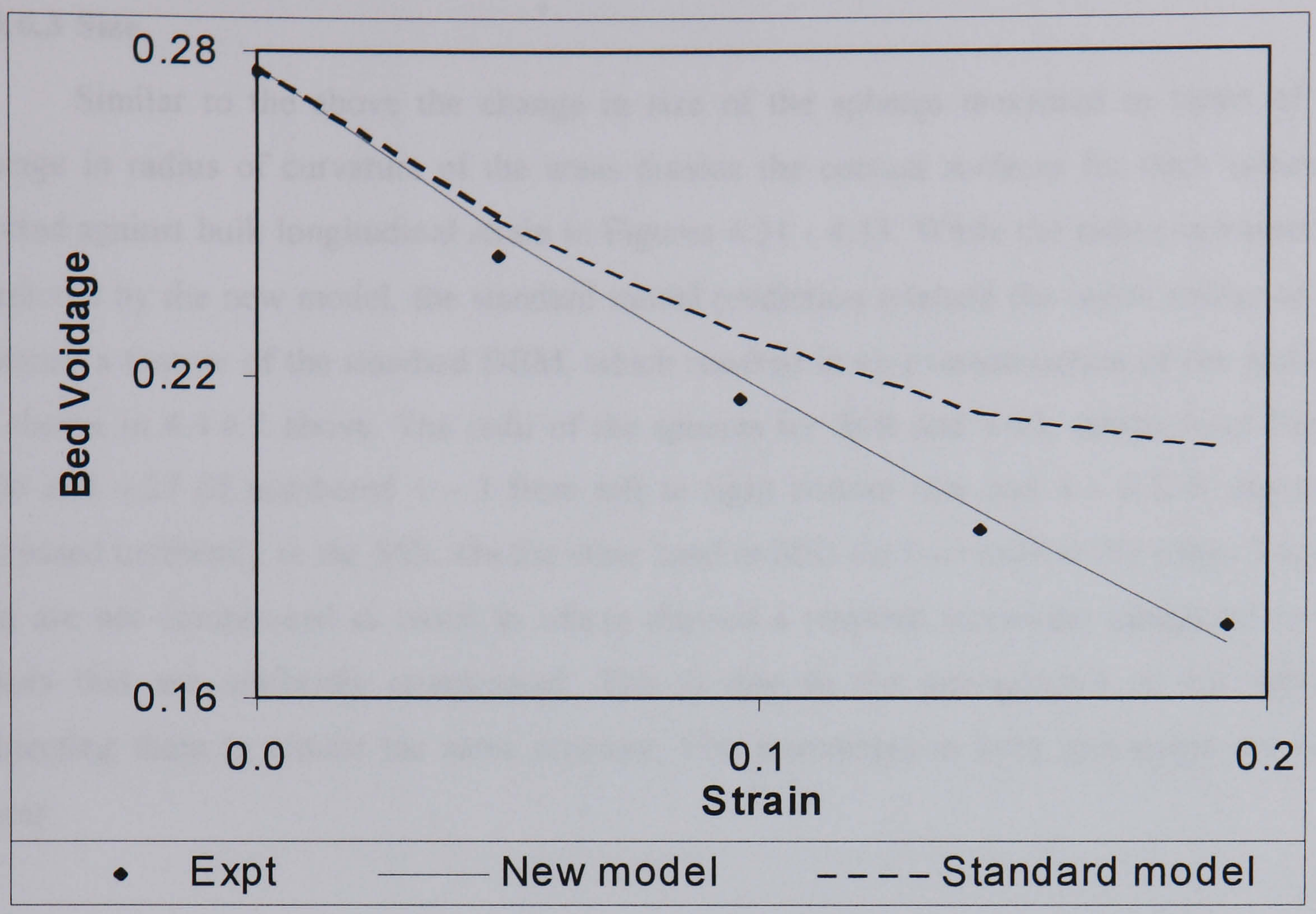

(a)

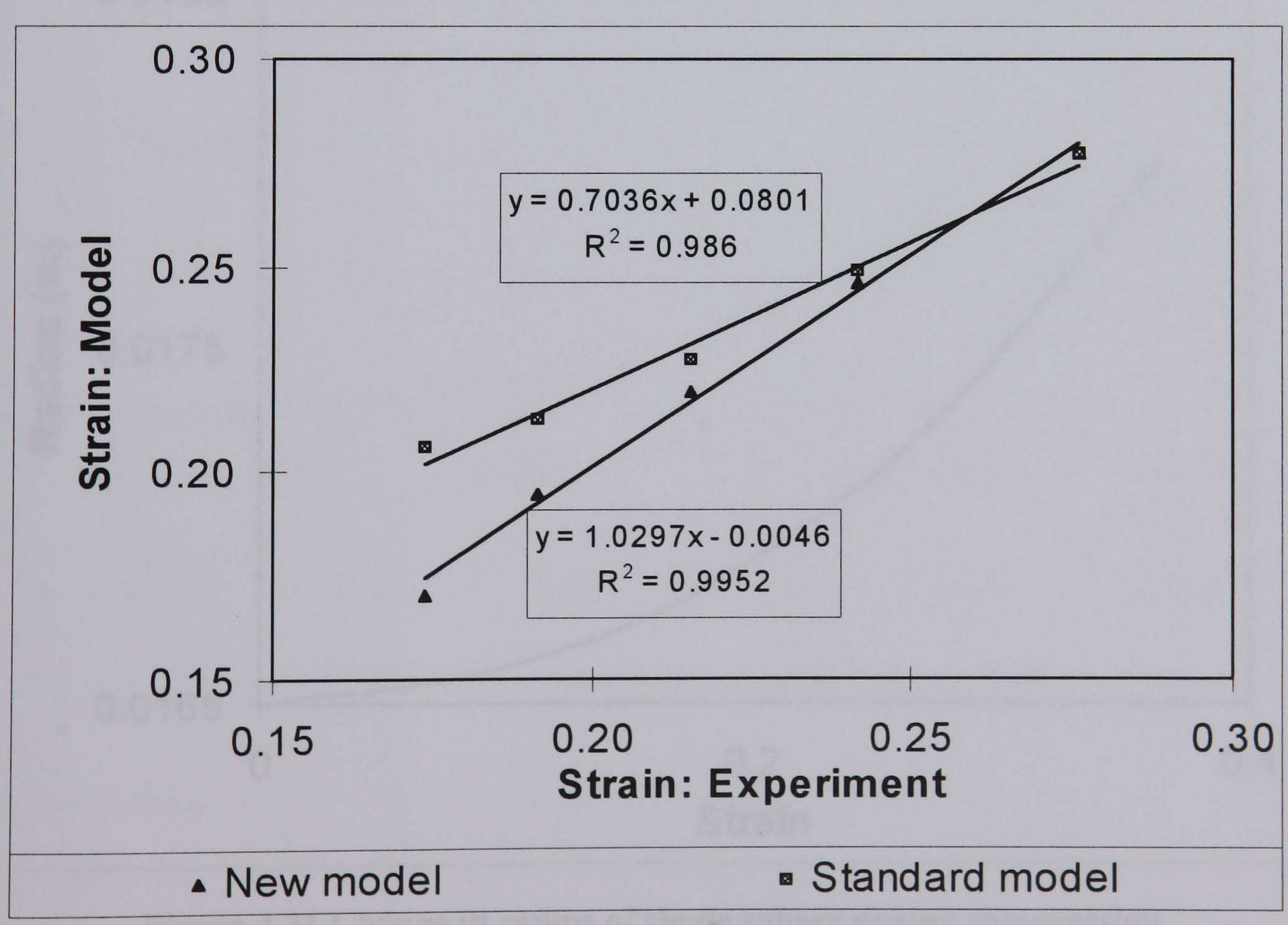

(b)

Figure 4.30 (a) Bed Voidage and (b) Line fit plot for S6D

4.3.6.3 Size

Similar to the above the change in size of the spheres measured in terms of the change in radius of curvature of the areas outside the contact surfaces for each sphere is plotted against bulk longitudinal strain in Figures 4.31 - 4.33. While the radius increased as predicted by the new model, the standard model prediction retained the initial radius of the spheres, a feature of the standard DEM, which resulted in an overestimation of the porosity as shown in 4.4.6.2 above. The radii of the spheres for S6R and S6D, which from Figure 4.26 and 4.27 (if numbered 1 - 3 from left to right bottom row and 4 - 6 L-R top row) increased uniformly in the S6R. On the other hand in S6D the two balls at the edges 1 and 6 that are not compressed as much as others showed a retarded increment compared to the others that are uniformly compressed. This is due to the arrangement of the spheres subjecting them to almost the same pressure. The increments in both specimens are non-linear.

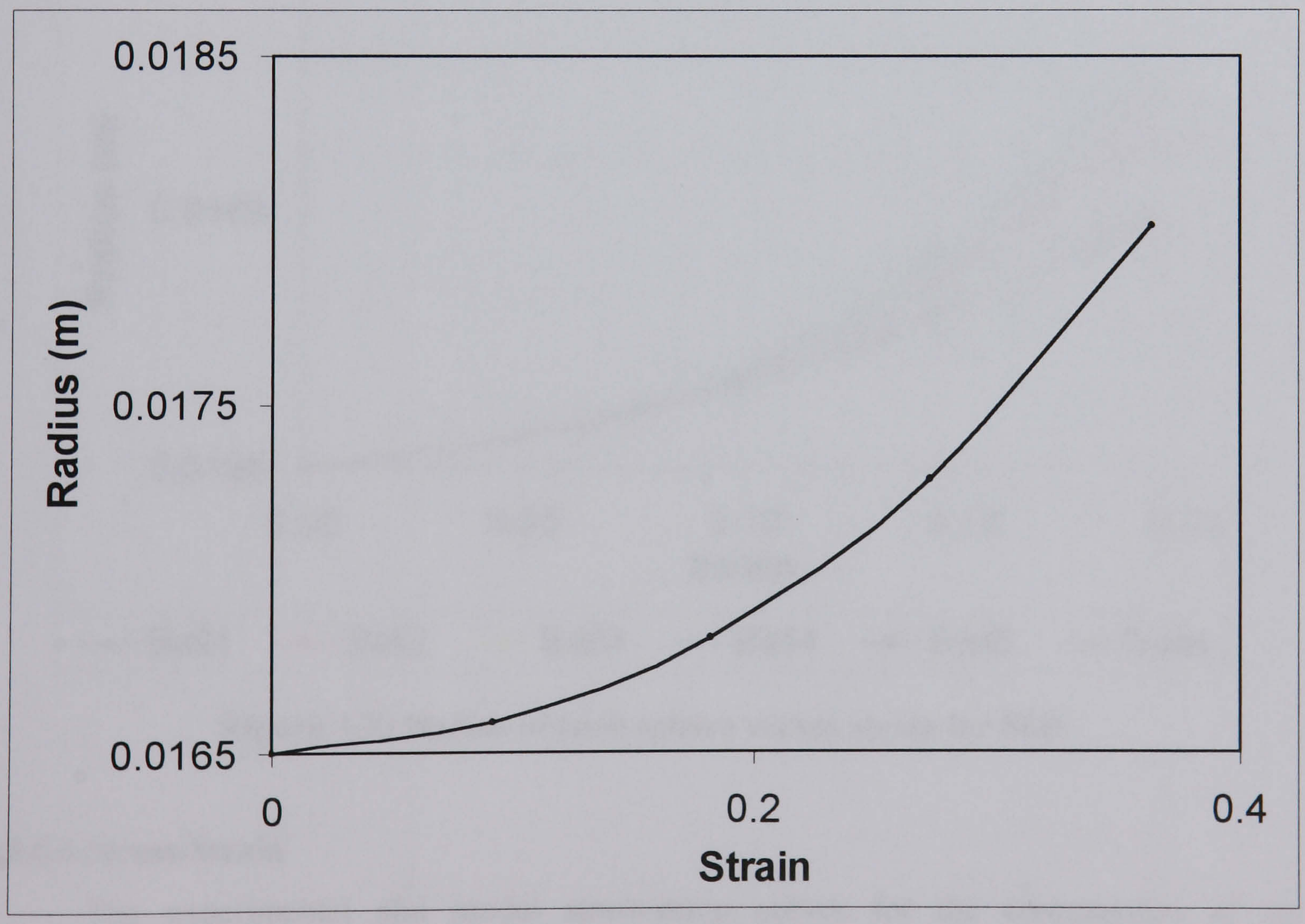

Figure 4.31 Change in radius of single sphere during compression

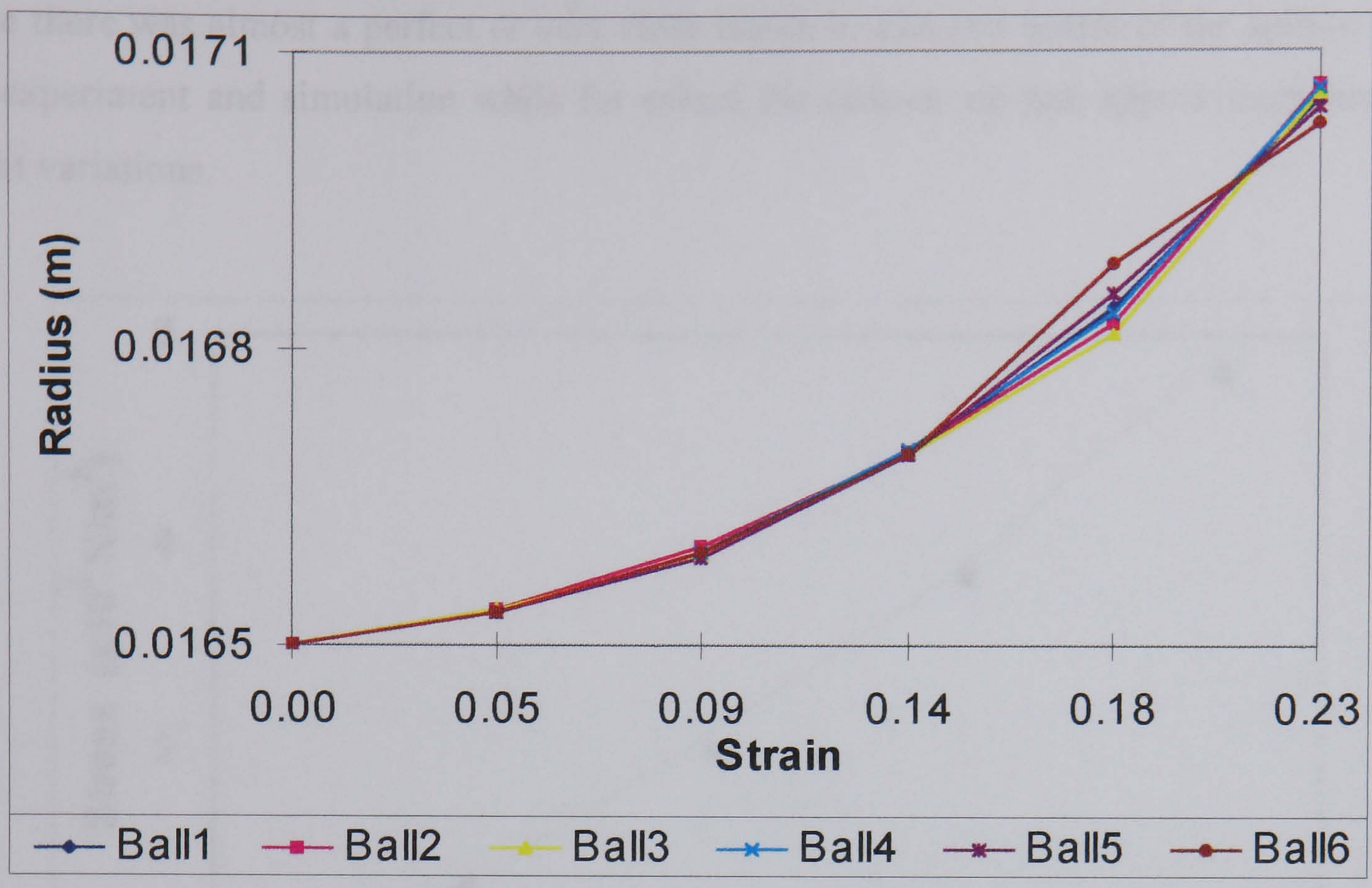

Figure 4.32 Radius of each sphere versus strain for S6R

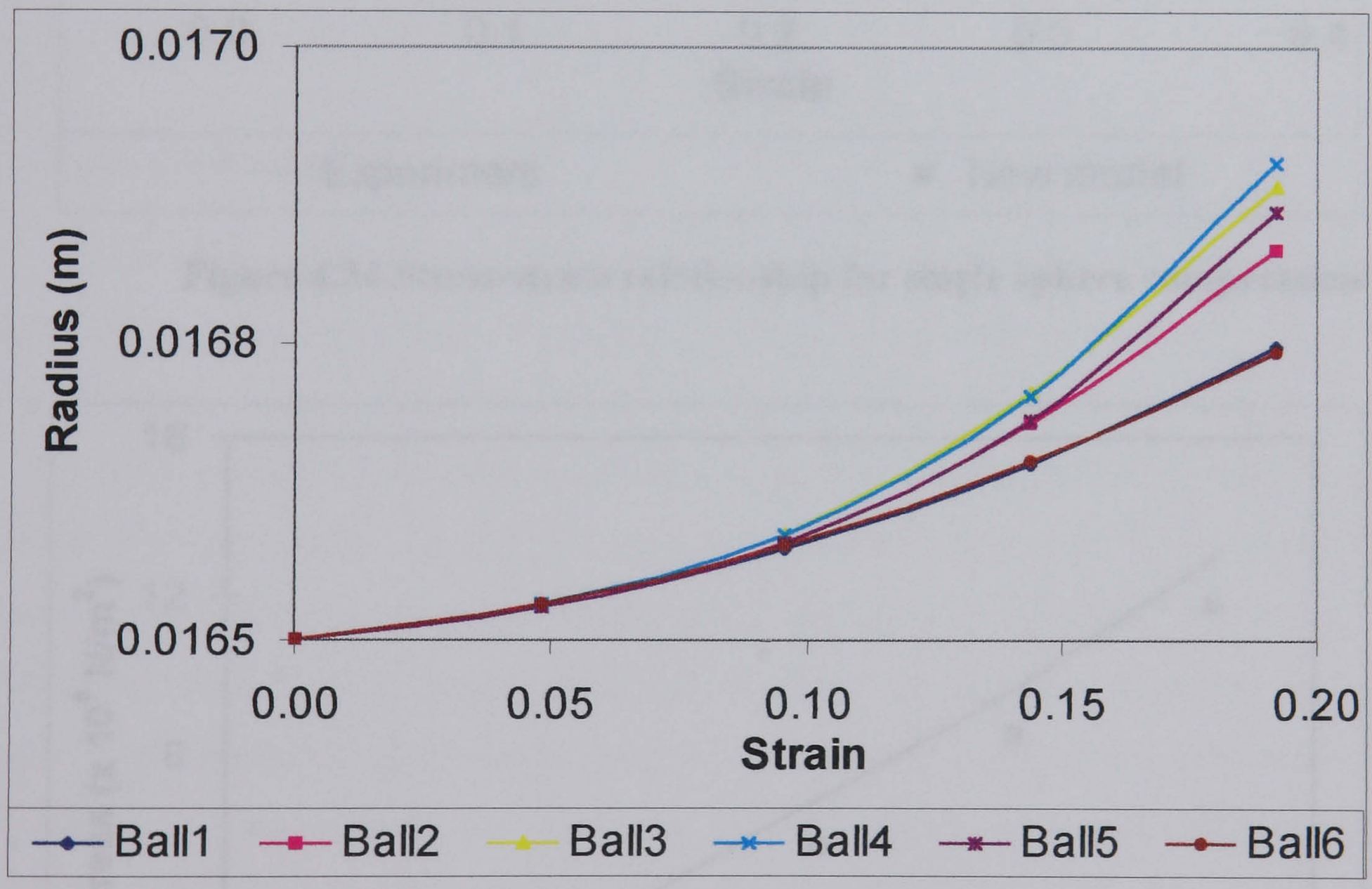

Figure 4.33 Radius of each sphere versus strain for S6D

4.3.6.4 Stress-Strain

The experimental and model stress-strain curves for the compression of the assemblies are shown respectively in Figures 4.34, 4.35 and 4.36. The simulation values also showed a reasonable correspondence with experiment similar to the other parameters discussed above. Generally there was a very close correspondence with the single particle

since there was almost a perfect or very close match in size and centre of the sphere in both the experiment and simulation while for others the centres are just approximate hence the slight variations.

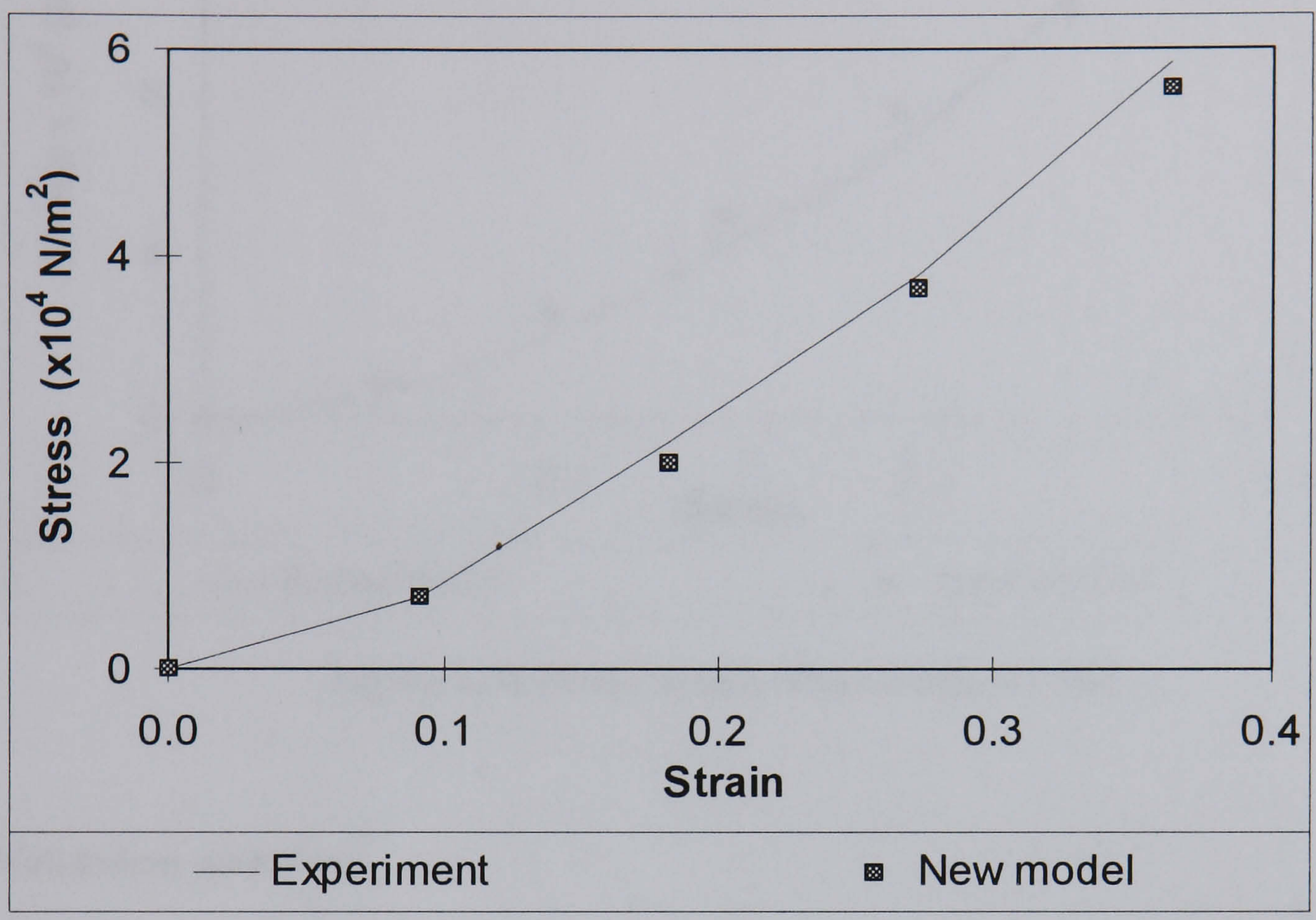

Figure 4.34 Stress-strain relationship for single sphere compression

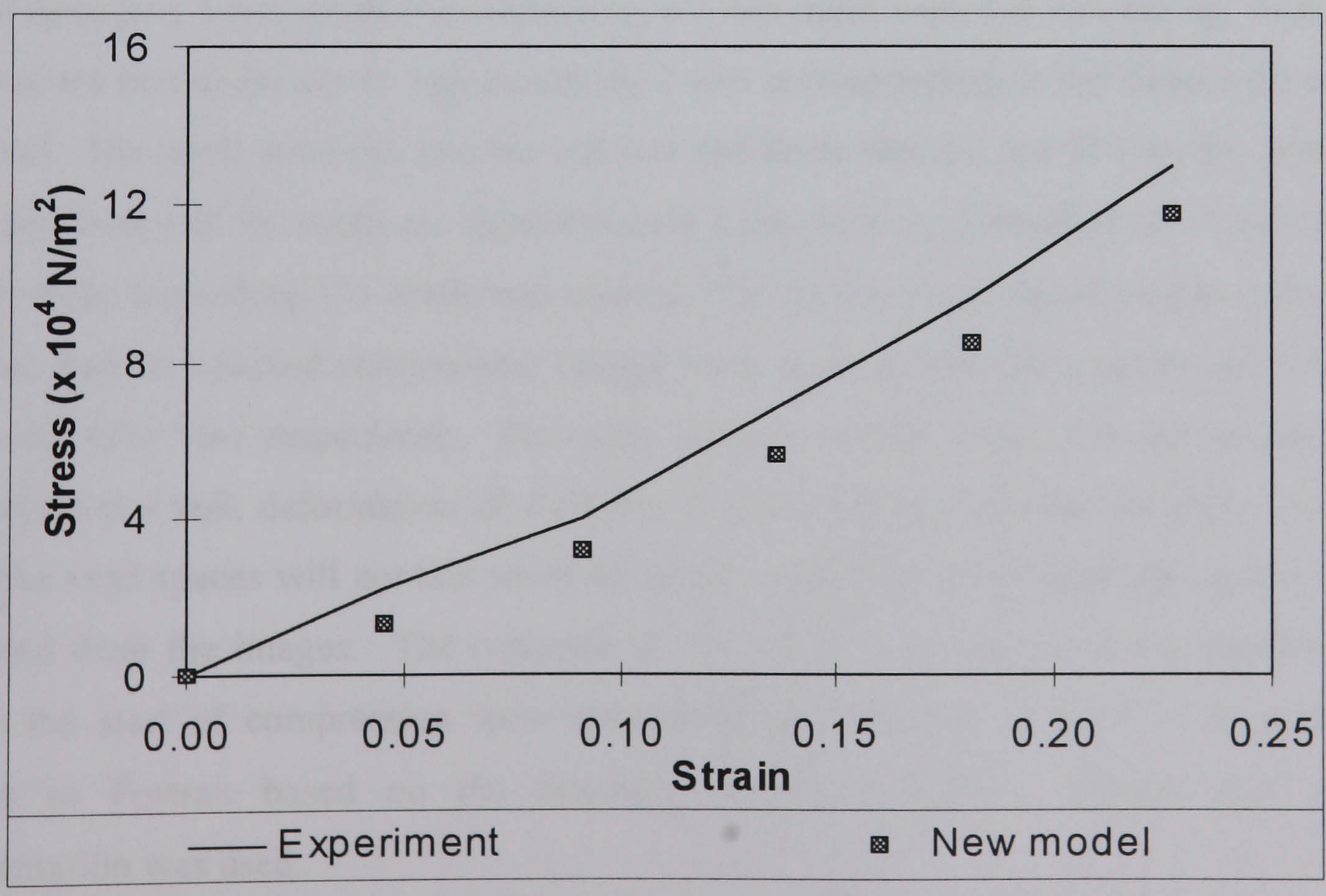

Figure 4.35 Stress Strain relationship for S6R

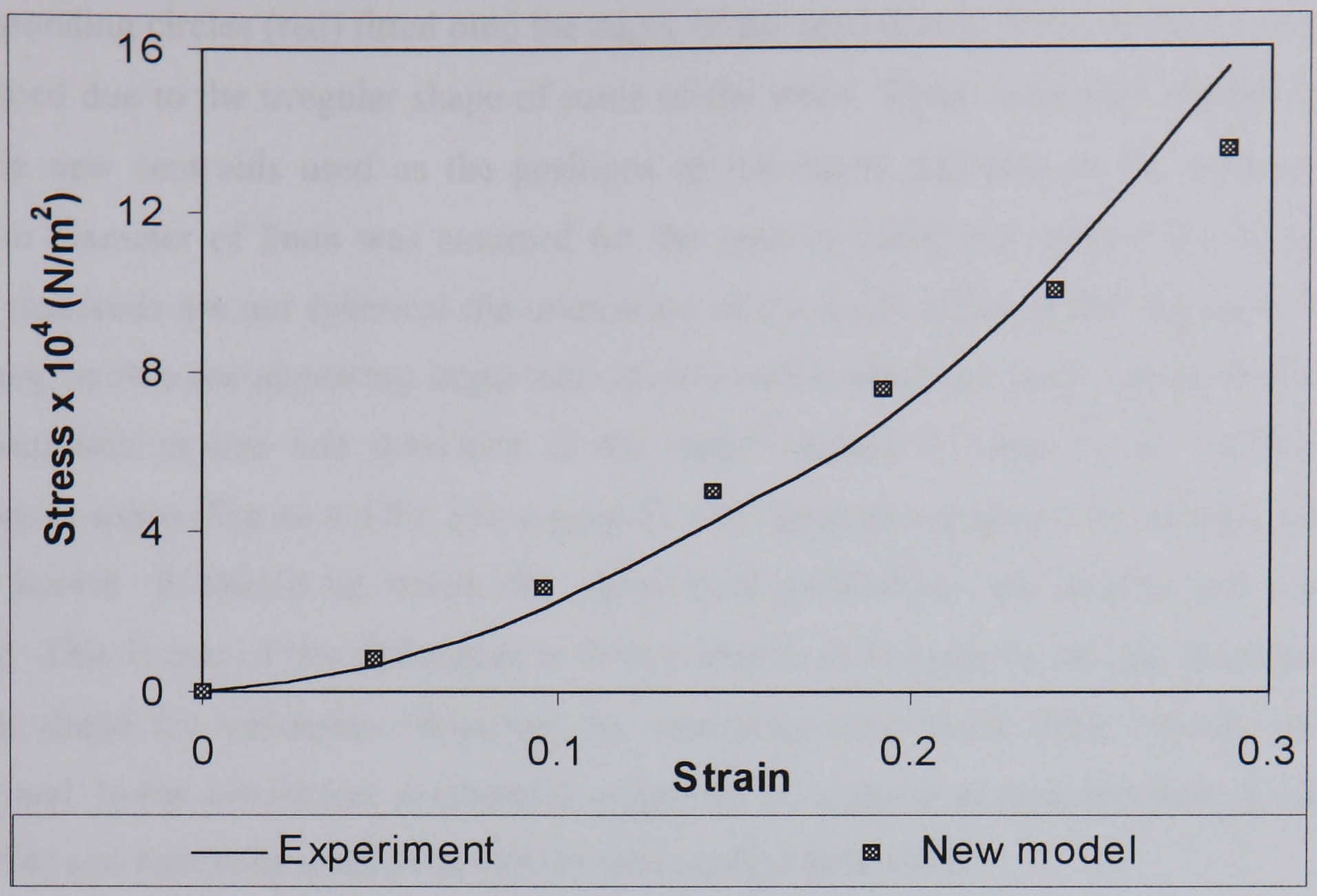

Figure 4.36 Stress Strain relationship for S6D

4.4 Validation with Seed

In order to validate the model on small particles, experiment and simulation similar to those for the large spherical balls were performed. Rapeseed was sieved and those that passed through a 3 mm mesh and retained on a 2 mm mesh were fed into the rig. The rig test box was set to a thickness of approximately 2 mm corresponding to the chosen diameter of the seeds. The seeds were fed into the test box and those that did not fit into the space were discarded hence all the seeds are approximately 2 mm in size. A seedbed of 14 mm high by 41 mm wide containing 133 seeds was created. The rig was then placed on the compressive machine and the seedbed compressed. Images were taken at bulk deformation of 0.00, 1.29, 2.99 and 4.00 mm respectively. To make image analysis easier the compression was terminated at a bulk deformation of 4.00 mm in order not to reach the oil point. At the oil point the void spaces will contain some oil which would have degraded the quality of data extracted from the images. The centroids of the seeds in the image of the seedbed taken before the start of compression were determined as described in 4.3.4.4. A programme written in Fortran based on the principle of image erosion, dilation and centroid determination was used.

Figure 4.37 shows the centroids (small square boxes) obtained with the

corresponding circles (red) fitted onto the edges of the seed (blue). Some of the centroids are misplaced due to the irregular shape of some of the seeds. These were then manually fitted and the new centroids used as the positions of the model particles in the simulation. A uniform diameter of 2mm was assumed for the seed in fitting the spheres for simulation. Since rapeseeds are not spherical the orientation of the seeds affected the size and shape in the image with some appearing larger and others smaller compared to the assumed diameter. This variation in size and sphericity of the seeds resulted in some of the fitted objects hanging in space (Figure 4.37b). For a good fit the diameter and sphericity of each seed has to be known. It should be noted that agricultural particulates are usually not regularly shaped. This is one of the difficulties in fitting images of irregularly shaped materials with regular shape for validation. However the simulation with these fitted objects was still performed. In the simulation, mechanical properties of rapeseed as obtained from Bilanski *et al* (1994) and Faborode and Favier (1996) were used (Table 4.4.).

Table 4.4 Properties and data used in simulation

Elastic Modulus* (MPa)	Density* (kg/m^3)	Diameter (mm)	Friction Coefficient		Coeff. of Restitution	Strain Rate (s^{-1})
			Wall-seed	Seed-seed		
30	1053	2	0.3	0.5	0.6	250

(* Bilanski *et al*, 1994 & Faborode and Favier, 1996. The walls have infinite radius and EM_w is assumed to be far greater than that of the seed hence $1/R_w$ and $1/EM_w$ are negligible).

Figure 4.38 shows the change in bed porosity with volumetric strain for the experiment and simulation. There was no significant difference between the new and the original code at the initial stage of compression. This is because the particle deformation during the simulation was still very low at this bed strain. The particles were therefore rearranging their positions to fill the extra space created in the fitted image. Also both had no significant correspondence with the experiment due to the difference in the initial set-up. The strain intervals at which the porosity was calculated were the same in the experiment and simulation but the particles positions at these strain intervals were not completely the same indicating they represent 'slightly different' systems. The difference between the prediction from the model and the experiment was therefore probably a result of the variation in the size and sphericity of the seeds.

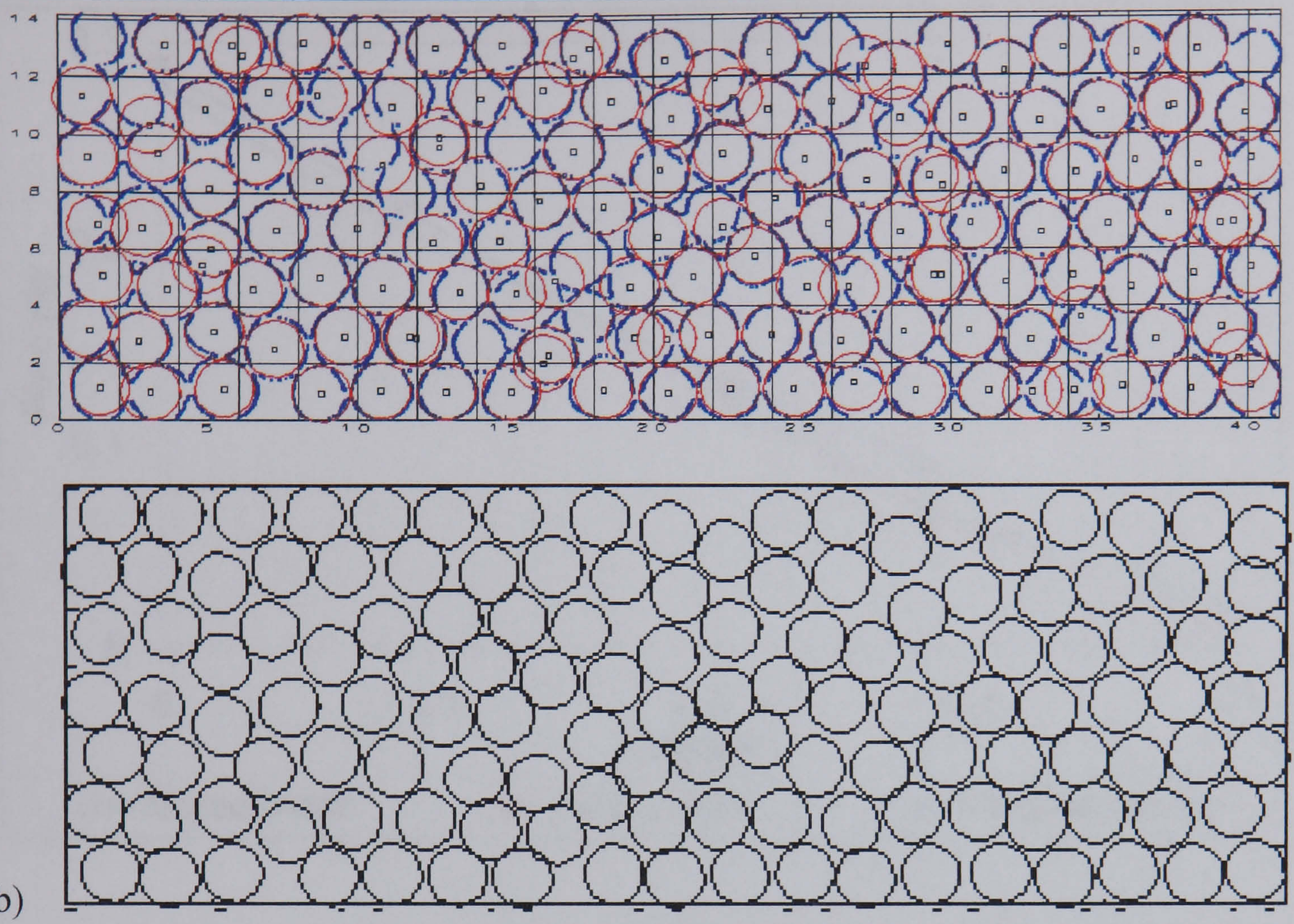

Figure 4.37 Sperical centroid determination (a) centroids and fitted circles (b) and fitted image

In order to compare the new and the original code, the compression was extended further to a strain of about 0.4 in the simulation. With this further compression which took the simulation to particle deformation stage, a divergence in porosity between the new and the original was predicted. The porosity with the original code, which neglected overlapped volume, was less than that with the new code. It is expected that the divergence will increase with further compression. However, the seed is an oil-seed and further compression beyond this stage will (i) take the process closer to the oil point and oil may be released to the void spaces creating errors in the estimated porosity and (ii) estimate a zero or negative porosity (2D) although the volumetric porosity (3D) has not yet approached zero.

The correlation between the predicted porosity in simulation and experiment were analysed using line fit plots (Figure 4.39). The differences between the new and original models compared to the experiment (Figure 4.39) were negligible with slopes closer to unity and the intercept on Y-axis being very close to 0. This shows that using fewer, more uniformly shaped and larger particles (to ease image analysis) with appropriate method to determine the size of each seed, a closer prediction could be obtained.

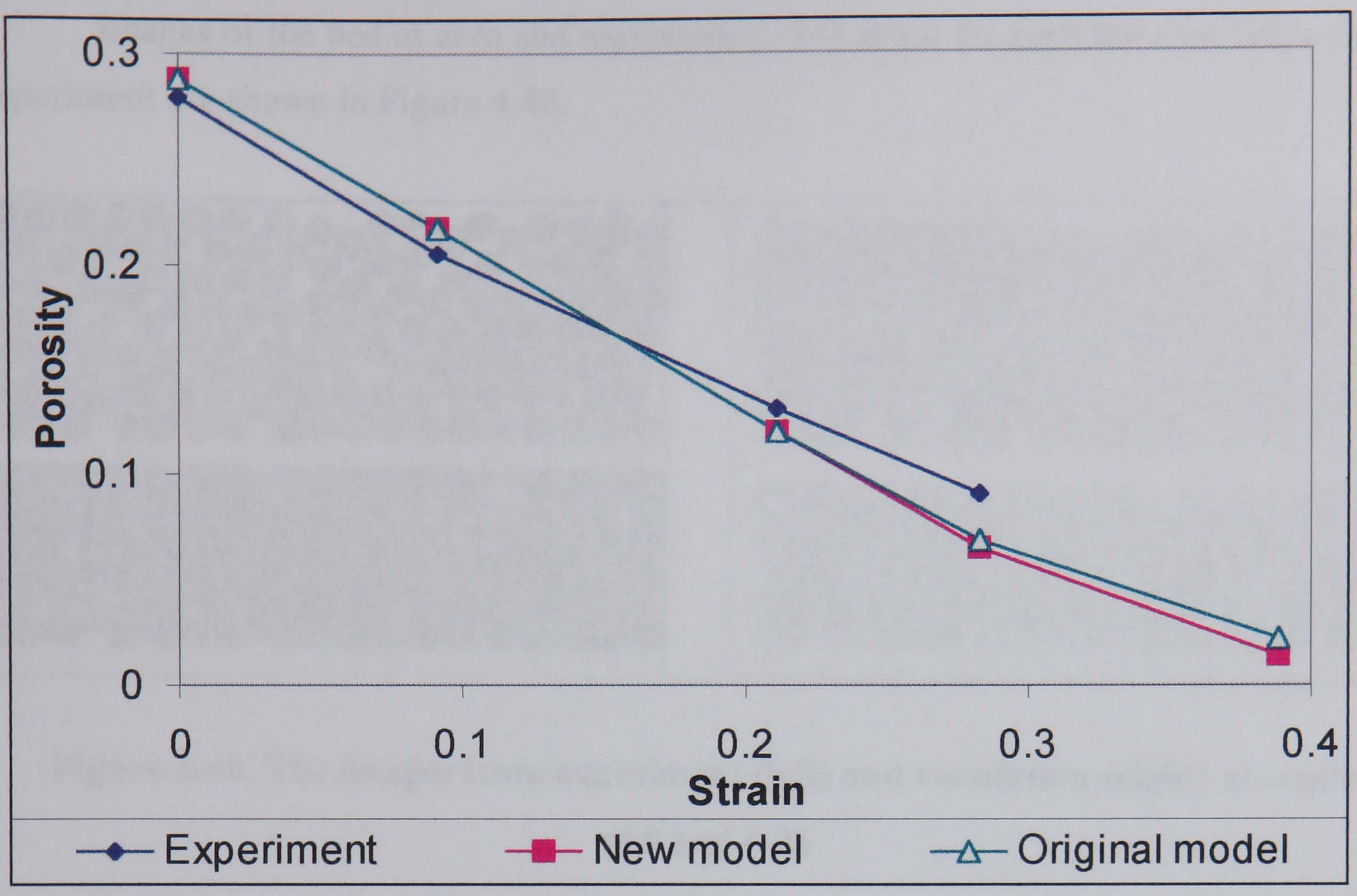

Figure 4.38 Porosity

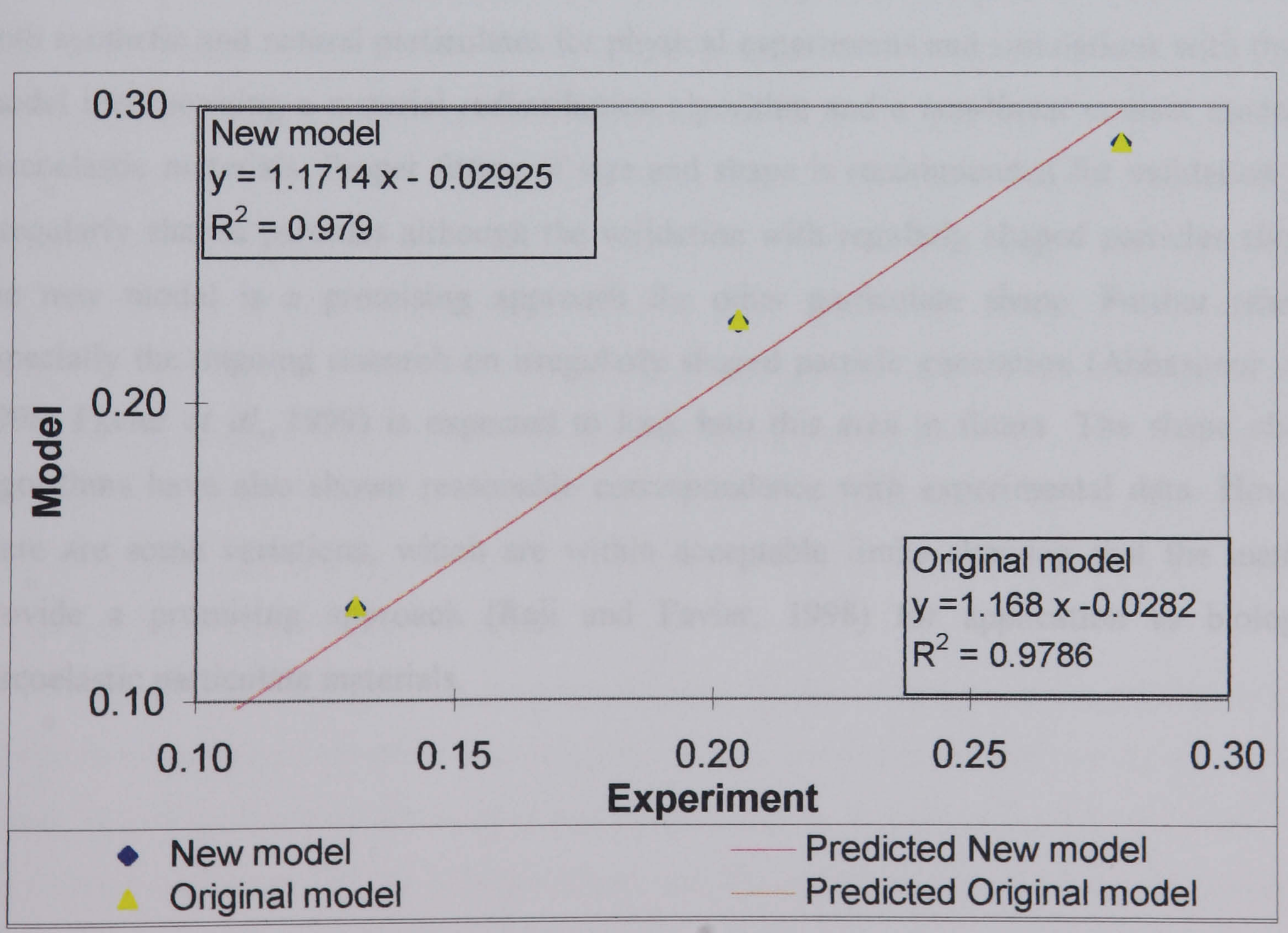

Figure 4.39 Line fit plot for the Porosity

Images of the bed at zero and maximum (0.28) strain for both the simulation and the experiment are shown in Figure 4.40.

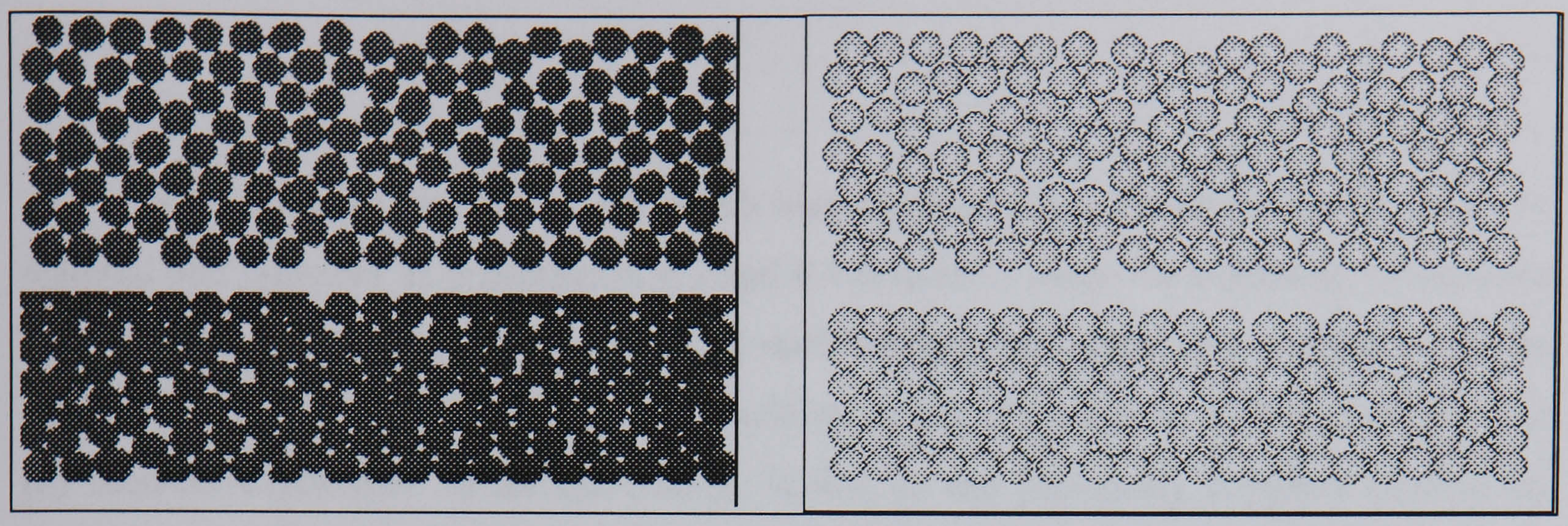

Figure 4.40. The images from experiment (left) and simulation (right) at strain of 0 and 0.28

4.5 Summary

Good correlation was achieved between the results of compression experiments on both synthetic and natural particulates for physical experiments and simulations with the DE model incorporating a material redistribution algorithm and a non-linear contact model for viscoelastic materials. Proper fitting of size and shape is recommended for validation with irregularly shaped particles although the validation with regularly shaped particles showed the new model is a promising approach for other particulate shape. Further research especially the ongoing research on irregularly shaped particle generation (Abbaspour *et al*, 1998; Favier *et al*, 1999) is expected to look into this area in future. The shape change algorithms have also shown reasonable correspondence with experimental data. However there are some variations, which are within acceptable limits showing that the methods provide a promising approach (Raji and Favier, 1998) for application to biological viscoelastic particulate materials.

5 APPLICATION OF DE MODEL TO AGRICULTURAL MATERIALS HANDLING AND PROCESSING

In this chapter the new model which was validated using spheres made of synthetic material and rapeseed as presented in 4.3 and 4.4 is used to study the behaviour of selected agricultural particulates in specific fruit and seed handling and processing operations. These applications are (i) determination of safe padding or belt thickness for a fruit conveyor and (ii) seed-oil expression. In all the studies, similar to the previously reported studies, an assumption of spherical shape was made and appropriate material properties used.

5.1 Impact Studies

As discussed in 4.2.2.3, if the material stiffness properties and deformation rules in impact studies of a falling object are reversed such that its stiffness properties are far greater than those of the plane surface, the deformation at contact is assumed to be totally that of the soft plane surface. Therefore the maximum deformation obtained at any drop height represents the minimum thickness of a padding surface or belt (supported below with a harder surface) required for preventing damage or bruising to the falling material. If the difference in the stiffness is such that the falling fruit (the harder material) also experiences some deformation (which is expected to be very small compared to the softer plane surface) the system can still be modelled as a system with very hard falling object compared to the plane contact surface. The deformation obtained (which is expected to be an addition of the deformation in both contacting objects) when taken as the required thickness of the contact surface ensures that a tolerance has been provided. This is because the required thickness will be less than the predicted thickness.

Simulations were performed using the new model to determine the padding surface thickness for different materials that could be used in the design of step conveyors for apple falling from one conveyor to the other in a processing line. Recalling Equations 2.5 and 2.20, the contact stiffnesses in the F-D equations are dependent on the modulus of rigidity or elastic modulus (EM), geometry and Poisson ratio. Four contact surface materials having elastic modulus of 4, 6, 8 and 10 times less than apple's EM represented by M1, M2, M3 and M4 respectively were considered. The EM for each material was therefore 1.175, 0.783,

0.587 and 0.470 MPa for M1, M2, M3 and M4 respectively. Simulations were performed for four drop heights of 5, 10, 20 and 30 cm and the damping coefficients were varied. The coefficient of restitution (on which the damping coefficient depends) of apple ranges between 0.4 and 0.8 (Mohsenin, 1986). Therefore three different damping coefficients D1 (0.28), D2 (0. 22) and D3 (0.16) equivalent to coefficients of restitution of 0.4, 0.5 and 0.6 respectively were considered in the simulation.

5.1.1 Results and Discussion

Figures 5.1 – 5.4 shows the results of the belt thickness (deformation at contact) obtained for different heights of drop for each material stiffness at different damping coefficients. The deformation obtained for each material type at different damping coefficient is as shown in Figure 5.5. Figures 5.6 and 5.7 show the energy regained after impact (as a percentage of the total kinetic energy before impact) and the height of rebound after impact respectively. The contact force during impact for all the materials at a damping coefficient of 0.22 is as shown in Figure 5.8

The deformation obtained during impact on surfaces with elastic modulus 4 and 6 times less than the fruit's ranged between a value of about 1.5 mm with a damping coefficient of 0.28 at a drop height of 5 cm to 6 mm with a damping coefficient of 0.16 at a drop height of 30 cm. The range of deformation for surfaces with EM 8 and 10 times less than the fruit's was 2.0 mm with a damping coefficient of 0.28 at a drop height of 5 cm to 7.4 mm with a damping coefficient of 0.16 at a drop height of 30 cm. Similar to the trend in Chapter Four the deformation increased with decreasing damping coefficient within the range used. Therefore the lower the damping coefficient of a material the thicker must be the padding surface or belts made from it. The required thickness is also directly related to the height of drop in all the cases.

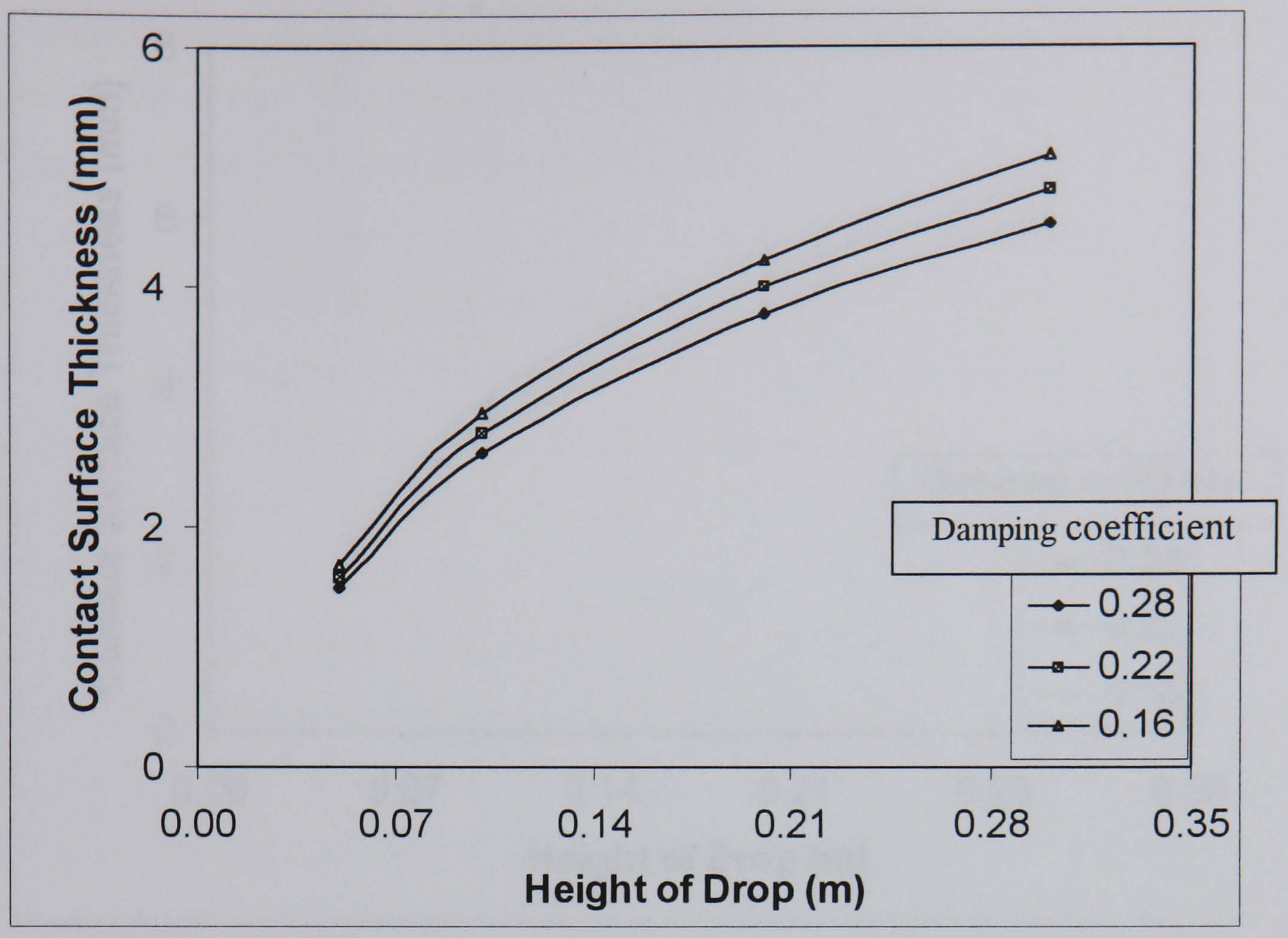

Figure 5.1 Contact surface thickness for material with E = 1.17 MPa

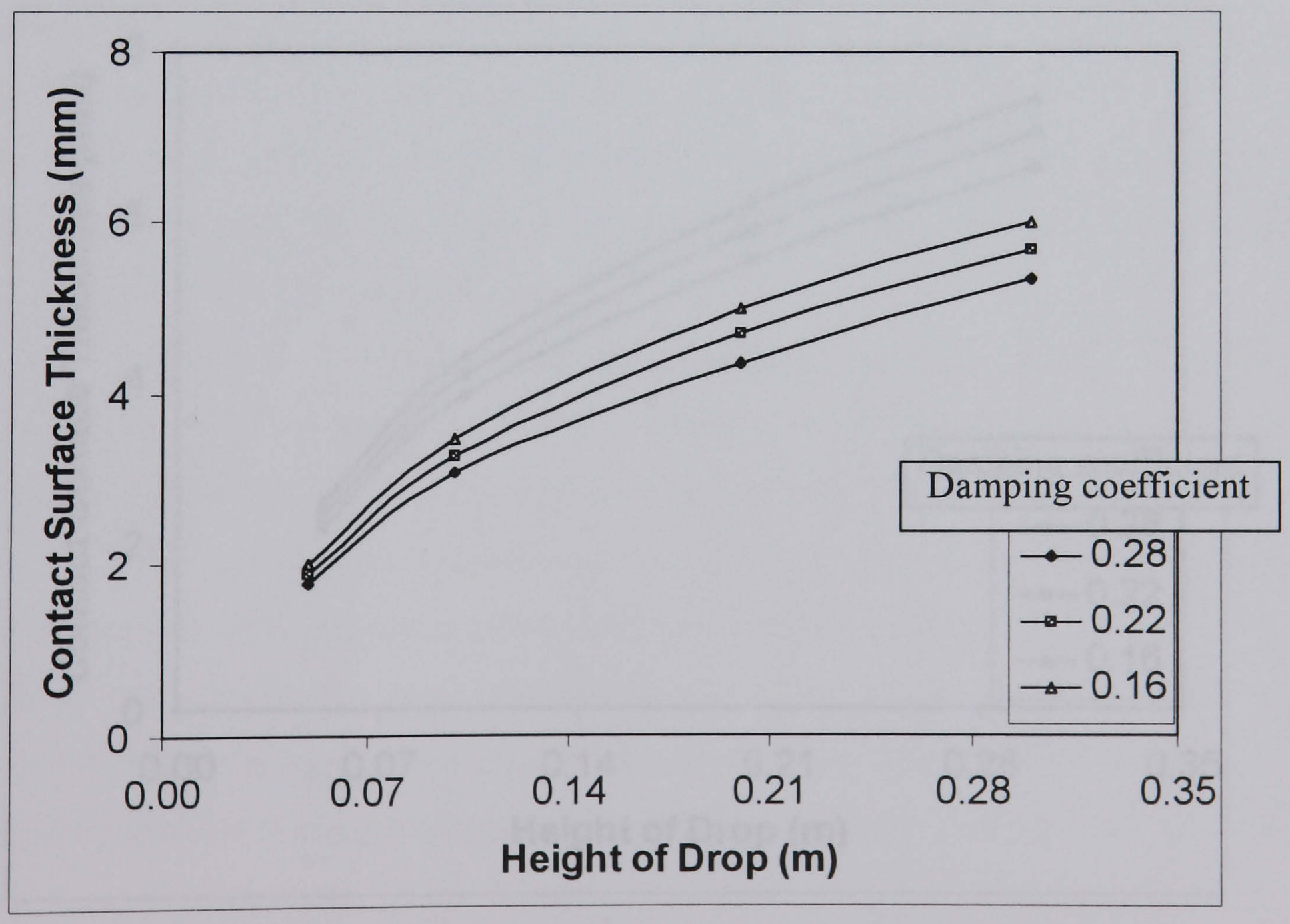

Figure 5.2 Contact surface thickness for material with E = 0.78 MPa

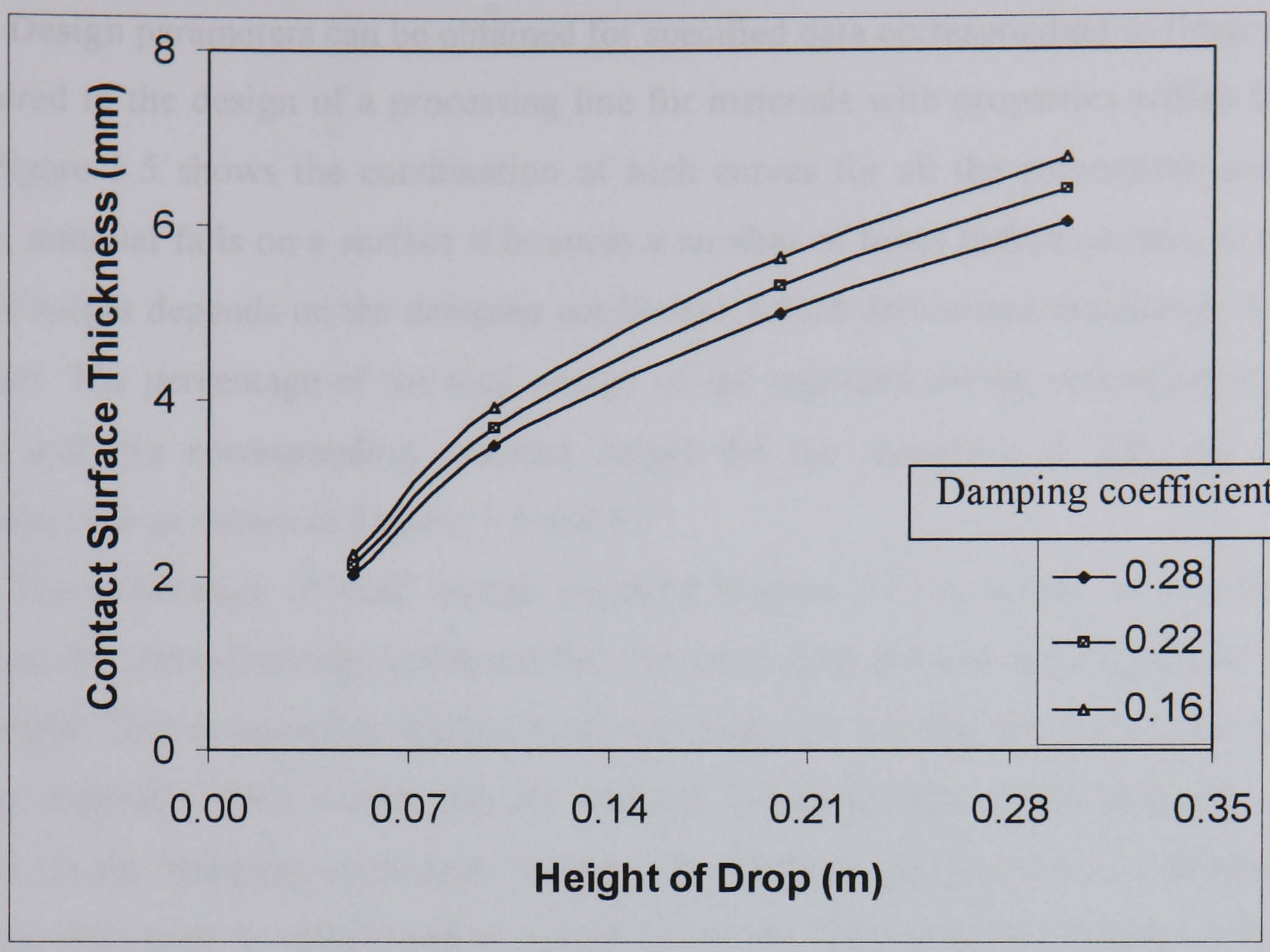

Figure 5.3 Contact surface thickness for material with E = 0.59 MPa

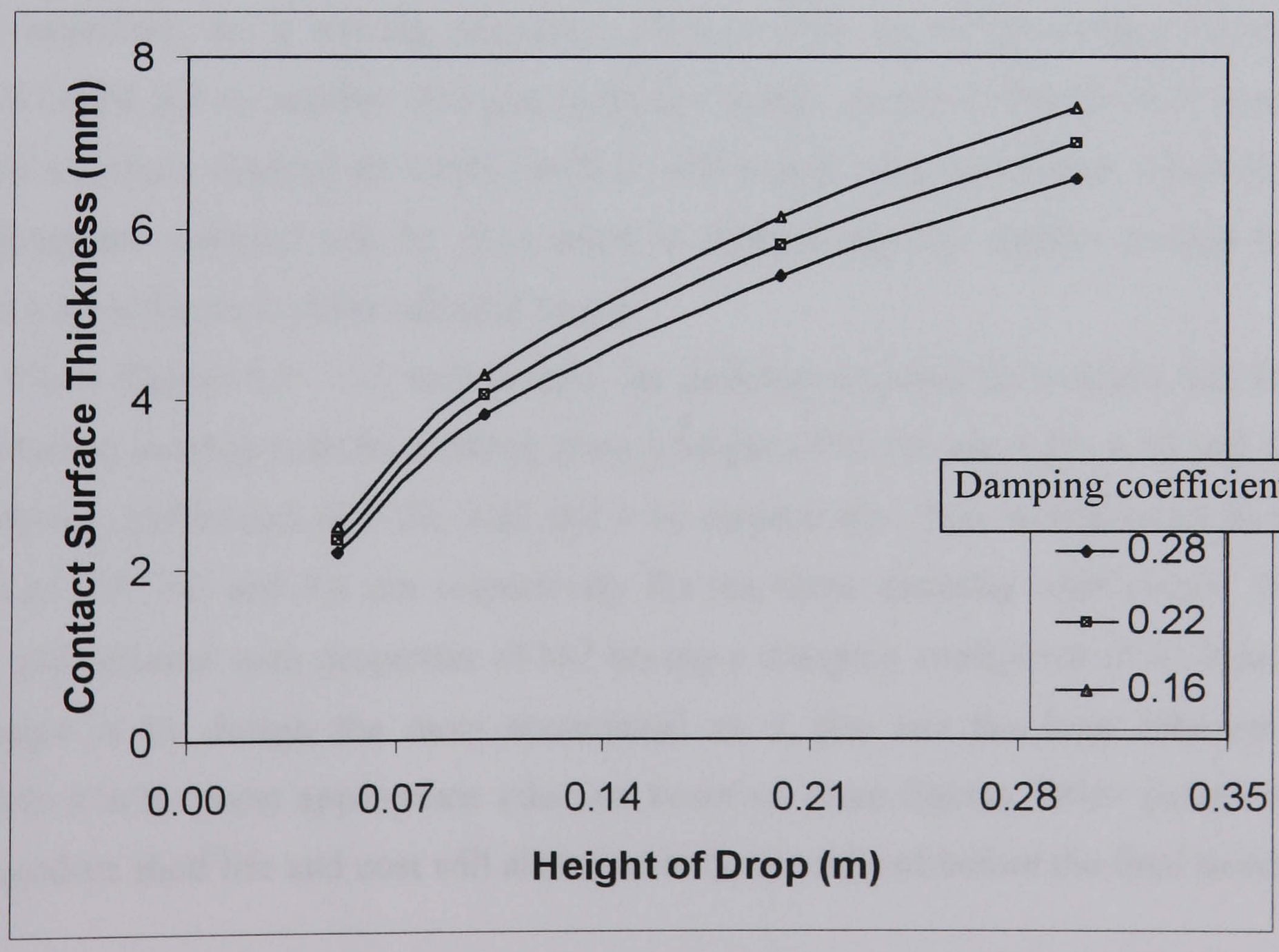

Figure 5.4 Contact surface thickness for material with E = 0.47 MPa

Design parameters can be obtained for specified data corresponding to those obtained or required in the design of a processing line for materials with properties within the range used. Figure 5.5 shows the combination of such curves for all the parameters considered. When a material falls on a surface it bounces a number of times before coming to rest. The rebound height depends on the damping coefficient, which determines the energy dissipated at impact. The percentage of the total energy of fall regained during unloading at the first contact and the corresponding rebound height for the materials at different damping coefficients are as shown in Figures 5.6 and 5.7.

The percentage of total energy regained (Figure 5.6) is equal for different drop heights at the same damping coefficient but decreases with increasing damping at the same drop height. This relationship applies to all the materials and the figures are the same for different materials. This shows that the rebound is independent of the material type but depends on the damping coefficient between the contact surfaces. This is another useful parameter that must be considered in design hence the information in Figure 5.5 has to be combined with those from Figures 5.6 and 5.7. The contact force shown in Figure 5.8 showed an inverse relation compared to the deformation with different material properties.

It is desirable to keep the rebound height to the minimum so as to reduce fruit to fruit impact especially on a moving conveyor where a fruit on its downward journey after rebound might fall on another fruit just dropping on the conveyor. Therefore it is necessary to select a surface material on which the fruit will almost stick on contact. The selection of the appropriate material will be incomplete in determining the contact surface thickness without a consideration of the rebound height.

From Figures 5.5 - 5.7, for example, the thickness required for material M2 for use as the contacting surface with fruit falling from a height of 20 cm are 4.38, 4.72 and 4.99 mm for damping coefficients of 0.28, 0.22 and 0.16 respectively. This would result in rebound heights of 5.8, 7.2 and 8.8 cm respectively for the three damping coefficients. From the above, any material with properties of M2 having a damping coefficient of 0.28 on contact with apple is by design the most economical as it also has the least rebound height. Therefore it is the most appropriate selection based on these figures. Other parameters such as the product shelf life and cost will also need to be considered before the final selection.

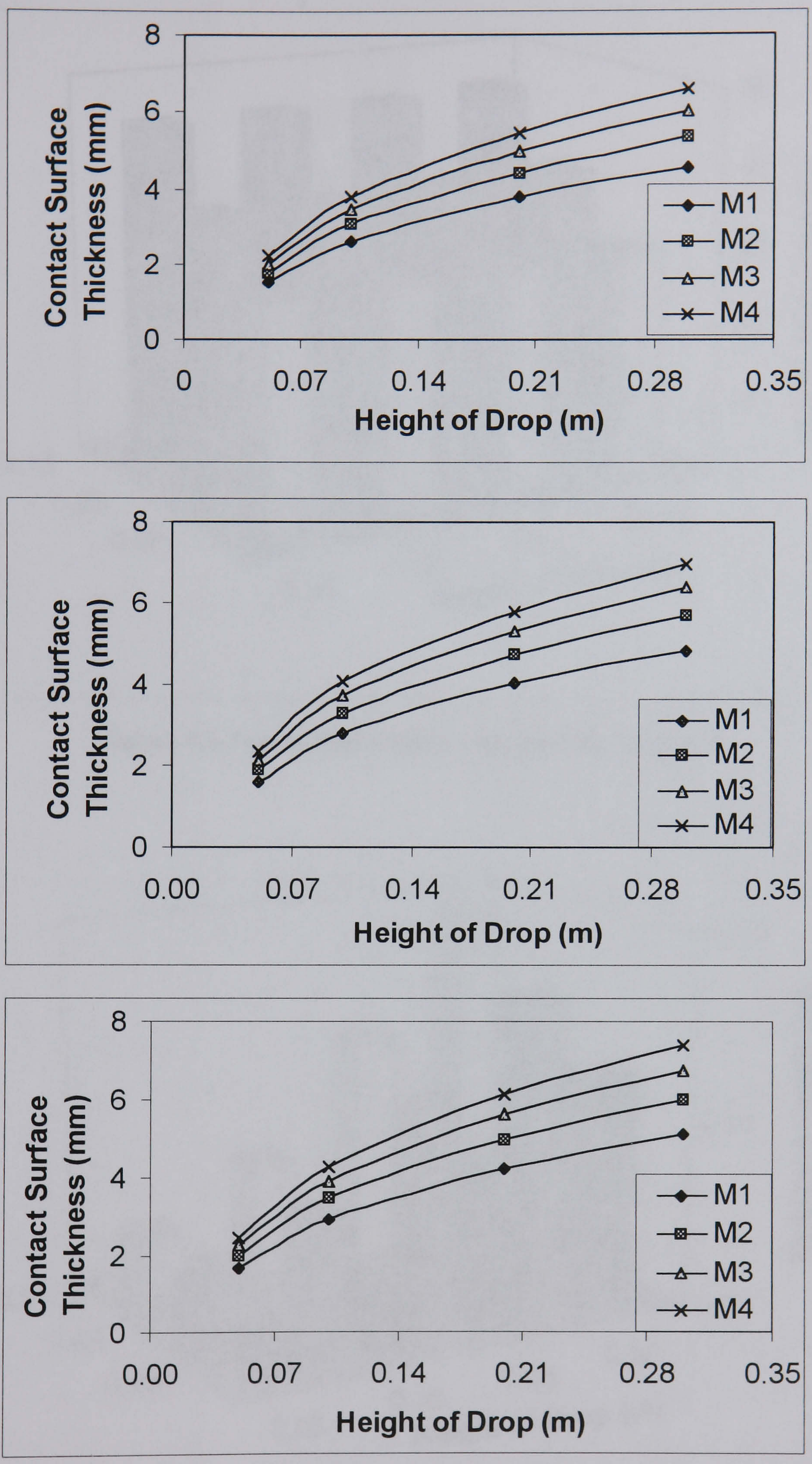

Figure 5.5 Contact surface thickness for different materials with damping coefficient 0.28 (top), 0.22 (middle) and 0.16 (bottom).

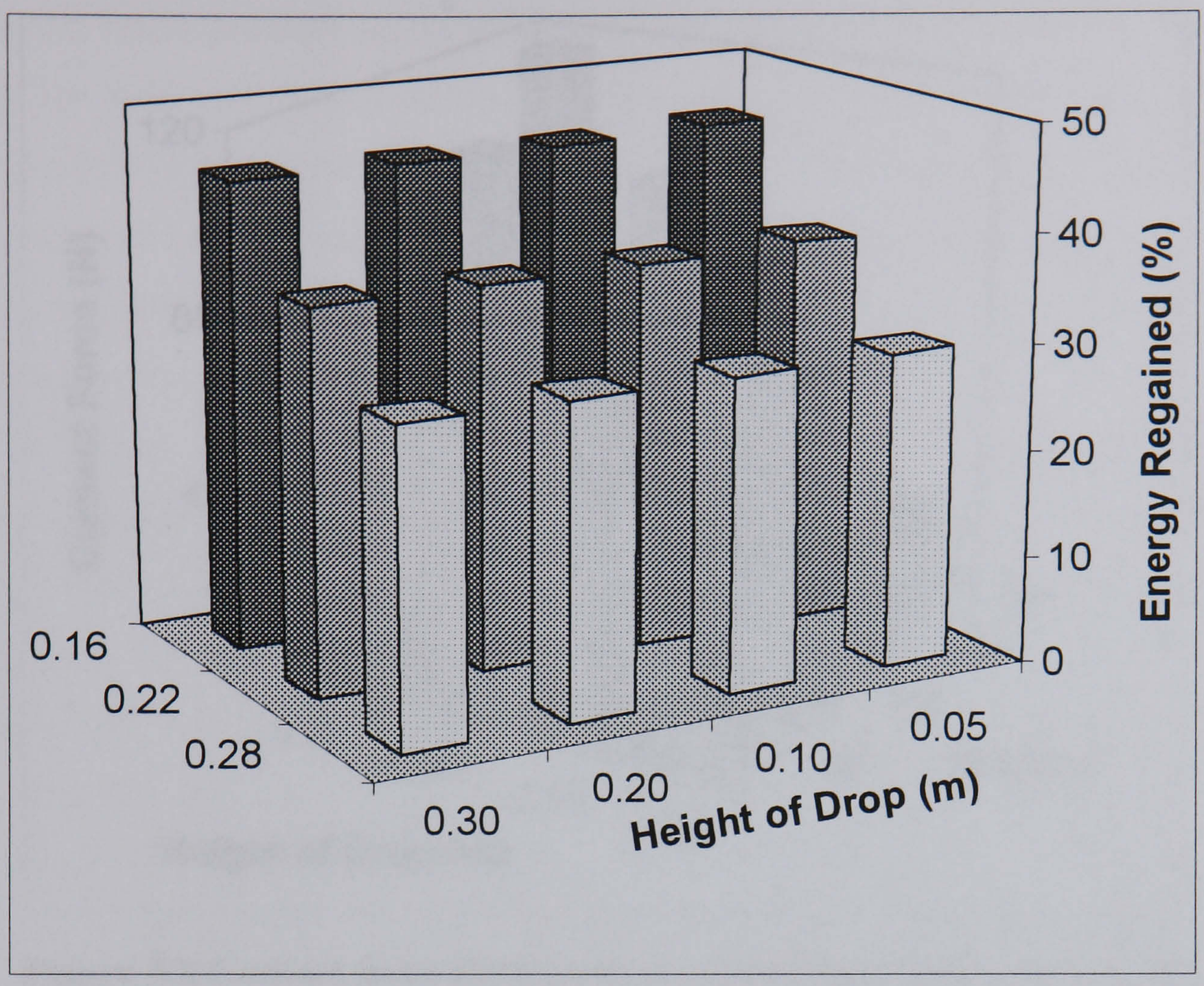

Figure 5.6 Percentage energy regained for rebound

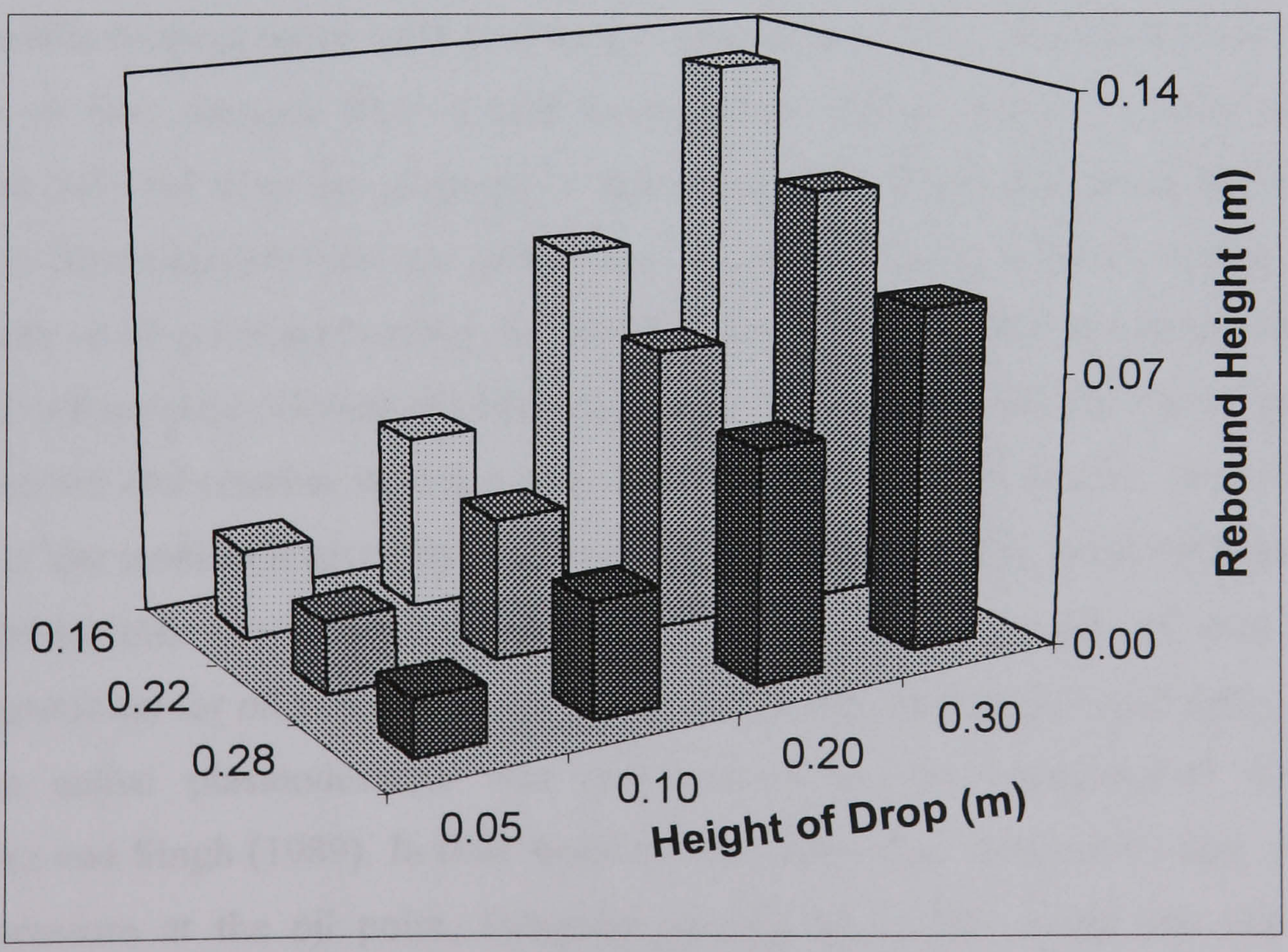

Figure 5.7 Rebound height after first impact

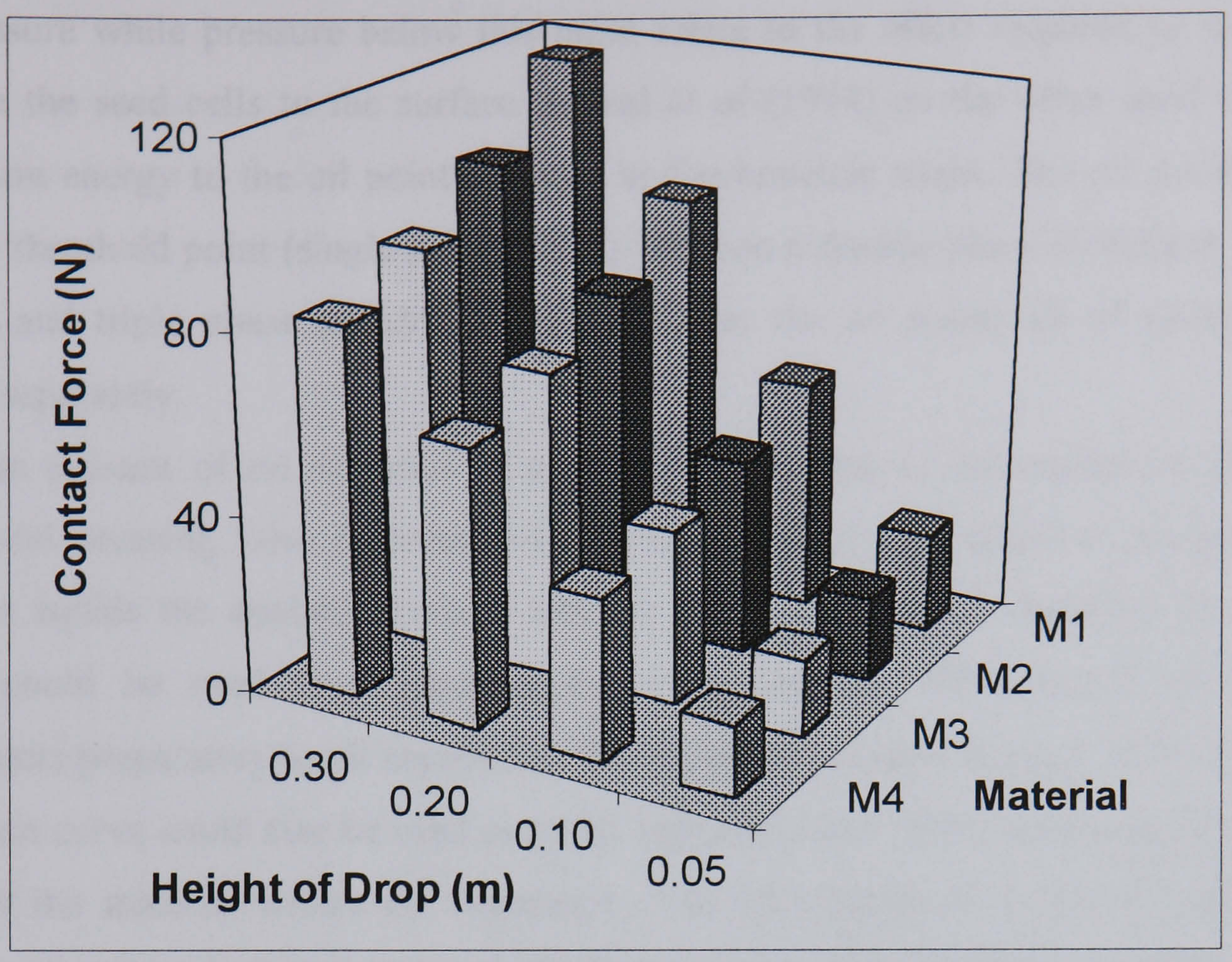

Figure 5.8 Contact force during impact (Damping coefficient = 0.22)

5.2 Seed Oil Expression

Faborode and Favier (1996) in a study of oil expression in seeds developed a theory relating seedbed compression with seed kernel properties. A threshold compressive pressure at which oil first emerges from a seed kernel in a seedbed during mechanical seed-oil expression (referred to as the oil-point) is theoretically related to the kernel density, which enables its determination from the initial bulk properties of the seedbed. Theoretically the bulk density at oil point approaches the kernel density and the volumetric strain approaches the initial bed porosity. Mrema and McNulty (1985) therefore stated that the oil point is the limit in kernel deformation before a reduction in kernel volume occurs. Also the elastic modulus of the seedbed is given by the inverse of the compressibility at the oil point.

The hypothesis put forward by Mrema and McNulty (1985) that cell wall rupture is not a precondition for oil expression and that the oil moves through the permeable cell walls via pores called plasmodesmata was corroborated by the experimental findings of Sukumaran and Singh (1989). In their studies on a method for dynamically determining the applied pressure at the oil point, Faborode and Favier (1996) stated that the potential advantages of identifying the oil point include the need to predetermine the effective pressure required for oil expression. Sukumaran and Singh (1989) stated that the effective applied pressure for oil expression is considered to correspond to some value above the oil

point pressure while pressure below this point relate to the effort required to mobilise oil flow from the seed cells to the surface. Fornal *et al* (1994) on the other hand related the compression energy to the oil point pressure and volumetric strain. The oil point therefore marks the threshold point (single phase: solid) between a double phase (solid/gas i.e. before oil point) and triple phase (solid/liquid/gas i.e. after the oil point) all of which must be modelled separately.

The amount of oil removed in a pressing operation is influenced by the applied pressure and pressing time (Mrema and McNulty, 1985). The effective pressure for oil expression equals the applied pressure less the oil point pressure, therefore the oil point pressure could be used as a measure for evaluating the effectiveness of alternative pretreatments preparatory to oil expression. The oil point pressure being a point on the load-deformation curve could also be used as a first approximation to the work expended per unit volume of the material before oil expression. The knowledge of oil point, which makes estimation of some parameters such as bulk density at the point possible and used to estimate the effective length beyond which oil expression can take place is helpful in analysing the design and performance of oil expellers.

In a bulk system, the volumetric strain is expressed as the ratio of the change in volume to the original volume. For monotonic unidirectional (e.g. vertical) loading where there is no lateral deformation, the volumetric strain is simplified as the ratio of the vertical deformation to the original/initial bed height. For a compression process, the volumetric strain is proportional to the pressure increment applied. If constant material properties is assumed, the bulk compliance is given as the compressibility of the porous bed system (Faborode and Favier, 1996) and it is the inverse of the bulk compression modulus (B) (Faborode and O'Callaghan, 1986; Mohsenin, 1986). Therefore

$$\Delta V/V_i = -S\Delta P \qquad 5.1$$

where V is the volume, subscript i indicates initial, P, the pressure and S is the compressibility. The ratio of the bulk modulus (B_o) to the bulk density (ϖ_o) of the material bed at the oil point gives the specific energy of compression (E_o, kJ/kg) (Sitkei, 1986).

$$E_o = \frac{B_o}{\varpi_o} = \left[S_o \varpi_o\right]^{-1} \qquad 5.2$$

Sukumaran and Singh (1989) reported that the oil point strain and pressure are functions of the moisture content and deformation rate. Figure 5.9 shows the variation of the bed compressibility, specific energy, and applied pressure for palm kernel in the experimental work reported by Faborode and Favier (1996). Most reported work on oil expression

presented only the values at the initial and oil point. The DEM simulation, which permits a step-by-step determination of parameters in a bulk system, is a useful tool for modelling the oilseed bed compression. The variation in the relevant parameters before the oil point can easily be estimated at any point and the necessary information extracted.

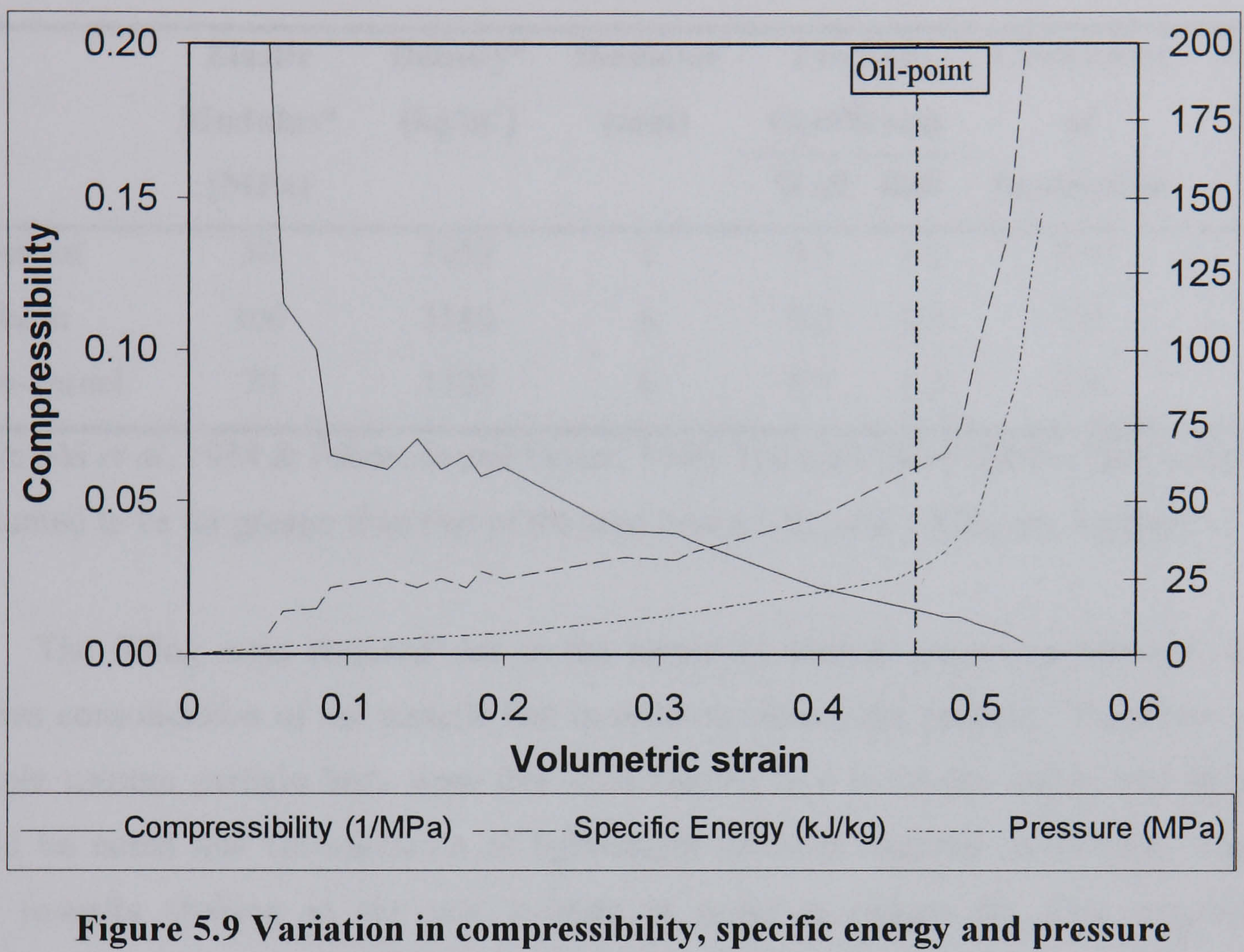

Figure 5.9 Variation in compressibility, specific energy and pressure during compression for palm-kernel (Faborode and Favier, 1996)

5.2.1 Simulation

Having established the validity of the new model for deformation and shape prediction as discussed in Chapter Four, the model was used for simulation of compression of four oilseed beds from three types of oilseed; oilseed rape, soybean and palm-kernel. The first is the seedbed used in the experiment reported in 4.4 with a single vertical layer of oilseed rape and this will be referred to as R1. The second bed of oilseed rape (R2) was prepared by randomly generating seeds in a box of size 0.01 x 0.02 x 0.01 m^3 hence a seedbed many particles thick was obtained. For the other studies, two seedbeds using the mechanical properties of soybean and palm-kernel were also prepared by generating particles randomly into a box of size 0.03 x 0.06 x 0.03 m^3. A particle diameter of 6mm was assumed for both soybean and palm kernel and for the three seedbeds, 156 particles were generated resulting in a filling ratio of 0.624. This ratio is with respect to filling the box with

particles uniformly arranged in stack on top of each other vertically and placed side by side horizontally which would result in a total of 250 particles for the specified box size. Table 5.1 shows the relevant physical properties of the seeds and data used in the simulation.

Table 5.1 Oilseed material properties and data used in simulation

	Elastic Modulus* (MPa)	Density* (kg/m^3)	Diameter (mm)	Friction Coefficient		Coefficient of Restitution	Strain Rate (s^{-1})
				Wall	Ball		
Rapeseed	30	1053	2	0.3	0.5	0.6	250
Soybean	100	1180	6	0.3	0.4	0.5	250
Palm-kernel	70	1125	6	0.3	0.4	0.4	230

(* Bilanski *et al*, 1994 & Faborode and Favier, 1996. The walls have infinite radius and EM_w is assumed to be far greater than that of the seed hence $1/R_w$ and $1/EM_w$ are negligible)

The filling ratio obtained due to the nature of random particle generation usually requires consolidation of the particle bed in order to reduce the porosity. Therefore all the multiple column particle beds were first consolidated to a relatively stable bed height. It should be noted that consolidation of lightweight particles requires an externally applied force (usually shaking in the real system) in order to reduce the time required for consolidation and to obtain a closely packed bed. In DEM this can be in form of increasing the acceleration due to gravity, application of alternating acceleration horizontally (shaking or vibration), application of strain rate or increasing the particle density. In DEM, after consolidation with these methods, the forces and velocities may be set to zero such that the system is assumed to represent a freshly generated bed. In this study only the lightest of the seeds, rapeseed (R2), was assisted in consolidation by increasing the particle density. Its true density was then used during the compression process. Soybean and palm-kernel were allowed to settle under self-weight to a stable height after which they were compressed slowly to allow further settling of the materials.

Constant instantaneous strain rates 250, 250 and 230 s^{-1} was applied on the loading wall during compression for oilseed rape, soybean and palm-kernel respectively. The reason for using these figures which appear 'too' high was due to the very short time of compression with the very low time steps that were used. As discussed in 4.2.2.2, a method was proposed and used for the determination of time step, which gave accurate prediction of

contact force. This time step was found appropriate in the compression of rigid or large soft particles, consolidation and flow. However it resulted in computation instability in the compression of small particles at high pressure as a result of the sudden push or release of a particle from a trapped position during particle rearrangement. A particle in contact with a wall having some unoccupied space around it experiences a sudden push due to the high pressure from the wall and in turn collides with other particles at high velocity causing instability. Ng (1989) noted that the approximation for computation of contact forces and area deteriorates as the difference between the radii of the contacting bodies increases. Therefore the difference in particle radius and the infinite wall radius as well as the large difference in the stiffness properties of these soft materials and the hard wall may also contribute. This requires further research. A sudden push or movement may result in very high velocity, which places the particle outside the box or deep into another particle at the next time step.

As discussed earlier, the computational instability can be corrected by reducing the time step. Therefore in each study the time step was reduced further each time an unstable computation occurred until an appropriate one was obtained. The selection or determination of the appropriate fraction of time step constituted the bulk of the computation time. In each case the instability was usually obtained after about 12-24 hours real time (approximately 8-20 hours CPU time depending on the period of computation on the time- sharing SUNs Ultra systems with 128Mb RAM). This resulted in repeated simulation before stability was obtained almost up to the oil point.

The fractions of time step used in each of the simulations reduced as porosity reduced such that very low fractions were used towards the end of the compression stage. The fractions of time step ranged from 0.05 to 0.002, 0.4 to 0.002, 0.05 to 0.0007 and 0.05 to 0.0005 resulting in approximately 6×10^5, 3×10^5, 1.54×10^6 and 2×10^6 iteration cycles before the oil point for rapeseed beds R1and R2, soybean and palm-kernel respectively. Details of the changes in the time step with number of cycles can be obtained from the input file for each simulation process in Appendix E.

The simulations were repeated until stable conditions that enabled computation up to or near the oil points were obtained. This process involved reducing the time step before the position at which instability occurred. An instability was indicated by a particle placed outside the box or too deep into another particle such that their centres almost coincided. The programme was either terminated automatically if the index for instability was turned on or allowed to go through a number of iteration cycles and the point of instability noted. This

trial and error method is commonly used in DEM. Therefore the determination of appropriate time step for simulation in DEM requires further research.

Each of the seedbeds was compressed to the oil point. This is the point, as stated earlier at which the bulk density of the seedbed approaches the seed kernel density. This indicates that there is no void space within the seedbed. However according to Mrema and McNulty (1985) the seed kernel reduction in volume occurs (permanent deformation) from this point onwards, which allows further compression. Oil is also released into the bed. The available data (bulk density) at oil point from the experiment by Faborode and Favier (1996) were used to determine the oil point at which the simulations were terminated.

5.2.2 Results and Discussion

Table 5.2 shows the summary of the time steps and the computation time for each case. During each simulation, the volumetric porosity with the new model and original code, bulk density, number of contacts (particle-particle, particle–wall), coordination number (number of contacts per particle), average contact area, pressure (reaction of the bed on the loading wall), compressibility, and specific energy were recorded with time.

Table 5.2 Fractions of time step *(frac)*, iteration cycles and computation time.

		R1	R2	Soybean	Palm-kernel
Time step (s)	Critical	0.11×10^{-7}	0.11×10^{-7}	0.37×10^{-7}	0.33×10^{-7}
Frac		0.005 - 0.002	0.4 – 0.002	0.05 - 0.0007	0.05 - 0.0005
Time step used (s)	Min	5.35×10^{-11}	2.14×10^{-11}	2.92×10^{-11}	1.95×10^{-11}
	Max	2.14×10^{-9}	4.28×10^{-9}	1.25×10^{-9}	1.63×10^{-9}
No. of cycles		6×10^{5}	3×10^{5}	1.54×10^{6}	2×10^{6}
Computation time	Real (h:m:s)	41:28:32	36:45:23	60:34:17	62:36:33
	$\frac{CPU}{Real}(\%)$	98%	88%	99%	98%
	Actual (s)	0.0030	0.0420	0.0380	0.0381

5.2.2.1 Compression of Single Kernel Thickness Seedbed

The results of compression of the one seed thick bed (R1) are as shown in Figures 5.10 - 5.14. Figures 5.10 – 5.12 shows the variation of the bed height and porosity average contact area and co-ordination number with volumetric strain; the total number of contacts

and wall contacts with time, during compression. The bed was compressed from a height of 14.16 mm to 6.2 mm with the porosity (volumetric) dropping to 0.6053×10^{-4} from an initial value of 0.5214 (Figure 5.10). In Figure 5.11 the co-ordination number (a measure of the number of contacts per particle) increased sharply at the initial stage of compression following the same trend as the number of contacts (Fig. 5.12) and became almost constant as the bed stabilised. The number of contacts on the wall also followed the same trend. The trend can also be observed in the variation in the average contact area which increased sharply (steeper slope) as the bed stabilised. This shows that the initial stage is the stage of particle rearrangement after which further compression results in bulk particle movement with contacts maintained. Change in bed height from that point is largely accounted for by particle deformation, hence the rise in contact area. From Fig. 5.11 the bed stabilised (constant co-ordination number) at a time of 0.0015 s corresponding to a volumetric strain of 0.31.

The variations in the bulk parameters relevant to oil expression are as shown in Figure 5.13. There is no available experimental data to be fitted onto this plot but data at oil point available are used for comparison as presented in Table 5.4. The compressibility of the bed was high at the initial stage corresponding to the stage of particle rearrangement and this dropped sharply as the number of contacts increases. The changes in energy of compression showed a direct inverse relation to compressibility while pressure increased with compression. As stated in the theory, the compressibility, energy and pressure at the oil point are the values at the point when the bulk density of the bed approaches the kernel density of the seed. The vertical dashed line in Figure 5.13 indicates the predicted or the approximate oil point at bulk density of 1040 kg/m^3. The values for all the simulation are summarised in Table 5.3. The trends of variation as plotted are found similar to that in Figure 5.9.

Figure 5.14 shows the images of the compressed bed (initial bed in Figs. 4.37 and 4.40) during simulation at volumetric strains of 0.285, 0.332, 0.382, 0.431 and 0.502. The porosity and bed height can be obtained from Figure 5.10. The bounding box is not shown hence the round edges of the particles in contact with the walls. The bed in Figure 5.10 was compressed with fraction of time step ranging between 0.005 – 0.002 (Table 5.2) while that in Figure 4.40 was compressed with a *frac* of 0.003 hence the difference in particle arrangement.

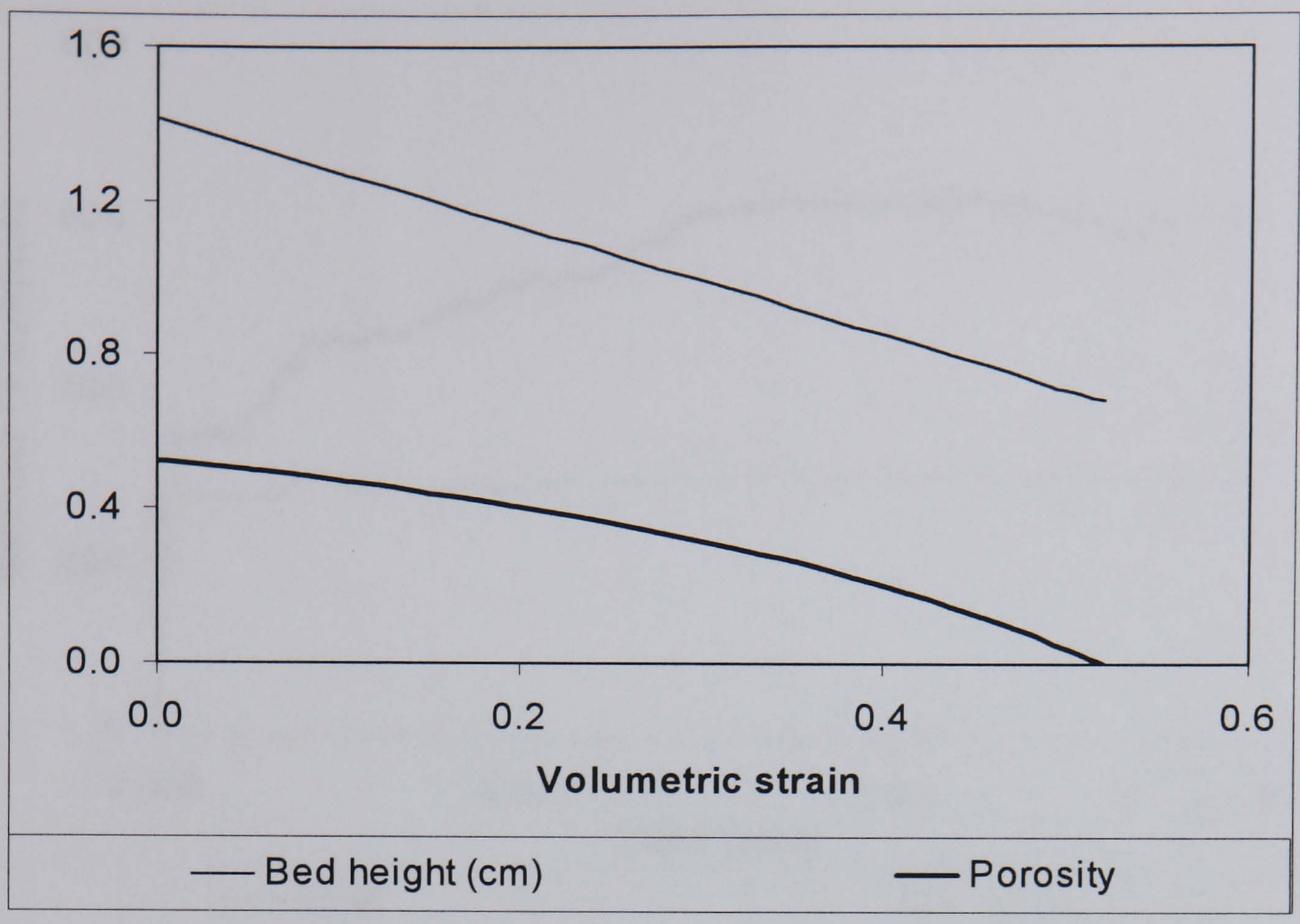

Figure 5.10 Changes in bed height and porosity during compression of R1

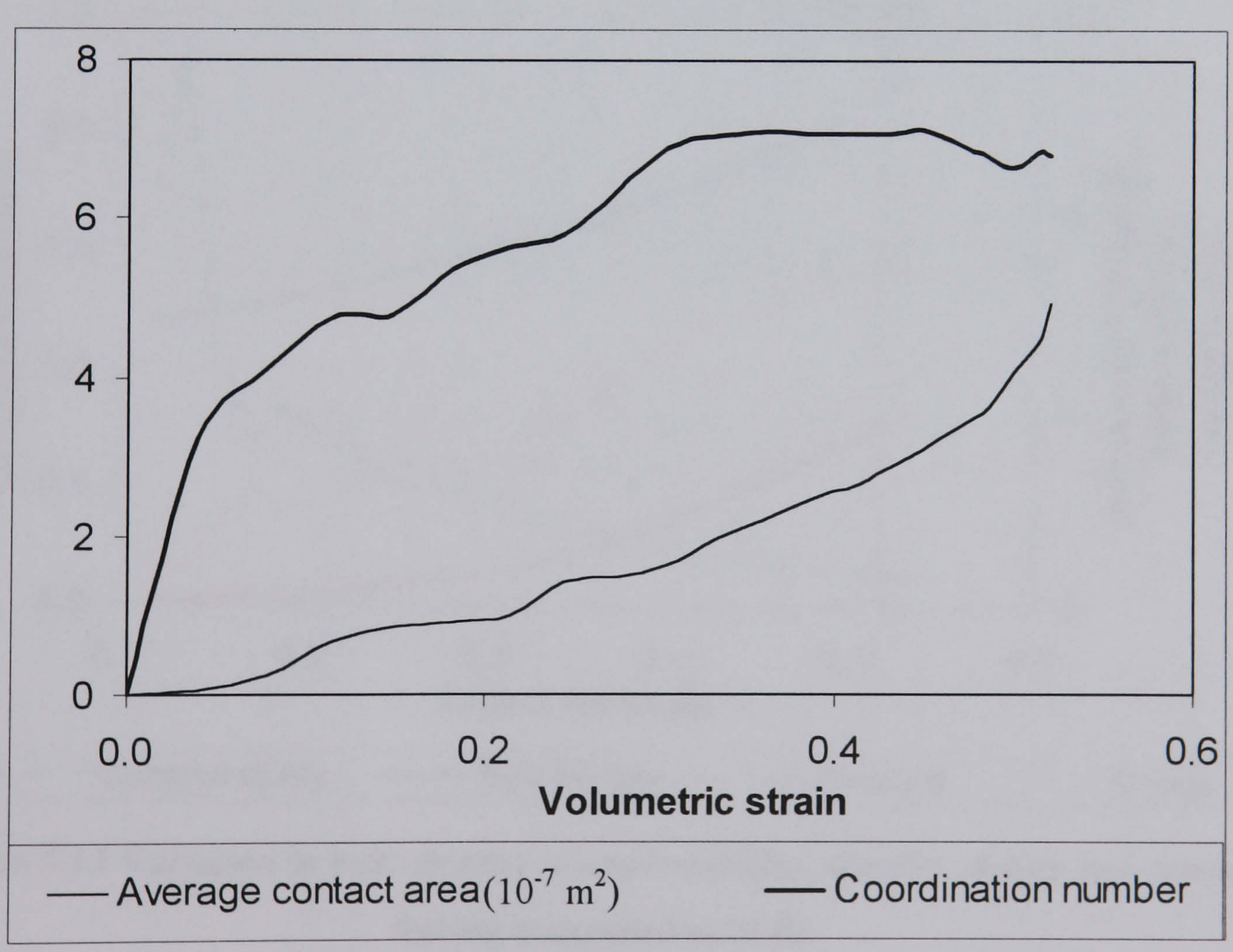

Figure 5.11 Average contact area and coordination number for R1

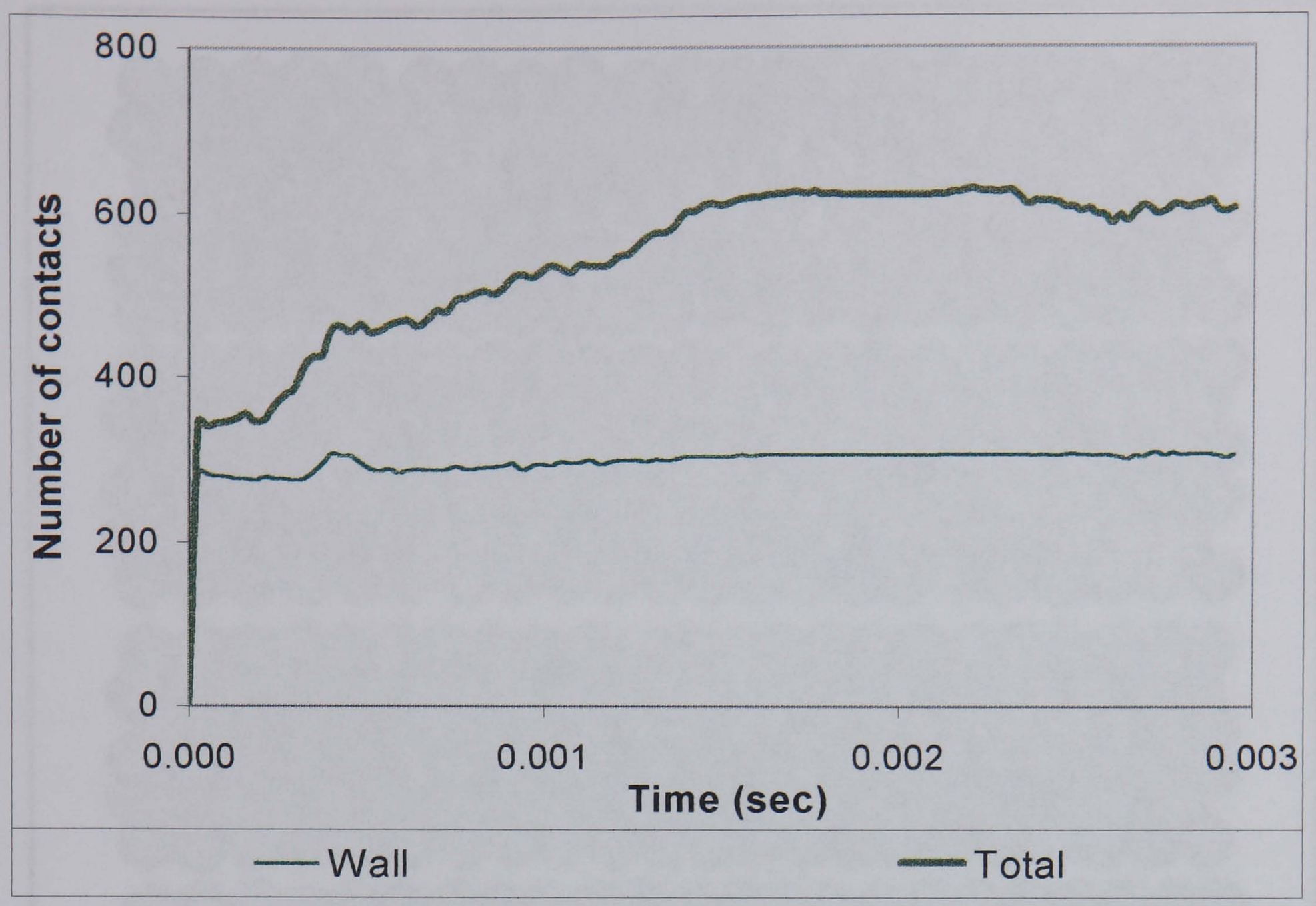

Figure 5.12 Number of contacts during compression of R1

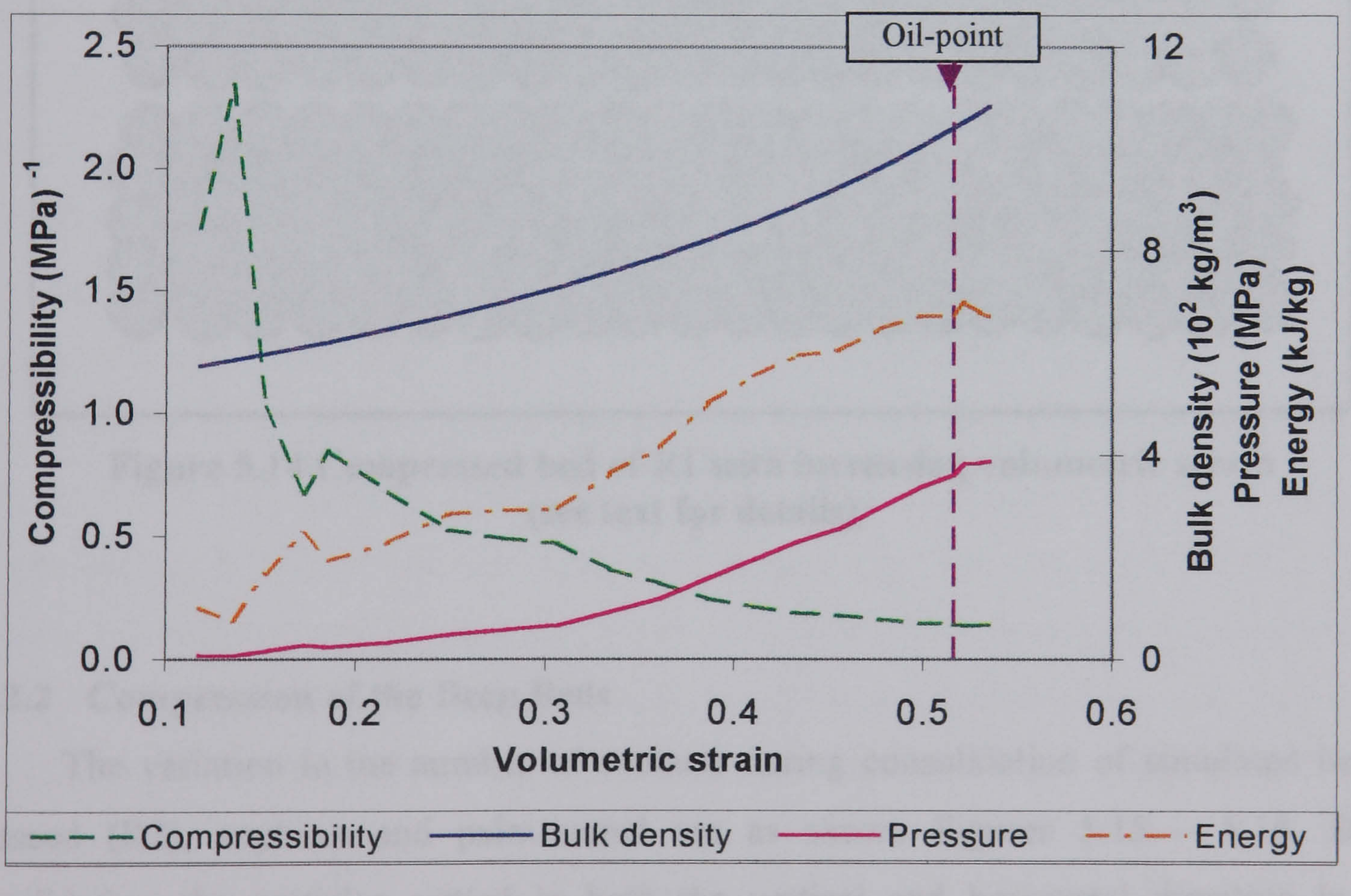

Figure 5.13 Variation in bulk density, compressibility, specific energy and pressure during compression of R1

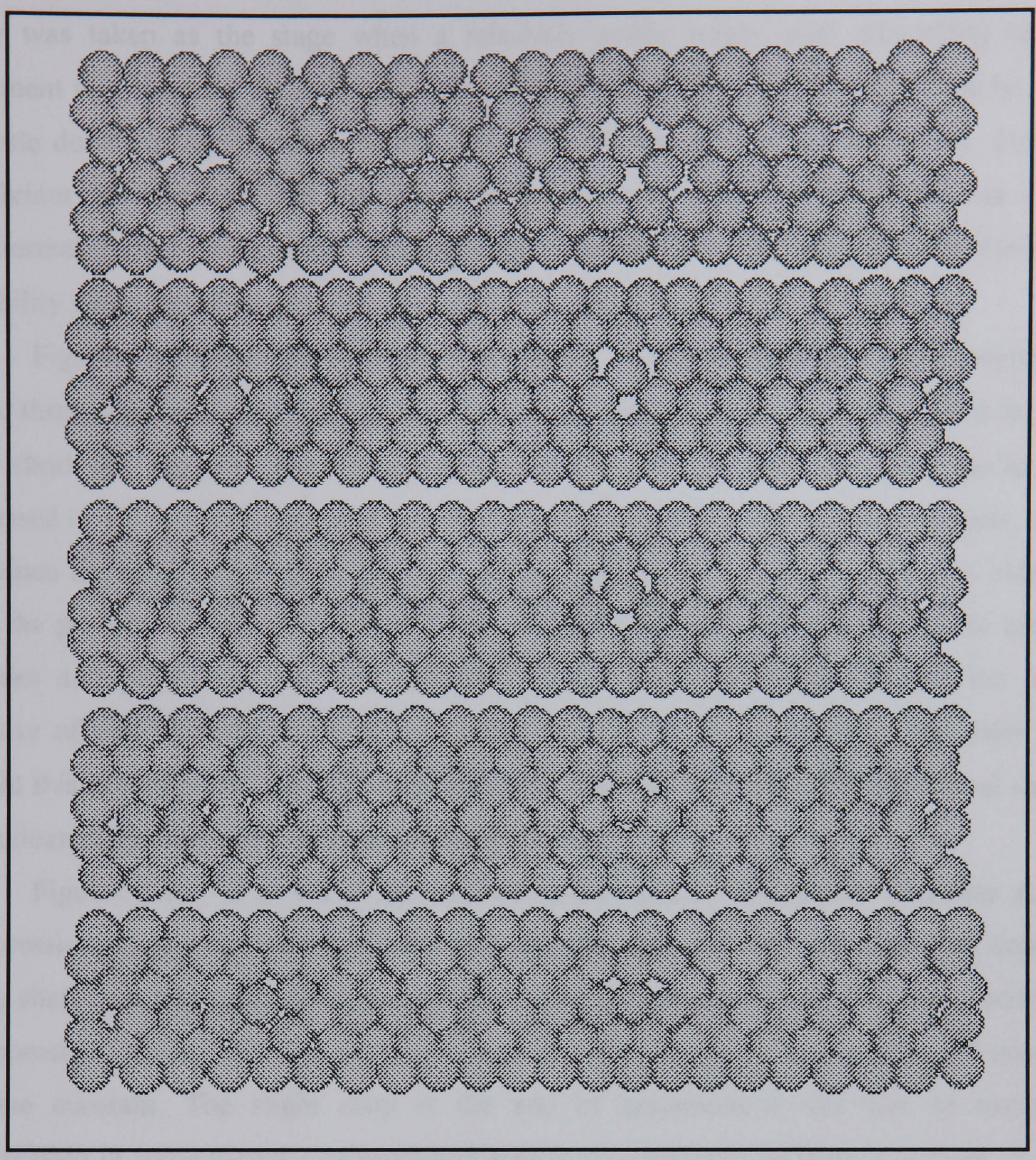

Figure 5.14 Compressed bed of R1 with increasing volumetric strain (see text for details)

5.2.2.2 Compression of the Deep Beds

The variation in the number of contacts during consolidation of simulated beds of rapeseed (R2), soybean and palm-kernel are as shown Figures 5.15 – 5.16. During consolidation the particles settled in both the vertical and horizontal direction but the downward movement was faster as they were consolidating under self-weight, hence the sharp rise in particle to particle contacts. This resulted in an increase in the number of contacts on the walls as the particles started spreading out towards the walls. In DEM it takes some time to obtain a stable bed, as the particles on the surface will tend to bounce a number of times before coming to rest. Therefore the end of the consolidation stage in this

study was taken as the stage when a relatively stable height with alternating contact increment was obtained before compression. The bed in Figures 5.15 and 5.16 can be made to settle down (to equilibrium) by introducing global damping or increasing the damping coefficient. However this was not introduced in this study, as it was desired to work within the normal particle parameters although this contributed to some of the problems of instability encountered later.

Figure 5.17 shows the changes in bed height during consolidation and compression of the three samples. From this figure it can be seen that the real compression periods were very short but required more computation time for the reasons discussed earlier. As discussed in 5.2.1, consolidation of sample R2 was achieved by increasing its density, so as to reduce the computation time required. A reduction of 40% in bed height was obtained with the porosity dropping to 0.4965 from an initial value of 0.6732 while in the case of soybean and palm-kernel, a 15% reduction in bed height was obtained and the initial porosity of 0.6732 dropped to 0.6367. From Figure 5.16 it can be seen that under self-weight this is the height to which the sample generated for soybean and palm-kernel can be consolidated, as the number of contacts had stabilised.

Figures 5.18 – 5.20 show the variation in the number of contacts with time during compression. From the figures a general trend can be observed with the number of contacts rising sharply as the particles rearranged due to the applied pressure as discussed above. As the porosity reduced and the system approached the oil point, the number of contacts became constant. The slight drop at the end of compression was due to excessive deformation in some particles as explained earlier resulting from sudden movement of such particles which were already under high pressure, when there was suddenly a free space around leading to loss of contacts with some neighbours. The nature of DEM in which particles will move as soon as they are free to do so affected the predicted pressure since the pressure was computed as the contact force of the particles on the loading wall. This can be corrected by further reduction of the time step or through some other methods that will be discussed later.

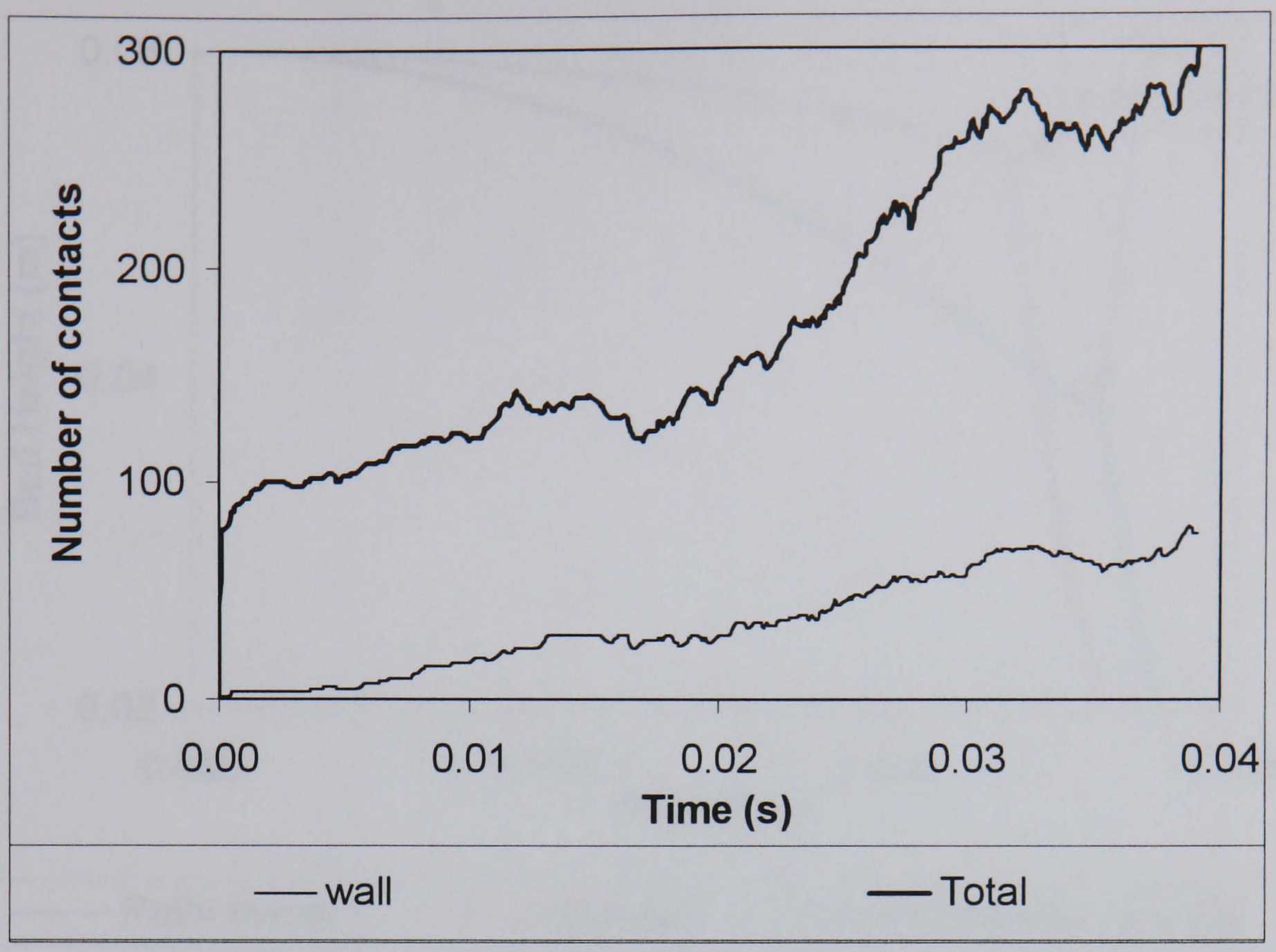

Figure 5.15 Number of contacts during consolidation of R2

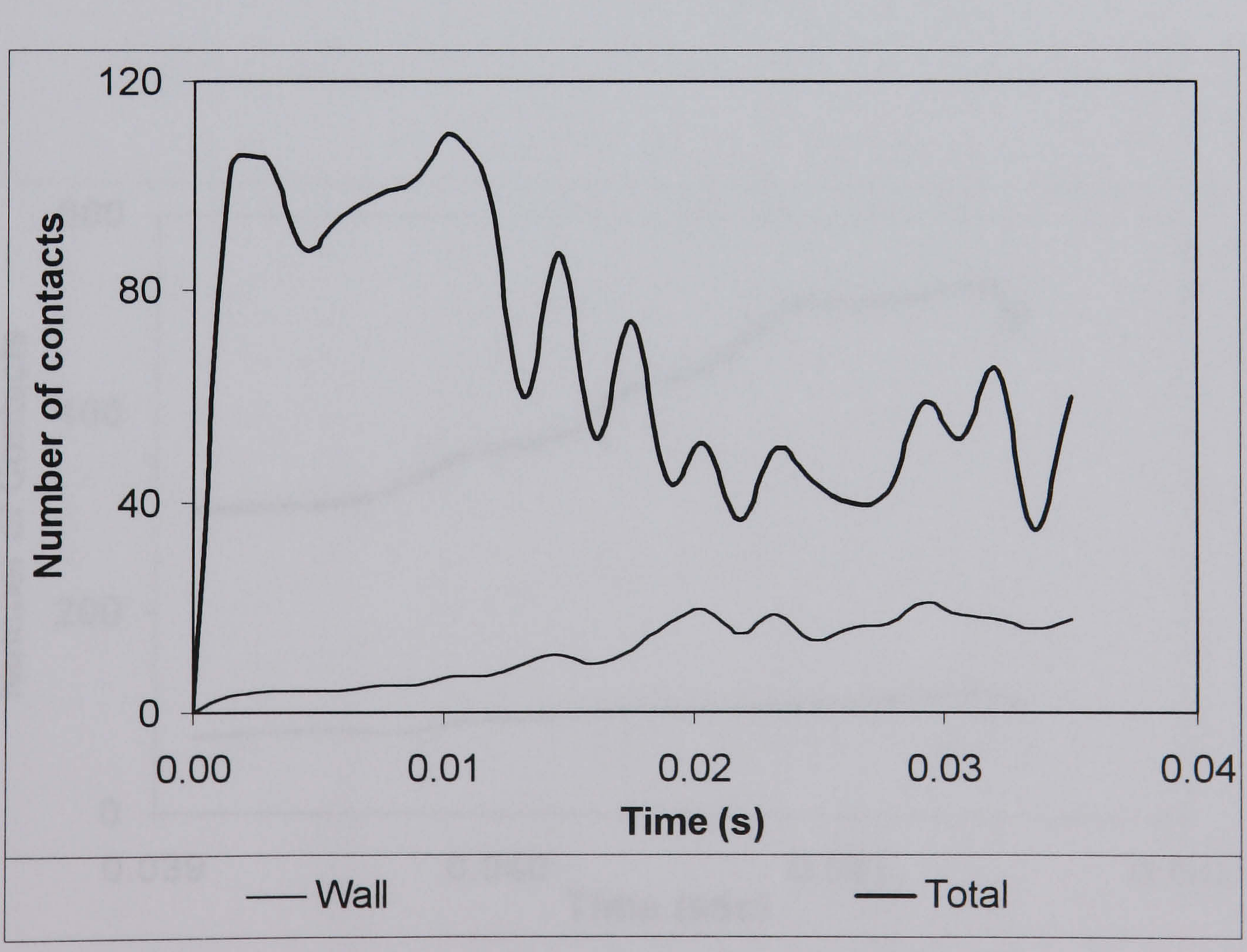

Figure 5.16 Number of contacts during consolidation of the sample used for soybean and palm-kernel.

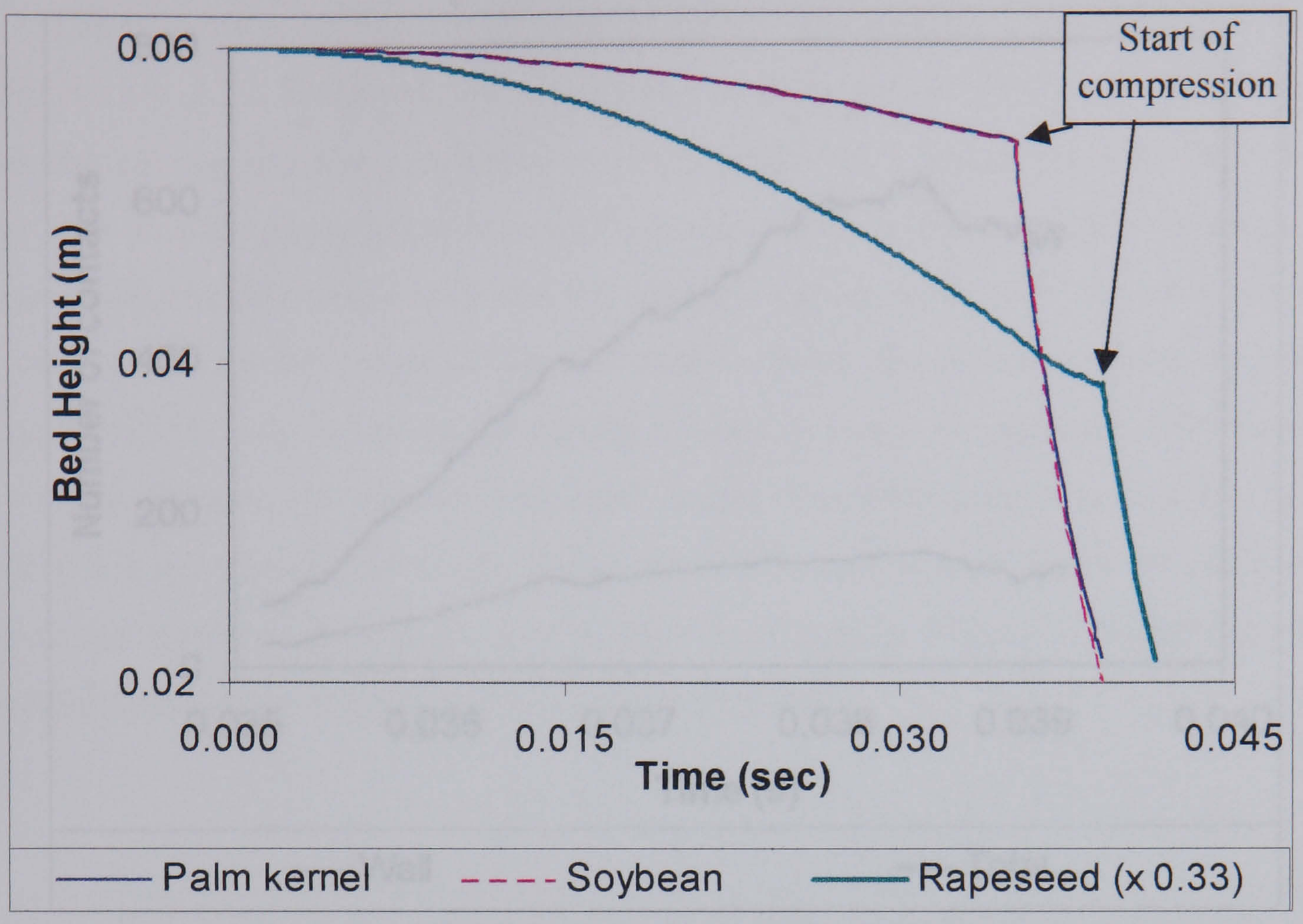

Figure 5.17 Variation in bed height during consolidation and compression of R2, soybean and palm-kernel

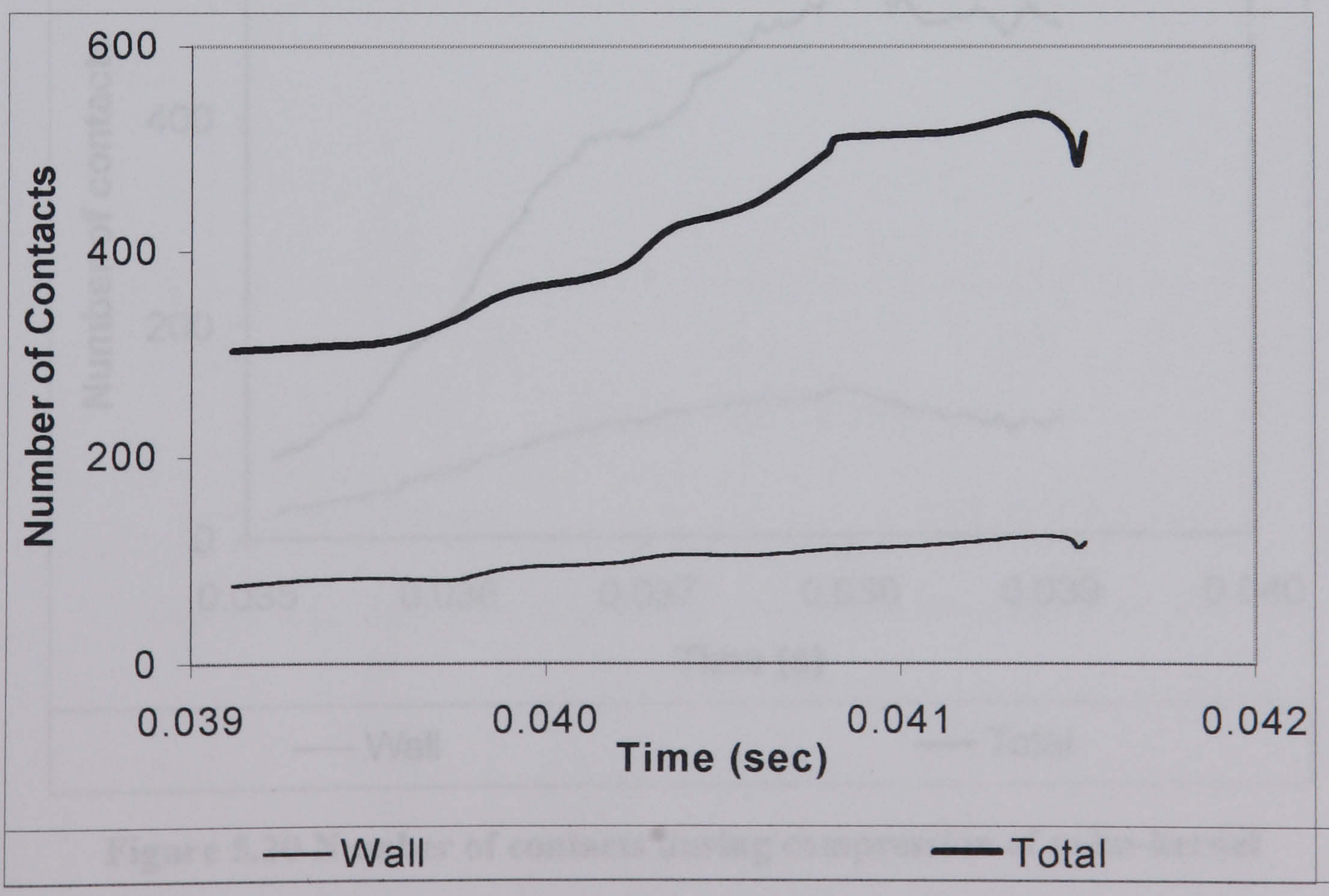

Figure 5.18 Number of contacts during compression of R2

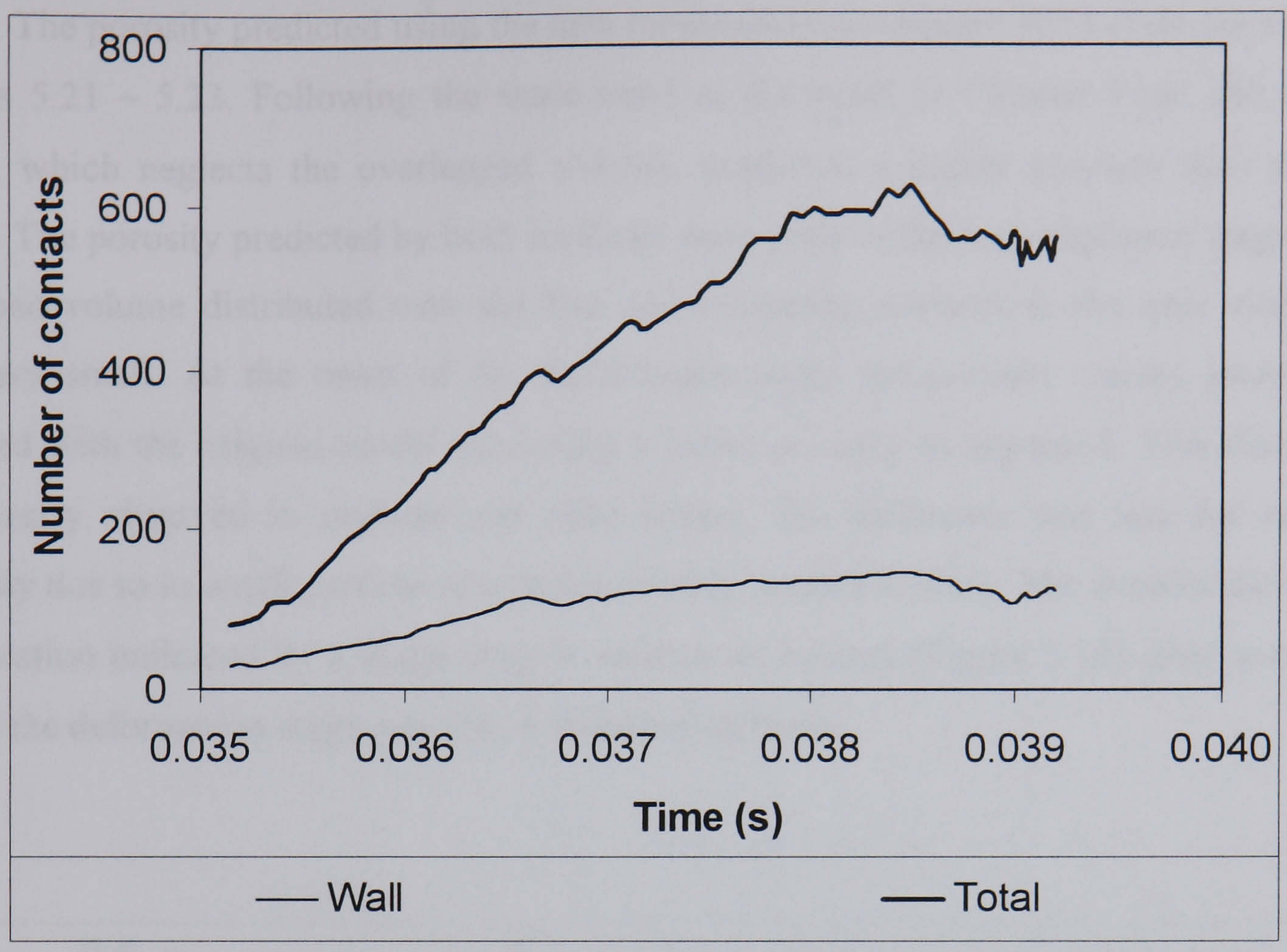

Figure 5.19 Number of contacts during compression of soybean

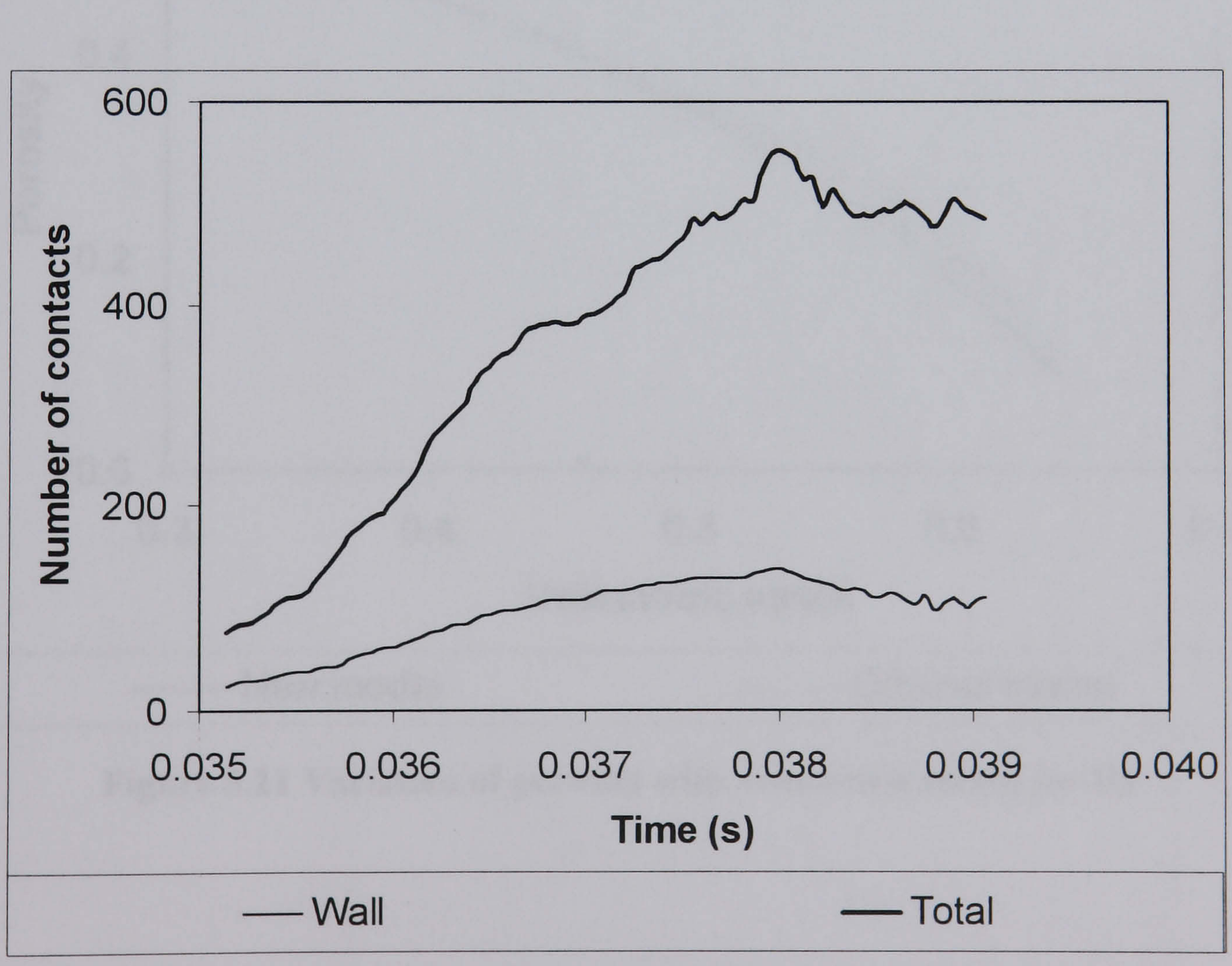

Figure 5.20 Number of contacts during compression of palm-kernel

The porosity predicted using the new model and the original DEM code are shown in Figures 5.21 – 5.23. Following the same trend as discussed in Chapter Four, the original model, which neglects the overlapped volume, predicted a higher porosity than the new model. The porosity predicted by both methods were close in the rearrangement stage, as the deformed volume distributed over the free non-contacting surfaces in the new model was still very small. At the onset of the deformation stage the porosity values increasingly diverged with the original model predicting a lower porosity as expected. This divergence was clearly observed in soybean and palm kernel. The difference was less for rapeseed probably due to its small particle size, hence smaller contact volume. The deterioration in the computation indicated by a slight drop in number of contact (Figure 5.18) after some time during the deformation stage was also a contributing factor.

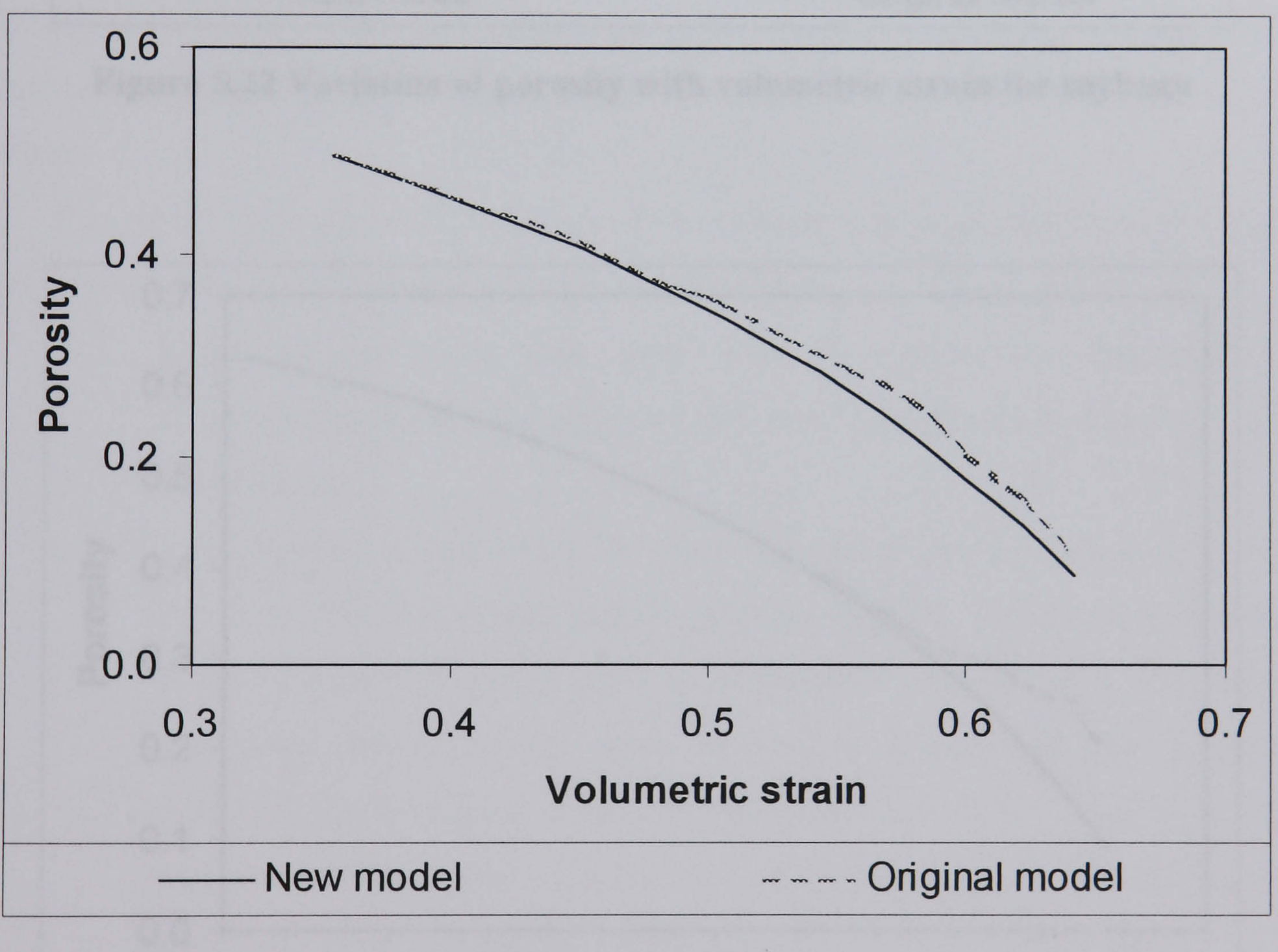

Figure 5.21 Variation of porosity with volumetric strain for R2

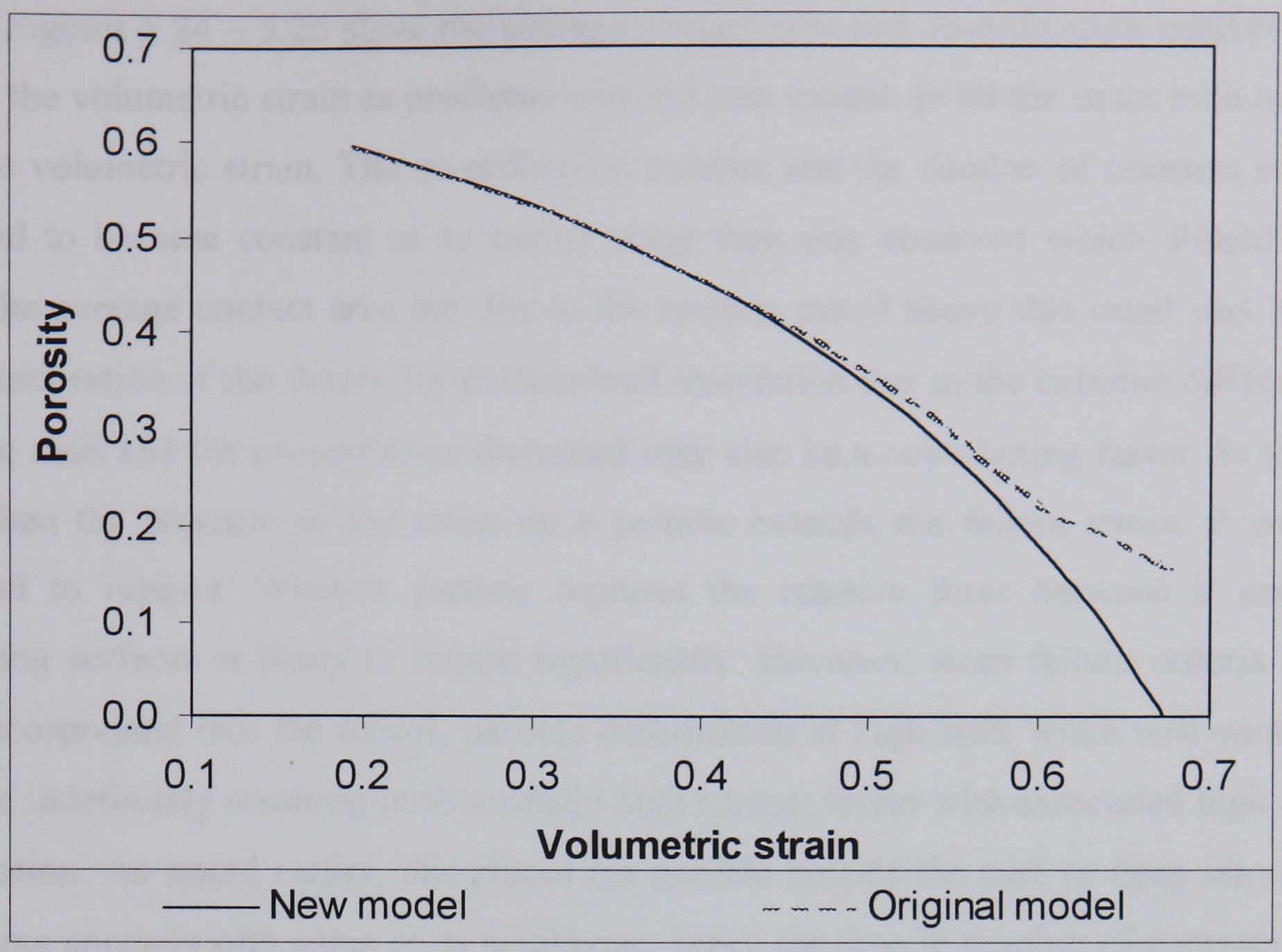

Figure 5.22 Variation of porosity with volumetric strain for soybean

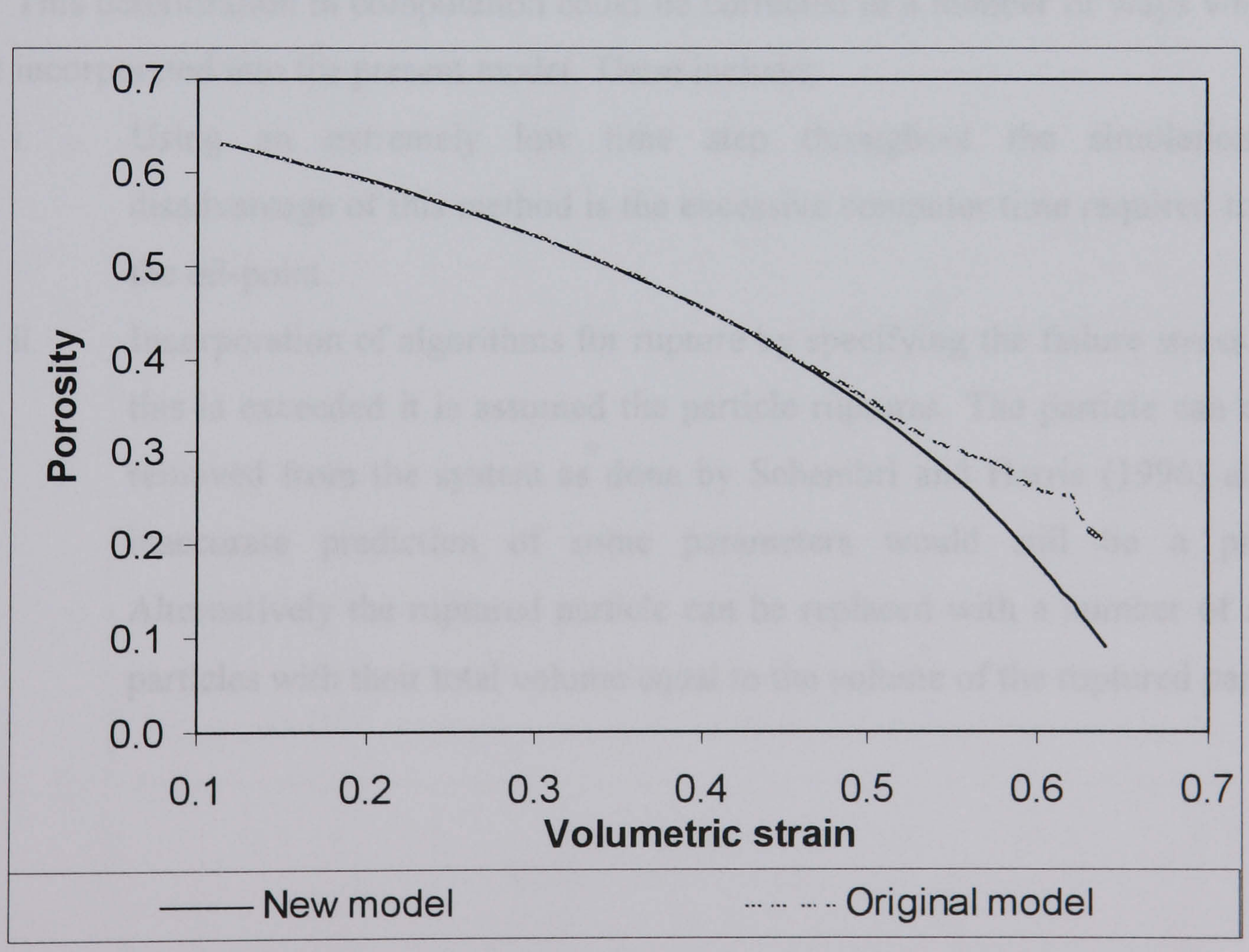

Figure 5.23 Variation of porosity with volumetric strain for palm-kernel

Figures 5.24 – 5.26 show the average contact area and co-ordination number plotted against the volumetric strain as predicted with the new model. In all the cases both increased with the volumetric strain. The co-ordination number and the number of contacts would be expected to become constant at an earlier stage than was observed which should in turn affect the average contact area but due to the reasons stated above this trend was delayed. The deterioration of the theory for particle-wall interaction due to the extreme differences in both the radii and the properties as discussed may also be a contributing factor. In the ideal case when the pressure or the stress on a particle exceeds the failure stress, it would be expected to rupture. When a particle ruptures the reactive force between it and other contacting surfaces is likely to reduce significantly. However, since failure criteria has not been incorporated into the model, particle deformation at high bulk strain will continue to increase indefinitely resulting in abnormally high contact forces with associated high particle acceleration. As stated earlier, this placed the particle outside the wall or deep into another ball losing contacts with some of its neighbours hence the drop in number of contacts. It also resulted in a drop in the predicted pressure and other relevant oil-point parameters as will be seen later.

This deterioration in computation could be corrected in a number of ways which are not yet incorporated into the present model. These include;

i. Using an extremely low time step throughout the simulation. The disadvantage of this method is the excessive computer time required to get to the oil-point.

ii. Incorporation of algorithms for rupture by specifying the failure stress. When this is exceeded it is assumed the particle ruptures. The particle can then be removed from the system as done by Schembri and Harris (1996) although inaccurate prediction of some parameters would still be a problem. Alternatively the ruptured particle can be replaced with a number of smaller particles with their total volume equal to the volume of the ruptured particle.

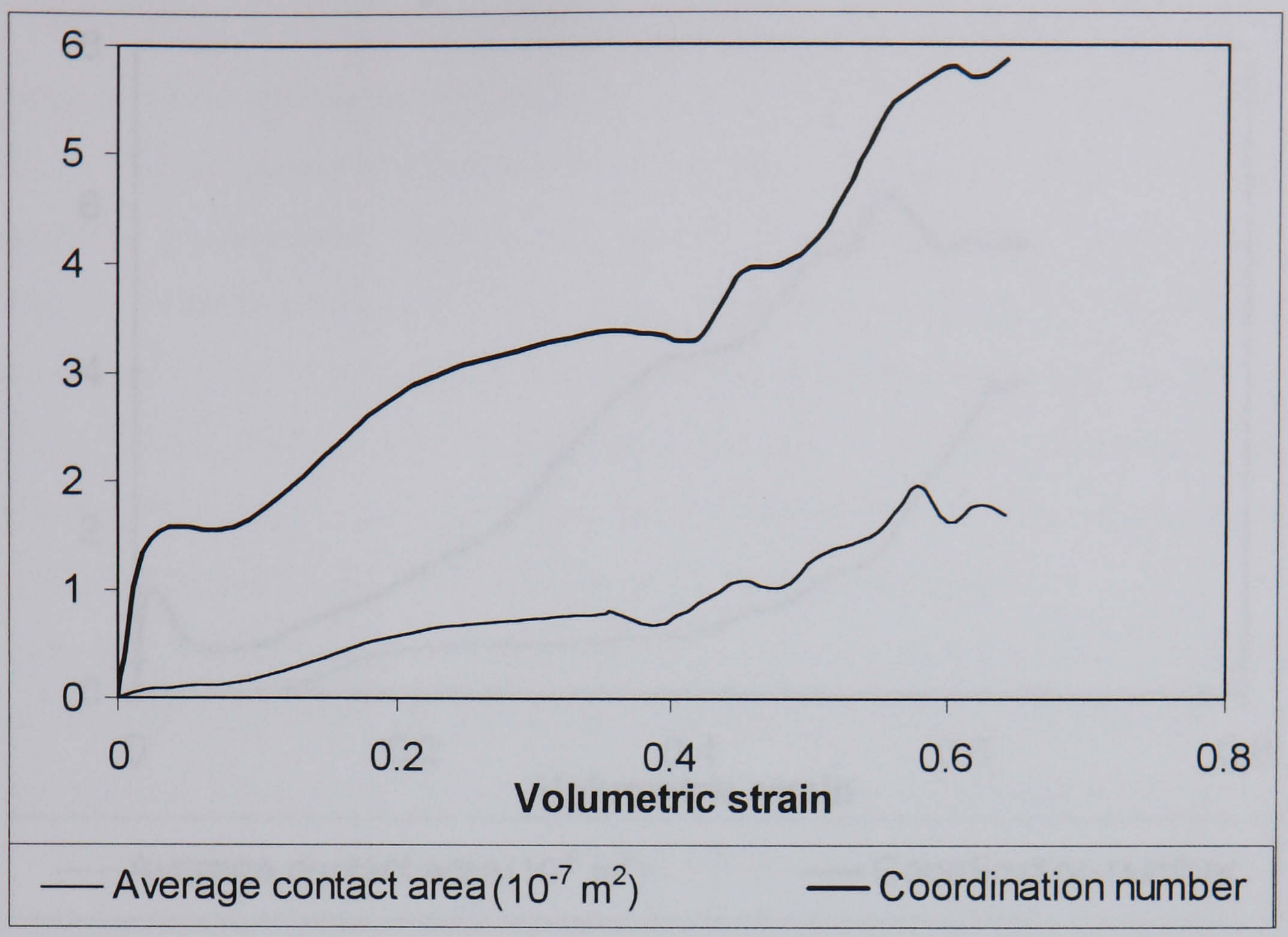

Figure 5.24 Average contact area and coordination number for R2 as predicted with the new model

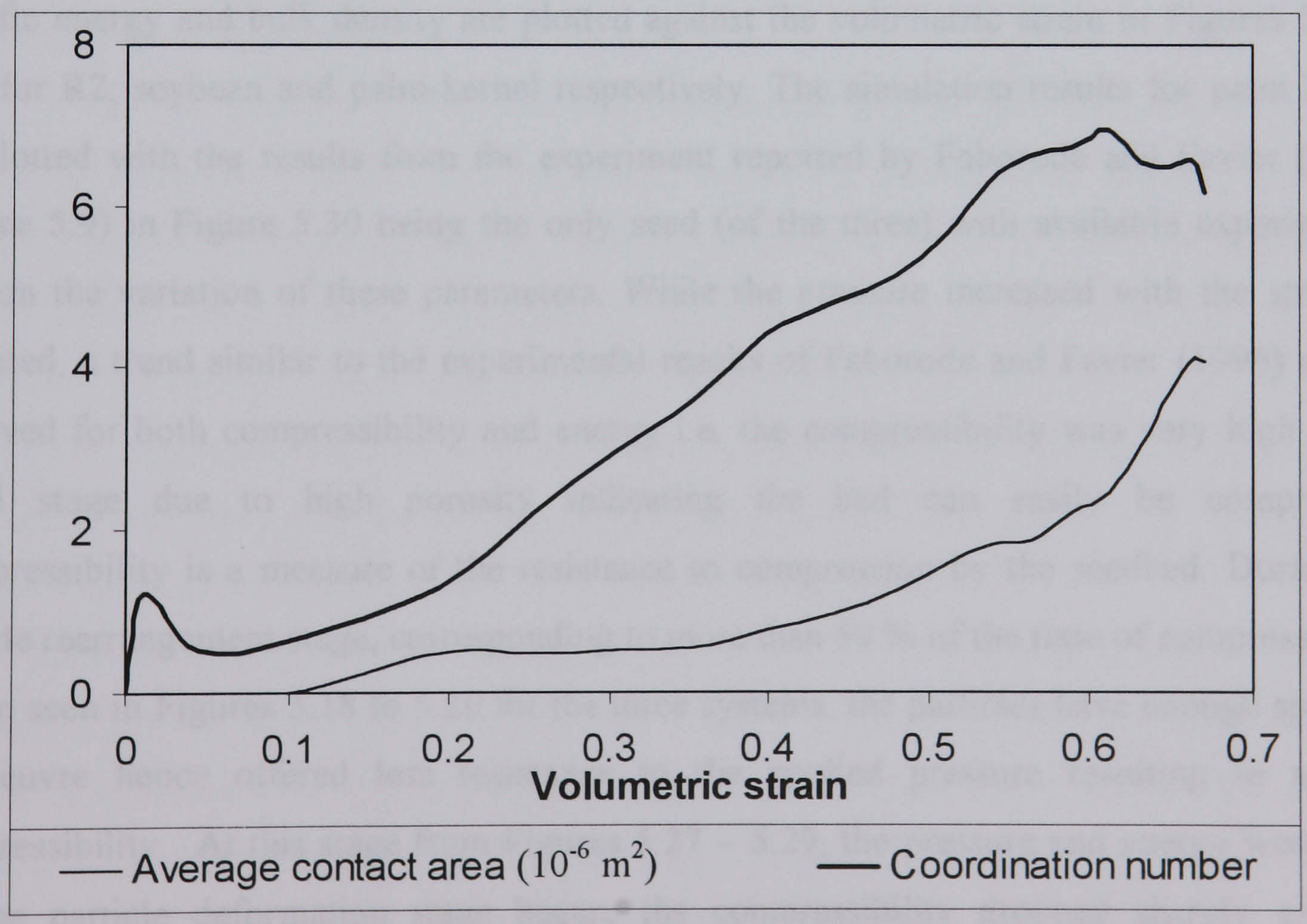

Figure 5.25 Average contact area and coordination number for soybean as predicted with the new model

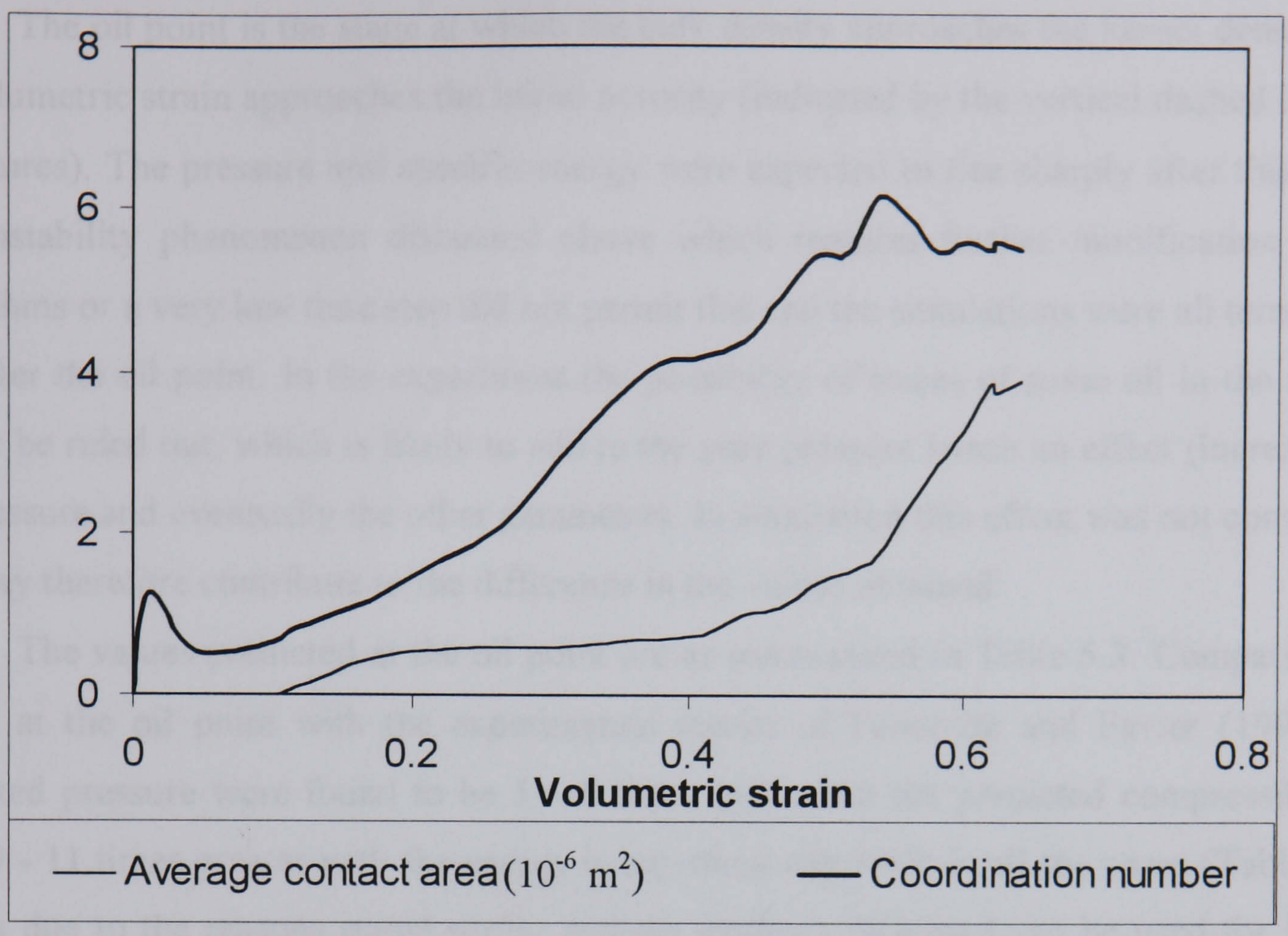

Figure 5.26 Average contact area and coordination number for palm-kernel as predicted with the new model

The bulk parameters for the determination of the oil point; pressure, compressibility, specific energy and bulk density are plotted against the volumetric strain in Figures 5.27 – 5.29 for R2, soybean and palm-kernel respectively. The simulation results for palm kernel are plotted with the results from the experiment reported by Faborode and Favier (1996) (Figure 5.9) in Figure 5.30 being the only seed (of the three) with available experimental data on the variation of these parameters. While the pressure increased with the strain as expected, a trend similar to the experimental results of Faborode and Favier (1996) can be observed for both compressibility and energy i.e. the compressibility was very high at the initial stage due to high porosity indicating the bed can easily be compressed. Compressibility is a measure of the resistance to compression by the seedbed. During the particle rearrangement stage, corresponding to more than 50 % of the time of compression as can be seen in Figures 5.18 to 5.20 for the three systems, the particles have enough space to manoeuvre hence offered less resistance to the applied pressure resulting in a high compressibility. At this stage from Figures 5.27 – 5.29, the pressure and energy were low. As the particle deformation stage began, the compressibility dropped sharply and the pressure and energy rose, indicating more energy and pressure were needed for compressing the system i.e. deforming the particles.

The oil point is the stage at which the bulk density approaches the kernel density and the volumetric strain approaches the initial porosity (indicated by the vertical dashed lined in the figures). The pressure and specific energy were expected to rise sharply after this point. The instability phenomenon discussed above which requires further modification in the algorithms or a very low time step did not permit this and the simulations were all terminated just after the oil point. In the experiment the possibility of traces of some oil in the system cannot be ruled out, which is likely to add to the pore pressure hence an effect (increase) on the pressure and eventually the other parameters. In simulation this effect was not considered and may therefore contribute to the difference in the values obtained.

The values predicted at the oil point are as summarised in Table 5.3. Comparing the values at the oil point with the experimental results of Faborode and Favier (1996) the predicted pressure were found to be 5 – 8 times less while the predicted compressibilities were 9 - 11 times greater with the energy being about one tenth in all the cases (Table 5.4). This is due to the reasons stated earlier and the methods discussed can be used for further investigation. The die charge i.e. the weight of the seeds used is of the order of ten less than that used in the experiment. This might be a contributing factor especially the constant 10 fold difference observed throughout the stages up to the oil point. However the trend of the variation predicted during the simulation is similar to that from the experiment in all the cases as shown in Figure 5.30.

When the pressure (from both the experiment and simulation) were normalised against the values for rapeseed, the normalised values for the simulation are 1.0, 1.005 and 1.86 for rapeseed, palm-kernel and soybean as compared to 1.0, 1.63 and 2.48 respectively for the experimental results. The trend is therefore similar in the simulation and the experiment with higher values obtained for soybean compared to palm-kernel. This indicates that the DE simulation was able to qualitatively represent the same differences between the response of different seed types as in the experiment. The introduction of other algorithms to handle rupture and instability effect may provide a closer prediction.

Generally, apart from the reasons stated, the results of both systems, simulation and experiment did not match except in the trend of variation since the two systems are not the same in all the cases in initial material arrangement, particle size, shape and the weight of the seed-bed. However as stated above, the similarity in trend shows that the model, with the necessary modification, is a promising approach for modelling the compression of bulk systems of particulates.

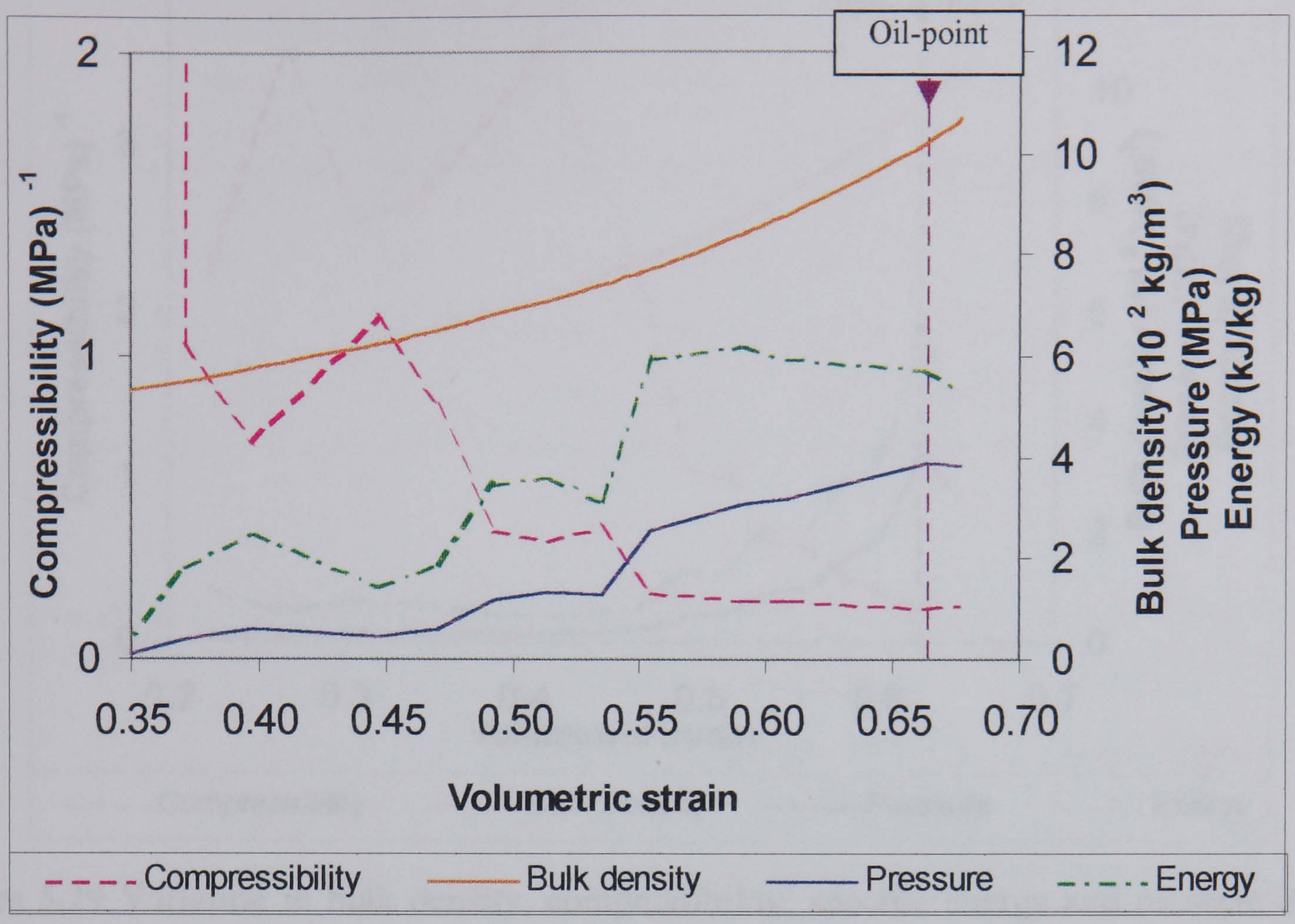

Figure 5.27 Variation in bulk density, compressibility, specific energy and pressure during compression of R2

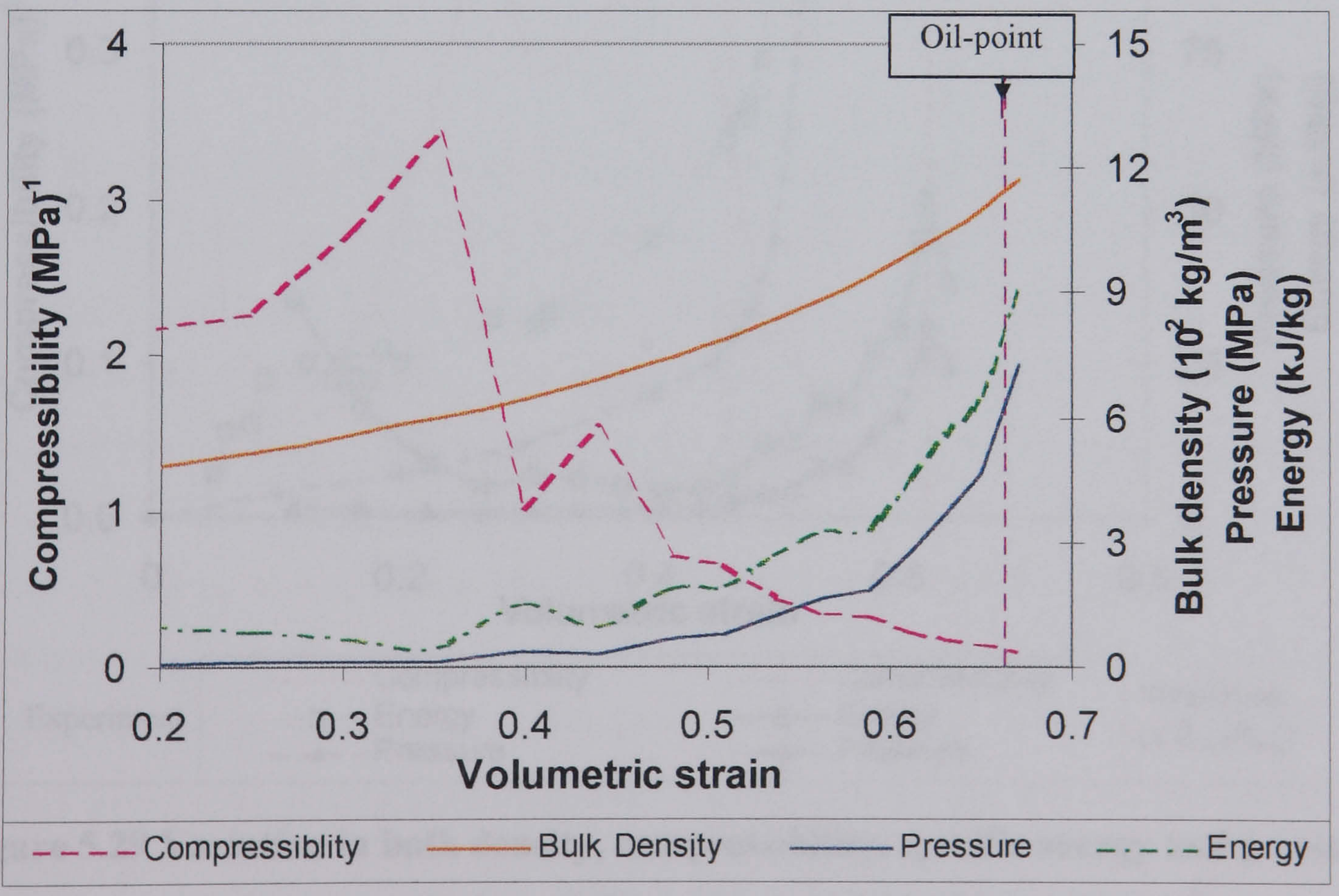

Figure 5.28 Variation in bulk density, compressibility, specific energy and pressure during compression of soybean

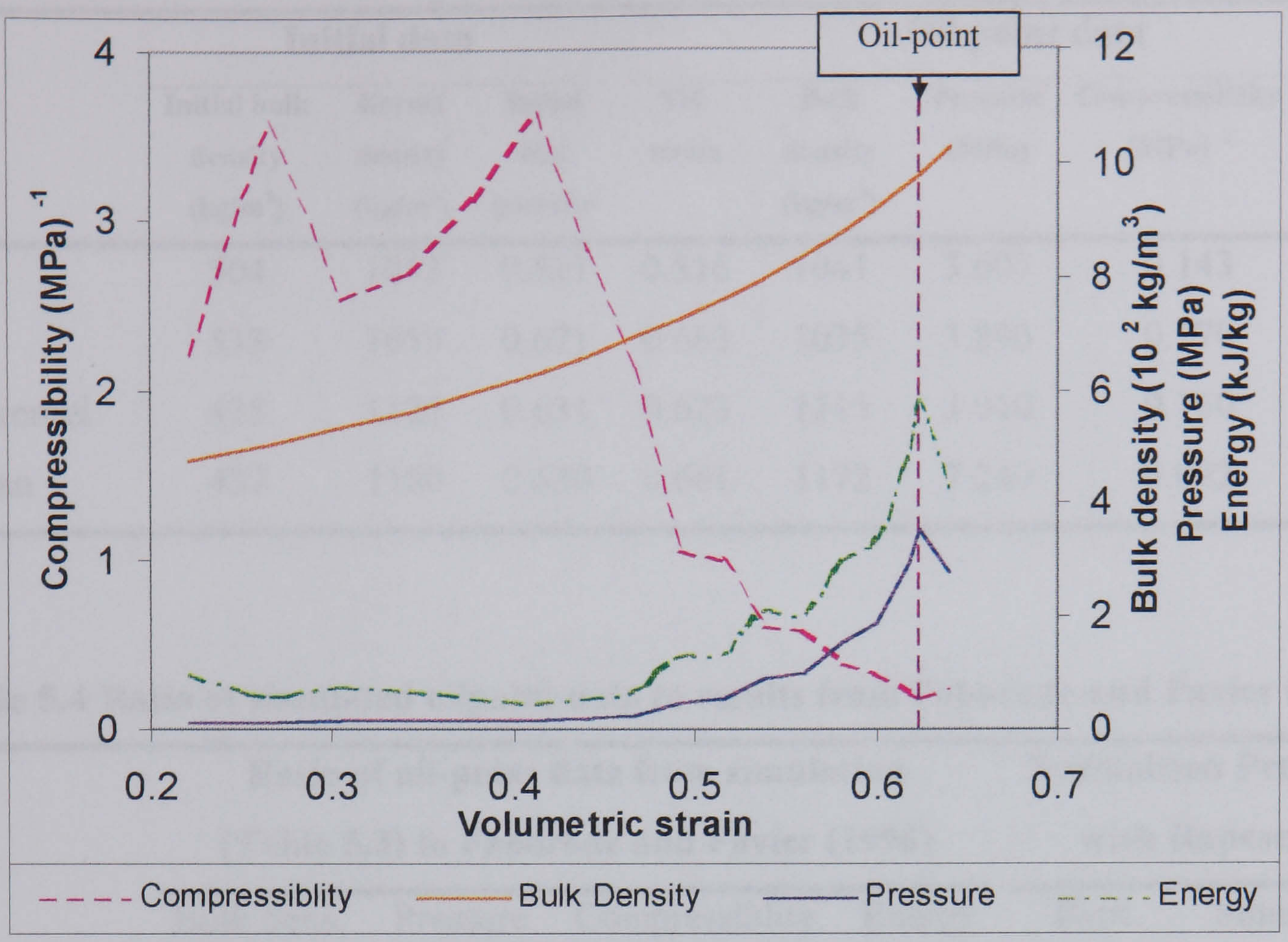

Figure 5.29 Variation in bulk density, compressibility, specific energy and pressure during compression of palm-kernel

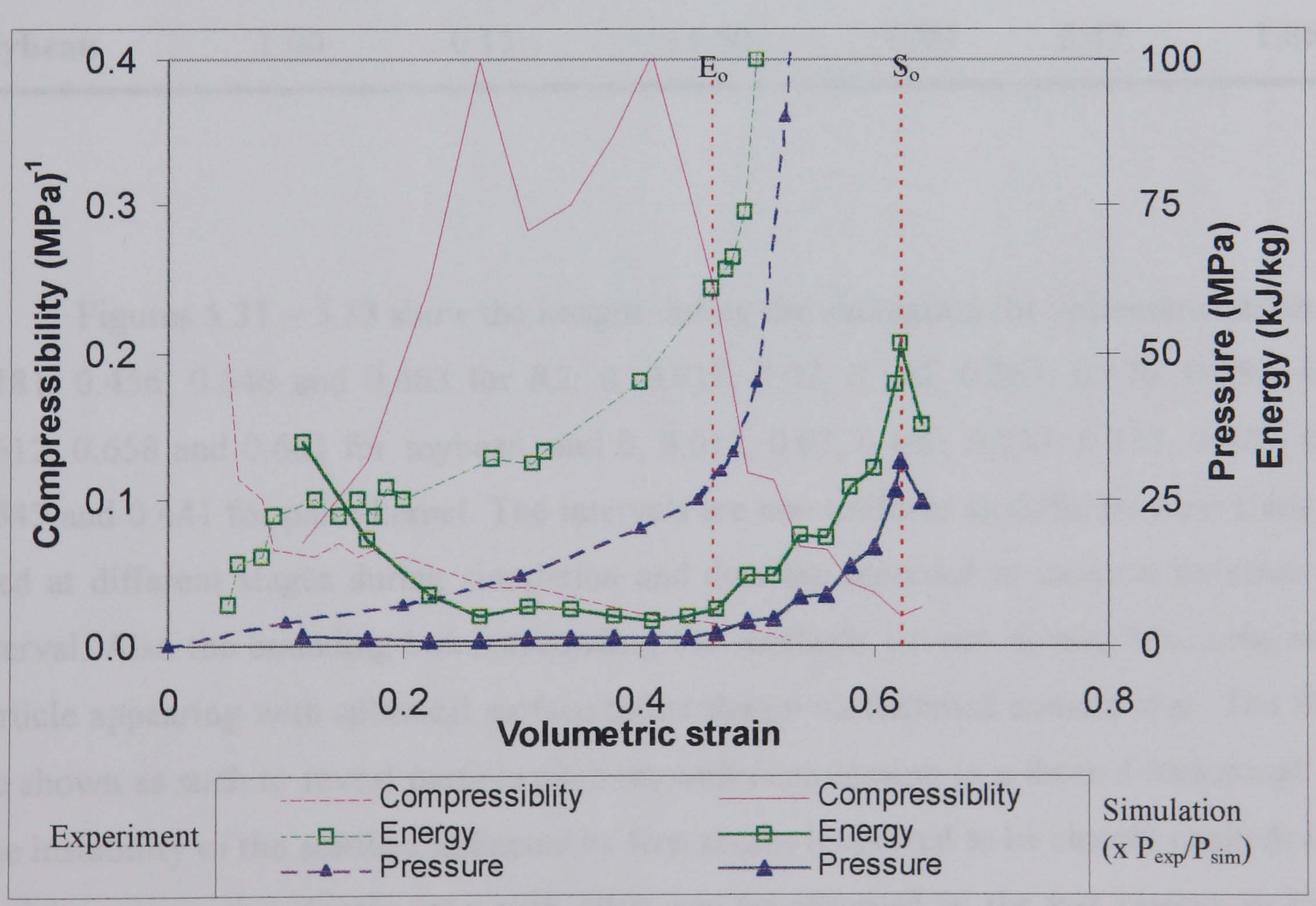

Figure 5.29 Variation in bulk density, compressibility, specific energy and pressure during compression for palm-kernel (Experiment =dashed lines, E and S represent experiment and simulation and subscript o indicates oil point).

	Initial data			Oil point data				
	Initial bulk density (kg/m^3)	Kernel density (kg/m^3)	Initial bed porosity	Vol. strain	Bulk density (kg/m^3)	Pressure (MPa)	Compressibility $(MPa)^{-1}$	Energy (kJ/kg)
R1	504	1053	0.521	0.516	1041	3.607	0.143	6.71
R2	533	1053	0.671	0.663	1035	3.890	0.170	5.75
Palm-kernel	415	1125	0.631	0.623	1115	3.910	0.160	5.77
Soybean	437	1180	0.630	0.661	1172	7.240	0.092	9.19

Table 5.4 Ratio of simulated oilpoint data to results from Faborode and Favier (1996)

	Ratio of oil-point data from simulation (Table 5.3) to Faborode and Favier (1996)				Normalised Pressure with Rapeseed	
	Bulk dens.	Pressure	Compressiblity	Energy	Expt.	Simulation
Rapeseed	1.00	0.20	8.95	0.11	1.00	1.00
Palm-kernel	1.00	0.12	10.66	0.09	1.63	1.01
Soybean	1.00	0.15	11.50	0.09	2.47	1.86

Figures 5.31 – 5.33 show the images during the simulation for volumetric strain of 0, 0.181, 0.456, 0.546 and 0.663 for R2, 0, 0.017, 0.07, 0.100, 0.251, 0.376, 0.480, 0.551, 0.612, 0.658 and 0.661 for soybean, and 0, 0.017, 0.07, 0.100, 0.233, 0.333, 0.420, 0.485, 0.543 and 0.641 for palm-kernel. The intervals are non-uniform as different time steps were used at different stages during simulation and data are recorded at uniform iteration cycle interval. Also the bounding box surrounding the seedbeds are not shown, hence the surface particle appearing with spherical surface rather than with flattened contact area. The images are shown as such to reveal particle position with compression in a three dimensional view. The instability of the seedbed indicated by free spaces (expected to be closely packed) and/or particles penetrating deeply into each other can be observed in the last images in Figures 5.32 and 5.33.

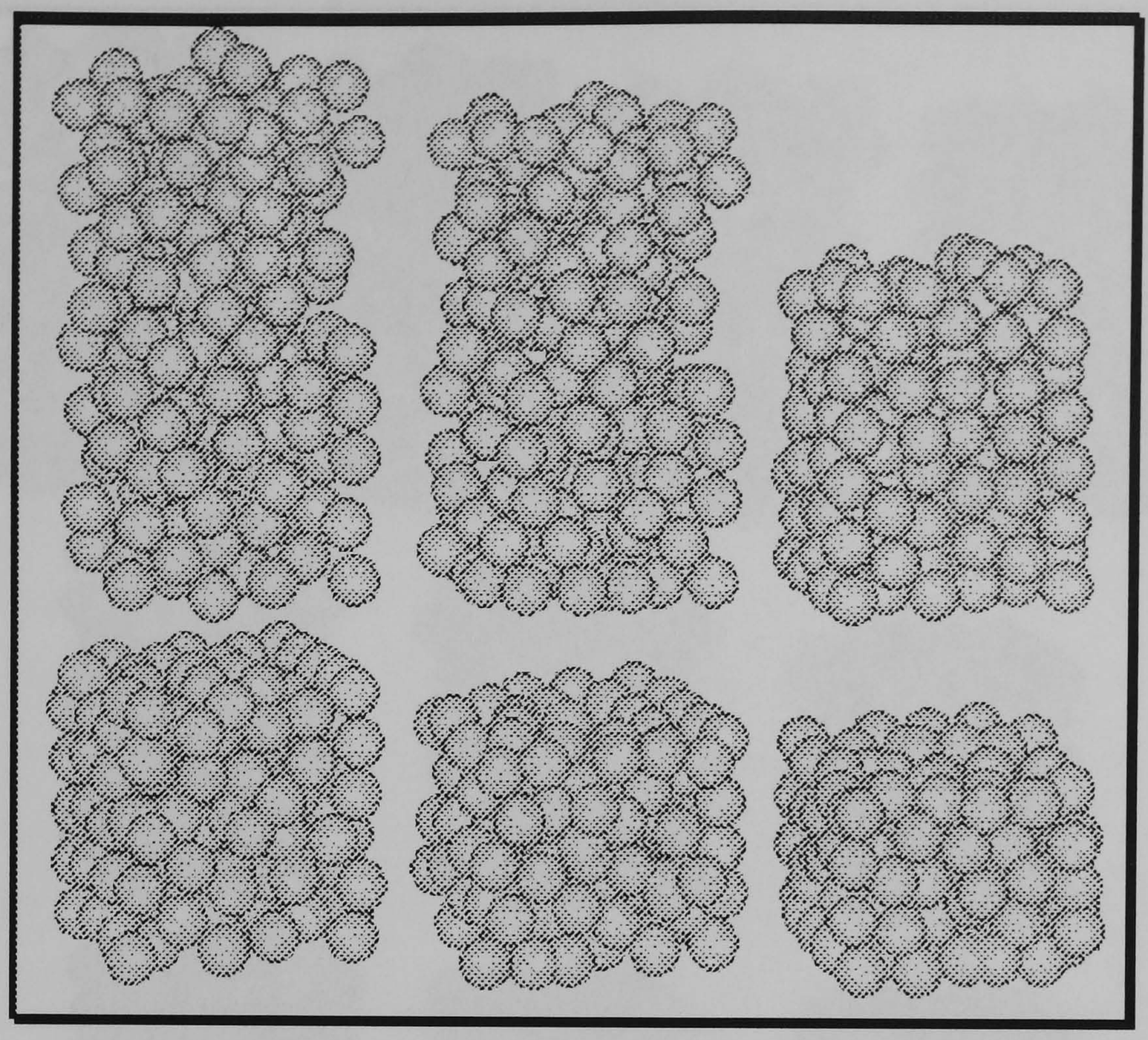

Figure 5.31 R2 consolidation (top) and compression (bottom)

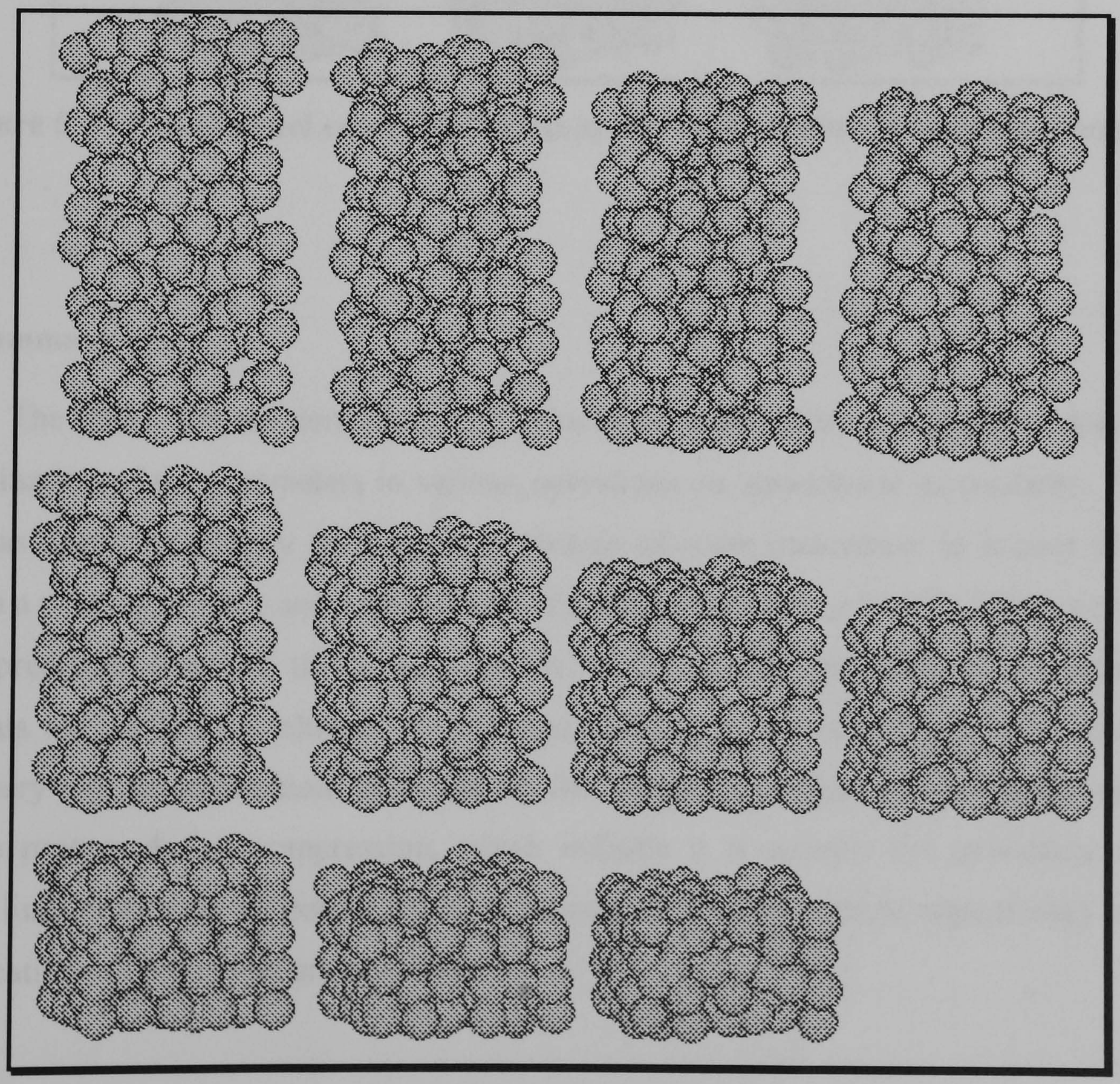

Figure 5.32 Soybean consolidation (top) and compression (bottom)

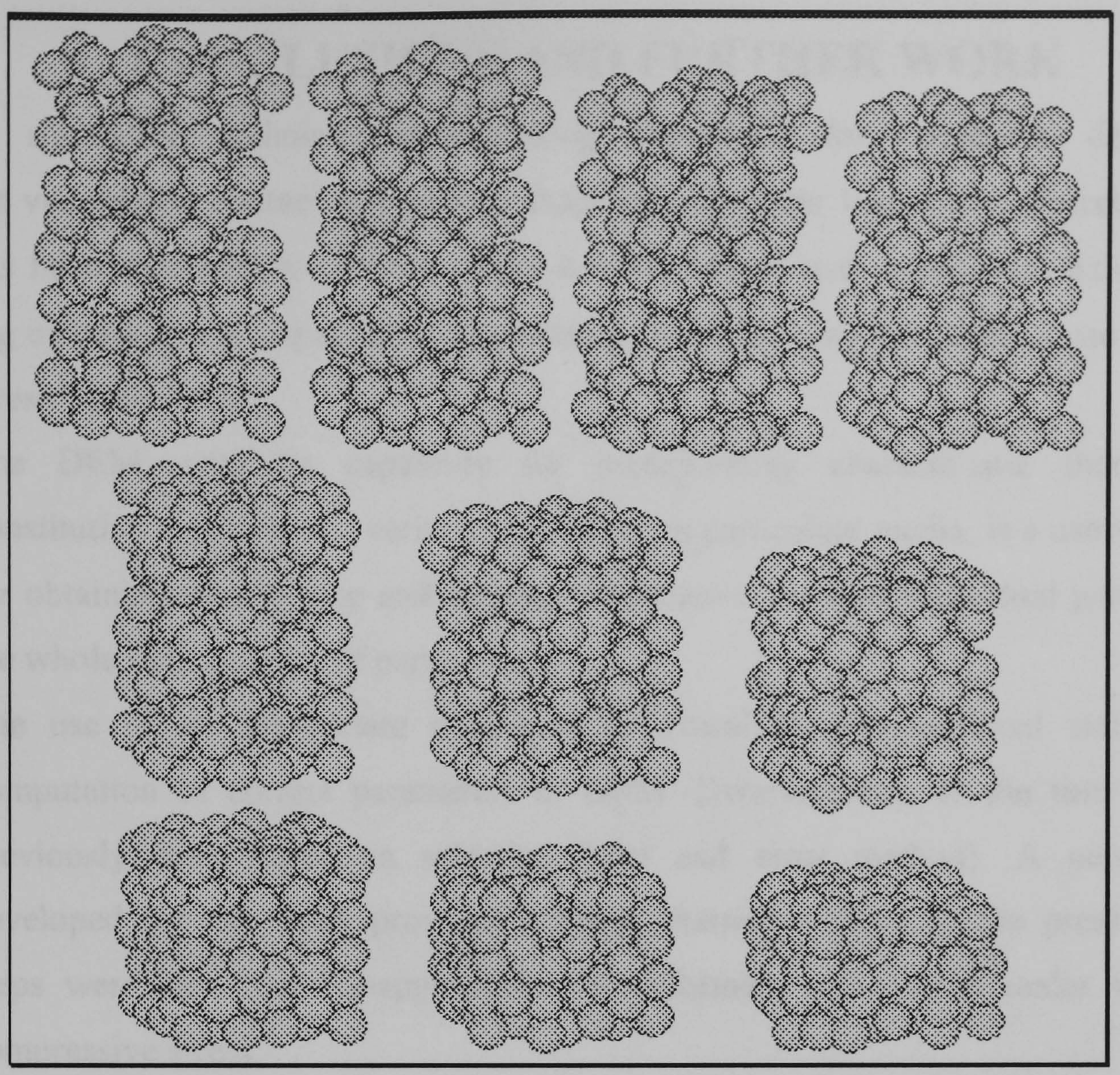

Figure 5.33 Palm-kernel consolidation (top) and compression (middle and bottom)

5.3 Summary

The DEM with the new algorithms introduced in this study can permit a step by step determination of the parameters in various operations on agricultural particulates. The new code has been successfully used in the prediction of some parameters in impact drop of a fruit on a padding surface and compression of assemblies or beds of seeds. These parameters when predicted provided useful information in the design and selection of appropriate materials for handling machinery components and pre-operation planning and selection of machinery for oil expression. However in the model, provision has not been made for particle rupture during compression, which indicate it is suitable for prediction up to a certain limit before the oil point or slightly beyond after which particle rupture may start and modifications of the model are required.

6 CONCLUSIONS AND FURTHER WORK

A simulation technique incorporating algorithms for non-linear deformation dependent viscoelastic contact and particle shape change under load into a discrete element model has been successfully used to model key aspects of two agricultural handling and processing operations i.e. impact and compression. The following conclusions can be drawn from the results presented:

(i) The DEM, with its capability for incorporating characteristic theories and constitutive equations for various operations on particulate media, is a useful method for obtaining step by step and detailed information for both individual particles and the whole bulk systems of particulates.

(ii) The use of an appropriate time step is critical to computational stability and computation of correct parameters in DEM. Determination of the time step has previously been based on selection (trial and error method). A new method developed for this study provided a better alternative although the predicted time steps were also found inappropriate for deforming particulates under very high compressive stress.

(iii) The new code provided a good prediction of particle behaviour during compressive loading (impact and compression) of viscoelastic particulates (agricultural and non-agricultural) undergoing a change of shape

(iv) The behaviour of viscoelastic particulates are better represented by the deformation dependent damping relationship which modelled a residual deformation upon load removal which is typical of viscoelastic particulates. Deformation and other related parameters modelled with the new code were found to be in close agreement with experimental results from literature.

(v) Only selected damping values were examined in impact simulations of apple against hard surface but the agreement with available results showed that using the appropriate parameters, the technique could be a useful tool in the study of the effects of damping and strength parameters on prediction of damage to agricultural particulates under impact load.

(vi) The model is also a promising approach for obtaining necessary data for design of some components of handling machinery in direct contact with product in order to reduce impact damage

(vii) Though an approximate method the particle shape change algorithm (incorporated into the new code) provided a closer approximation to experimental results for compression of both synthetic and natural spherical particles than the original code (without particle shape change). In particular better predictions of bed porosity were attained which suggests that this method could be useful for applications in which estimation of porosity is important.

(viii) The increase in predicted particle-to-particle contact area resulting from the use of the shape change algorithm should also provide a more accurate basis for modelling of particle rupture if this were added to the model.

(ix) Particle rearrangement and compression stages were clearly distinguished in bulk compression of three agricultural particulates in mechanical oil expression. The model enables prediction of particle and bulk physical property and parameter values during any stage of the bulk compression of particulates.

6.1 Recommendations for Further Work

Based on the results and problems encountered in this study and the general requirements for a closer prediction of agricultural particulates bahaviour considering their properties and the available work, the following are recommended for research:

i. The deformation and shape change of agricultural particulates with the new theories on viscoelastic behaviour have only been studied under loading conditions. The study needs to be extended to the unloading conditions and this will involve the recovery of the residual deformation for individual particle and the bulk.

ii. Modelling the behaviour of the bulk agricultural particulates during loading also requires the incorporation of other algorithms to handle other phenomena such as particle rupture. This will enable a closer prediction at very high compressive stress.

iii. Further research on the appropriate time step for simulation with the DEM for loaded and deforming systems needs to be carried out.

iv. This study approximate the shapes of particles as spherical, with homogeneous properties for individual particle and uniform size distribution within the bulk although real agricultural particulates will differ in varying degrees from these simplifying assumptions. The extent to which the inter-particle behaviour is affected by the shape and size distributions of the constituent particles as well as inhomogeneity in particle structure need to be studied to improve the accuracy of the prediction of the bulk behaviour.

REFERENCES

Abbaspour, M. H; Raji, A. O. and J. F. Favier; (1998). Discrete Element Method of the modelling of irregularly shaped particulate agricultural materials. Paper No. 98-A-057. International Conference on Agricultural Engineering, Oslo.

Anandarajah, A; (1995). Discrete element method for simulating the behaviour of cohesive soil. J. of Geotechnical Engineering. 120(9):1593-1613.

Anazodo, U. G. N. and S. C. Chikendu; (1983). Poisson's ratio and elastic modulus of radially compressed biomaterial I: Small modulus of deformation approximation. Trans ASAE, 26(3): 923-929.

Arzt, A; (1982). The influence of an increasing particle co-ordination on densification of spherical powders. Acta Metallurgy Vol. 30:1883-1890.

Barr, A. H; (1981). Superquadrics and angle-preserving transformations. IEEE Computer Graphics and Animation. Vol. 1, pp. 11-23.

Barthurst, R, J. and L. Rothenburg; (1986). Investigation of micromechanical features of idealised granular assemblies using DEM. Proceeding of first US Conference on DEM, Golden, Colorado.

Becker, A; (1996). Boundary element method for engineering problems. NAFEMS Seminar on Alternative Strategies for Computational Mechanics, Feb. 20, 1996, London.

Bilanski, W. K; Szot, B; Kushwaha, I. and A. Stepniewski; (1994). Comparison of strength features of rape pods and seeds for varieties cultivated in various countries. International Agrophysics, Vol. 8(4):177-184.

Carini, A. and G. Gioda; (1986). A boundary integral equation technique for visco-elastic stress analysis. International Journal for Numerical and Analytical Methods in Geomechanics, Vol. 10:586-608.

Chen, H. and J. D. Baedemeaker; (1995). Optimisation of impacted parameters for reliable excitation of apples during firmness monitoring. Journal of Agricultural Engineering Research, 61:275-282

Chen, P. and R. B. Fridley (1972). Analytical method for determining viscoelastic constants of agricultural materials. Trans ASAE, 15(6): 1103 -1106.

Chen, P. and R. Yazdani; (1991). Prediction of apple bruising due to impact on different surfaces. Trans ASAE, 34(3): 956-961.

Chen, P. and Y. Tjan; (1998). A real time impact sensing system for on-line firmness sensing of fruits. Paper No. 98-F-006. International Conference on Agricultural Engineering, Oslo.

Cundall, P. A; (1971). A computer model for simulating progressive large-scale movement in blocky rock system. Proceedings of International Symposium on Rock Fracture, Nancy P. II-8.

Cundall, P. A. and O.D.L. Strack; (1979). A discrete numerical method for granular assemblies. Geotechnique, 29(1):47-65.

Cundall, P. A. and R. P. Hart; (1992). Numerical modelling of discontinua. Engineering Computations, 9(2): 101-113.

Davies, E. R. (1991). Efficient image analysis techniques for automated visual inspection. In Computer Vision and Image Processing. Ed. A. Barrett. Chapman and Hall, London.

Dielwiche, M. J; Arevalo, H. and J. Mehlschau; (1996). Second generation impact response fruit firmness sorter. Trans ASAE, 39(3): 1025-1033.

Desai, S. C and J. T. Christian; (1977). Numerical Methods in Geotechnical Engineering. McGraw Hill Books, New York.

Dobry, R; Ng, T. T. and E. Petrakis; (1991). General model for contact law between two rough spheres. J. of Engineering Mechanics. 117(6): 1365-1381.

Dobry, R. and T.T. Ng; (1992). Discrete modelling of stress strain behaviour of granular materials at small and large strains. Journal of Engineering Computations, Vol. 9: 129-143.

Dougherty, E. R. and C. R. Giadina, (1987). Image Processing - Continuous to discrete I: Geometric Transform and Statistical methods. Prentice–Hall, Inc. New Jersey.

Faborode, M. O. and R. R. Dirinfo; (1994). A mathematical model of cocoa pod deformation based on Hertz theory. International Agrophysics: A Proceeding of 5th International Conference on Physical Properties of Agricultural Materials (fruits vegetables and root crops), Vol. l8, No 3.

Faborode, M. O. and J. F. Favier; (1996). Identification and significance of the oil-point in seed-oil expression. Journal of Agricultural Engineering Research, **65**:335-345.

Faborode, M. O. and J. R. O'Callaghan, (1986). Theoretical-analysis of the compression of fibrous agricultural materials. Journal of Agricultural Engineering Research. **35:** 175-191.

Favier, J. F; Abbaspour-Fard, M. H; Kremmer, M. and A. O. Raji; (1999). Shape representation of axi-symmetrical, non-spherical particles in discrete element

simulation using multi-element model particles. Accepted for publications in Engineering Computations.

Fluck, R. C. and E. M. Ahmed; (1973). Impact tests of fruits and vegetables. Trans ASAE, 16(4): 660-665.

Fornal, J; Sadowska, J; Jaroch, R; Kaczynska, B and T. Winnicki; (1994). Effect of drying of rapeseeds on their mechanical properties and technological usability. International Agrophysics, 8(2): 215-224.

Foultz, T. L; Thompson, S. A. and M. D. Evans; (1993). Comparison of loading response of packed grain and individual kernel. Trans ASAE, 36(2): 569-576.

Fridley, R. B; Bradley, R. A; Rumsey, J. W and P. A. Adrian; (1968). Some aspects of elastic behaviour of selected fruits. Trans ASAE, 11(1): 47-49.

Fuller, K. N. G. and Tabor; (1975). The effect of surface roughness on the adhesion of elastic solids. Proc. of the Royal Society of London, A.345: 327-342.

Ghaboussi, J. and R. Barbosa; (1990). Three dimensional discrete element method for granular materials. Int. Journal for Numerical and Analytical Methods in Geomechanics. Vol. 14, pp. 451-472.

Ghadiri, M. and Z. Ning; (1997). Effect of shear strain rate on attrition of particulate solids in a shear cell. International Conference on Powders and Grains, Durham, North Carolina.

Goodman, L.E; (1962). Contact stress analysis of rough spheres. Journal of Applied Mechanics, 84: 515-522.

Greenspan, J; (1974). Discrete numerical methods in Physics and Engineering. Academy press, New York.

Hamman, D. D. and K. C. Diehl; (1978). Equation for dynamic complex uniaxial compression modulus of spheroidal shape foods. Trans. ASAE, 21: 1009-1014.

Heinstein, M. W; Attaway, S. W; Swegle, J. W and F. J. Mellow; (1993). A general contact detection algorithm for finite element analysis. Proceedings of First International Conference on Contact Mechanics. Computational Techniques, Southampton. pp 219-226.

Hertz, (1882). Uerber die Berhrunsfester elastischer korper. J.Renie Angew Math, 92: 156-171.

Herum, F. L; Mensah, J. K; Barre. H.J. and K Majizadeh; (1979). Viscoelastic behaviour of soybean due to temperature and moisture content. Trans ASAE, 22(4): 1219-1224.

Hocking, G; (1989). The DEM for analysis of fragmentation and discontinua. Proceedings of 1st US Conference on DEM, Golden, Colorado.

Hogue, C; (1998). Shape representation and contact detection for discrete element simulations of arbitrary geometries. Engrg. Computations. 15(3): 374-390.

Hogue, C. and D. E. Newland; (1994). Efficient computer simulation of moving granular particles. Powder Technology, **8**, pp. 71-66.

Holt, G.E; Schoorl, D and C. Lucas; (1981). Prediction of bruising in impacted multilayered apple packs. Trans ASAE, 24(1): 242-247.

Holt, G.E; Schoorl, D. and C. Lucas; (1985). A theoretical and experimental analysis of the effect of suspension and road profile on bruising in multilayered apple packs. Journal of Agricultural Engineering Research, Vol. 31.

Holst, J. M. F. G; Ooi, J. Y; Rotter, J. M. and G. H. Rong; (1999a). Numerical modelling of silo filling I: Continuum analysis. Journal of Engineering Mechanics, 125(1): 94-103.

Holst J. M. F. G; Rotter, J. M; Ooi, J. Y. and G. H. Rong; (1999b). Numerical modelling of silo filling II: Discrete element analysis. Journal of Engineering Mechanics, 125(1): 104-110.

Horabik, J. A; Ross, I. J. and C. V. Schwab; (1988). Effects of spatial orientation on grain load distribution. Trans ASAE 31(6): 1787-1793.

Horabik, J. and M. Molenda; (1989). Effects of moisture content on friction of wheat grain. Powder Handling and Processing, 1(3): 277-279.

Hryciw, R. D; Raschke, S. A; Ghalib, A. M; Horner, D. A. and J. F. Peters; (1997). Video tracking for experimentation of discrete element simulations of large discontinuous deformations. Computers and Geotechnics, Vol. 2(3): 235-253.

Hutchings, I. M; (1993).Mechanism of wear in powder technology: a review. Powder Technology, **76**: 13-22.

Hyde, G. M; Brown, G.K; Timm, E. J. and W. Zhang; (1992). Instrumented sphere evaluation of potato line impacts. Trans ASAE 35(1):65-69.

Issa, J. A. and R. B. Nelson; (1989). Numerical analysis of micromechanical behaviour of granular materials. Proc. 1st US Conf. on DEM.Gol. ,CO.

Jofriet J. C; Negi, S. C. and Lu, Z; (1997). A numerical model for flow of granular materials in silos. Part 3: Parametric study. Journal of Agricultural. Engineering Research, 68: 237-246.

Johnson, K. L; (1992). Contact Mechanics. Third Edition, Cambridge University Press, Cambridge.

Kafui, D. and C. Thornton; (1993) Computer simulated impact of agglomerate. Powder and Grains 93, the Proceedings of the 2nd Int. Conference on Micromechanics of Granular Media, A. A. Balkema, pp. 401-406.

Karakerezis, A. and K. Khodabandehloo; (1996). Simulation modelling for robotics grasping of flexible viscoelastic materials using a discrete element model. Mathematics and Computers in Simulation. 41: 595-614.

Krishnasamy, J. and M. S. Jakiela; (1995). A method to solve ambiguities in corner-corner interactions between polygons in the context of motion simulation. Engineering Computations, Vol. 12: 123-144.

Langston, P. A; Nikitidis, M. S; Tuzun, U; Heye, D. M. and N. M. Spyrou; (1997). Microstructural simulation and imaging of granular flows in two- and three-dimensional hoppers. Powder technology, Vol. 94, pp. 59-72.

Leavers, V. (1991). Use of the Randon transform of extracting symbolic representations of shape in two dimensions. In Computer Vision and Image Processing. Ed. A. Barrett. Chapman and Hall, London.

Lichtensteiger, M. J; Holmes, R. G; Hamdy, M. Y. and J. L. Blaisdell; (1988). Impact parameters of spherical viscoelastic objects and tomatoes. Trans ASAE 31(2): 595-602.

Loo, T. T; (1958). Effect of curvature on the Hertz theory for two circular cylinders in contact. Journal of Applied Mechanics, The ASMechE. **25**: 122-124.

Lu, Z; Negi, S. C. and J. C. Jofriet; (1997). A numerical model for flow of granular materials in silos. Part I: Model development. Journal of Agricultural Engineering Research, **68**: 223-229.

Lubkin, J. L. (1962). Contact Problems: Handbook of Engineering Mechanics. Mc-Graw Hill Book Co. New York.

Manbeck, H. G. and G. L. Nelson; (1972). Method and instrumentation for evaluating the stress strain behaviour of wheat en-masse. Trans ASAE, 25(5): 919-923.

Matthew, R. and G. M. Hyde; (1997) Potato impact damage thresholds. Trans ASAE 40(3):705-709.

McEwen, E; (1949). Stress in elastic cylinder in contact along a generatrix. Philosophical Magazine, Vol. 40: 454.

McGlone, V. A.; Jordan, R. B. and P. N. Schaare; (1997a). Obtaining mass from fruit impact response. Trans ASAE 40(5): 1417-1419.

McGlone, V. A; Jordan, R. B. and P. N. Schaare; (1997b). Mass and drop height influence on kiwifruit frimness by impact force. Trans ASAE 40(5):1421-1428

Meng, Q; Jofriet, J. C. and S. C. Negi; (1997). Finite element analysis of bulk solids flow: Part I, Development of a model based on a secant constitutive relationship. Journal of Agricultural Engineering Research, **67**: 141-150.

Meng, Q; Jofriet, J. C. and S. C. Negi; (1997). Finite element analysis of bulk solids flow: Part II, Application to a parametric study. Journal of Agricultural Engineering Research, **67**: 151-159.

Mindlin, R. D. (1949). Compliance of elastic bodies in contact. Journal of Applied Mechanics, 16(3): 259-266.

Mindlin, R. D. and H. Deresiewicz; (1953). Elastic spheres in contact under varying oblique forces. J. Applied Mechanics **20**, pp. 327-344.

Mohsenin, N. N; (1986). Physical properties of plant and animal materials. 2nd ed. Gordon Breach Science, Publ; New York.

Mohsenin, N. N; Jindal, V. K. and A.N. Manor; (1978) Mechanics of impact of a falling fruit on a cushioned surface. Trans ASAE 21(5): 594 - 600.

Molenda, M; Horabik, J. and I. J. Ross; (1993). Loads in model grain bins as affected by filling method. Trans ASAE 36(3): 915-919.

Morrow, C. T. and N. N. Mohsenin; (1968). Consideration of selected agricultural products as viscoelastic materials. J. Food Science, 33(6): 686-698.

Mrema, G. C. and P. B. McNulty; (1985). Mathematical-model of mechanical oil-expression from oilseeds. Journal of Agricultural engineering Research, **31**: 361-370.

Munjiza, A; Owen, D. R. J and N. Bicani; (1995). A combined Finite-Discrete element in transient dynamics of fracturing solids. Engineering Computation. 12: 145-174.

Negi, S. C; Rong, G. and J. C. Jofriet (1992). Discrete particle simulation of gravity flow of particulate materials. Powder Handling and Processing, 4:375-386.

Negi, S. C; Lu, Z. and J. C. Jofriet; (1997). A numerical model for flow of granular materials in silos. Part 2: Model validation. Journal of Agricultural. Engineering Research, 68: 233-236.

Ng, T. T. (1989). Numerical simulation of granular soil under monotonic loading: A particle mechanics approach. Ph.D Thesis, Renselvier Polythechnic Institute, New York.

Ng, T. T. and R. Dobry; (1990). CONBAL simulated granular material using quartz spheres with the DEM. Nat. Foundation Grant Paper number MSM8620334.

Ng, T. T. and R. Dobry; (1994). Numerical simulation of monotonic and cyclic loading of granular soils. J. of Geotechnical Engineering, 120(2):388 -403.

Ning, Z; (1995). Elasto plastic impact of fine particles and fragmentation of small agglomerates. Ph.D Thesis, Civil Eng; Aston University Birminghan.

Ning , Z; Boerefijn, R. and M. Ghadiri; (1997a). Effect of particle size and bond strength in impact breakage of weak agglomerates.

Ning , Z; Boerefijn, R; Ghadiri, M. and C. Thornton (1997b). Discrete element simulation of impact breakage of lactose agglomerates. Advanced Powder Technology, Vol.1:15-37.

Olukoko, O.A; Becker, A.. M and R. T. Fenner; (1993) Analysis of two-dimensional and axisymmetric contact and friction problems using boundary element software. Proceedings of First International Conference on Contact Mechanics Computational Techniques, Southampton. pp. 243-251.

Ooi, J. Y. and K. M. She; (1997). Finite element analysis of wall pressure in imperfect silos. International Journal of Solids and Structures, 34(16): 2061-2072

Ooi, J. Y; Chen, J. F. and J. M. Rotter; (1998). Measurement of solids flow pattern in a gypsium silo. Powder Technology, 99(3): 272-284

Pan, X. D. and M. B. Reed; (1989). A coupled discrete and finite element methods for large deformation analysis of rock masses. Proceedings of the first US Conference on DEM, Golden, Colorado.

Paulsen, M. R. (1978). Fracture resistance of soybean to compressive loading. Trans ASAE 21(4): 1210-1216.

Pei, S. and J. Horng; (1996). Optimum approximation of digital planar curves using circular arcs. Computer Pattern Recognition Vol. 29(3): 383-388.

Peleg, K. (1984). A mathematical model of produce damage mechanism. Trans ASAE, 27(1):287-293.

Princen, J; Illingworth, J; Kittler, J. and H. K. Yuen; (1991). Shape analysis using the Hough transform. In Computer Vision and Image Processing. Ed. A. Barrett. Chapman and Hall, London.

Rao, Y. N. M. and G. E. Skinner; (1986). Rheological properties of solid foods. In Engineering. Poperties of Foods. Ed. Rao M. A. and S. S. H. Rizvi. Marcel and Decker Inc. New York. pp 215-254.

Raji, A. O. and J. F. Favier; (1998). Discrete element modelling of deformation in particulate agricultural materials under bulk compressive loading. Paper No. 98-F-045. International Conference on Agricultural Engineering, Oslo.

Rogers, L. N. and J. Reeds; (1984). The adhesion of particles undergoing an elastic-plastic impact with a surface. J. Physics D: Applied Physics, Vol.17: 677-689.

Rong, G; Negi, S. C. and J. C. Jofriet; (1992). Simulation of the flow of particulate solids in storage vessels. ASAE Paper NO.92-4018.

Rong, G; Negi, S. C. and J. C. Jofriet; (1993). DEM simulation of in-transit fruit damage. ASAE Paper NO 93-6503.

Rong, G; Negi, S. C. and J. C. Jofriet; (1995a). Simulation of the flow behaviour of bulk solids in bins, Part 1: Model development and validation. Journal of Agricultural Engineering Research, 62: 247-256.

Rong, G; Negi, S. C. and J. C. Jofriet; (1995b). Simulation of the flow behaviour of bulk solids in bins, Part 2: Shear bands, flow, corrective inserts and velocity profile. J. of Agric. Eng. Research 62:257-269.

Ruiz-Altisent M; (1991). Damage Mechanism in the handling of fruits. In Progress in Agricultural Physics and Engineeeirng Ed. Mathews J. 231-258. C.A.B International Bristol.

Rumsey, T. R. and R. B. Fridley; (1977). Analysis of viscoelastic constant stresses in agricultural products using a finite-element method. Trans. ASAE 20(1): 162-166.

Sakaguchi, E; Kawakami, S. and F. Tobita; (1994). Simulation of flowing phenomena of grains by DEM. International Conference on Agricultural Engineering, Paper No. 94-G-025, Milano.

Sakaguchi, E; Kawakami, S; Suzuki, M; Urukawa, T. and J. F. Favier; (1998). Effective use of DEM simulation for development of grain processing technology: Application to shaking separation phenomenon of paddy and brown rice. Paper No. 98-F-021. International Conference on Agricultural Engineering, Oslo.

Schembri, M. G. and H. D. Harris; (1996). Modelling impact on a biological material (sugar cane) using DEM. Paper no. 96F-072, Int. Conf. On Agricultural Engineering, Madrid.

Segerlind L. J. (1984). Applied Finite Element Method. 2nd Ed. Wiley, New York.

Shahabasi, Y; Segerlind, L. J. and N. J. Carrol; (1995). A simulation model to determine the allowable depth for apples stored in bulk. Trans ASAE, 38(2): 587-591.

Sheriff, S. M; Segerlind, L. J.and J. S. Frame; (1976). An equation for the modulus of elasticity of a radially compressed cylinder. Trans. ASAE, 19(4): 782-785.

Sitkei, G. (1986). Mechanics of Agricultural Materials: Development in Agricultural Engineering, 8. Elsevier Science, Amsterdam.

Siyami, S; Brown, G. K; Burgess, G. J; Gerrish, J. B; Tennes, B. R; Burton, C. L. and R. H. Zapp; (1988). Apple impact bruise prediction models. Trans ASAE 31(4): 1039-1046.

Smith, J. O. and G. K. Liu; (1953). Stresses due to tangential and normal loads on an elastic solid. J. Applied Mechanics, 21: 371-378.

Sukumaran, C. R. and B. Singh; (1989). Compression of a bed of rapeseeds-the oil-point. Journal of Agricultural Engineering Research. **42**: 77-84.

Taylor, L. M. and D. S. Preece; (1992). Simulation of blasting induced rock motion using spherical element method. Engineering Computations 9(2): 243-252.

Thompson, S. A. and I. J. Ross; (1983). Compressibility and frictional coefficient of wheat. Trans ASAE 26(4): 1171-1176.

Thornton, C. and C. W. Randall; (1988). Application of theoretical mechanics to solid particulate system simulation. Micromechanis of Granular Materials, Ed. M. Satake and J. J. Jenkins. Elsevier Science. Amsterdam.

Thornton, C; and K. K. Yin; (1991). Impact of elastic spheres with or without adhesion. Powder Technology **65**:157-166.

Thornton, C; Yin K. K. and M. J. Adams; (1996). Numerical solution of the impact fracture and fragmentation of agglomerates. J. Physics D: Applied Physics 29: 424-435.

Timoshenko, S. P and J. N. Goodier; (1970). Theory of Elasticity. Third Edition. McGraw Hill, Tokyo.

Ting, J. M; Corkum, B. T; Kauffman, C. R; and C. Graco; (1989). Discrete numerical model for solid mechanics. J. Geotechnical Eng; **3**: 379-398.

Ting, J. M; Khwaja, M; Meachum, L. R. and J. D. Rowell; (1993). An ellipse based discrete element model for granular materials. Int. Journal for Numerical and Analytical Methods in Geomechanics. Vol. 17 pp. 603-623.

Tsuji, Y; Tanaka, T. and T. Ishida; (1992). Langrangian numerical simulation of plug flow of cohesionless particle in a horizontal pipe. Powder Technology. **71**: 239-250.

Tsuji, Y; Kawaguchi, T. and T. Tanaka; (1993). Discrete particle simulation of two fluidised bed. Powder Technology 77: 79-87.

Wall, S; John, W. and S. C. Georen; (1989). Application of impact adhesion theory to particle kinetic energy loss measurement. Particle on Surface, Ed; K. H. Mitted. Plenim Pub. Corp.: 19-34.

Walton, K; (1978). The oblique compression of two elastic spheres. J. Mechanics and Physics of solids, **26**: 139-150.

Walton, O. R; Bran, R. C; Mallon, R. G. and D. M. Cervelli; (1988). Particle dynamics calculation of gravity flow of inelastic frictional spheres. Micromechanics of Granular Materials, Ed. M. Satake and J. J. Jenkins. Elsevier Science. Amsterdam.

Watson, G. R. and J. M. Rotter; (1996). A finite element kinematics analysis of planar granular solids flow. Chemical Engineering Science, 51(6): 3967-3978

Williams, J. R. and R. O'Connor; (1995). A linear complexity algorithm for DE simulation of arbitrary geometries. Engineering Computations, **12**: 185-201.

Williams, J. R; O'Connor; R. and N. Rege; (1996). Discrete element analysis of granular vortex formation. Research Report, Intelligent Engineering Systems Laboratory (Web Page).

Williams, J. R. and A. P. Pentland; (1989). Superquadrics and modal dynamics for discrete elements in concurrent design. Proc. 1st US Conf. on DEM, Golden, Colorado.

Williams, J. R. and N. Rege; (1997). The development of circulation cell structures in granular materials undergoing compression. Powder Technology, **90**: 187-194.

Wronski, M. and M. Jean; (1995). Some computational aspects of structural dynamic problem with frictional contact. Proceedings of First International Conference on Contact Mechanics Computational Techniques, Southampton. pp. 163-173.

Xu, B. H. and A. B. Yu; (1997). Numerical simulation of the gas-solid flow in a fluidised bed by combining discrete particle method with computational fluid dynamics. Chemical Engineering Science. Vol. 52, No 16, pp2785-2890.

Xu, S; Zhang, O. and M. G. Britton; (1996). An endochronic constitutive model for grain en-masse. Journal of Agric Engrg. Research, Vol. 63, pp 121-128.

Zhang, Y. and P. A. Cundall; (1986). Numerical simulation of slow deformations. Proc. Symp. on the Mechanics of Particulate Media. 10th U.S. National Congress on Applied Mechanics, Texas.

Zhang, D. and W. J. Whitten; (1996). The calculation of contact forces between particle using spring and damping models. Powder Technology, **88**: 59-64.

Appendix A

Consider two contacting spheres shown in Figure A.1(a)

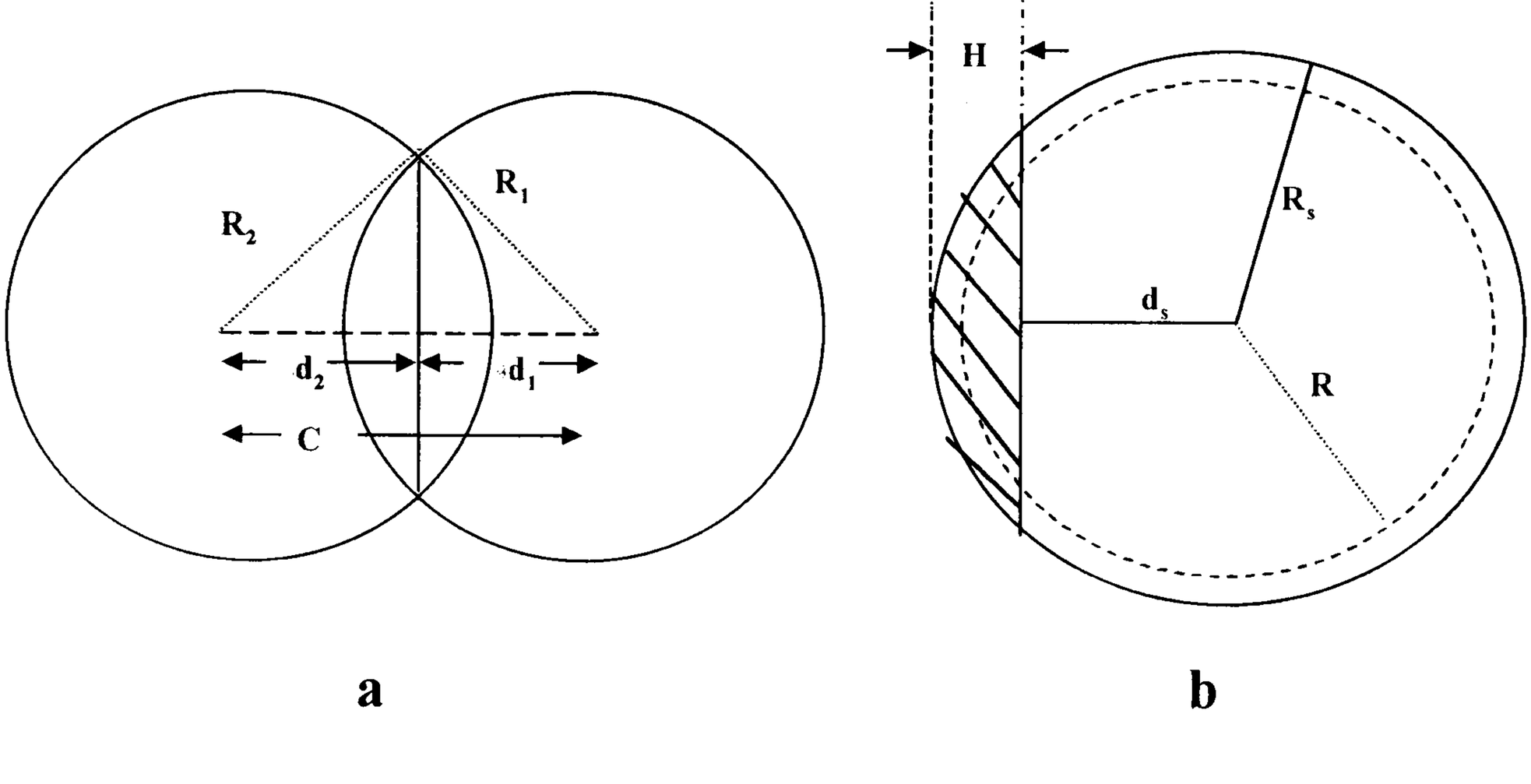

Figure A.1 (a) Two contacting spheres (b) Excess volume distribution after contact

The distance between the two spheres L can be obtained as stated in 2.7.2.2 and considering all the assumptions and the properties of the contact surface the distance between the centre of the each of the sphere i, and the contact surface, d_i, is geometrically given by

$$d_1 = \left(L^2 + R_1^2 - R_2^2\right)\frac{1}{2(L)}$$

$$d_2 = \left(L^2 + R_2^2 - R_1^2\right)\frac{1}{2(L)}$$

for contact between a sphere and a flat plate e.g. a wall $d_i = L$ is simply the distance between the centre of sphere I and the surface of the flat plate (also the contact surface)

The volume of the spherical cap formed between contact surface and the surface of the a sphere of radius R_s is

$$V_{sc} = \pi H_s^2 \left(R_s - \frac{H_s}{3} \right)$$

where H_s is the height of the spherical cap (Arzt, 1982)

In Figure A.1(b) we assume the inner sphere with a radius of R formed a contact with another body and has a deformed portion given by the spherical cap shown.

Then if this volume is distributed evenly across the other surface, forming a larger sphere of radius R_s. The volume of the new object formed (the unshaded portion) should be equal to the volume of the original sphere of radius R which is given by the volume of the new sphere less the volume of the spherical cap (shaded volume), i.e.

$$\frac{4}{3}\pi R^3 = \frac{4}{3}\pi R_s^3 - \pi H_s^2 \left(R_s - \frac{H_s}{3} \right)$$

By geomery $H_s = R_s - d_s$

then

$$\frac{4}{3}\pi R^3 = \frac{4}{3}\pi R_s^3 - \frac{\pi}{3}\left(R_s - d_s\right)^2 \left(2R_s + d_s\right)$$

For a system with N contacts, then

$$R^3 = R_s^3 - \frac{1}{4}\sum_{i-1}^{N}\left[\left(R_s - d_{s_i}\right)^2 \left(2R_s + d_{s_i}\right)\right]$$

from which R_s can be calculated numerically.

Appendix B

The finite difference forward approximations (FDA) are;

$$\ddot{x} = \frac{\dot{x}_{T+\Delta T} - \dot{x}_{T}}{\Delta T}$$

$$\dot{x} = \frac{\dot{x}_{T+\Delta T} + \dot{x}_{T}}{2}$$

$$\dot{x}_{T+\Delta T} = \dot{x}_{T} + \ddot{x}(\Delta T)$$

The general equation for the FDA known as Newmark's generalised acceleration method

$$(\dot{x})_{T+\Delta T} = (\dot{x})_{T} + \{1-\zeta\}(\ddot{x})_{T}\,\Delta T + \zeta \Delta T(\dot{x})_{T+\Delta tT}$$

for an explicit scheme where $\zeta = 1$ while $\zeta = 0$ for an implicit scheme (Desai and Christian, 1977).

Appendix C

The normalised displacement for the linear equation is

i) for b > 1; $$\hat{u}(\hat{T}) = \frac{\exp\left\{-\left[b-\left(b^2-1\right)^{\frac{1}{2}}\right]\hat{T}\right\}}{2\left(b^2-1\right)^{\frac{1}{2}}} - \frac{\exp\left\{-\left[b+\left(b^2-1\right)^{\frac{1}{2}}\right]\hat{T}\right\}}{2\left(b^2-1\right)^{\frac{1}{2}}} \qquad C1$$

(ii) for b < 1; $$\hat{u}(\hat{t}) = \frac{\sin\left\{\left(-b^2-1\right)^{\frac{1}{2}}\hat{T}\right\}\exp(-b\hat{T})}{\left(-b^2-1\right)^{\frac{1}{2}}} \qquad C2$$

iii) for b = 1; $$\hat{u}(\hat{T}) = \frac{\hat{T}}{\exp(\hat{T})} \qquad C3$$

The normalised velocity for the linear equation is

(i) Case a > 1

$$\hat{v}(\hat{t}) = \frac{d\hat{x}(\hat{t})}{d\hat{t}} = \frac{\left[-a+(a^2-1)^{\frac{1}{2}}\right]\exp\left\{-\left[a-(a^2-1)^{\frac{1}{2}}\right]\hat{t}\right\}}{2(a^2-1)^{\frac{1}{2}}} - \frac{\left[-a-(a^2-1)^{\frac{1}{2}}\right]\exp\left\{-\left[a+(a^2-1)^{\frac{1}{2}}\right]\hat{t}\right\}}{2(a^2-1)^{\frac{1}{2}}}$$

(ii) Case a < 1

$$\hat{v}(\hat{t}) = \frac{d\hat{x}(\hat{t})}{d\hat{t}} = \cos\left[\left((-a^2+1)^{\frac{1}{2}}\hat{t}\right)\right]\exp(-a\hat{t}) - \frac{\sin\left[\left((-a^2+1)^{\frac{1}{2}}\hat{t}\right)\right](a)\exp(-a\hat{t})}{(-a^2+1)^{\frac{1}{2}}} \qquad C5$$

(iii) Case a = 1

$$\hat{v}(\hat{t}) = \frac{d\hat{x}(\hat{t})}{d\hat{t}} = \frac{\hat{t}}{\exp(\hat{t})} + \frac{1}{\exp(\hat{t})} \qquad C6$$

The force is

(i) Case a > 1

$$\hat{f}(\hat{t}) = \frac{d\hat{v}(\hat{t})}{d\hat{t}} = \frac{\left[-a+(a^2-1)^{\frac{1}{2}}\right]^2\exp\left\{-\left[a-(a^2-1)^{\frac{1}{2}}\right]\hat{t}\right\}}{2(a^2-1)^{\frac{1}{2}}} - \frac{\left[-a-(a^2-1)^{\frac{1}{2}}\right]\exp\left\{-\left[a+(a^2-1)^{\frac{1}{2}}\right]\hat{t}\right\}}{2(a^2-1)^{\frac{1}{2}}}$$

(ii) Case a < 1

$$\hat{f}(\hat{t}) = \frac{d\hat{v}(\hat{t})}{d\hat{t}} = \sin\left[\left((-a^2+1)^{\frac{1}{2}}\hat{t}\right)\right](-a^2+1)^{\frac{1}{2}}\exp(-a\hat{t}) - 2\cos\left[\left((-a^2+1)^{\frac{1}{2}}\hat{t}\right)\right](a)\exp(-a\hat{t}) + \frac{\sin\left[\left((-a^2+1)^{\frac{1}{2}}\hat{t}\right)\right](a)^2\exp(-a\hat{t})}{(-a^2+1)^{\frac{1}{2}}} \quad C8$$

(iii) Case a = 1

$$\hat{f}(\hat{t}) = \frac{d\hat{v}(\hat{t})}{d\hat{t}} = \frac{\hat{t}}{\exp(\hat{t})} - \frac{2}{\exp(\hat{t})} \quad C9$$

Appendix D

SET UP - Starts or restarts a new problem. The arrays and variables are initialised, constants specified, material properties and parameters needed for particle generation are read and necessary calculation done. The information are saved when starting a new problem while in restarting they are recalled.

NEXT- Interprets the command lines for each operation and locates the position for reading or calculating the necessary parameters from the input line for the successive operations

HALT- Terminates the programme when there is an error or at the end of the operations

TIDY - Eliminates the blanks in the input lines and make index to location of parameters by recognising the separator between parameters and the terminator at the end of a line. The characters before a separator are recognised as making up a parameter while all parameters before a terminator are attached to the operational keyword at the beginning of a line.

MATCH- Matches input string to keyword in table of data in the programme which are index to the parts of the programme where the parameters following the keyword are required.

SAVE- Saves or restores state of parameters, data, information and results

GETFN- To create files, it interprets the filename parameter in the input line as a filename.

GEN- Generates particles (with different size distribution) randomly within a 3-D periodic space.

TRBRAN- A function under GEN to generate pseudo-random numbers.

SEARCH- Search for neighbouring particles which are potential contact particles and assign identification address to each contact.

BBTEST- Test for contact between particles.

UPDATE- Updates particles position, create and put particles in position when necessary. Identifies and initialises memory block for storing data for each contact.

INITP- Performs calculation of initial parameters prior to the calculation cycles e.g. mass and time step.

CYCLE- Cycle through main calculation loop - Calculates and updates the periodic space, velocity, acceleration, displacement and forces.

FORD- Applies force-displacement law to each ball-ball contact to obtain the contact forces and deformation etc.

SETSRV- Inputs the stress variable/factor

CONP- Tests for sliding and the yield points using the Mindlin solution.

APLOT- Prepare the plotting file.

PRINT- Prepare the general print out routine i.e. the output data.

In order to make the programme CONBAL suitable for the operations needed in this work, nearly all the subroutines were modified but major changes are made on the followings while some others added are listed below

GEN: as before but with additional tasks of recognising the real boundaries and generating a single column stack of particles when necessary

REBOX- As before with additional tasks of locating positions and inclination of walls with respect to the sub-boxes (mapping the walls to the box(es) it occupies) within the main box. BBTEST, SEARCH and UPDATE dependent on REBOX are modified accordingly.

FORD and CYCLE are also modified accordingly to handle the wall options and damping.

Recognise other forms of loading.

CONP- The whole set changed though still performing the same function but the elastic plastic nature changed to handle visco-elastic

Additional Routines

BUCVOL – Computes the new particle size and shape in conjunction with others such as PRVBAL, PREVOL, PRVWAL : For shape data computation

ATEFUN: Moving or changing the wall position.

WALPAR, WALLS, WALDIS: For creating appropriate containers (walls); flat or inclined

NEWCIR, ROBOTO, KOPI, KOPI1- for graphics

There are a numbers of other functions for other minor operations.

Appendix E

Input file for consolidation and compression of soybean

(The input file for other simulations and other references made to this appendix can be found in the attached disk {Appendix F})

```
Start,0.03,0.06,0.03,250,260,6
CONSOLIDATIONSOY                              !comment
radius,0.003,1,
gravity,0,-9.81,0,
fric, 0.2
frac, 0.04,
damp,0.0,0.7
gen,20,1,10!generate uniform radius spheres(1), 20x10 times
dens, 1180
shear,40.00e06          !rigidity modulus
save, conssoy,
-----------------------------Consolidation-----------------
news,                                 !index for restart
restart, conssoy,                     !read saved information
cycle,10000,10,1
cycle,10000,10,1
cycle,10000,4,1
save,comsoy1
news
-----------------------------Compression-------------------
restart,comsoy1,
frac, 0.001,
compress,0.0,1.0,0.0,0.0,0.0,0.0
grid,0.0,-250,0.0,0.0,0.0,0.0
cycle,20000,10,0
save,comsoy2,
news
restart,comsoy2,
compress,0.0,1.0,0.0,0.0,0.0,0.0
grid,0.0,-250,0.0,0.0,0.0,0.0
cycle,20000,10,0
save,comsoy3,
news
restart,comsoy3,
compress,0.0,1.0,0.0,0.0,0.0,0.0
grid,0.0,-250,0.0,0.0,0.0,0.0
cycle,20000,10,0
save,comsoy4,
news
restart,comsoy4,
frac, 0.0008,
compress,0.0,1.0,0.0,0.0,0.0,0.0
grid,0.0,-250,0.0,0.0,0.0,0.0
cycle,20000,10,0
```

```
save,comsoy5,
news
restart,comsoy5,
frac, 0.0007,
compress,0.0,1.0,0.0,0.0,0.0,0.0
grid,0.0,-250,0.0,0.0,0.0,0.0
cycle,20000,10,0
save,comsoy6,
news
restart,comsoy6,
frac, 0.0006,
compress,0.0,1.0,0.0,0.0,0.0,0.0
grid,0.0,-250,0.0,0.0,0.0,0.0
cycle,20000,10,0
stop
```

APPENDIX F

Thesis Title: Discrete Element modelling of the Deformation of Bulk Agricultural Particulates

Author: A.O. RAJI
Degree: Ph.D

Filename	Type
BIODEM.F	main prog
BIODEM.DAT	input
AORCOM1, AORCOM2	include

Year: 1999

CONTAINS

DISKETTE